An Abstract of the Thesis of

Tony Michael Allen for the degree of Master of Science in Civil Engineering presented on April 18, 1983.

Title: PROPERTIES OF GEOTEXTILES IN COLD REGIONS APPLICATIONS

Abstract approved: Redacted for Privacy

Ted S. Vinson

Geotextiles are experiencing increased use in arctic and subarctic construction in separation, reinforcement, erosion control, and drainage applications. The use of geotextiles as capillary cutoff layers to prevent frost heave has been proposed as well.

In recognition of the need to investigate properties of geotextiles in cold regions applications, a laboratory test program was conducted with five representative geotextile types. Freeze-thaw durability of geotextiles in fresh and saline water was studied. Geotextile strength before and after 300 freeze-thaw cycles showed no serious degradation. Geotextile load-deformation-time relationships were determined at +22°C and -12°C by wide strip tensile and static creep tests. Temperature had little effect on strength, but creep was significantly affected. Lower temperatures resulted in lower creep rates and delayed the onset of tertiary creep. Geotextile structure and polymer type were significant to creep. Polypropylene geotextiles were affected to a greater extent by the temperature differences considered than were polyester geotextiles.

A preliminary laboratory investigation was performed to determine the potential of geotextiles to serve as capillary breaks to reduce

frost heave. Three columns of a highly frost susceptible Alaskan silt were frozen simultaneously from the top at a constant rate. Free water was available at the bottom for two columns - one contained a geotextile layer and one did not. The third column, a control specimen, was frozen without free water or a geotextile layer. Heave and water content increase during freezing were determined for each soil column. The results indicate select geotextiles have the potential to significantly reduce frost heave. There were substantial differences between the effectiveness of the five geotextiles considered.

PROPERTIES OF GEOTEXTILES IN COLD REGIONS APPLICATIONS

By

Tony Michael Allen

A THESIS

submitted to

Oregon State University

in partial fulfillment of
the requirements for the
degree of
Master of Science

Completed April 18, 1983

Commencement June 1983

APPROVED:

Redacted for Privacy

Professor of Civil Engineering in charge of major

Redacted for Privacy

Head of Department of Civil Engineering

Redacted for Privacy

Dean of Graduate School

Date thesis presented: April 18, 1983

Typed by Jane Jarvi for Tony Michael Allen.

ACKNOWLEDGEMENTS

The author gratefully acknowledges the financial support provided by the Crown Zellerbach Corporation. The contents of this thesis reflect the views of the author who is responsible for the facts and the accuracy of the data presented herein, and do not necessarily reflect the views or policies of the Crown Zellerbach Corporation.

The author is indebted to his major professor, Dr. T.S. Vinson, and Dr. J R. Bell for their advice and guidance throughout this research project. The author is also grateful to Andy Brickman and the engineering shop machinists, Chuck Svenson and Lauren Sundberg, for their advice and assistance on the building and debugging of the equipment used in the test program.

A special thanks also goes to the following people for their assistance and encouragement: Tuyet-Mai Chau, Ted Hammer, Barry Kellems, Terri Reynolds, Ross Rieke, Terry Whitehill, and Chuck Wilson. The efforts of Jane Jarvi, who typed this report, are greatly appreciated.

TABLE OF CONTENTS

TABLE OF CONTENTS (continued)

TABLE OF CONTENTS (continued)

LIST OF FIGURES

List of Figures (continued)

List of Figures (continued)

List of Figures (continued)

LIST OF TABLES

LIST OF TABLES (continued)

NOTATION

Term	Description	Dimensions
E	Modulus of elasticity of Geotextiles (open spring constant)	Newtons/m (lbs/in.)
$\overline{E}$	Experimental activation energy	Calories/mole
E_p	Constant for parallel spring element	Newtons/m (lbs/in.)
ΔF	Free energy of activation	Calories/mole
K	Constant of the series open viscous element	$\frac{mm}{mm}sec^{-1}(\frac{in.}{in.}\ sec^{-1})$
K_p	Constant of the parallel closed viscous element	Newtons/m (lbs/in.)
M	Geotextile mass per unit area	Grams/m^2 (lbm/yd^2)
M_a	Average mass per unit area of three geotextiles (creep test)	Grams/m^2 (lbm/yd^2)
M_n	Nominal mass per unit area of a geotextile	Grams/m^2 (lbm/yd^2)
n	Number of specimens	Dimensionless
P_u	Percent of wide strip tensile strength	Percent
R	Universal gas constant	$\frac{Calories}{mole°K}$
S	Standard deviation of the sample population	Dimensions Vary
S_N	Normalized geotextile strength	Newtons/m (lbs/in.)
$\overline{S}_N$	Mean normalized strength of five geotextile specimens	Newtons/m (lbs/in.)
S_u	Ultimate Geotextile Strength	(Newtons/m) (lbs/in.)
T	Absolute temperature	°K (°R)
Tg	Glass transition temperature	°C (°F)
t	Time	Minutes

Notations (continued)

Term	Description	Dimensions
t_1	Time at which one half of the total primary creep strain has occurred	Minutes
$t_{n-1,\ \alpha}$	Standard normal deviate in which n is the number of samples and α is the probability of exceeding a confidence level of $1-\alpha$	Dimensionless
α	Constant of the series open viscous element	m/Newton (in./lbs)
α'	Slope of deviator stress versus log strain rate response of geotextiles	m/Newton (in./lbs)
α_p	Constant of the parallel closed viscous element	m/Newton (in./lbs)
ε	Total creep strain at time t	mm/mm (in./in.)
$\dot{\varepsilon}$	Strain rate	$\frac{mm}{mm\ sec.}$ ($\frac{in.}{in.\ sec.}$)
ε''	Ratio of the primary creep at time $t=2t_1$ to the total primary creep strain	Dimensionless
ε_0	Instantaneous creep strain (elastic)	mm/mm (in./in.)
ε_d	Secondary creep strain	mm/mm (in./in.)
$\dot{\varepsilon}_d$	Secondary creep rate	$\frac{mm}{mm\ sec.}$ ($\frac{in.}{in.\ sec.}$)
ε_p	Primary creep at time t	mm/mm (in./in.)
ε_p^*	Total primary creep	(mm/mm) (in./in.)
λ	Distance flow units move in the direction of stress	(mm) (in.)
λ_1	Distance between flow units	(mm) (in.)

Notations (continued)

Term	Description	Dimensions
λ_2 λ_3	Cross sectional area of flow units	mm^2 ($in.^2$)
μ	Maximum or minimum value of the mean of a normal distribution	Dimensions vary
σ	Stress	Newtons/m^2 (lbs/in^2)

PROPERTIES OF GEOTEXTILES IN COLD REGIONS APPLICATIONS

1. INTRODUCTION

1.1 Background

In the past decade considerable attention has been focused on the cold regions of the world owing to the abundance of natural resources which exist there, in particular oil and gas reserves. Owing to the exploitation of these natural resources, roadways, embankments, and buildings are being constructed in cold regions at an ever increasing rate. The design and construction of these structures in cold regions is intimately associated with freezing related phenomena of initially unfrozen ground, and thawing related phenomena of initially frozen ground. Due to freezing related phenomena such as frost heave and thermokarst formation, ground surfaces can heave during the winter, resulting in the disruption of foundations or embankments placed on or within the zone of freezing. Thawing of ice-rich soils can result in loss of bearing strength and settlement, termed thaw instability.

As geotextiles have been used successfully as filtration and separation and/or reinforcing layers on very weak, saturated soils in the temperate regions of the world, geotextiles are now also being used on the weak and saturated soils (when thawed) found in cold regions. While the primary use of geotextiles in cold regions has been as filtration, separation, and reinforcing layers, unique applications of geotextiles are also being considered to deal with phenomena resulting

from freezing of soil. In particular, engineers have suggested that geotextiles might act as capillary barriers when placed in frost-susceptible soils, which would reduce frost heave problems.

1.2 Problem Statement

While successful applications of geotextiles have been made, many questions remain unanswered relative to the performance of geotextiles in cold environments. For example, the influence of subfreezing temperature on the load-strain-strength and creep characteristics of geotextiles is largely unknown. The effect of freeze-thaw cycles in fresh water and saline water environments on the durability of geotextiles is also presently unknown.

Frost heave is an important problem in cold regions in areas where frost-susceptible soils are present. At this time the methods available to alleviate frost heave are either very expensive or inefficient. Geotextiles as capillary breaks could provide an inexpensive but efficient alternative to the presently available frost heave solutions. However, more must be learned about the ability of geotextiles to act as a capillary break, as well as the geotextile properties involved, before geotextiles can be used to prevent frost heave.

In summary, the need to determine the effect of a freezing/thawing environment on the load-strain-strength and creep characteristics of geotextiles, and the need to determine the ability of geotextiles to act as a capillary barrier, is evident. Only after the effect of a freezing/thawing environment on geotextile properties is determined can

more economical and efficient designs of structures employing geotextiles be made.

1.3 Purpose and Scope

The purposes of this study are to (1) investigate the influence of freeze-thaw cycles in a freshwater and a saline water environment on the load-strain-strength characteristics of geotextiles, (2) develop an understanding of the effect of temperature on the load-strain and creep characteristics of geotextiles, (3) evaluate the load-strain-time parameters of selected geotextiles at temperatures in a range experienced in cold regions, and (4) determine the feasibility of using a geotextile as a capillary break to prevent frost heave.

The report presents a literature survey of the geotextile applications which pertain to cold regions. Field and laboratory data pertaining to these applications are reviewed. Background on the load-strain-time behavior of geotextiles at the molecular level is included.

Experimental work is limited to laboratory investigations. The scope of this study is limited to the load-strain and creep behavior of five geotextiles commonly used in road subgrade stabilization, embankment stabilization, and erosion control applications. The effect of temperature on the load-strain and creep characteristics of geotextiles at two temperatures (+22°C and -12°C) are measured. The effect of 50 and 300 freeze-thaw cycles on geotextile durability in fresh water and saline water environment is also investigated. A qualitative study of the ability of a geotextile to prevent water migration to the freezing

front in a soil which is known to be frost- susceptible is made through frost heave tests on specimens with and without a geotextile layer.

2.0 LITERATURE REVIEW ON LOAD-STRAIN-TIME PROPERTIES OF GEOTEXTILES IN COLD REGIONS APPLICATIONS

2.1 General

Information is provided which includes a summary of the past experience with geotextiles in cold regions and geotextile properties which are important for different applications. This is followed by a review of the literature on tensile strength and creep behavior of geotextiles. Finally, a discussion of load-strain-time behavior of geotextiles at the molecular level is presented.

2.2 Applications of Geotextiles Used in Cold Regions

2.2.1 Past Experience with Geotextiles in Cold Regions

Little specific information has been published about the uses and performance of geotextiles in cold regions. Therefore, the following list of typical geotextile applications in cold regions is general and by no means complete.

Subgrade stabilization has been the most common application of geotextiles in cold regions. The city of Calgary, Alberta, has consistently used geotextiles as a separation medium in the construction of their primary roads (77). Roads in Alaska have been more stable when a geotextile layer was used (43). A needlepunched polypropylene geotextile was used as a separation/reinforcement layer in the construction of a low embankment on muskeg in southeast Alaska

(28). Nonwoven geotextiles were also used near James Bay in eastern Canada as separation layers in roads over muskeg and in permanent rockfill structures (56). Cragg (18) reported that geotextiles are frequently used as separation layers in the construction of temporary and permanent access roads over weak soils on Ontario hydroelectric projects. Kerr and Townsend (40) reported that geotextiles were used as separation layers in log and lumber yards in northern Alberta and British Columbia. A geotextile was also used in northeastern Alberta as a separation/reinforcement layer in a highway embankment over muskeg (14). Burwash (14) reported that this geotextile layer performed adequately for the first four months after construction. Tart and Luscher (71) reported the use of a high strength geotextile layer to stabilize a fill for an airstrip on the North Slope of Alaska. They reported that the geotextile adequately stabilized the fill during the spring thaw period as well as during the winter months, preventing adverse differential heave of the runway surface.

Brantman, et al., (12) reported the use of Bidim as a separation layer and a capillary break (see also Section 3.3.1) in roadways constructed near Soyuzdornii in the U.S.S.R. They reported that tensile tests were performed on fabric specimens taken from the roadway one year after installation. These tests showed that the load-strain characteristics of the geotextile had not changed (12).

Little specific information about the use of geotextiles for the stabilization of embankments (other than low embankments in highways) in cold regions is available. In the only reference available on the use of geotextiles to stabilize embankments in cold regions, Broms (13) described the use of a polyester woven geotextile to increase the

stability of a bridge abutment in Sweden. He reported that the embankment has performed adequately since its construction.

Geotextiles have recently been incorporated in the design of gravel islands off the Alaskan North Slope to prevent erosion of the island core due to wave action (45). The performance of geotextiles in this application has not been determined.

2.2.2 Descriptions and Theories of Geotextile Applications in Cold Regions

The most common applications of geotextiles in cold regions are in road stabilization, embankment stabilization, and erosion control. A description of these applications follow. A fourth application which has the potential to become very common, the use of geotextiles as capillary breaks, is discussed in Chapter 3.

2.2.2.1 Geotextile Subgrade Stabilization Application

Geotextiles used in subgrade stabilization applications perform at least one of three possible functions: separation, reinforcement, and filtration. Geotextiles placed between the subgrade and the aggregate base almost always perform the separation function. The reinforcement function is only performed when the geotextile bridges very soft soil (CBR $\leqslant 2$) such as muskeg or when the geotextile bridges thermokarsts. The filtration function is usually performed in conjunction with the separation function when subgrade pumping is a problem. Descriptions of these subgrade stabilization functions follow:

(1) Separation and Filtration. The purpose of separation is to prevent a fine-grained subgrade material from entering a coarse-grained base material. By physically preventing these two dissimilar materials from mixing, the stability (strength) of the base layer can be preserved (5).

The migration of fines into the coarse-grained base material can be divided into two modes. Fine soil particles can move into the base material due to the action of water. This water movement, which is caused by the sudden application of a load, is known as pumping (5). A geotextile layer placed between the subgrade and the base as a separation layer may prevent the fine soil particles suspended in the water during pumping from migrating into the base coarse by acting as a filter. The second mode is the intrusion of fine subgrade particles into the base material by plastic flow due to the application of a load (5). The geotextile separation layer prevents this plastic flow by bridging across the voids in the coarse-grained base material (5).

A geotextile may not satisfy its separation function if its pores are so large that excessive fine material could pass through the geotextiles (5). If the strength of the geotextile is inadequate, the geotextile may burst due to the pressures developed in the geotextile layer across the voids in the aggregate base layer (5).

In light of the phenomena involved in the separation (and filtration) function, Bell, et al., (5) concluded that the important properties to consider for a geotextile separation layer are the burst and tensile strength, puncture resistance, extension at failure, dynamic creep, and pore size.

(2) Reinforcement. In roads with very soft subgrades (such as muskeg), the normal stress transmitted to the subgrade may exceed the allowable load. Under many load applications, failure in the form of a rut is developed due to the accumulation of small, inelastic strains in the subgrade (5). However, if a geotextile layer is placed between the subgrade and the base, as the rut deepens, the geotextile strains and takes on a permanent tension, inducing a shear and normal stress on the subgrade as shown in Figure 2.1.

Kinney (41) proposed that a geotextile layer be used to bridge thermokarsts in roadways. In this application the geotextile would support the soil above it by membrane action (41). Figure 2.2 shows schematically how the geotextile layer would prevent severe road settlements when the ice melts.

Kinney (42) found that the improved bearing capacity of a soil-geotextile-aggregate system could be attributed to geotextile induced shear and normal stress on the subgrade and base. He also observed that the stress developed in the soil-geotextile-aggregate system depended on the dynamic modulus and creep characteristics of the geotextile layer (42).

Webster and Watkins (76) performed a full scale test using a geotextile as a separation/reinforcement layer over a soft subgrade soil. They found that the two geotextile properties which best related to performance were breaking strength and elongation.

Kinney (41) proposed that a geotextile layer used to bridge thermokarsts have high modulus and strength. The geotextile layer must also exhibit low static creep during the thaw period (41).

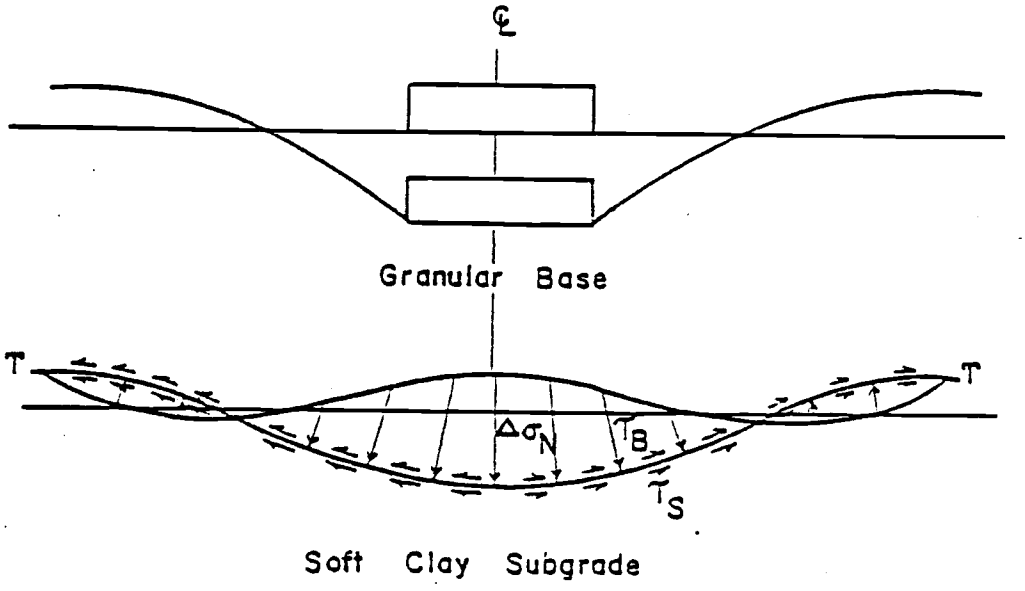

Legend:

τ_B = Friction between base and fabric.
τ_S = Friction between subgrade and fabric.
$\Delta\sigma_N$ = Fabric induced normal stress.
T = Tension in fabric.

Figure 2.1: Typical fabric induced shear and normal stresses (after Kinney (42)).

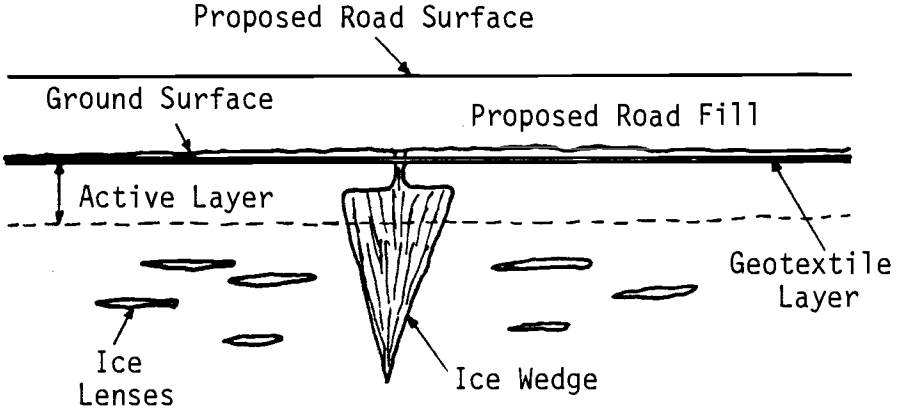

a. Initial conditions (frozen state)

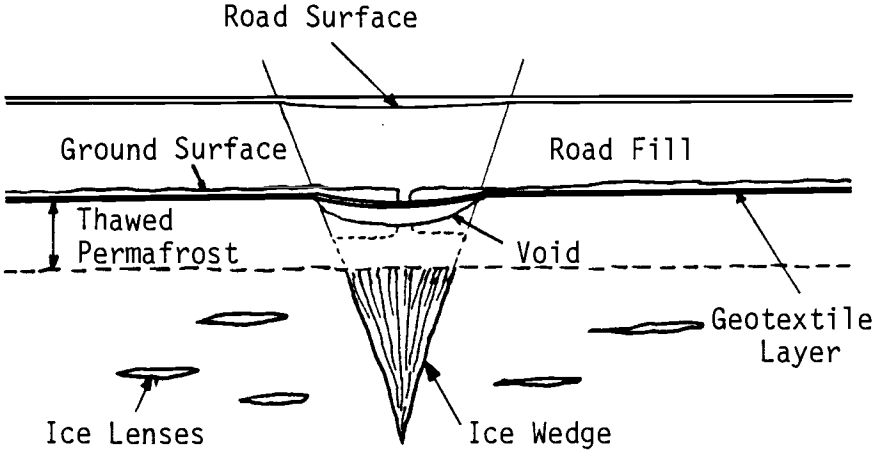

b. Conditions after thawing

Figure 2.2: Geotextile layer to prevent severe settlement during the spring thaw of a road bridging a thermokarst (after Kinney (41)).

2.2.2.2 Embankment Stabilization Application

The stability of embankment foundations may be improved by the placement of a geotextile layer underneath the body of the embankment. The geotextile layer provides tensile forces across the potential failure surface of an embankment, thereby increasing the stability of the embankment (5). Figure 2.3 shows schematically the possible modes of failure for embankments reinforced with geotextiles.

Geotextiles may also be used to reinforce embankments with vertical faces. The geotextile itself may form the facing element, or the geotextile may be tied to facing elements made of concrete, timber, or steel (5). The forces imposed on the geotextile layers are similar to the forces occurring in sloping embankments (5). These forces include the vertical forces due to the weight of the soil mass and the lateral earth pressure forces as well (5).

If a geotextile layer is to provide increased embankment stability, the tensile strength of the geotextile layer must become fully developed through a movement of the soil mass, causing the geotextile to become strained (5). If this soil movement is to be sufficiently small to preclude a failure of the embankment, the modulus and tensile strength of the the geotextile must be very high (5, 29). However, Haliburton, et al. (29) postulated that the geotextile should have the ability to undergo large deformations without rupture as well. Haliburton, et al. (29) also noted that the geotextile should exhibit low static creep at the working load. Maagdenberg (47) stressed the importance of geotextile creep by stating that a factor of safety of

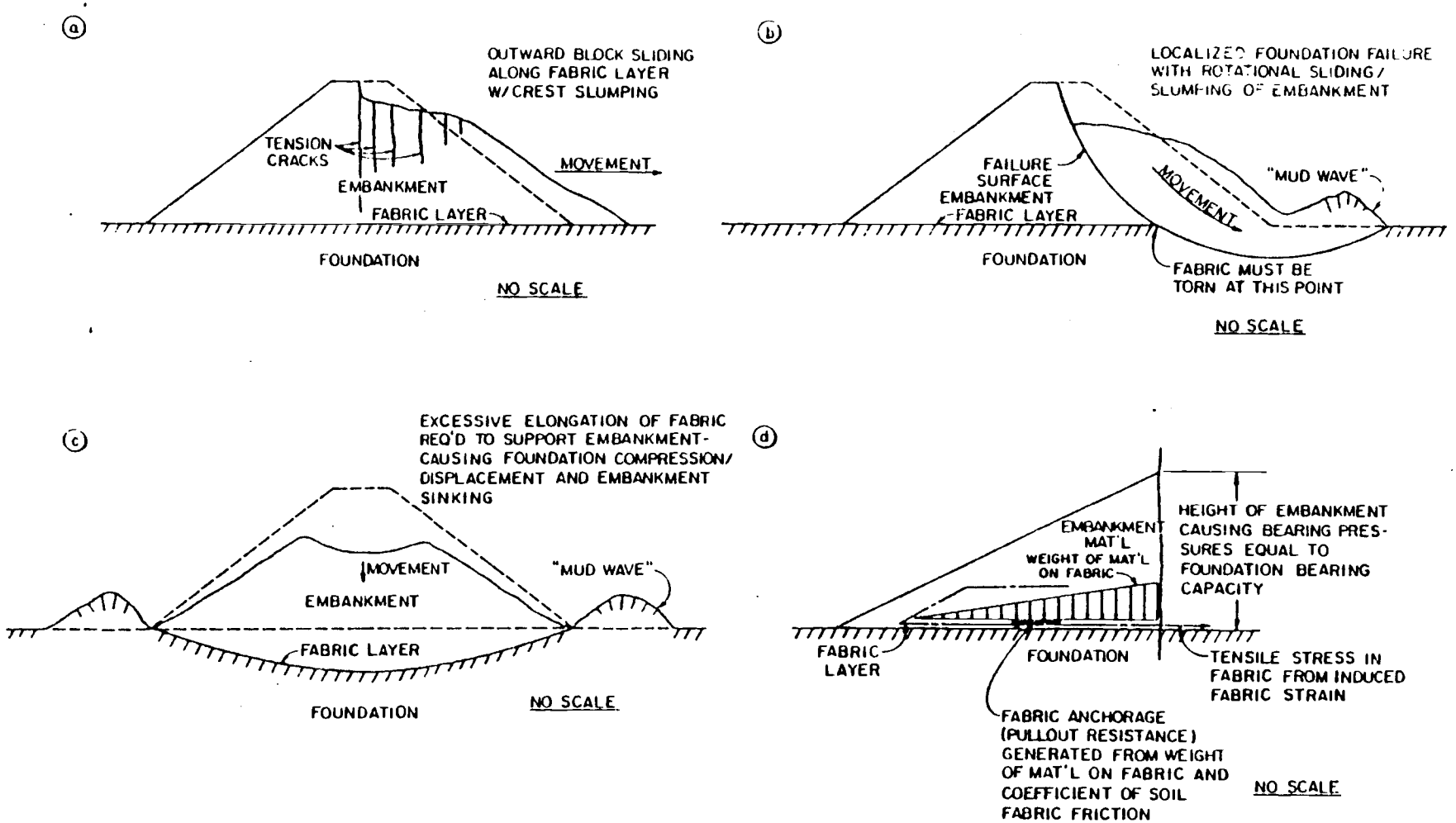

Figure 2.3: Potential unsatisfactory behavior which might occur for fabric-reinforced embankments (after Haliburton, et al. (29)).

2.0 be used to select the strength of a geotextile to allow for creep and stress relaxation.

Greenway and Bell (28) observed that the geotextile tension developed under traffic live load in a low embankment on muskeg was significantly greater than the geotextile tension developed under the embankment dead load. They suggested that for low embankments the dynamic creep strength may be of greater concern than the static creep strength of the geotextile.

Another geotextile property which is important in the embankment stabilization application is the soil-geotextile frictional resistance. If the desired geotextile strain, and therefore tensile strength, is to be obtained, the soil-geotextile frictional resistance must be reasonably high (29).

2.2.2.3 Erosion Control Application

The erosion control application is described in terms of a specific example, the gravel islands off the Alaskan North Slope.

The core of a gravel island can be protected from the scouring action of waves through the placement of a geotextile layer on the surface of the island. To keep the geotextile from moving around due to wave action, riprap is placed on the geotextile layer. In the case of the offshore Alaskan gravel islands, riprap is often in the form of large geotextile bags filled with sand or gravel (45). Figure 2.4 depicts schematically the geotextile layer and the sand filled geotextile bags in place on an island.

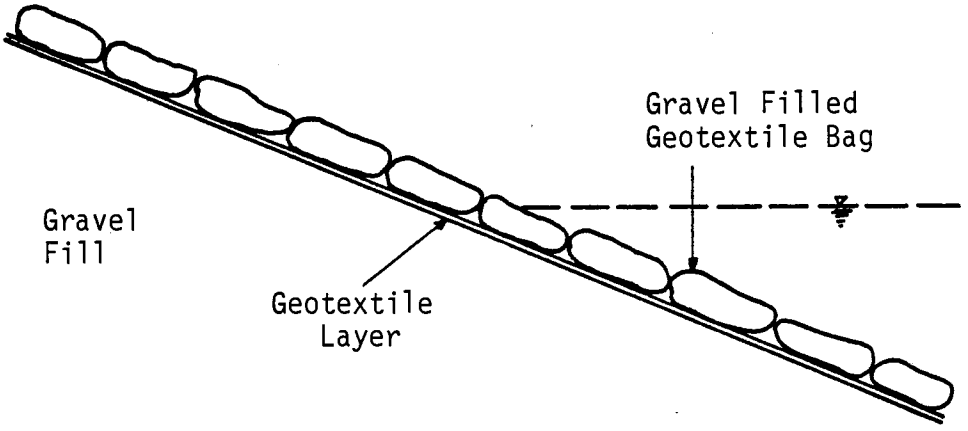

Figure 2.4: Schematic cross section of Alaskan North Slope gravel island slope using geotextiles for scour protection.

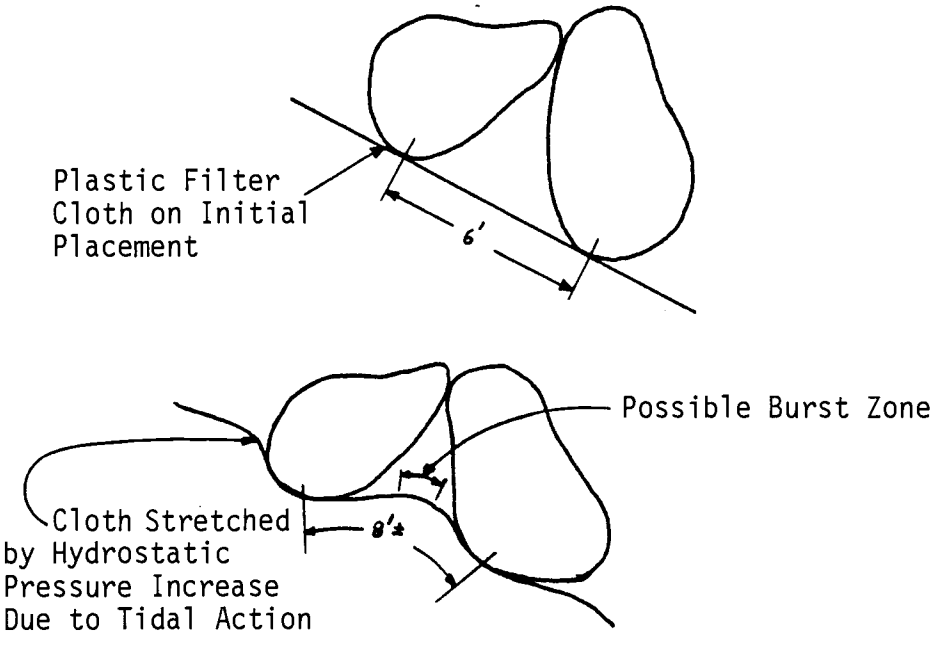

Figure 2.5: Ballooning effect with large stones on slope (after Dunham and Barret (20)).

Since the use of geotextiles in gravel island construction has only been for a very short time, many questions remain unanswered. The size of the waves which the geotextile layer can tolerate is not known. Large waves could cause a large differential in head, resulting in soil movement from the area under the sand filled bags to the area between the bags, causing the geotextile layer to balloon, as shown in Figure 2.5 (5). Ballooning would be especially likely if the geotextile permeability was too low, or if the geotextile became clogged (5). The resistance of geotextiles to the impact and abrasion of drifting ice may also be of prime concern (45). Therefore, geotextile strength, abrasion resistance, and permeability are important properties to consider. The frictional characteristics of the geotextile layer are also important, as movement of the geotextile bags due to wave action would be undesirable. Handling of the geotextile bags during their placement on the embankment is also of concern (45). Since these geotextiles will be exposed to the freezing and thawing action of seawater, the freeze-thaw durability of the geotextiles, as well as their resistance to seawater, may be important factors to consider. Geotextile ultraviolet radiation resistance is also important as geotextiles used in this application will be exposed to sunlight (45).

2.2.3 Summary of Geotextile Properties

Based on the literature survey, the geotextile properties which should be considered when evaluating a geotextile for use in the road subgrade, embankment stabilization, and erosion control applications in a temperate climate are given in Section 2.2.3.1. Following the

summary of the temperate climate properties, conclusions are given in Section 2.2.3.2 as to which of these properties are most likely to be affected by the freezing/thawing environment found in cold regions.

2.2.3.1 Summary of Geotextile Properties Important in Temperate Climates

(1) A geotextile used in the subgrade stabilization application should have a high burst strength and tensile strength, high modulus, high elongation at break, high friction, high resistance to puncture and tearing, and should be resistant to static and dynamic creep. The strength and stiffness required for reinforcing layers is higher than that required for separation layers. Furthermore, the pore size of a geotextile used for separation must be small, but it must still have high permeability. The geotextile should also be very durable.

(2) Geotextiles used in the embankment stabilization application should have high tensile strength and high elongation at failure, high modulus, and high soil-geotextile friction. Geotextiles used in this application should exhibit low static and dynamic creep and be durable.

(3) Geotextiles used in the erosion control application should have high tensile strength and high modulus, as well as high puncture and tear resistance. The geotextile should also have high frictional characteristics. The permeability of the geotextile should be high, but the pore size of the geotextile must be small enough to prevent the embankment material from eroding away. The geotextile should also be very durable. Resistance to abrasion and ultraviolet radiation are also important.

Table 2.1: Important temperate climate geotextile properties for three geotextile applications.

Geotextile Property	Application			
	Subgrade Stabilization		Embankment Stabilization	Erosion Control
	Separation	Reinforcement		
Tensile Strength	1	3	4	2
Modulus	1	3	4	2
Failure Elongation	4	4	4	4
Burst Strength	3	2	1	4
Durability	4	4	1	4
Puncture Resistance	4	2	1	3
Static Creep Resistance	2	3	4	1
Dynamic Creep Resistance	4	2	1	3
Soil-Geotextile Friction	1	3	4	2
Permeability	2	N/A	N/A	3
Pore Size	1	N/A	N/A	3

Note: The geotextile properties are rated on a scale of 1 to 4, in which "1" is the lowest and "4" is the highest magnitude of the property. Where the property is not applicable for the particular application, N/A appears.

The important temperate climate geotextile properties for the three geotextile applications previously noted are also summarized in Table 2.1. An attempt is also made in Table 2.1 to determine the relative magnitudes of the geotextile properties required for each geotextile application.

2.2.3.2 Geotextile Properties Most Likely to be Affected by a Freezing/Thawing Environment

To determine which geotextile properties are most important when considering geotextiles in cold regions structures, one must postulate how below freezing temperatures and the freezing and thawing of water could affect geotextile properties. Bell, et al. (6) suggested that low temperature could have a significant effect on the modulus and creep characteristics of geotextiles used as a separation/reinforcement layer. This suggestion seems quite reasonable considering that many polymers become stiffer at low temperatures.

As was stated in Section 2.2.2.3, the freezing and thawing action of fresh water as well as seawater could adversely affect the strength of a geotextile. The salts contained in seawater might also affect geotextile strength.

The pore size, permeability, and soil-geotextile friction are most likely not affected by a freezing/thawing environment. Therefore, these three properties do not need to be considered for further study as these properties can be applied to cold regions applications using their temperate climate values. Furthermore, since

burst strength and puncture resistance are related to tensile strength, a study of the effect of temperature on tensile strength is sufficient.

In light of the above discussions, the geotextile properties which should be considered for a study of the effects of freezing/thawing environments on geotextile properties are geotextile load-strain and creep behavior, and geotextile durability in a saline and fresh water freezing/thawing environment.

2.3 Review of Previous Work on Tensile and Creep Behavior and Durability of Geotextiles

2.3.1 Load-Strain Behavior of Geotextiles

Researchers have determined that the load-strain behavior of geotextiles is controlled by the fiber polymer properties and construction characteristics of the geotextile (5). The construction characteristics of the geotextile tend to dominate the load-strain behavior, at least when the geotextile is not confined in soil (5).

At low strains, the geotextile load-strain behavior depends on the crimp heights and/or the amount of fiber entanglement, and the ability of the fibers to reorient during application of the load (5 , 31). Once reorientation and decrimping have occurred, as is generally the case at relatively high loads, the load-extension properties of the geotextile are almost entirely governed by the load-extension properties of the filaments themselves (31).

For geotextiles in which there is a large amount of entanglement but with many fibers which are free to move, such as the needlepunched geotextiles, much of the total strain (even at failure) is due to fiber reorientation (5, 69). Hence the needlepunched geotextiles tend to have a low modulus and high strain at failure (5). However, the load-strain behavior of geotextiles of relatively simple construction, such as the woven geotextiles, tends to be governed by the load-strain behavior of the filament, even at very low strains. Hence, the woven geotextiles tend to have a high modulus and a low strain at failure. In both cases the maximum tensile strength of the geotextile depends primarily on the fiber polymer type and the degree of crystalline orientation within the fiber, this orientation being controlled by the amount which the fiber is drawn (discussed in Section 2.4.2)(5). Of course, the total geotextile strength also depends on the number and the diameter of fibers stressed by an applied force.

McGown (51) has summarized in graphical form the typical behavior of geotextiles of various construction types. His summary is shown in Figure 2.6.

Haliburton, et al. (29) performed uniaxial tension tests on several geotextile types. Tests were performed on 150 mm (6.0 in.) wide specimens with an initial 300 mm (12.0 in.) specimen length between grips. The tests were conducted at a deformation rate of 1% strain per minute. The results of the load-strain testing of the pertinent geotextile types are summarized in Table 2.2.

Table 2.2: Results of fabric tension tests conducted by Haliburton, et al. (29).

Fabric Trade Name	Woven (W) or Nonwoven (N)	Warp (W) or Fill(F)	Ultimate Tensile Load (kN/m)	Strain at Failure Percent	Secant Modulus at 10% E (kN/m)
Stabilenka T-100	N	W	4.78	36	30.1
		F	3.36*	50*	15.4
Typar 3401	N	W	5.25	34	39.4
		F	7.32	43	50.3
Bidim C-34	N	W	15.3	45	17.5
		F	10.0	37	12.6
Polyfilter-X	W	W	54.5	35	180
		F	32.3	33	115
Advance Type I	W	W	44.1	29	188
		F	24.0	29	88.4
Lotrak 16/15	W	W	15.3	30	63.9
		F	8.67	19	66.2

*Test stopped at 50% strain.

Note: Three specimens in the warp and three specimens in the fill direction of each geotextile type were tested.

1 kN/m = 5.71 lbs/in.

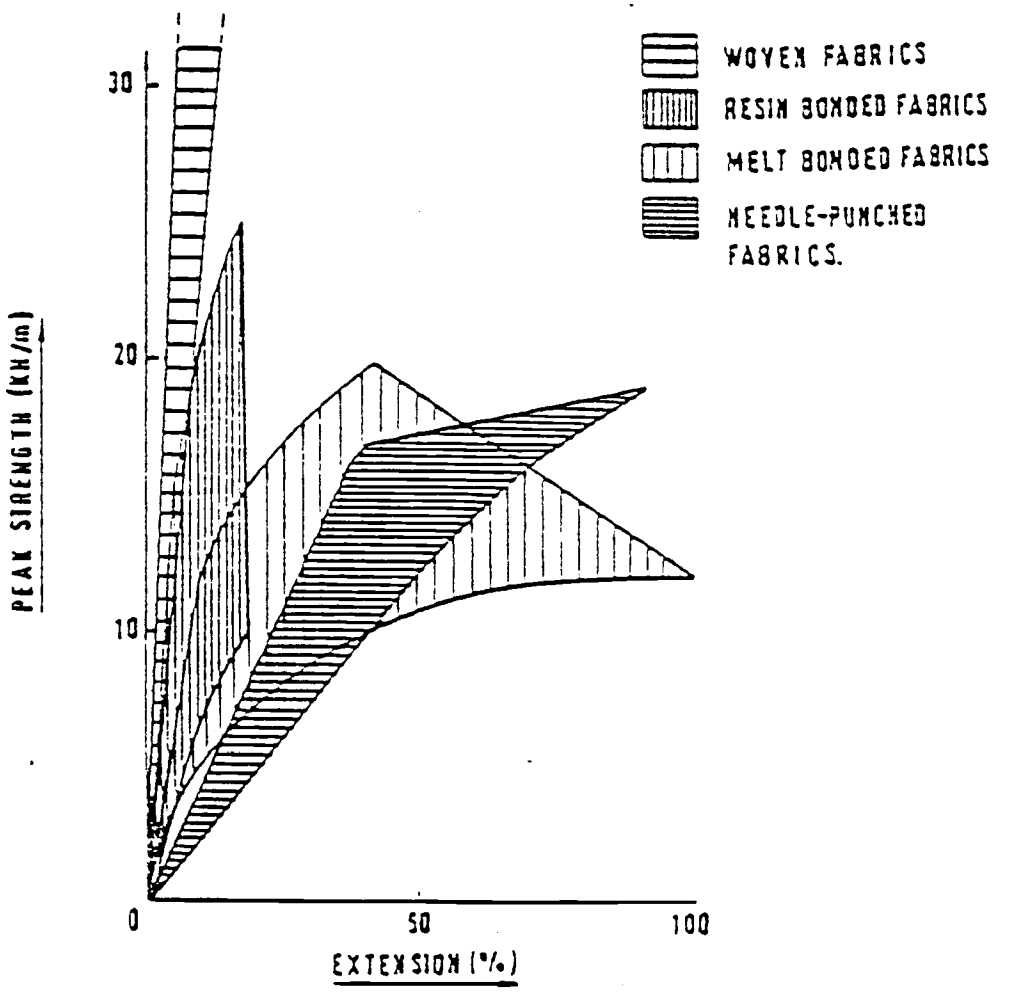

Figure 2.6: In-isolation plane strain load deformation behavior of various fabric types (normalized to 300 g/m^2 fabric) (after McGown (51)).

Since the load-strain characteristics of geotextiles are also greatly influenced by the test conditions, a discussion of these conditions follows:

(1) Specimen size and aspect ratio. Shrestha and Bell (67) found that the specimen size and aspect ratio did not significantly influence the ultimate strengths of geotextiles tested in strip tensile tests, whereas the strain at failure varied considerably. They recommended that a specimen 200 mm (8.0 in.) wide with a 100 mm (4.0 in.) gauge length be used for routine laboratory testing. At this specimen size they found that plane strain loading conditions could be adequately approximated without the use of a restraining device to limit lateral contraction.

(2) Specimen orientation. The results of strip tensile tests conducted by Steward, et al. (69) demonstrate the variation in strength and strain at failure of geotextiles tested in the warp and fill directions. These results are presented in Table 2.3. The results of tests conducted by Haliburton, et al. (29) also demonstrate variation in ultimate strength and strain with specimen orientation, as shown in Table 2.2. Therefore, if reliable conclusions are to be made when comparing the various geotextile types, careful attention must be paid to the direction in which the geotextile specimens are stressed.

(3) Rate of loading. Although the ultimate tensile strengths of geotextiles are not greatly affected by the rate of loading, the moduli are greatly affected, as modulus increases with loading rate (5). Therefore, a common loading rate is needed if the results of various tests are to be compared.

Table 2.3: Summary of results of fabric tension tests (modified cut strip tests) conducted by Steward, et al. (69).

Type of Fabric	Average Strength (kN/m) Dry	Wet	Standard Deviation (Dry)	Percent Strain (%) Dry	Wet	Standard Deviation (Dry)	Direction
Fibretex 320*	17.3	21.5	1.21	183	209	13.04	Warp
Fibretex 320*	21.2		0.35	161.8		17.54	Fill
Bidim 4 oz.	13.5	11.0	1.96	49	32	14.19	Warp
Bidim 4 oz	8.48	8.98	0.50	59.3	67	5.91	Fill
Typar 4 oz	5.78	5.25	0.39	30.8	18	2.21	Warp
Typar 4 oz	8.76	9.16	0.72	45.5	53	6.61	Fill
Mirafi 140	7.13	6.97	0.38	87.2	85	14.10	Warp
Marafi 140	5.73	5.25	0.82	68	68	10.12	Fill

Note: Specimens were 100 mm (4.0 in.) wide with a 76 mm (3.0 in.) gauge length. Five specimens of each fabric type (in both directions) were tested. All specimens were tested using a loading rate of 300 mm/min. (12 in./min.). All specimens were tested at room temperature.

* Gauge length for these specimens was 50 mm (2.0 in.).

1 kN/m = 5.71 lbs/in.

Standard strip tensile tests (i.e., ASTM D-1682) are conducted at a strain rate of 300 to 400% per minute (59). Slower strain rates, such as 1% per minute, are more compatible with the strain rates normally used in soil testing, (29, 59). Shrestha and Bell (67), however, found that the tensile properties of geotextiles did not vary significantly between strain rates of 1¼% to 12½% per minute. They concluded that a strain rate of 10% per minute could be used for routine tensile testing.

(4) Specimen variability. The results of the uniaxial tensile tests performed by Steward, et al. (69) show that a standard deviation of up to 2.0 kN/m (11 lbs/in.) for strength and a standard deviation of up to 18% for strain may be expected in a series of tests (see Table 2.3). Shrestha and Bell (66) observed a variation of as much as 30% between the load-strain properties of specimens obtained from the same lot.

These large variations may be partially reduced through the use of large specimens, as large specimens will tend to average out the variations (5). Increasing the number of specimens tested will also increase the reliability of the mean strength obtained. Shrestha and Bell (66) recommended that at least five specimens in the warp direction and five specimens in the fill direction of each geotextile type be tested when a reliable estimate of the coefficient of variation for the geotextile in question is not available. If an estimate of the coefficient of variation is available, select the number of specimens such that at the 95% probability level, the test is within 10% of the true mean (66).

2.3.1.1 Effect of Temperature on Load-Strain Behavior

The effect of temperature on the load-strain characteristics of seven geotextiles was investigated by Calhoun (15). Grab tensile tests were performed on five woven polypropylene geotextiles, one woven vinylidene chloride geotextile, and one needlepunched polypropylene geotextile. The tests were performed in accordance with ASTM D-1682 (15). Ten specimens of each geotextile type, five in the warp and five in the fill direction, were tested at each of the following temperatures: -18°C (0°F), 23°C (73°F), 43°C (110°F), 66°C (150°F), and 82°C (180°F). Calhoun (15) found that tensile strength was not significantly affected by temperature, but that the strain at failure of all of the geotextiles tested tended to increase with increasing temperature, indicating that the modulus of the fibers was affected somewhat. The results of these grab tensile tests are presented in Table 2.4.

Calhoun (15) also performed low-temperature brittleness tests on ten specimens of each of the seven geotextile types. The tests were performed in accordance with U.S. Army specification CRD-C 570-64. An alcohol heat transfer medium was used to cool the samples. He found that none of the geotextiles were excessively brittle at -51°C (-60°F).

Information from the supplier of Mirafi 140 fabric indicates that Mirafi 140 retains 100% of its room temperature strength at -57°C

Table 2.4: Summary of grab tensile test results showing the effect of temperature and freezing and thawing on geotextile load-strain behavior (after Calhoun (15)).

Geotextile Description	Woven Monofilament Vinylidene Chloride		Woven Monofilament Polypropylene		Woven Monofilament Polypropylene		Woven Monofilament Polypropylene		Woven Mono- and Multifilament Polypropylene		Nonwoven Heat Bonded Needlepunched Polypropylene		Woven Monofilament Polypropylene	
	warp	fill	warp	fill	warp	fill	warp	fill	warp	fill	warp	fill	warp	fill
Tensile test (ASTM D-1682-64) Grab Method														
at -18°C strength, N	890	668	1690	1120	894	868	1870	1170	472	1100	174	454	783	561
Strength, % of 23°C, strength	97	132	98	98	97	97	105	107	83	107	126	98	95	84
Strain, %	16.8	26.2	23.0	23.0	18.0	15.8	16.8	24.0	9.0	24.6	10.0	31.4	16.8	8.0
23°C Strength, N	917	503	1730	1140	926	899	1780	1090	565	1030	138	463	828	668
Strain, %	22.2	27.4	22.4	26.8	23.6	16.6	17.0	24.6	10.6	26.3	11.3	40.3	23.0	10.6
43°C Strength, N	828	507	1550	1060	961	930	1850	992	619	1080	147	463	765	699
Strength, % of 23°C strength	90	101	90	93	104	103	104	91	109	105	106	100	92	105
Strain, %	23.4	33.0	25.4	25.4	23.6	17.5	21.0	26.4	16.0	25.8	8.0	41.6	22.8	12.2
66°C Strength, N	908	485	1520	1110	983	912	1930	988	663	1070	111	436	814	668
Strength, % of 23°C, strength	99	97	88	97	106	101	109	91	117	104	81	94	98	100
Strain %	25.4	31.8	25.4	29.0	19.4	24.2	23.0	27.6	20.6	28.5	7.4	38.4	25.0	11.0
82°C Strength, N	917	498	1760	1180	992	903	1880	917	672	1090	102	405	872	614
Strength, % of 23°C, strength	100	99	102	104	107	100	106	85	119	106	74	88	105	92
Strain %	28.0	32.2	26.6	35.6	21.6	23.4	28.0	32.6	23.8	30.6	8.0	41.0	28.4	112.0
Freeze-thaw (300 cycles) (CRD-C 20-69)														
Strength, N	886	481	1600	1120	952	783	1820	979	645	1100	147	423	819	694
Strength, % of 23°C, Strength	97	96	93	98	103	87	103	90	114	107	106	91	99	104
Strain, %	25.0	37.0	25.5	29.5	20.6	17.8	21.8	28.0	15.7	26	11	43.3	23.6	11.7

Note: 1 lb = 4.45 N

(-70°F). However, only 40% of the strain at room temperature was obtained for Mirafi 140 (53).

This geotextile load-strain-temperature behavior is in contrast to the behavior exhibited by the polymers of which the geotextiles are made. Figure 2.7 shows the effect of temperature on the tensile strength of polypropylene. Obviously, the tensile strength of polypropylene increases with decreasing temperature. This strength versus temperature curve was not derived for high tenacity yarns (the molecules within the polymer tested were only slightly oriented), which may in part account for this discrepancy. Also, part of this discrepancy may be due to the structure of the geotextiles. Plying and entanglement of the yarns in geotextiles may hide, at least somewhat, the effect of temperature on polymer tensile strength. However, more study is needed in this area to support these statements.

2.3.1.2 Effect of Moisture on Load-Strain Behavior

Steward, et al. (69) performed wet and dry strip tensile tests on several nonwoven geotextiles (see Table 2.3). However, they found that the inconsistency in the load-strain data precluded the establishment of any trends. The strength of some geotextiles increased upon wetting whereas for other geotextiles the strength decreased. Koerner, et al. (44) concluded that since geotextile fibers are relatively insensitive to moisture regain (polypropylene being negligible and polyester being about 0.5%), any observed effect on geotextile load-strain behavior caused by moisture was most likely

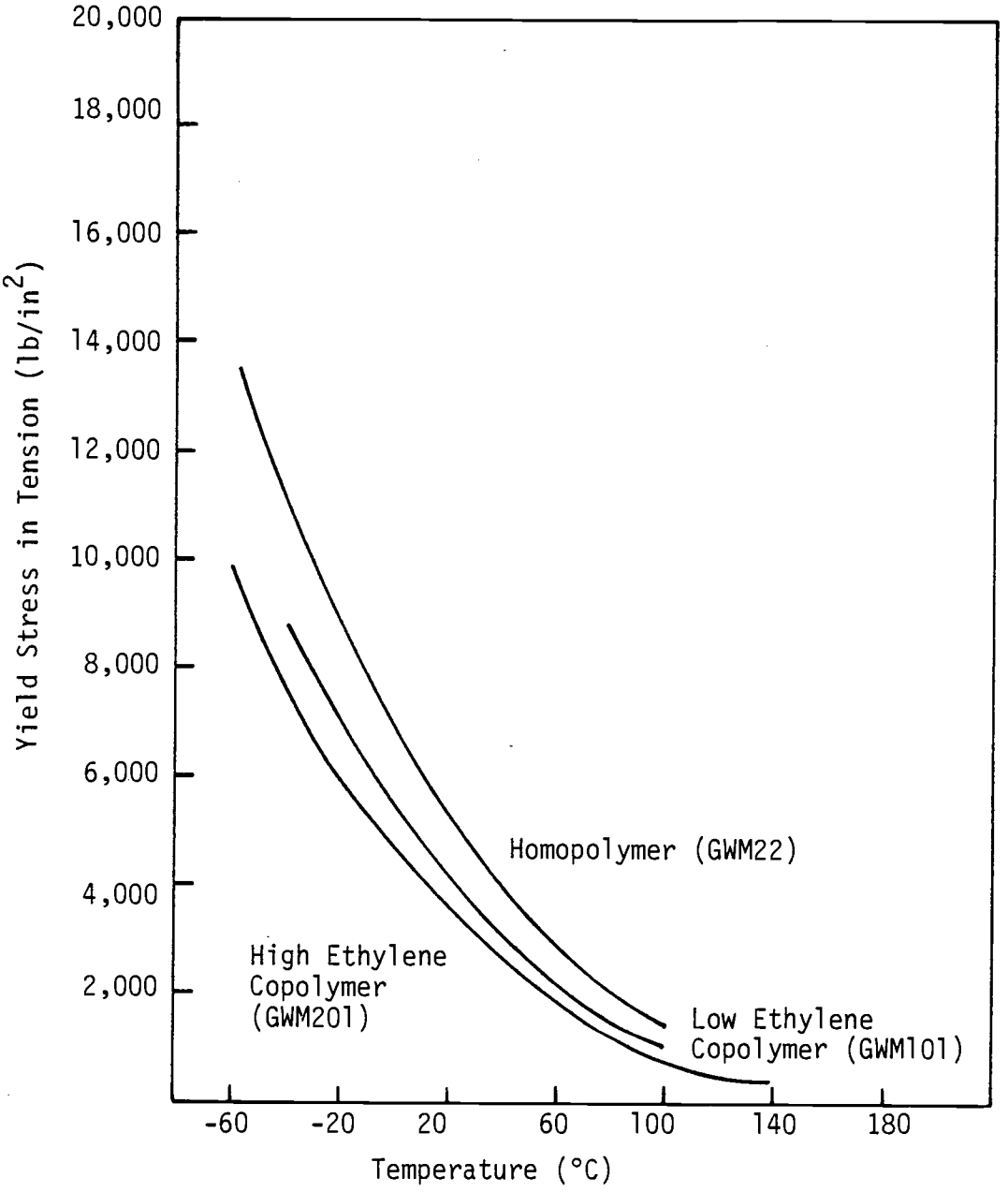

Figure 2.7: Yield stress in tension vs. temperature: 50% per minute strain rate. Propylene homo- and co-polymers ('Propathene' GWM22, GWM101, GWM201) (after Ogorkiewicz (55)).

the result of moisture affecting the geotextile bonding mechanisms.

Haliburton, et al. (29) performed uniaxial strip tensile tests on four woven geotextiles (three specimens each) after they had been immersed in artificially simulated seawater for a period of five weeks. One geotextile was a woven polyamide monofilament (Nicolon 66186), one was a woven polypropylene multifilament (Nicolon 66475), and the other two geotextiles were polypropylene monofilaments (Advance Type I and Polyfilter-X). A substantial reduction in the ultimate strength of both of the polypropylene monofilaments was noted, while the two Nicolon geotextiles showed minimal strength losses, as shown in Table 2.5 (29). The two Nicolon materials did absorb a relatively large amount of water when compared to the amount of water absorbed by the Advanced Type I and the Polyfilter-X geotextiles (29). The water contents of tne Nicolon geotextiles was probably biased on the high side, however, as a saturated-surface-dry condition could not be obtained for these two geotextiles (29). Haliburton, et al. (29) felt, though, that the amount of unblotted free water left in the Nicolon specimens could not account for the large differences in water content between the Nicolon geotextiles and the Polyfilter-X and advance Type I. They concluded that water absorption had minimal effect on ultimate tensile strength.

2.3.1.3 Effect of Freezing and Thawing on Load-Strain Behavior

Tensile tests were performed by Calhoun (15) on geotextile specimens which were subjected to 300 two hour freeze-thaw cycles in water in accordance with U.S. Army standard CRD-C 20-69. The

Table 2.5: Results of salt water immersion on tensile strength - fabric warp direction (after Haliburton, et al. (29)).

Material	Unsoaked Ultimate Strength (kN/m-width)	Soaked Ultimate Strength (kN/m-width)	Strength Loss (%)	Average Water Content[1] (%)
Nicolon 66475	158	148	6.4	20.2
Polyfilter-X	54.5	37.1	31.8	1.8
Nicolon 66186	39.6	36.3	8.4	25.7
Advance Type I	44.1	36.4	17.5	1.4

[1] water content = $\frac{\text{wet weight - dry weight}}{\text{dry weight}}$ x 100. Specimens blotted until all visible free water removed. Both Nicolon specimens had a dense weave and were difficult to blot; test data are probably high.

Note: 1 kN/m = 5.71 lbs/in.

Note: Three specimens of each geotextile type were tested.

temperature in the test was varied from -18°C to 4°C (0°F to 40°F). Ten specimens of seven geotextile types (these geotextiles are described in Section 2.3.1.1 of this report) were tested in tension. Calhoun found that none of the geotextiles tested showed significant strength losses, while some specimens even showed slight gains in strength. The results of these freeze-thaw tests are presented in Table 2.4.

2.3.1.4 Load-Strain Behavior of Geotextiles Confined in Soil

The individual fibers of geotextiles confined in soil are tightly gripped by the soil, preventing large amounts of fiber realignment during loading (69). This prevention of fiber realignment due to the confining effect of the soil could cause the modulus of the geotextile to increase.

El-Fermaoui and Nowatzki (22) investigated the effect of soil-fabric frictional characteristics and confining pressure on the load-strain characteristics of three woven geotextiles (Polyfilter-X, Mirafi 100X, and Mirafi 500X) and three nonwoven geotextiles (Mirafi 140S, Typar 3601, and Bidim C-34). They observed that substantial increases in the tensile strength of both woven and nonwoven geotextiles occurred when confined in sand and/or gravel. They also found that confining a geotextile in materials of relatively high frictional characteristics caused greater increases in geotextile tensile strength than when confined in materials of relatively low frictional characteristics (see Figure 2.8). The presence of water in the geotextile and soil caused the tensile strength of the confined geotextile to decrease, indicating that moisture tends to decrease this frictional interaction between the

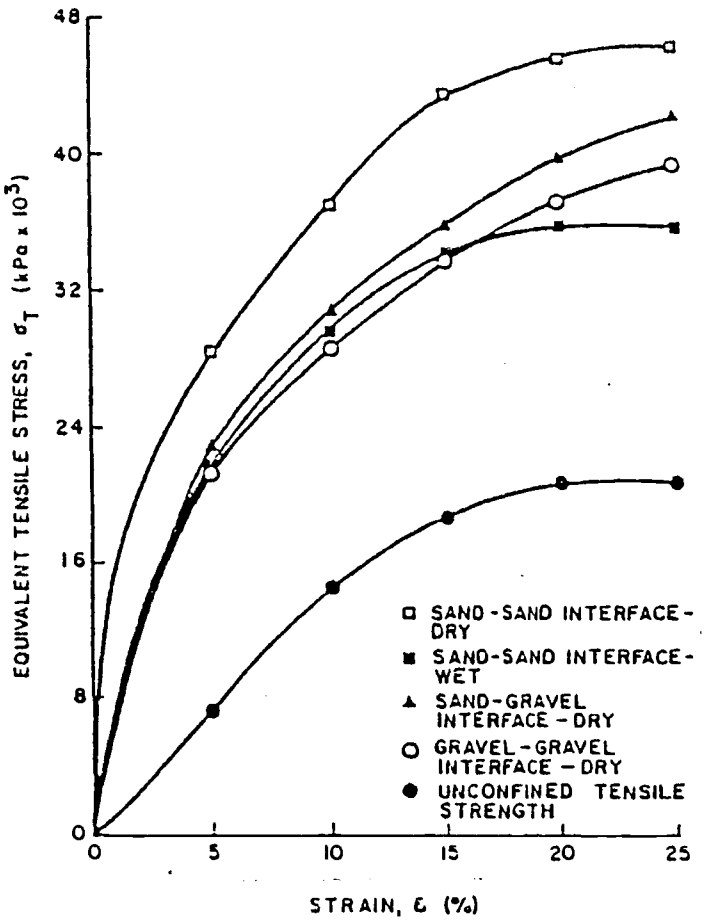

Figure 2.8: Stress vs. strain for Polyfilter-X (woven fabric) under 383.2 kPa (4 Tsf) normal stress for various combinations of cover and support materials (after El-Fermaoui and Nowatzki (22)).

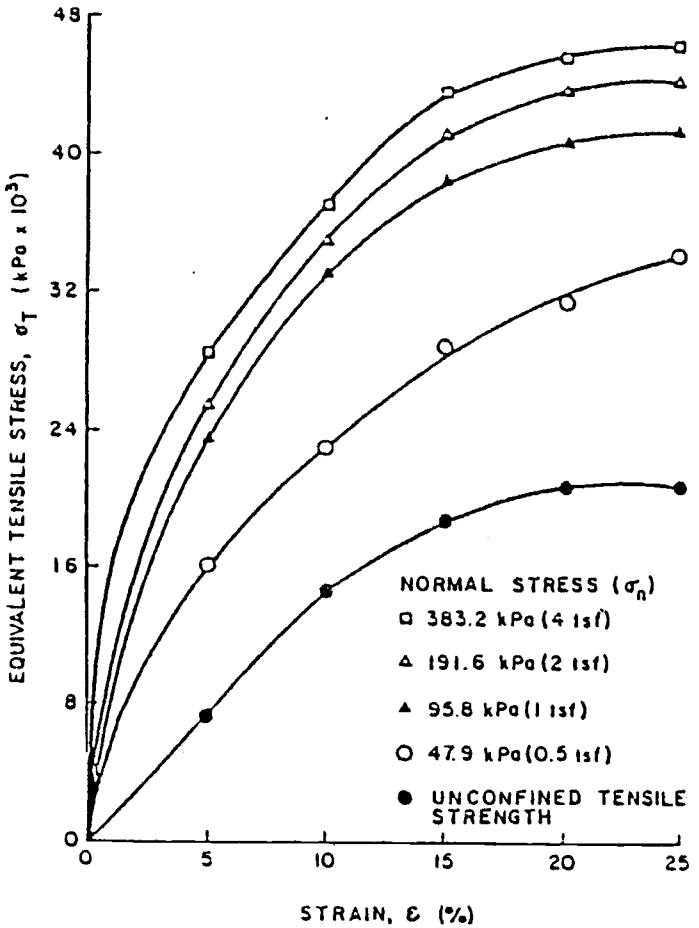

Figure 2.9: Stress vs. strain for poly-filter-X (woven fabric); support and cover material = dry #30 Ottawa sand (after El-Fermaoui and Nowatzki (22)).

geotextile and the soil (22). Increasing the confining stress also caused the tensile strength of the geotextile to increase, as shown in Figure 2.9 (22). In general, the work done by El-Fermaoui and Nowatzki (22) showed that the tensile strength of geotextiles confined in sand or gravel at a confining pressure of 95.6 kPa (1 Tsf) in a wet condition increased 50% for nonwovens to 90% for wovens over the tensile strength of geotextiles tested in isolation.

McGown, et al. (50) tested four geotextile types confined in soil. Two were nonwoven, one was woven, and one was a composite woven and nonwoven. McGown, et al. (50) noted that an increase in the moduli of the two nonwoven and one composite geotextiles occurred when those geotextiles (in a saturated condition) were subjected to an in-soil (sand) confining stress of 100 kPa (1 Tsf). The increase in the secant modulus at 20% strain for the two nonwoven and one composite geotextiles varied from only 16% to 64% (see Table 2.6). The woven geotextile (Lotrak 16/15) actually showed no increase in its secant modulus when subjected to a confining stress. McGown, et al. (50) concluded that the aligned tapes of the Lotrak 16/15 were not affected by soil confinement.

Part of the difference between the results obtained by El-Fermaoui and Nowatzki (22) and McGown, et al. (50) may be attributed to the difference in the size and aspect ratio of the specimens tested by the two groups of investigators. El-Fermaoui and Nowatzki (22) used a 50 mm by 50 mm (2 in. by 2 in.) specimen size, whereas McGown, et al. (50) used a 200 mm by 100 mm (8 in. by 4 in.) specimen size.

The effect of the specimen size on load-strain behavior of geotextiles was investigated by Shrestha and Bell (67), as described in

Table 2.6: Changes from unconfined in-isolation load-strain curves due to confinement in-soil at 100 kPa (1 Tsf) confining stress (after McGown, et al. (50)).

Measured Value	Lotrak 16/15	Terram 1000	Bidim U24	Propex 6067
Initial Slope	+8%	+78%	+270%	+254%
5% Secant Slope	+1%	+46%	+206%	+ 39%
20% Secant Slope	-1%	+16%	+ 64%	+ 16% (18% strain)

Section 2.3.1. In light of the discussion in Section 2.3.1, the 50 mm by 50 mm (2 in. by 2 in.) specimen would tend to elongate, and also neck down, more than the 200 mm by 100 mm (8 in. by 4 in.) specimen when tested in isolation. However, the confining effect of the soil would tend to restrict the specimens such that neither specimen size would exhibit necking when confined. Therefore, the confining effect of the soil would show its greatest effect on the modulus of the 50 mm by 50 mm (2 in. by 2 in.) specimen, thereby accounting for some of the differences in the results obtained by the two groups of investigators. The effect of specimen size (confined and unconfined) on geotextile load-strain behavior can be readily seen in the results obtained by McGown, et al. (50), as shown in Figure 2.10.

However, the effect of specimen size only accounts for the differences obtained for the nonwoven geotextiles, as the woven geotextiles do not neck down very much (22). Another factor which could account for the differences obtained by these two groups of investigators is that El-Fermaoui and Nowatzki (22) used a fabric pull-out test to perform their investigation whereas McGown, et al. (50) loaded the geotextile specimen in simple tension. When a geotextile specimen is tested confined in-soil using the pull-out method, the normal stress at the soil-geotextile interface may be considerably higher than the applied normal stress, as the shear stresses induced into the system by the anchor plate (see reference 22) tend to confine the soil, increasing the normal stress at the soil-geotextile interface. This increase in the normal stress would increase the confining effect of the soil on the geotextile, possibly causing the large increases in geotextile modulus due to soil confinement obtained by El-Fermaoui and

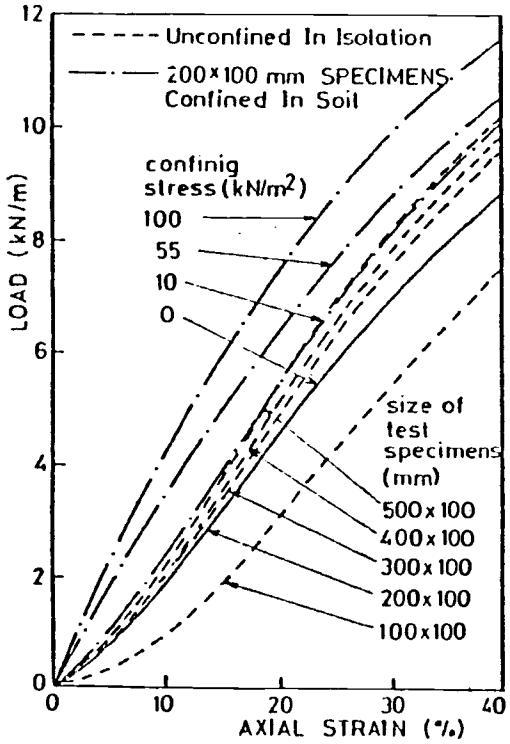

Figure 2.10: Unconfined in-isolation and confined in-soil load-axial strain data for Bidim U24 (after McGown, et al. (50)).

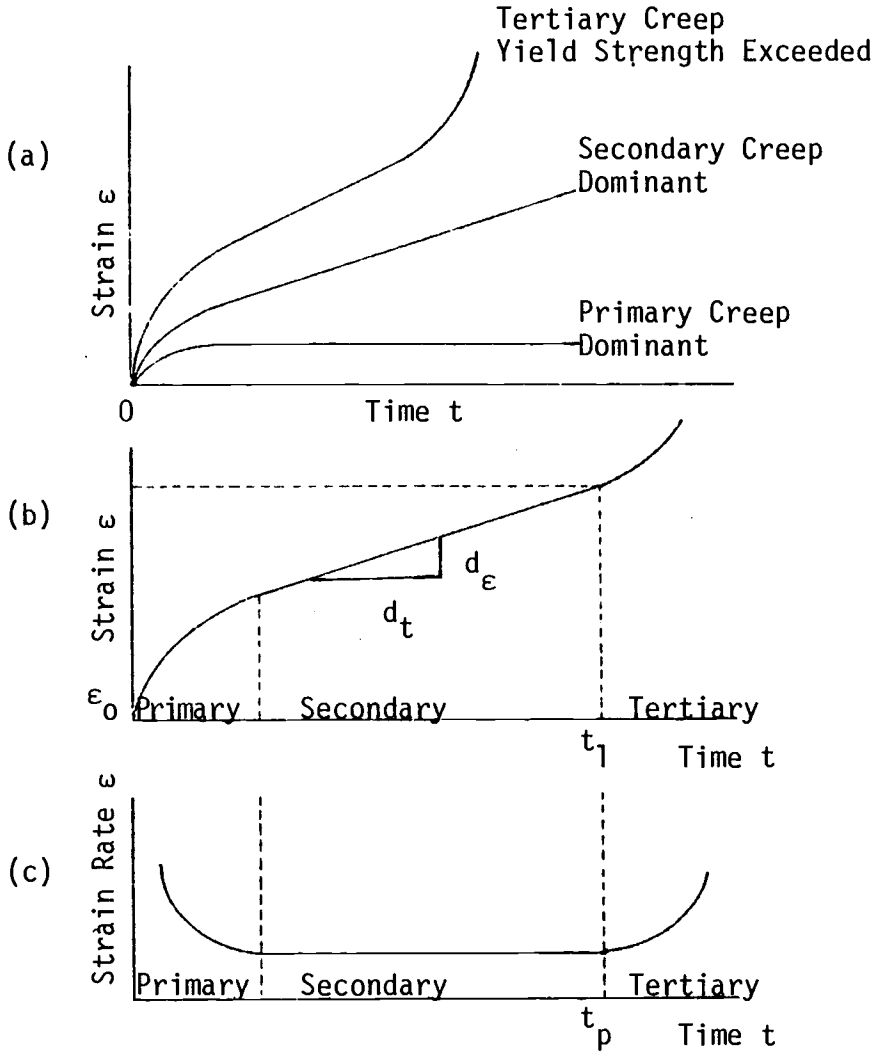

Figure 2.11: Constant-stress creep test: (a) creep curve variations: (b) basic creep curve: (c) true strain rate vs. time (after Andersland and Anderson (2)).

Nowatzki (22). In view of the testing method used by El-Fermaoui and Nowatzki (22), the results obtained by this group of investigators should be viewed with caution.

In conclusion, design strengths and moduli for geotextiles should be determined by testing the geotextiles confined in soil, if possible (50). Research on the effect of soil confinement on geotextile load-strain behavior should be continued to determine the magnitude of the modulus and strength increase due to soil confinement more accurately.

2.3.1.5 Summary

The goal of load-strain testing of geotextile specimens is to provide reliable load-strain data which can be applied accurately to the moisture, temperature, and stress conditions which exist at the construction site. Based on the literature review of geotextile load-strain behavior, the following conclusions can be made:

(1) To simulate field loading conditions (plane-strain) a specimen 200 mm (8.0 in) wide with a 100 mm (4.0 in.) gauge length should be used.

(2) The orientation of the load on the geotextile specimen is important and careful attention should be paid to the specimen orientation to obtain valid, useful results.

(3) The specimen should be loaded at a rate compatible with soil testing rates. Therefore, since the tensile properties of geotextiles do not vary significantly at strain rates of 1¼% to 12½% per minute,

the 10% per minute loading rate recommended by Shrestha and Bell (67) should be used.

(4) To account for geotextile varibility, at least five specimens of each geotextile should be tested, as recommended by Shrestha and Bell (67).

(5) Since little data on the effect of temperature on the load-strain behavior of geotextiles are available at this time, additional study in this area is needed if conclusions are to be made.

(6) Since no trends have been established on the effect of moisture on geotextile load-strain behavior, additional study in this area is needed. Further study is needed for the determination of the degradation in strength which may occur when geotextiles are subjected to salt water immersion or freeze-thaw cycles.

(7) If possible, the design strength and modulus of a geotextile should be determined by tensile testing the geotextile confined in-soil, as recommended by McGown, et al. (50). Additional study in this area is needed.

2.3.2 Geotextile Creep

In applications such as stabilization of embankments, reinforcement of earth walls, and to some extent stabilization of roads, geotextiles may be subjected to high loads for long periods of time. The time dependent load-strain behavior of a geotextile under this condition is known as "static creep" (continual strain under a constant load) (5).

In applications such as the stabilization of roads, where dead loads are typically low but live loads (due to traffic) are typically high, geotextiles may be subject to many repetitive loads. Geotextiles subjected to repetitive loads may fail due to dynamic creep (5).

2.3.2.1 Static Creep

If a geotextile is subjected to a constant tensile load of sufficient magnitude that after a period of time it ruptures, three stages of creep can be noted. If the geotextile strain under a constant load is plotted as a function of time, a curve of the form shown in Figure 2.11(b) results (2). Immediately after the load is applied, an instantaneous, elastic deformation occurs. With the passage of time, the first stage of creep, known as primary or transient creep, occurs. This primary creep is characterized by a creep rate which decreases with time (see Figure 2.11(c)). After the geotextile has gone through the first stage of creep, the second stage of creep, known as secondary creep, occurs. Secondary creep is characterized by a creep rate which is nearly constant (34). After an extended period of time, the creep rate increases and rupture occurs (25). This third stage of creep, known as tertiary creep, is a catastrophic process, possibly initiated by defects in the material itself (25).

If a geotextile is subjected to a constant tensile load which is a small to moderate percentage of its ultimate tensile strength (e.g., less than 20%), creep rupture may not occur, or at least not within the time of interest (25). Under these low stress conditions, the

geotextile may exhibit only primary creep and eventually reach equilibrium.

The amount of creep which occurs in a geotextile may vary depending upon the geotextile material and construction, and the environment in which it is placed. These factors which affect creep are discussed as follows:

(1) Geotextile Filament Material. Typically, polyester geotextiles have been observed to have creep characteristics which are superior to those of polypropylene geotextiles, considering geotextiles which are of the same weight and construction (5). Creep tests were conducted by Rhone-Poulenc-Textile Company (73) to investigate the creep characteristics of polypropylene and polyester filaments. They found that the polypropylene filament was far more susceptible to creep than the polyester filament, as shown in Figure 2.12.

A large amount of investigative work on the tensile creep characteristics of polypropylene has been performed by the plastics industry (55). Typical creep test results for a propylene homopolymer are shown in Figure 2.13. Many of the creep tests for the polyproplylene were also taken to failure, which resulted in the creep rupture versus time to failure curves shown in Figure 2.14. However, as can be seen in Figure 2.14, the stress level at which failure never occurs (or at least does not occur for a very long period of time, such as 30 years) is unknown. It has been suggested that the phenomenon of run-away creep, resulting in creep rupture (tertiary creep), is related to the yield point in conventional tensile tests (55). If a relationship between creep rupture and the conventional tensile yield point could be obtained, this critical stress level could be estimated.

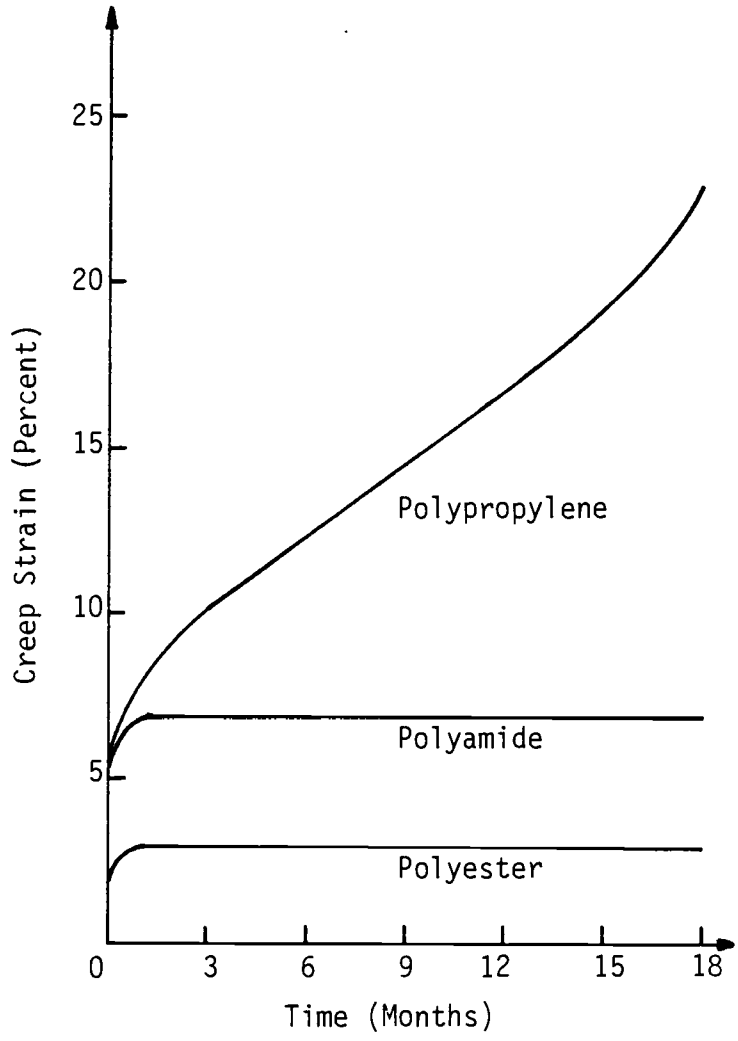

Figure 2.12: Creep curves of filaments subjected to a constant stress equal to 20% of ultimate strength (73).

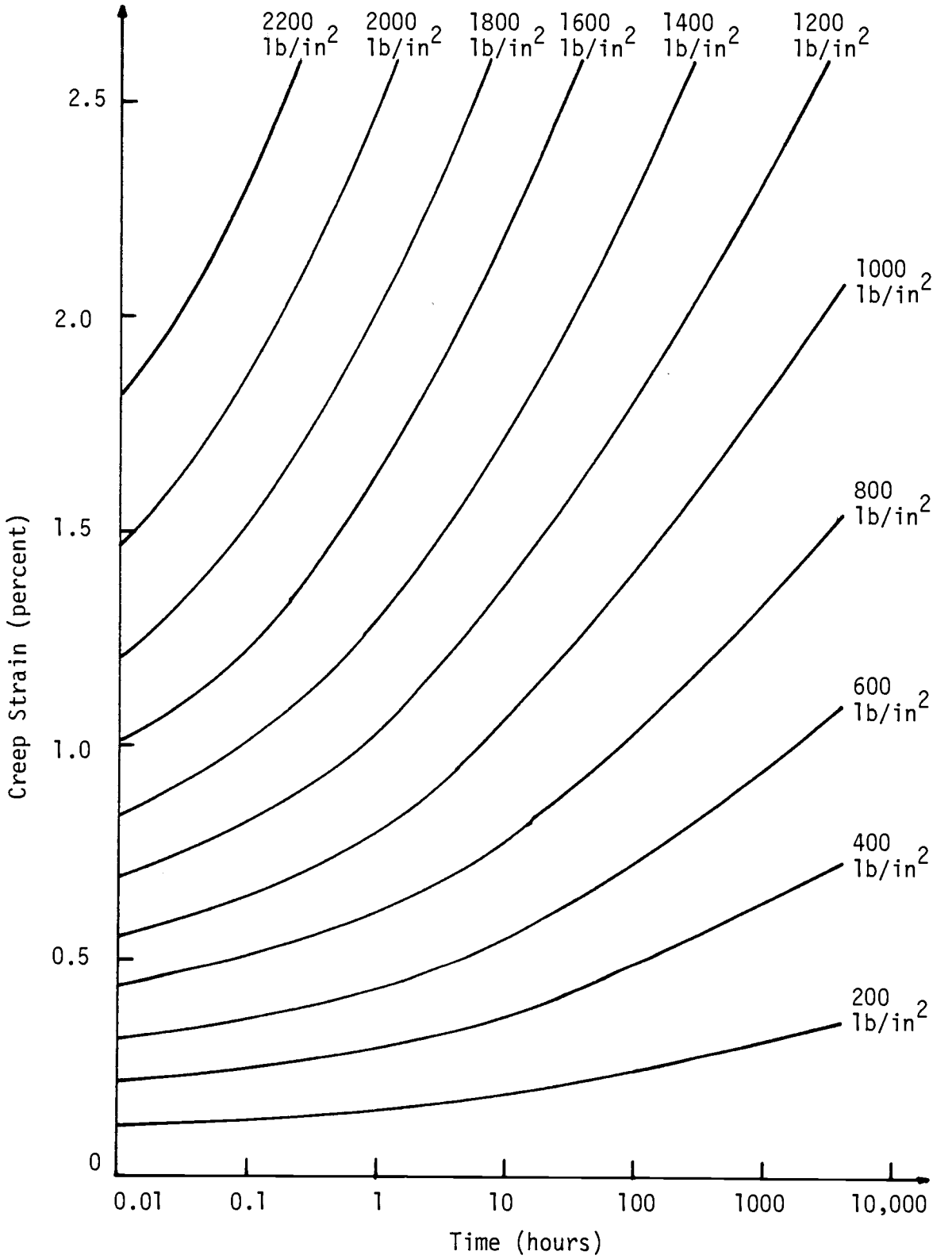

Figure 2.13: Creep curves in tension: 20°C. Propylene homopolymer, density 0.909 g/cm^3 ('Propathene' GSM 34)(after Ogorkiewicz (55)).

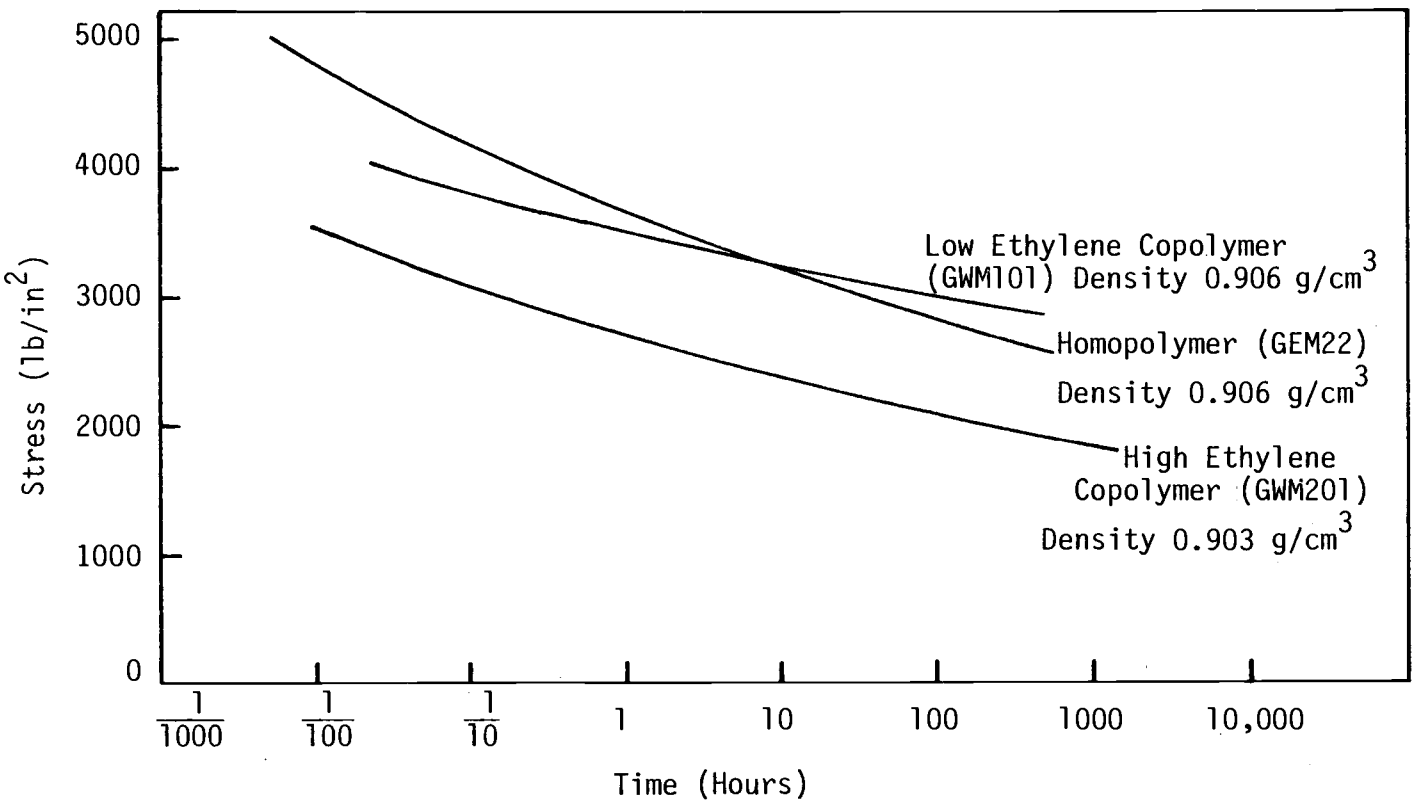

Figure 2.14: Creep rupture stress in tension vs. time to failure: 20°C Propylene homo- and co-polymers ('Propathene' GWM 22, GWM 201)(after Ogorkiewicz (55)).

Finnigan (25) performed creep tests on high tenacity polyester and polyamide yarns (1100 dtex polyester and 940 dtex polyamide). He found that the strain, when plotted as a function of the log of time, was nearly linear for up to 1000 hours, allowing the creep behavior of the yarns to be characterized by the creep rate (using log of time). Typical creep curves for the polyester yarn at various loads are shown in Figure 2.15.

Recent work has also shown that for polyester yarn loaded to less than 50% of its ultimate strength, creep rupture is unlikely to occur before 1,000,000 minutes (25). Furthermore, when either polyester or polyamide yarns are loaded to 20% of their breaking strengths, only a 1% change in length of those yarns over 10 years may be expected (25).

(2) Fiber Drawing Ratio. Finnigan (25) investigated the effect of drawing ratio on the creep characteristics of 5-fold polyester and polyamide yarns (see Section 2.4.2 for discussion of fiber drawing). He found that the creep rates of both yarns were dramatically reduced as the drawing ratio of the yarns was increased, as shown in Figure 2.16. Therefore, the amount which a filament has been "drawn" is an important creep variable.

(3) Geotextile Construction Method. In general, as the complexity of the structure of the geotextile increases, the magnitude of the creep exhibited increases (25). Therefore, lower plies and straighter warps will all reduce creep in structured items (25).

Finnigan (25) compared the effect of plying on creep of polyester and polyamide yarns with that of individual filaments. The yarns consisted of five filaments twisted together at 100 turns per meter. Polyester yarns were also woven into a fabric and compared with the

Note: The breaking load for the polyester yarn was approximately 8 kg (18 lbs).

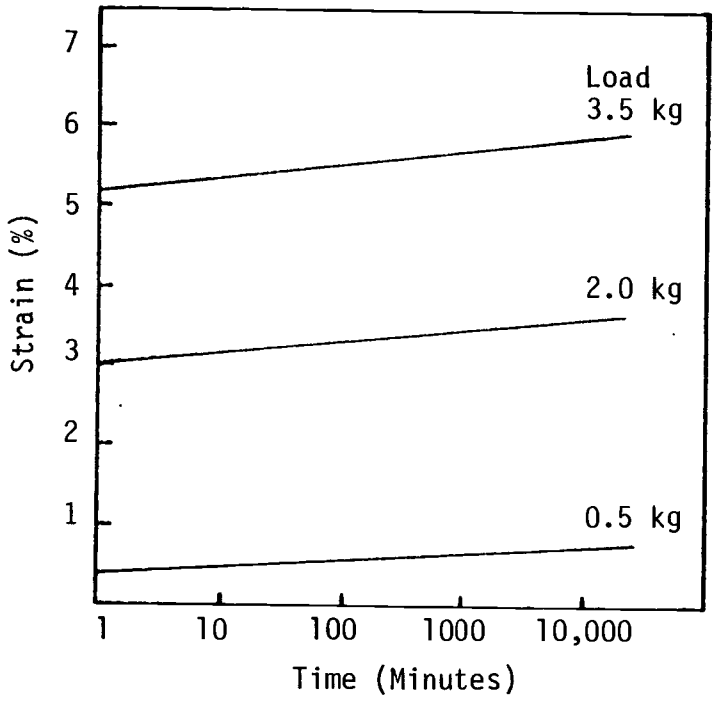

Figure 2.15: Extension of 1100 dtex high tenacity polyester vs. logarithm of time (static frame tests) (after Finnigan (25).

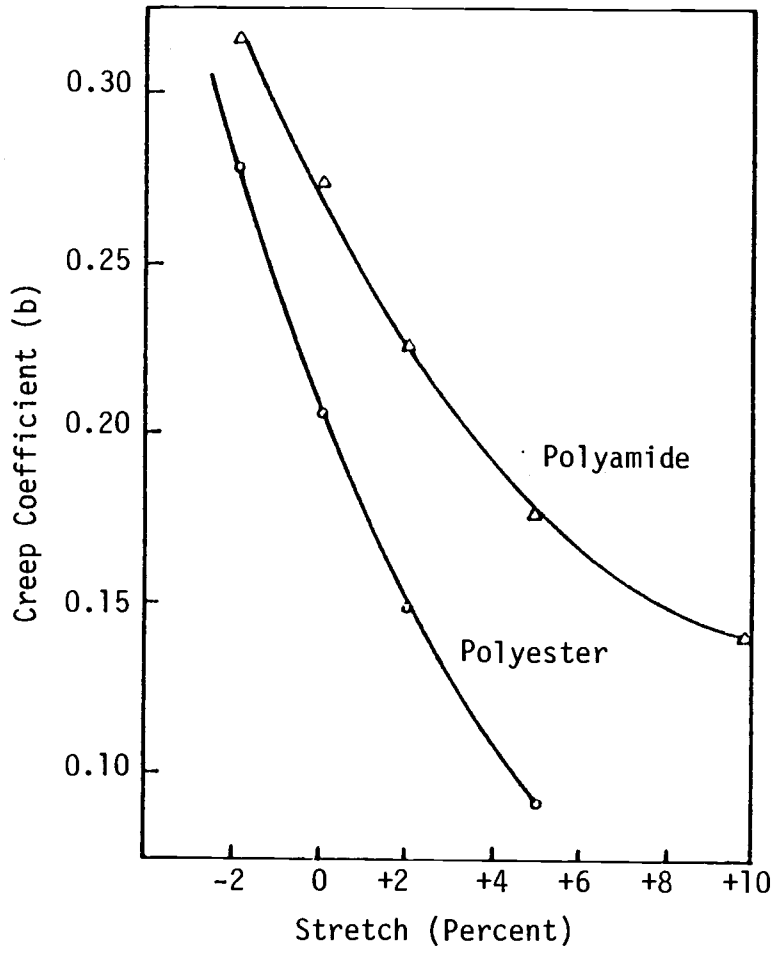

Figure 2.16: The effect of drawing ratio on the creep tendency of 5-fold polyester and polyamide yarns (after Finnigan (25)).

creep obtained with individual filaments. Finnigan found that plied yarns and woven fabrics showed slightly higher creep rate values (typically 20 to 50% higher, respectively) than did their constituent filaments (25).

Observations of creep of the various geotextile types has shown, in general, that the woven geotextiles and the bonded nonwovens exhibit less creep, all other factors being equal, than the needlepunched geotextiles (5, 73). These observations are reasonable, considering that the filaments within the needlepunched geotextiles can reorient to a greater degree under load than can the filaments within the wovens and the bonded nonwovens, as this reorientation induces an additional strain (5). Typical examples of the creep curves of various geotextile types are shown in Figure 2.17.

(4) Effect of Load on Geotextile Creep. In general, increasing the level of the load placed upon a geotextile increases the rate of geotextile creep. However, the amount of increase in creep which occurs with increasing load levels may vary depending upon the geotextile filament material and construction.

Finnigan (25) studied the effect of load on the logarithmic creep rate (slope of the primary creep curve plotted on a log of time scale) of polyester and polyamide yarns. He observed, as shown in Figure 2.18, that the creep rate of the polyester filament increased rapidly until a load level of about 25% of its breaking load was reached, where a distinct saturation in creep potential occurred. However, for the polyamide yarn the creep rate actually decreased with increasing load until the load reached 45% of its breaking load, where a minimum in

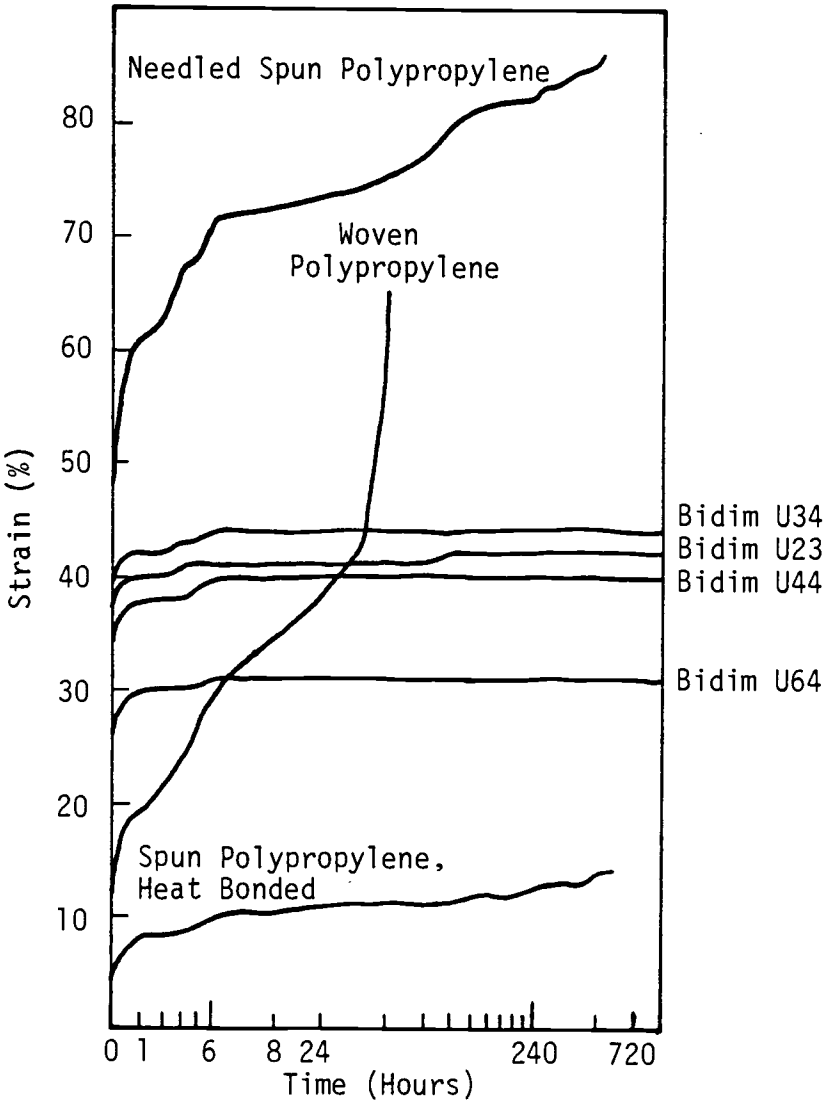

Figure 2.17: Creep of different fabrics under a load level of 40% breaking load (73).

Note: The breaking load for the polyester and the polyamide yarns was approximately 8 kg (18 lbs).

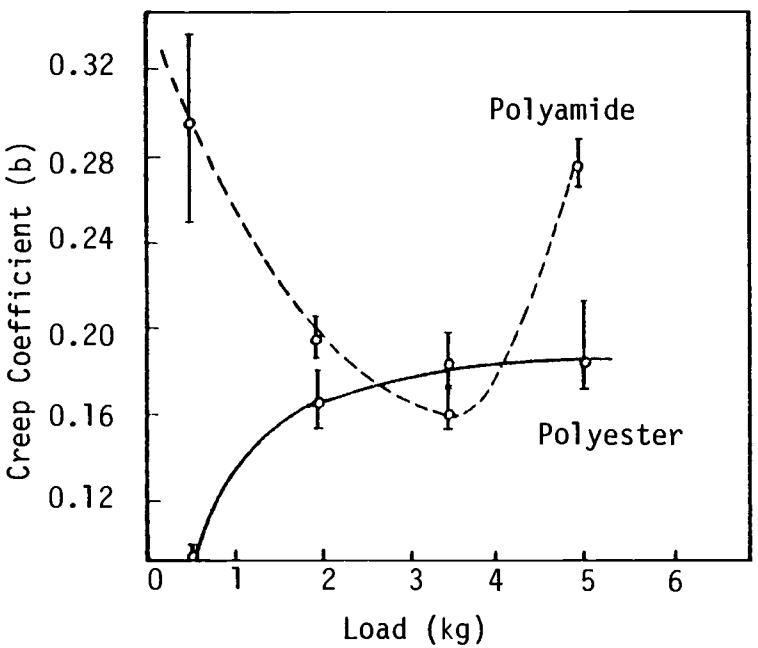

Figure 2.18: The effect of load on the rate of creep of polyester and polyamide. (The uncertainty bars represent 95% confidence limits on the mean value of b)(after Finnigan (25)).

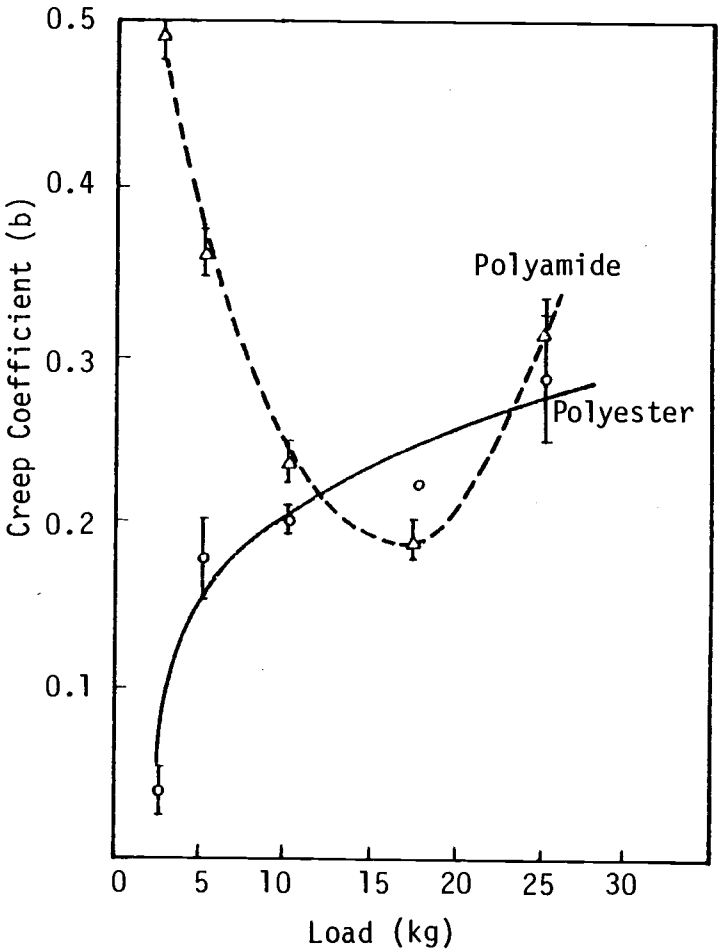

Figure 2.19: Effect of load on the creep coefficient of plied polyester and polyamide yarns (after Finnigan (25)).

creep rate was obtained (25). At load levels above 45%, the creep rate of the polyamide yarn increased rapidly (25).

Finnigan (25) also performed creep tests on 5-fold plied polyester and polyamide yarns, as well as on a fabric woven from polyester yarns. He found that the plied polyester yarns as well as the polyester fabric still showed a saturation in creep potential at around 25% of their breaking loads, though the saturation point was not as distinct as for the individual yarn. The plied polyamide yarns also showed a minimum creep rate at about 45% of the breaking load of the yarns (25). Figure 2.19 shows the effect of load level on the primary creep rate of plied polyester and polyamide yarns.

Of the various geotextile construction methods, the nonwoven geotextiles with continuous polypropylene filaments tend to show the greatest sensitivity to load levels, while the nonwoven geotextiles with staple polypropylene filaments tend to show the least sensitivity to load levels, as shown by Table 2.7 and Figures 2.20 and 2.21 (66). The woven geotextiles tend to show a moderate to high sensitivity to load levels (see Table 2.7) (66).

(5) Effect of Temperature on Geotextile Creep. The mechanical properties of all of the polymers typically used in geotextiles are sensitive to changes in temperature (5, 55). The modulus of the polymers tends to decrease as the temperature increases (5).

There are no data available on the effect of temperature on geotextile creep. However, some information is available on the effect of temperature on polymer creep. Specifically, Figure 2.22 shows the relationship between temperature and the 100 second tensile creep modulus at 0.2% strain for polypropylene at temperatures above room

TABLE 2.7: Creep of geotextiles tested by Shrestha and Bell (66).

Fabric Type	Creep measured in 20 hours			
	Stress[1] Level %	Creep %	Stress[1] Level %	Creep %
Resin bonded Continuous filaments Polyester	40	3	57	4
Heat bonded Continuous filaments Polypropylene	35	5	63	27
Needlepunched Continuous filaments Polypropylene	33	9	57	31
Needlepunched Staple filaments Polypropylene	33	20	56	22
Woven Monofilament 85% polypropylene	31	11	44	16
Woven slit film Polypropylene with Needlepunched nylon	36	5	55	8

[1] Stress level was reported as a percent of the wide strip tensile strength.

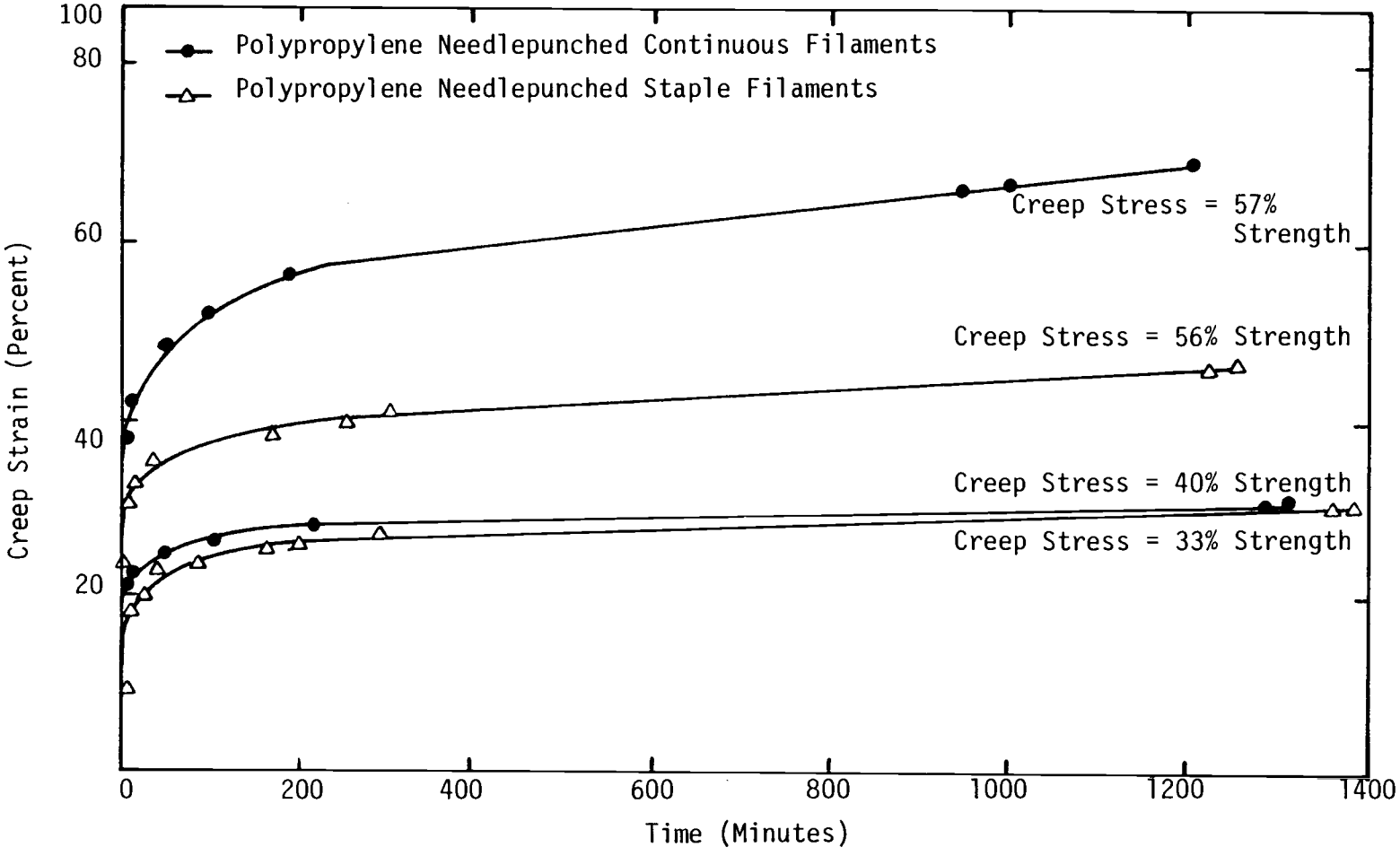

Figure 2.20: Creep strain vs. time for two polypropylene needlepunched geotextiles (after Shrestha and Bell (66)).

Note: Stress level was reported as a percent of the wide strip tensile strength.

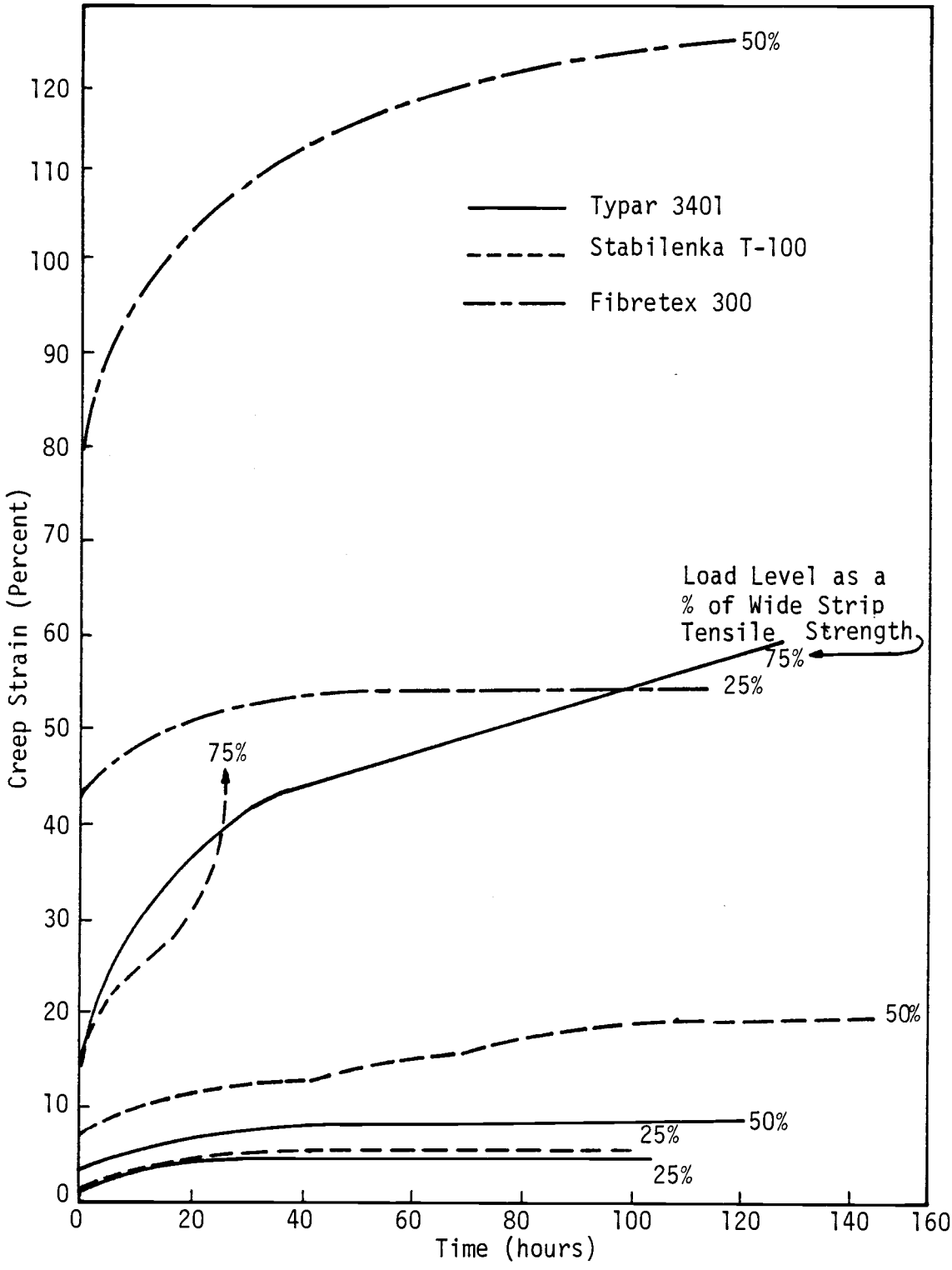

Figure 2.21: Creep strain vs. time at three load levels for three nonwoven geotextiles (74).

Note: Specimens were 5 cm (2 in.) wide by 10 cm (4 in.) long.

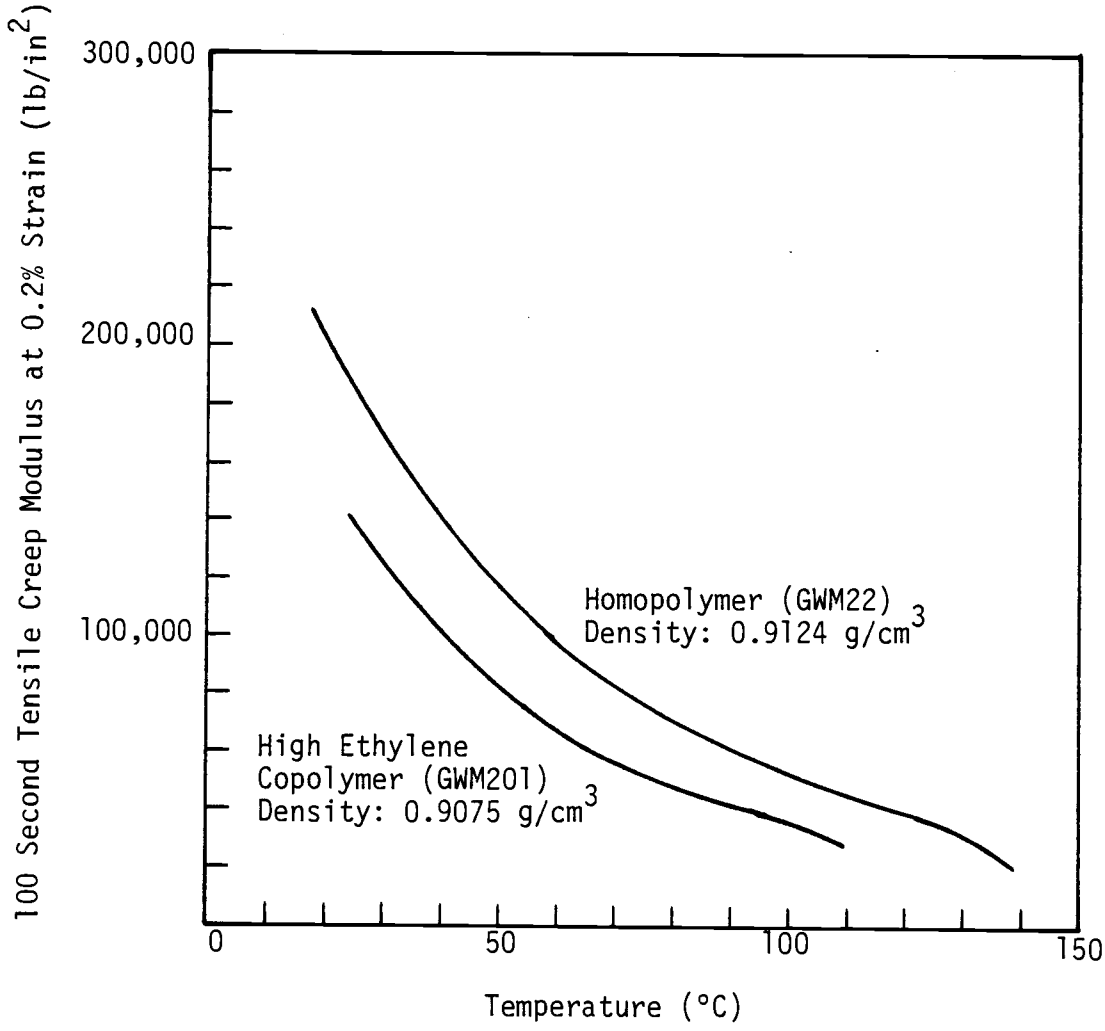

Figure 2.22: Tensile creep modulus (100 sec., 0.2% strain) vs. temperature. Propylene homo- and high ethylene copolymer ('Propathene' GWM22, GWM201) (after Ogorkiewicz (55)).

temperature. This figure shows that the tensile creep modulus for polypropylene decreases dramatically with increasing temperature. No temperature versus creep data for polyester was available.

(6) Effect of Soil Confinement on Geotextile Creep. The creep behavior of a geotextile confined in-soil (specifically sand) was observed by McGown, et al. (50) to be substantially different than that of the same geotextile tested in isolation. The primary creep strains of both of the specimens tested, Terram 1000 (Mirafi 140S) and Bidim U24, decreased 40 to 60% when confined relative to their in-isolation values, while the creep which occurred during secondary creep decreased by an even greater amount, as shown in Figure 2.23. McGown, et al. (50) subsequently concluded that unconfined in-isolation creep testing grossly overestimates the long term creep strains which would occur confined in soil.

(7) Geotextile Creep Testing Methodology. The geotextile specimen size and aspect ratio, the specimen orientation (warp, fill, or bias), and the specimen variability affect the results obtained from geotextile creep tests. The effects these factors have on geotextile creep are similar to the effects of these factors on geotextile load-strain behavior (re. Section 2.3.1).

2.3.2.2 Dynamic Creep

Live loads due to traffic may be greater than the embankment dead load for many highway embankment applications, implying that cyclic creep rather than static creep may be of major concern (28).

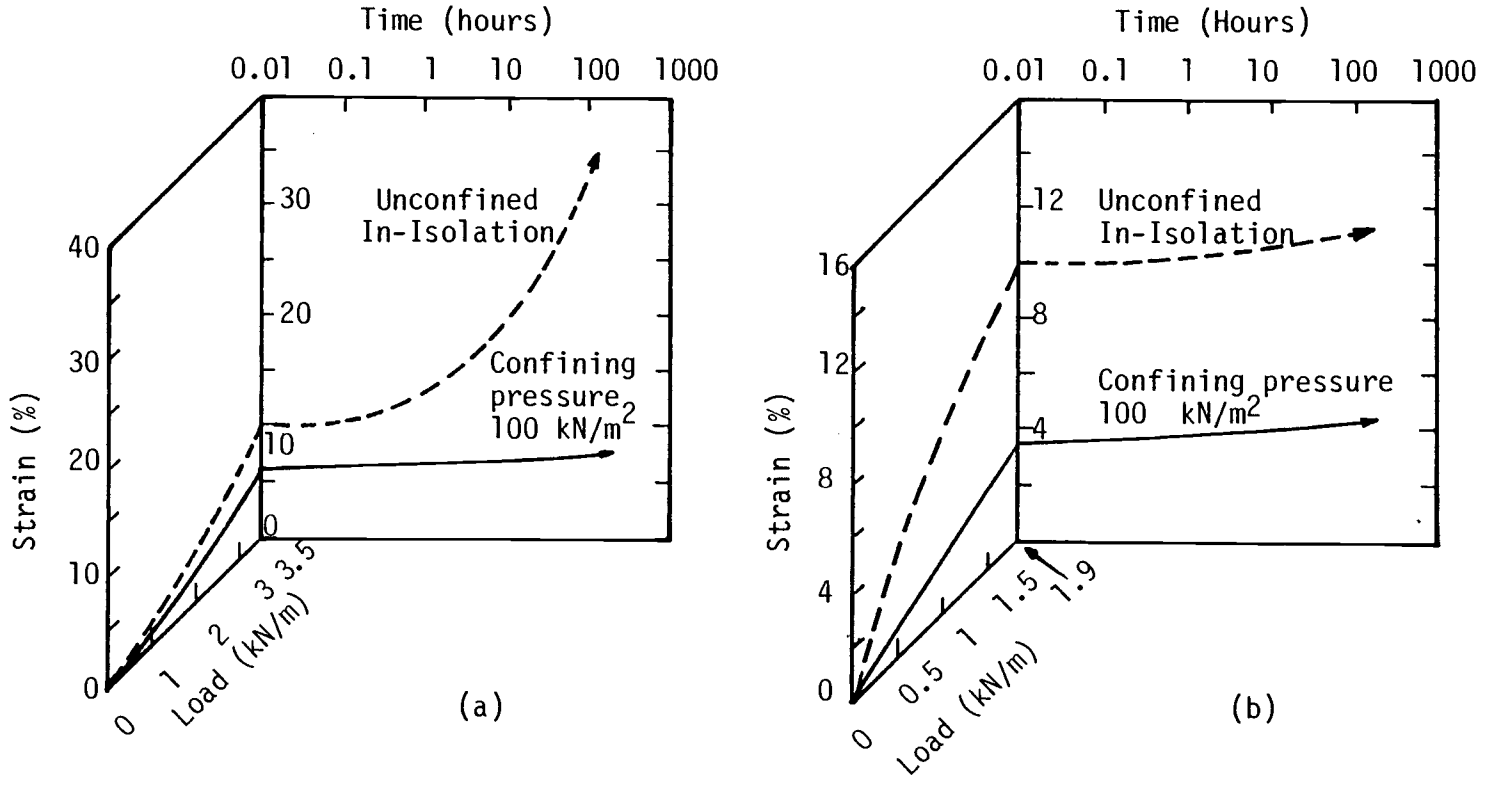

Figure 2.23: Creep test data for (a) Terram 1000 and (b) Bidim U24 (after McGown (50)).

Fatigue tests performed by Bell and Lavansiri (7) on Fibretex 400 (Fabric A) and three other nonwoven geotextiles demonstrated that the relative load to produce failure by cyclic creep ranged from 30 to 60 percent of the single application failure load. The results of these tests as reported by Greenway and Bell (28) are shown in Figure 2.24.

Figure 2.25 shows the effect of repeated loading on the modulus of Fibretex 400 (Fabric A) and Mirafi 140 (Fabric D) at various geotextile tensions. For the repeated loading curves, the geotextile modulus is a resilient modulus, which is defined as the ratio of the deviator load to the recoverable strain (7). For the single loading curves (i.e., constant rate of strain), the geotextile modulus is a secant modulus. As shown in Figure 2.25, the resilient modulus of the Fibretex was about 2.5 times the static modulus at low geotextile tension, but at high geotextile tension the two modulii were nearly equal (28, 66). Mirafi 140, however, exhibited a resilient modulus which at very low tension levels was higher than the static modulus, but at moderate tension levels the resilient modulus was lower than the static modulus. Raumann (59) reported similar variations in the results for a needled polyester and a bonded polypropylene geotextile when comparing the resilient modulus to the static modulus.

The relationship between the cyclic creep strain and the number of load repetitions for Fibretex 400 is shown in figure 2.26. This figure shows the cyclic creep of Fibretex 400 at three levels of tensile load. At a load level of 48% of the ultimate strength of the geotextile, the geotextile failed by cyclic creep at 600 load repetitions (7).

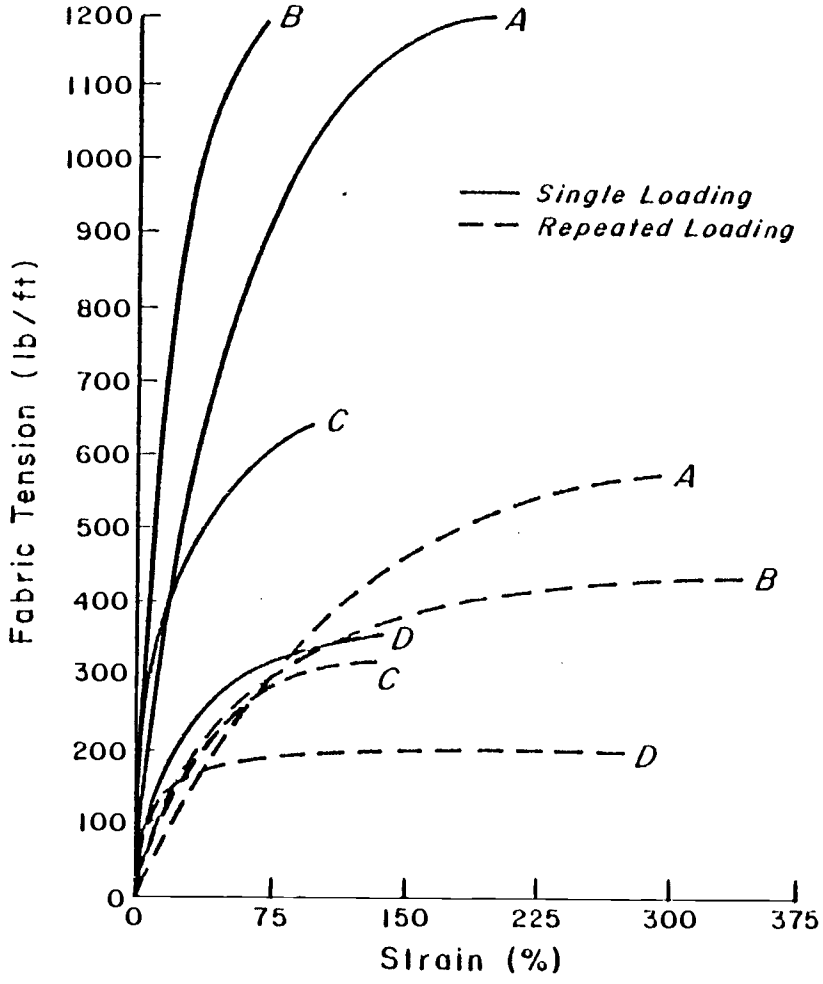

Figure 2.24: Effects of repeated loading on Geotextile load-strain relationships (after Greenway and Bell (28)).

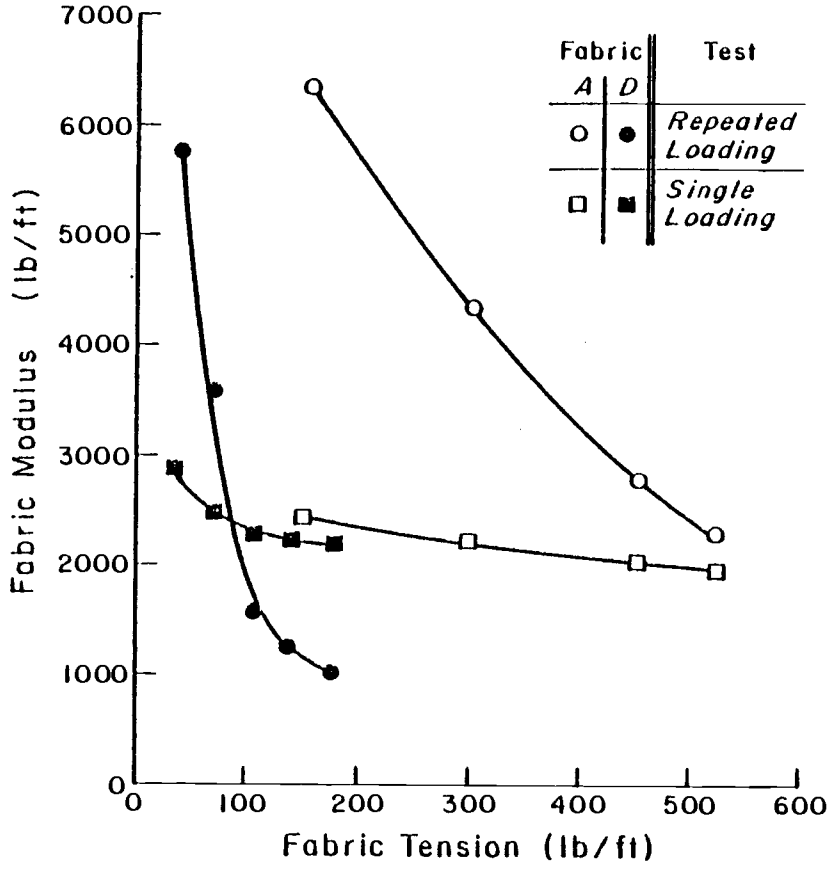

Figure 2.25: Modulus relationships for fabrics A (Fibretex 400) and D (Mirafi 140) (after Greenway and Bell (28)).

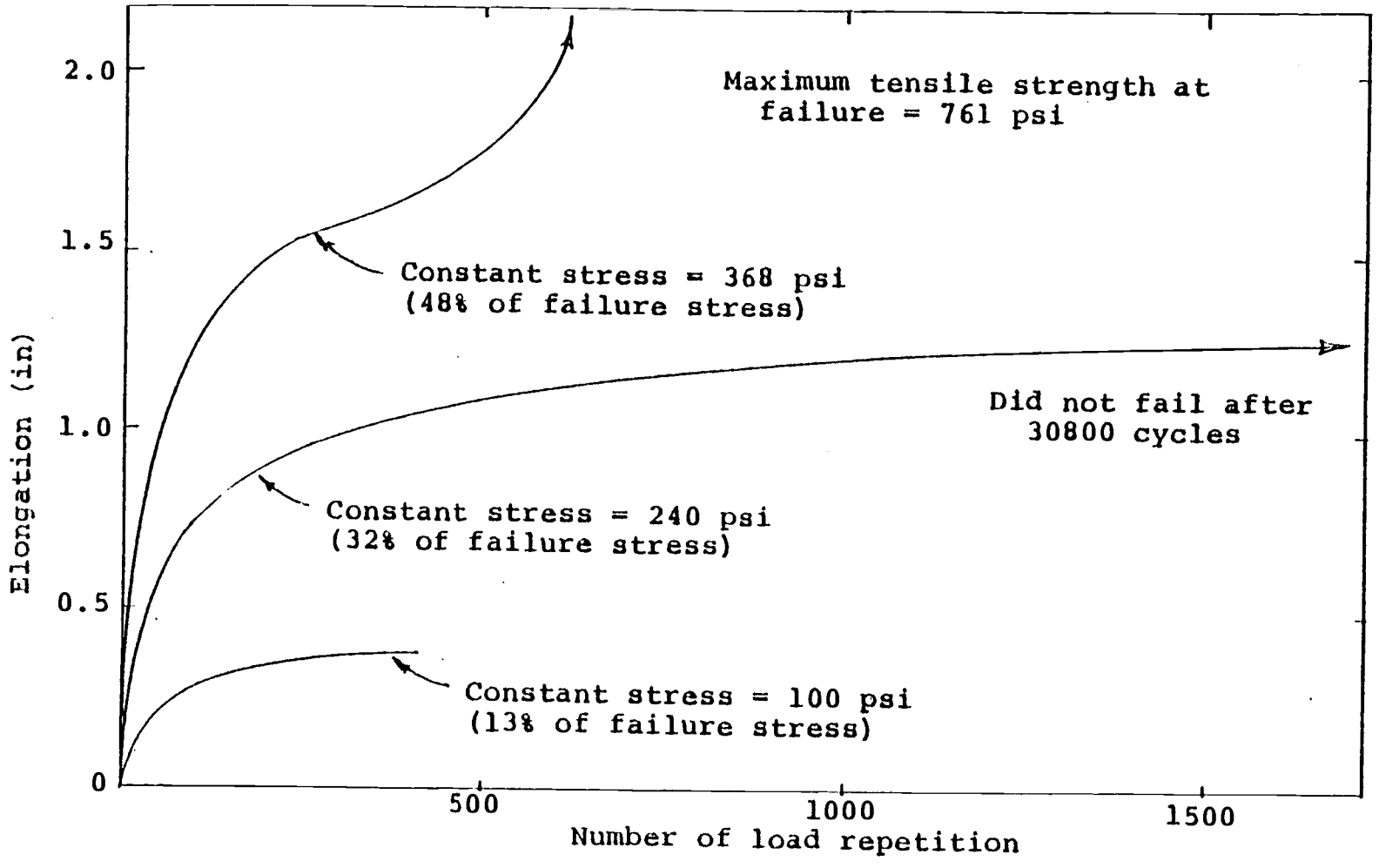

Figure 2.26 Relationship between elongation and number of load repititions for Fibretex 400 (after Bell and Lavansiri (7)).

In light of the variations observed in the dynamic behavior of the various geotextiles tested for cyclic creep thus far, definite trends cannot be summarized. Only the following conclusions can be made at this time:

1. The resilient modulus is generally greater than the static modulus, especially at low geotextile tensions.
2. Rupture due to cyclic creep at relative strengths of about 30 to 60% of the static tensile strength can be expected for many geotextiles.

2.3.2.3 Summary

As is true for geotextile load-strain testing, the goal of geotextile creep testing is to provide a reliable working load and/or strain for the geotextiles in question, considering the temperature, moisture, and stress conditions which exist at the construction site. In light of this goal, based on the literature review of geotextile creep behavior, the following may be concluded:

(1) Considering the three stages of creep (primary, secondary, and tertiary), the most critical stage of creep is most likely the secondary stage, as secondary creep always preceeds tertiary creep, and failure is inevitable once the tertiary stage of creep is reached (i.e., is there some critical load level which will always result in the occurrance of secondary creep?).

(2) When temperatures are expected to be above freezing, polyester geotextiles are likely to perform more satisfactorily than polypropylene geotextiles, as the polyester geotextiles exhibit creep

characteristics which are superior to those exhibited by polypropylene geotextiles.

(3) The filament drawing ratio has a great effect on the creep characteristics of the filament and should be taken into account during the geotextile selection (i.e., other factors being constant, geotextiles constructed of the highest tenacity filaments will have the best creep characteristics).

(4) Geotextiles of the simplest construction tend to exhibit the lowest creep strains (e.g., woven geotextiles will have lower creep strains than needlepunched geotextiles), all other factors being equal.

(5) Typically, for the same polymer, nonwoven geotextiles with continuous filaments have the greatest sensitivity in their creep characteristics to changes in load levels, while the geotextiles with staple filaments are the least sensitive. Woven geotextiles have an intermediate sensitivity to changes in load levels. However, data on the effect of load level on creep are limited, and more information is needed to verify these trends.

(6) Temperature has been demonstrated to have an effect on the creep of the polymers of which geotextiles are typically made. Creep tends to decrease rapidly with decreasing temperature for amorphous polypropylene. However, the effect of temperature on the creep characteristics of geotextiles is largely unknown, and research in this area is needed.

(7) Geotextile creep tests conducted in-isolation tend to grossly overestimate the long term creep strains which would most likely occur in the field (i.e., when the geotextile is confined in-soil). Therefore, to get a true measure of the creep which could be expected

in the field, the specimens should be tested confined in-soil. More creep data are needed to confirm the results obtained thus far.

(8) Creep tests should simulate plane-strain conditions as much as possible. The specimen size and aspect ratio recommended for tensile testing should also be used for creep testing (i.e., the specimen size should be 200mm by 100mm).

(9) Rupture due to cyclic creep at relative strengths of about 30 to 60% of the static tensile strength can be expected for many geotextiles. More research is needed to verify the results obtained thus far.

2.4 Load-Strain and Creep Behavior of Polymer Filaments at the Molecular Level

To understand and interpret the load-strain-strength and creep behavior of geotextiles which are subjected to various temperature and loading conditions, one must look at the behavior of the individual filaments at the molecular level. Therefore, background information is provided which includes a brief discussion of polymer structure, bonding energy, and the effect molecular thermal energy on molecular structure and mobility (specifically, the glass transition). A discussion of the deformation and failure mechanisms currently believed to hold true for polymers is also presented. Finally, some of the theories which are currently being used to predict deformation and failure in polymers are presented. Special emphasis is placed on polypropylene and polyester polymers in these discussions of polymer deformation and fracture.

2.4.1 Polymer Structure

A polymer is formed by the union of thousands of structural units called mers. These mers join together in a linear fashion, forming very long molecular chains. The polyethylene mer, the simplest of the vinyl polymers, is shown below (55):

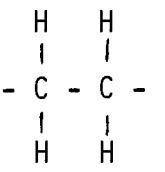

Due to thermal agitation, the ability of the C-C bond to rotate, and the great molecular length of polymers, polymeric molecules are continuously kinked and can become entangled with adjacent molecules (75).

The ability of polymeric molecules to be extended and moved past one another when under a tensile load, termed chain mobility, is restricted due to several factors (33):

(1) The C$^{\diagup C \diagdown}$C bond angle is fixed at 109.5°;

(2) The C-C bond length is also fixed, which means that chain flexibility can only arise from rotational motions about C-C bonds:

(3) Rotational motions of bonds and certain modes of molecular motion may be impeded by neighboring molecules;

(4) As the temperature falls, various types of molecular motion are progressively precluded (discussed in Section 2.4.3);

(5) The more highly crystalline a polymer, the less mobile are the individual molecules.

As the first three factors, the bond angle, bond length, and neighboring molecules, are common to all polymers, only the last two factors, temperature and crystallinity, are discussed in further detail. Since the effect of temperature on molecular mobility is discussed in Section 2.4.3, only the effect of crystallinity on molecular mobility is discussed presently.

The degree of crystallinity in a polymer is determined primarily by the molecular structure, and the thermal and mechanical history of the polymer (30, 33). The molecular structure (specifically, its packing efficiency) determines the maximum degree of crystallinity possible for the polymer (30, 33). The thermal and mechanical history of the polymer determines the actual degree of crystallinity obtained (30).

Chain packing in crystalline polymers is accomplished through repeated chain folding (33). Many of these folded molecules packed together form a flat, ribbonlike crystal called a lamellae, as depicted in Figure 2.27 (33). These ribbonlike lamellar units fan out in all directions from a nucleus, such that a spherical development is established (30). This spherical, macro-crystalline structure is called a spherulite (30). Though much of the material within the spherulite is crystalline, some amorphous material does exist between the lamellar units, as well as between the spherulites themselves (30).

As reported by Hertzberg (33), Clark (16) postulated that some disorder must exist at the lamellar fold surface due to imperfect chain folding. This imperfect chain folding would result in loose loops and chain ends which extend beyond the surface of the lamellae. Some of these disordered molecules could also extend into adjacent lamellae,

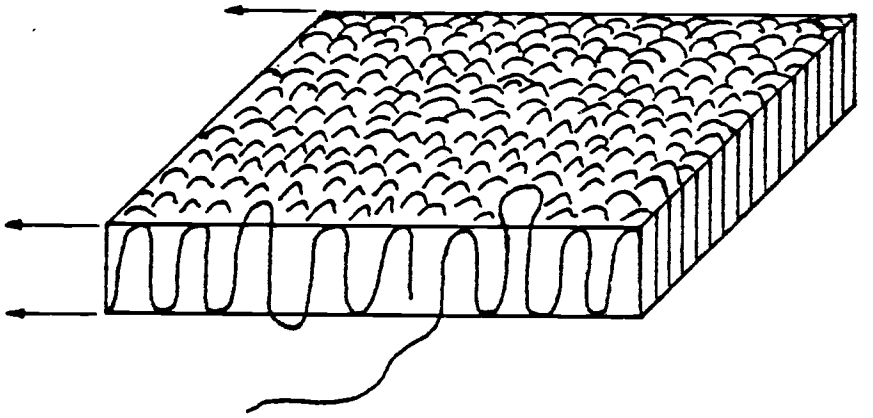

Figure 2.27: Model of part of a lamellar crystal with a folded chain structure (after Geil (26)).

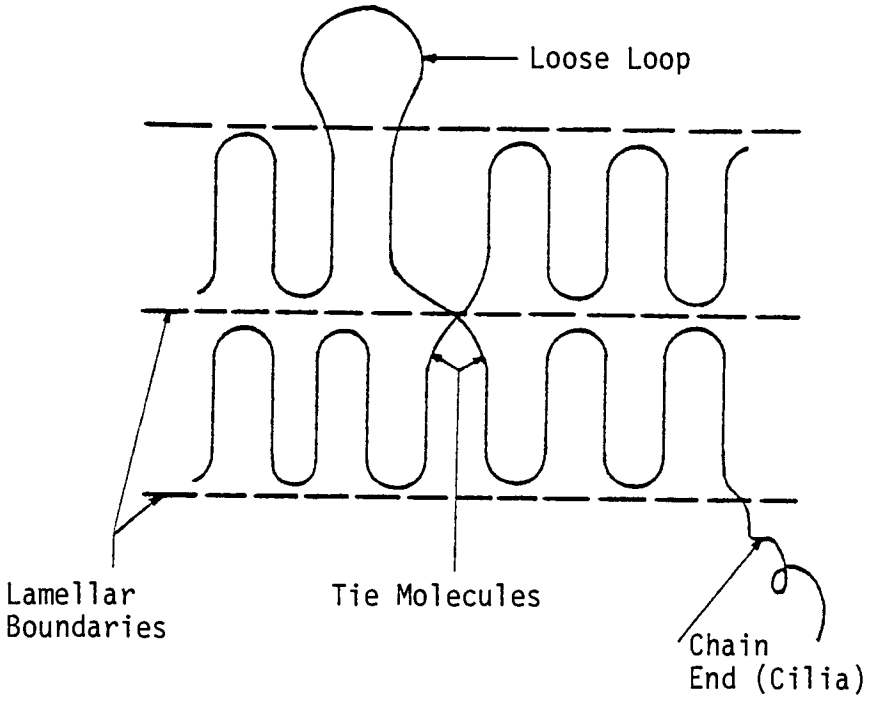

Figure 2.28: Schematic representation of lamellar chain folding with tie molecules, loose loops, and chain ends.

forming what are termed tie molecules, as shown in Figure 2.28 (30, 33). These tie molecules become very important during fiber drawing.

Also due to inefficient packing and molecular thermal vibration, voids on the order of molecular dimensions or smaller can be found within the polymeric material (23). These voids are termed the free volume (23). In order for molecules to move relative to each other, voids in the material must be present. Though the tie molecules present restrict the ability of a polymer to deform (discussed in Section 2.4.2), the amount of free volume present also restricts polymer deformation in that the free volume affects the rates of relaxation processes (23).

2.4.2 Effect of Deformation on Polymer Molecular Structure

Large deformation of a polymer solid can bring about changes in the crystalline structure of the polymer. For example, the crystalline structure of a polymer fiber can be favorably modified through a process which involves large strain deformation known as "drawing." Fiber drawing transforms the polymer morphology based on the spherulite into one based on the microfibril (30).

This morphological transformation is depicted in Figure 2.29. This transformation begins with the breaking of the lamellae into smaller blocks, with the molecular chains maintaining their folded conformation (33). As the drawing continues, these blocks become aligned in the direction of drawing, and the folded molecules become extended and oriented in the direction of drawing as well, forming microfibrils (30, 33). The tie molecules which inevitably form during

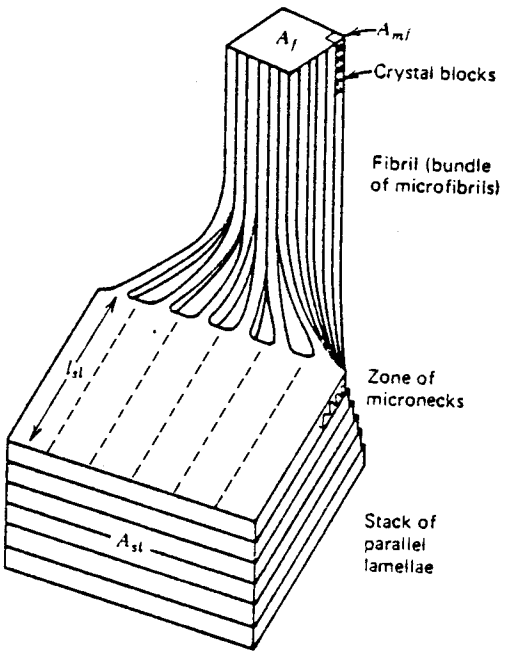

Figure 2.29: Model depicting transformation of a stack of parallel lamellae into a bundle of densely packed and aligned microfibrils (after Peterlin (58)).

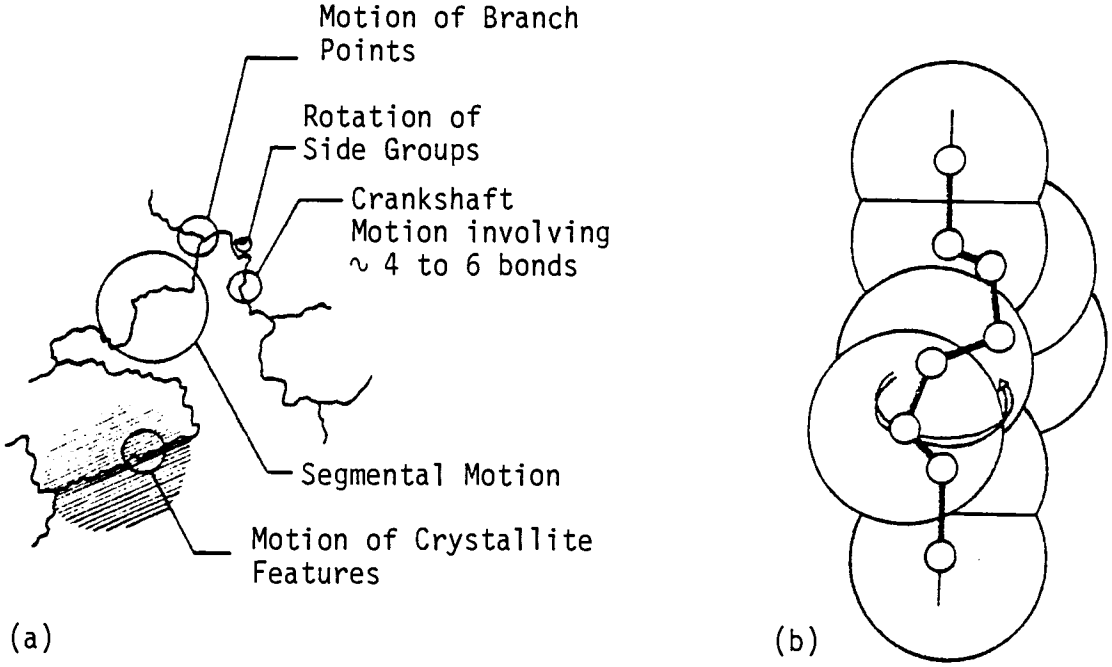

Figure 2.30: (a) Various types of molecular and microstructural motion. (b) Crankshaft motion in a linear chain, illustrated by a short segment of a polyethylene chain comprising eight backbone carbon atoms (after Hall (30)).

the unfolding of chains from the original lamellae, as well as the tie molecules already existing between lamellae, become fully extended (30). Due the many fully extended tie molecules and the oriented bundles of molecules obtained during this drawing process, the load is borne by the primary covalent bonds within the molecules rather than the weak van der Waals forces between the molecules (33).

Since the energy needed to break a covalent bond in a polymer is about 80 Kcal/mole, and the energy to break a van der Waals bond is about 5 to 10 Kcal/mole, the strength of the polymer is significantly improved due to drawing (10, 33). Creep resistance of a polymer is also significantly improved due to drawing as covalent bonds hold atoms very tightly together and do not reform with other adjacent atoms once they are broken (10, 19). However, van der Waals forces hold atoms or molecules together very loosely and can reform with another atom or molecule after the bond is broken (10, 20). Therefore, for polymers in which the load is borne by covalent bonds, little creep can be expected. Polymers in which the load is borne by van der Waals forces, however, tend to creep a great deal under load, as the molecules within the polymer can move relative to each other by stretching, breaking, and reforming the van der Waals bonds.

This oriented, polymer molecular structure can be "frozen in" if the fiber is drawn at a temperature well above the glass transition temperature (discussed in Section 2.4.3) of the polymer and is subsequently quenched to a temperature well below the temperature at which the fiber was drawn (33).

The degree of orientation "frozen" into the drawn polymer fiber may vary depending upon the amount which the fiber is drawn, termed the

drawing ratio (27). Therefore, the creep that a particular polymer fiber exhibits depends upon its drawing ratio. This variation in creep with the polymer drawing ratio supports the results obtained by Finnigan (see Figure 2.16) (25).

2.4.3 Effect of Temperature on Polymer Strength and Creep Characteristics at the Molecular Level

At absolute zero (0°K), a polymer has so little thermal energy that the atoms within the polymer are stationary (30). As the temperature rises, thermal energy is distributed between all of the possible modes of molecular motion (30). These modes are illustrated in Figure 2.30. The different modes of motion, however, require different amounts of energy to become activated (30). Therefore, there is a threshold temperature required for the activation of each mode of motion (30). Experimentally, these threshold temperatures can be detected as transitions in certain physical parameters (30).

One such transition, the principal or primary one which is observed, is the glass transition (30). At temperatures below the glass transition temperature, Tg, a polymer behaves as a glassy, elastic solid because molecular mobility is very low (1). Only a few molecular modes of motion are possible below Tg. Tie molecules are firmly entangled, allowing little deformation to take place upon the application of a load (21).

At temperatures above Tg more extensive deformation can take place because more molecular modes of motion are available (1). At these temperatures the molecular chains are wriggling about from one conformation to another, and even their centers of gravity can wonder at random (slow self-diffusion of entire chain molecules) (1). A tensile stress imposed on these chains causes this random motion to be biased in a direction parallel to the stress, leading to stretching of the macroscopic specimen (1). Tie molecules are also held more loosely at temperatures above Tg because of the increase in free volume with temperature which occurs above Tg, allowing deformation to occur with greater ease (21).

Tg is primarily determined by the chemical composition of a polymer and is relatively insensitive to molecular architecture (e.g., molecular chain length, branching, and crosslinking) (1). However, two chemically different polymers can be compared at "corresponding temperatures" (i.e., at temperatures which bear the same relation to the glass transition temperatures of the individual polymers). At these "corresponding temperatures," the two chemically different polymers in question will exhibit similar viscoelastic properties (1). This principle is known as the "Principle of Corresponding States" (1). For example, Tg of polypropylene is approximately 0°C (32°F)(39), and Tg of polyester is approximately 110°C (230°F)(27). Given the principle of corresponding states, the viscoelastic properties of polypropylene at -10°C (14°F) will be similar to those of polyester at 100°C (212°F).

The degree of crystallinity and/or orientation in a polymer also has an effect on the transition in viscoelastic properties which occurs

at Tg. In highly crystalline materials, as well as materials with high crosslink densities (or entanglements, as would be the case in a drawn fiber), the glass transition may become less pronounced (62). Changes in polymer viscoelastic response with temperature in general may be less pronounced (62).

2.4.4 Prediction of Polymer Viscoelastic Response to Load

The majority of the theories available for the prediction of the viscoelastic response of polymers to load only apply to linearly viscoelastic materials (i.e., materials which exhibit linear, time-dependent behavior) (30). These theories are based on a time-temperature correspondence, this correspondence allowing mechanical properties of a specimen obtained at high temperatures and short times to be directly related to the mechanical properties which would be obtained at lower temperatures and longer times (30). This correspondance implies that the various molecular motions which control the viscoelastic properties of the material in question all have the same temperature dependence (30). Due to this implication, time-temperature correspondence is only applicable to amorphous polymers (amorphous polymers exhibit linear viscoelastic behavior) (30).

Unfortunately, semicrystalline, as well as oriented polymers, exhibit nonlinear viscoelastic behavior (30). Owing to this nonlinear behavior, the theories based on time-temperature equivalence are not applicable to semicrystalline and oriented polymers (30).

One theory which has been applied to many processes involving the time-dependent rearrangement of matter (e.g., creep) is the Absolute

Rate Process Theory. This theory has been applied successfully to materials such as soil, asphalt, textile fibers, and even geotextiles (54, 32, 17, 66). Shrestha and Bell (66) applied the Rate Process Theory to six geotextile types and found that for those six geotextiles, the Rate Process Theory adequately modeled the observed creep behavior of the geotextiles. However, they also concluded that more work was needed to ascertain the effectiveness of this model for geotextiles.

The basis of the Rate Process Theory is that the atoms and molecules participating in a deformation process are constrained from movement relative to each other due to the energy barriers which separate equilibrium positions (54). When an external force is applied to those atoms and molecules, energy is added to the system causing the energy barrier height to become distorted, as shown in Figure 2.31 (a) (34). If the energy added to the system is great enough to cause the atoms, molecules, or aggregates of molecules known as flow units to become "activated," flow of the material occurs (32). These flow units are depicted in Figure 2.31(b).

The creep exhibited by a geotextile can be analyzed through the use of Burger's four element rheological model (66). Burger's rheological model is shown in Figure 2.32. The Rate Process Theory is used to determine the constants for the viscous elements. Through the use of this theory, each viscous element can be represented by two constants, K and α, in which K is the rate of flow of the dashpot and is expressed in reciprocal seconds, and the constant α is the resistance of the element to external force and has the units of reciprocal stress (66). Through these two constants, K and α, the non-linearity of the

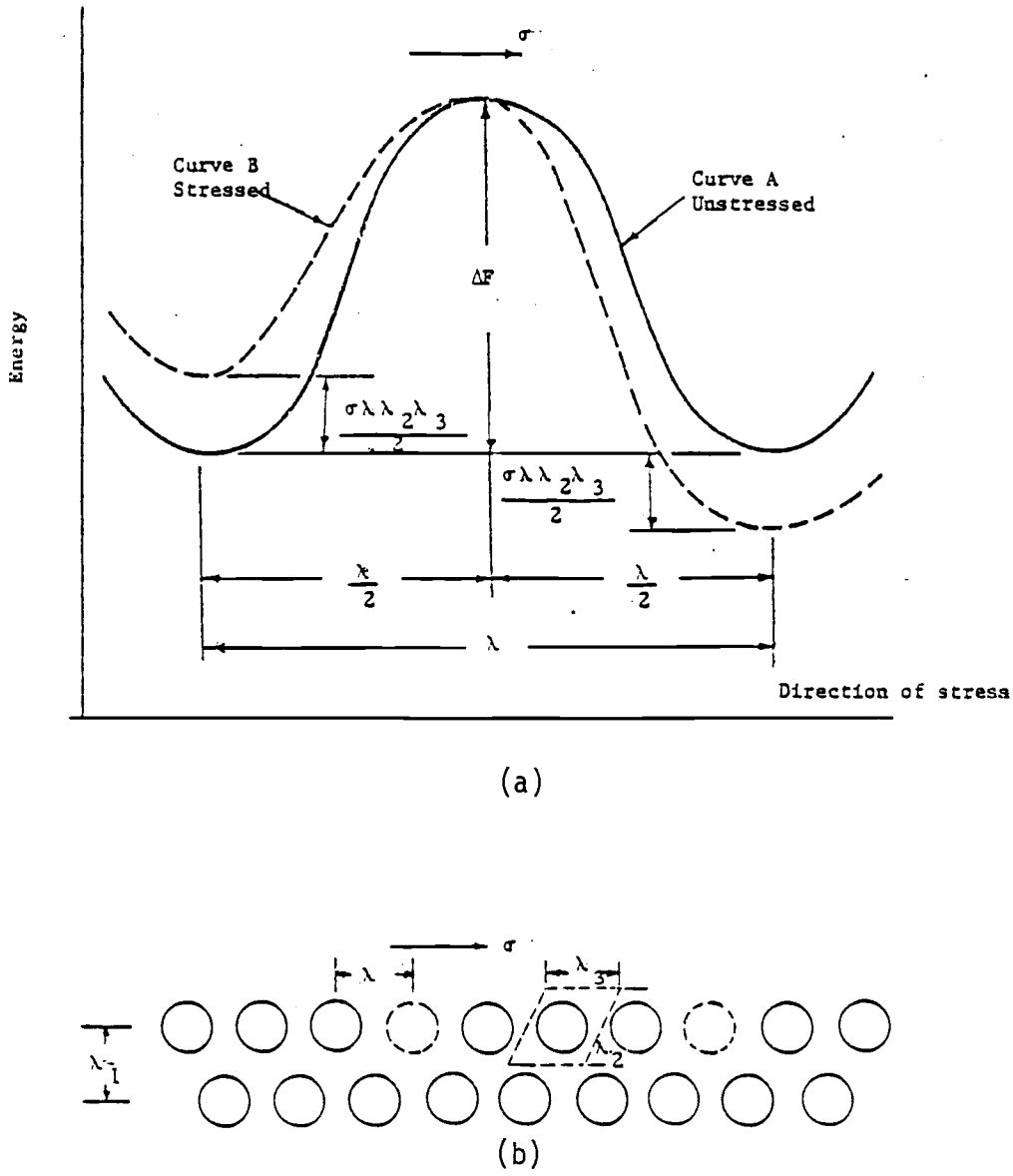

Figure 2.31: (a) Energy barriers for strain with and without external applied stress. (b) Distance that flow units move in the direction of strain and disances between flow units (after Hogan (34)).

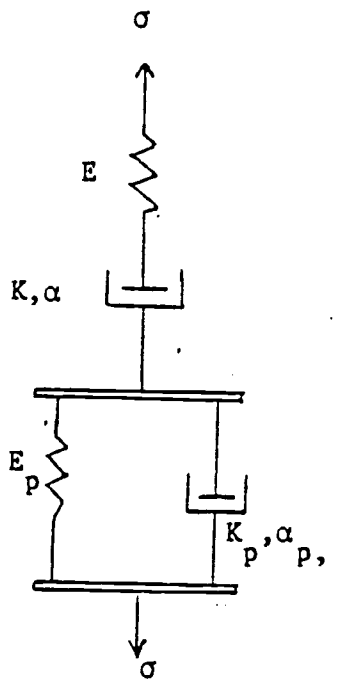

Figure 2.32: Burger's rheological model (after Hogan (34)).

viscous elements can be represented (66). The constant for each spring, E, can be determined from experimental results. The method of obtaining the constraints for Burger's rheological model using the Rate Process Theory is presented in Appendix C.

Given the creep versus time relationships for a given material at two or three load levels, the creep versus time relationship at other load levels can be predicted through this application of the Rate Process Theory to Burger's rheological model (66). A theoretical relationship between the creep rate and temperature can also be obtained from the Rate Process Theory, as described in Appendix C.

The onset of tertiary creep and failure by rupture cannot be predicted through the use of the Rate Process Theory and Burger's model by themselves. This problem of predicting when, and under what load, a material will fail is discussed in the following paragraphs.

2.4.5 The Prediction of Failure of Crystalline and Oriented Polymers

The theoretical strength of a material can be calculated from its molecular composition and structure (10). However, the strength obtained in the laboratory for a material typically is much lower than its theoretical value (10). In general, a material will fail prematurely due to local stress concentrations caused by flaws in the material (10). These flaws typically are molecular in size and take the form of loops, entanglements, loose ends, holes, density domains, and cross-link bunches (21). Unfortunately, the local stress at a flaw depends critically on the details of the flaw geometry, which is usually unknown (10). The theoretical strength of the material at the

tip of the flaw may also change with time as deformation proceeds, if structural changes are likely to occur there (10). These structural changes are especially likely to occur as deformation becomes large, as is the case when creep is a concern (10). The prediction of the failure of a polymer at the molecular level is very difficult.

Because of these difficulties, few theories have been developed to predict failure in polymers. Scientists disagree as to whether or not the few theories which have been made are useful or even valid.

Scientists do agree, however, that a theory of ultimate mechanical properties can only be obtained through a better understanding of the phenomenon known as crazing in terms of structure and its dependence on stress, time, and temperature (10).

A craze is a highly ordered, localized region of plastic deformation (38). It is similar in shape to a crack, and the plane of the craze is at right angles to the stress axis (38). The formation of crazes always occurs in amorphous polymers just prior to failure and is considered a phase of failure (52). Cracks usually form in semicrystalline polymers (e.g., polypropylene) instead of crazes prior to failure; however, cracks can be considered equivalent to crazes for the semicrystalline polymers (52).

Scientists do not agree on the conditions which cause crazes or cracks to form. For example, Menges (52) postulated that crazes will only form after certain threshold values of strain are exceeded. He further stated that this threshold value of strain was independent of the state of stress, load type (static, cyclic, or intermittent), and environmental conditions (temperature and the surrounding medium) as long as the structure of the material itself doesn't change. Menges

(52) also postulated that this threshold value of strain was valid for crack formation without crazing.

However, Sauer, et al. (10, 65) suggested that since craze size is a function of both time and stress, the details of its growth would be expected to be a function of the test temperature and the rate of loading. Therefore, the strain at failure would be expected to vary depending on the temperature, the stress level, and the rate of loading (10).

If a threshold value of strain could be established for a given material, the Rate Process Theory could be used to determine when the critical value of strain would be reached, allowing creep rupture to be predicted. Obviously, though, more study in this area is needed before failure can be predicted in this manner.

Another approach to predicting the failure of a polymer is to establish a failure envelope by determining a number of experimentally well-defined pairs of failure stresses and elongations (21). Though this approach works quite well for amorphous polymers, the failure envelope for semicrystalline and for oriented polymers tends to be different at different temperatures or different strain rates due to the non-linear viscoelastic behavior of these polymers (21, 30). Therefore, the establishment of a single failure envelope based on stresses and strains at failure for a given polymer fiber (or geotextile) may not be possible.

2.4.6 Summary

The following summary can be made about the deformational behavior of polymers at the molecular level:

(1) Since the amount which a polymer filament has been drawn directly affects the molecular structure in the fiber, and since changes in molecular structure affect the load-strain and creep behavior of the polymer filament, the drawing ratio of the filament in question must be considered when evaluating the filament (and therefore the geotextile) creep behavior.

(2) The glass transition temperature of a given polymer is important in that the deformational behavior of the polymer can radically change in the vicinity of this temperature.

(3) At "corresponding temperatures" (i.e., at temperatures which bear the same relation to the glass transition temperatures of the individual polymers) two chemically different polymers can be compared. At these corresponding temperatures, the two polymers will exhibit similar viscoelastic properties.

(4) The Rate Process Theory can be used to predict the creep behavior of materials which exhibit non-linear viscoelastic flow. These materials include geotextiles, though more work must be done to ascertain the effectiveness of this theory for geotextiles.

(5) There is little agreement at this time on a method to predict the occurrence of failure in a polymer. The effect of temperature and the rate of loading on the strain at rupture and the minimum stress

level (relative to the yield stress) required to cause rupture is presently unknown.

(6) If a critical strain level could be established for a particular polymer, or ultimately a geotextile, the Rate Process Theory could be used to determine when that critical strain would be attained. If a critical strain level cannot be established, the only alternative may be to predict when a given allowable creep strain might be reached when subject to a given sustained static stress, as suggested by Shrestha and Bell (66).

3.0 LITERATURE REVIEW ON THE USE OF GEOTEXTILES TO PREVENT FROST HEAVE

Recently, research has been conducted to investigate the ability of a geotextile layer to perform as a capillary break during the freezing of a frost-susceptible soil. However, most of this work has been restricted to laboratory testing. The only known field installations of geotextiles used as a capillary break were those reported by Hoover, et al. (37), Andersson (3), and Brantman, et al. (12).

This chapter reviews the previous research conducted to evaluate the ability of a geotextile layer to prevent frost heave. To understand how geotextiles can prevent, or at least reduce frost heave, a discussion of the factors important in frost heave must be made. Therefore, this chapter begins with a discussion of these factors. Following the discussion on the frost heave mechanisms, the methods used, to date, to prevent or reduce frost heave are presented. Finally, a summary of the laboratory and field investigations conducted to investigate the possible use of geotextiles to prevent frost heave is presented.

3.1 Frost Heave Factors

Segregated ice lenses, which form in frost susceptible soils, account for most of the volume increase which occurs during frost heaving. Ice lenses also account for the extremely high water contents found during the spring thaw in soils which experienced frost heave. During the spring thaw, ice lenses melt from the top down, and the

melting water is prevented from escaping due to the still frozen soil layers below. This trapped water causes the soil shear strength to become very low, resulting in what is termed "thaw instability."

The formation of ice lenses results from the interaction of three frost action factors (57):

(1) Below freezing soil temperature. The soil temperature and, therefore, the porewater temperature, must be below freezing if ice lenses are to form.

(2) A nearby water supply. Water sources (e.g., from the groundwater table, infiltration, or water held within the voids of the soil) must be available at the freezing front if ice lenses are to grow.

(3) A frost-susceptible soil. Only certain soils exhibit frost heave. The soil properties which are of the greatest importance to the frost heave phenomena appear to be the size of the pores and the diameter of the channels between pores. The pores and the channels between the pores must be large enough to allow water to flow freely to the freezing front, but they must be small enough to allow surface tension effects to occur, allowing the supercooling of pore water to occur. Typically, a frost-susceptible soil contains many silt sized particles. When supercooled porewater freezes, energy is released which is used for the development of heaving pressure and the creation of a suction gradient (57). Water is drawn to the freezing front due to this suction gradient.

If these frost action factors, freezing soil temperature, a water supply, and a frost-susceptible soil, are not acting simultaneously, frost heave will not occur.

3.2 Methods Used to Alleviate the Frost Heave Problem

The methods typically used to alleviate problems associated with frost heave attempt to control one or more of the frost action factors. Some methods are more effective than others in controlling these frost action factors. Some methods are also much more expensive than other methods. A summary of these methods (except for the capillary break method, which is discussed in Section 3.3) follows:

(1) Removal of the frost-susceptible soil and/or thickening of the pavement to preclude frost penetration into the frost-susceptible subgrade. The soil can be replaced to a depth such that no frost penetration into the subgrade occurs, or to a depth where only "adverse heaving" is prevented (78). As this method is quite expensive, the degree of effectiveness of this method depends upon how deep the soil can be economically replaced.

(2) Strengthening of the pavement structure to withstand thaw instability. This method does not prevent frost heave during the winter months.

(3) Installation of drainage systems. This method may be used alone, or in combination with methods "1" or "2". The main purpose of a drainage system is to lower the water table such that little water, if any, can migrate to the freezing front, thereby reducing or preventing frost heave (61). McGaw (49) found that if the depth of the water table below the freezing front was at least 2.4 m (8.0 ft.), frost heaving could be stopped. This method can be very expensive.

(4) Thermal barriers. Thermal barriers such as polystyrene boards control the thermal regime in the subgrade. The thermal barrier would, in effect, insulate the subgrade, preventing or reducing frost penetration into the subgrade. Unfortunately, differential surface icing between insulated and uninsulated sections of roadways has caused some safety problems which have not been resolved as yet (61).

(5) Chemical additives to modify soil hydraulic characteristics. This method controls the flow of water to the freezing front by changing the adsorption characteristics of the soil grains, making them hydrophobic (11). The chemical used in this method is called TBC (4-tert-butylcatechol) (11). This method has not completely stopped frost heave, however.

(6) Chemical additives to lower the freezing point of the void fluid. Salt may be mixed into the soil to lower the freezing point of the soil water (61). This method prevents frost heave as long as the temperature does not become so low that the salty pore water freezes (61). The main disadvantage of this method is that the soluble salts are removed by leaching (61).

(7) Cementing agents to stabilize frost-susceptible soil. Cementing agents such as portland cement, bitumen, lime, and lime-flyash may be used to chemically stabilize frost-susceptible soil (61). All of these cementing agents have been used successfully, though the cost of these agents can be exorbitant (61).

(8) Membrane encapsulation of roadbed soils. In this method the flow of water to the subgrade is controlled by encapsulating the subgrade soil to the desired depth with a waterproof barrier such as neoprene-coated nylon fabric (64). However, construction difficulties

such as puncturing of the barrier and obtaining a soil water content below the optimum water content have reduced the effectiveness of this method (61).

In summary, all of the methods used to prevent or reduce frost heave have drawbacks. These methods are either expensive, do not effectively stop frost heave, or are difficult to apply in the field. Therefore, new, inexpensive methods which are effective in preventing frost heave should be sought.

3.3 Use of a Capillary Barrier to Prevent Frost Heave

The use of a capillary barrier to prevent water migration to the freezing front has been proposed for many decades (46). Typically, this capillary barrier consisted of a layer of sand or gravel, the thickness of which depended on the capillarity of the cutoff material (4, 61). The presence of the capillary barrier allowed low quality, frost-susceptible material from the subgrade to be employed as backfill on the sand layer (60).

Capillary barriers consisting of a sand layer have been successfully used in some provinces of Canada (4). Taivainen (70) reported that sand layers have also been successfully used in Finland.

Rengmark (60) reported that sand capillary barriers have been used successfully in Sweden as well. In particular, a test road section was constructed in 1950 on a national highway in Sweden in which a sand layer 20 cm (7.9 in.) in thickness was used as a capillary break (60). The cross section of this test road is shown in Figure 3.1. Rengmark (60) stated that the road test section exhibited no frost damage during

its first twelve years of service, indicating that the sand layer completely cut off capillary flow to the freezing front. Rengmark (60) also stated that some capillary cut-off layers employed in other roads in Sweden failed when water percolated from the side ditches into the sand layer. Due to this problem, Rengmark (60) concluded that the sand layer should be placed at a level which is above the bottom of the side ditch. He also stated that in light of these failures, capillary cut-off layers should only be used on low volume roads.

A sand or gravel layer placed in frost-susceptible soil prevents the movement of capillary water to the freezing front owing to its low capillary conductivity. If the air-filled voids within the sand or gravel layer are so large that the layer cannot be bridged by capillarity, movement of capillary water to the freezing front is essentially stopped (63).

A capillary transmission barrier which employs an impervious material such as clay or asphalt treated felt has been used in Canada (4) and in Sweden (60), respectively. This type of barrier cuts off the flow of moisture to the freezing front whether in liquid form or in vapor form (46). However, this impervious barrier also trapped infiltration water from the surface, forming a perched water table near the frost line - a problem which has contributed to the scant use of such layers (61).

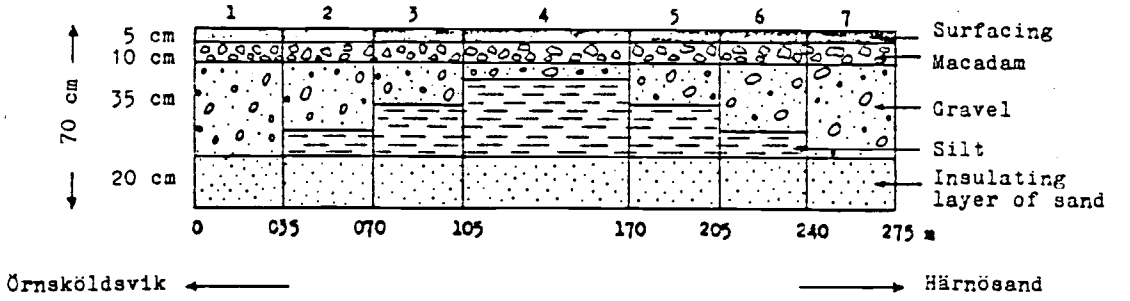

Figure 3.1 Cross section of the test road at Bjästa, Sweden (after Rengmark (60).

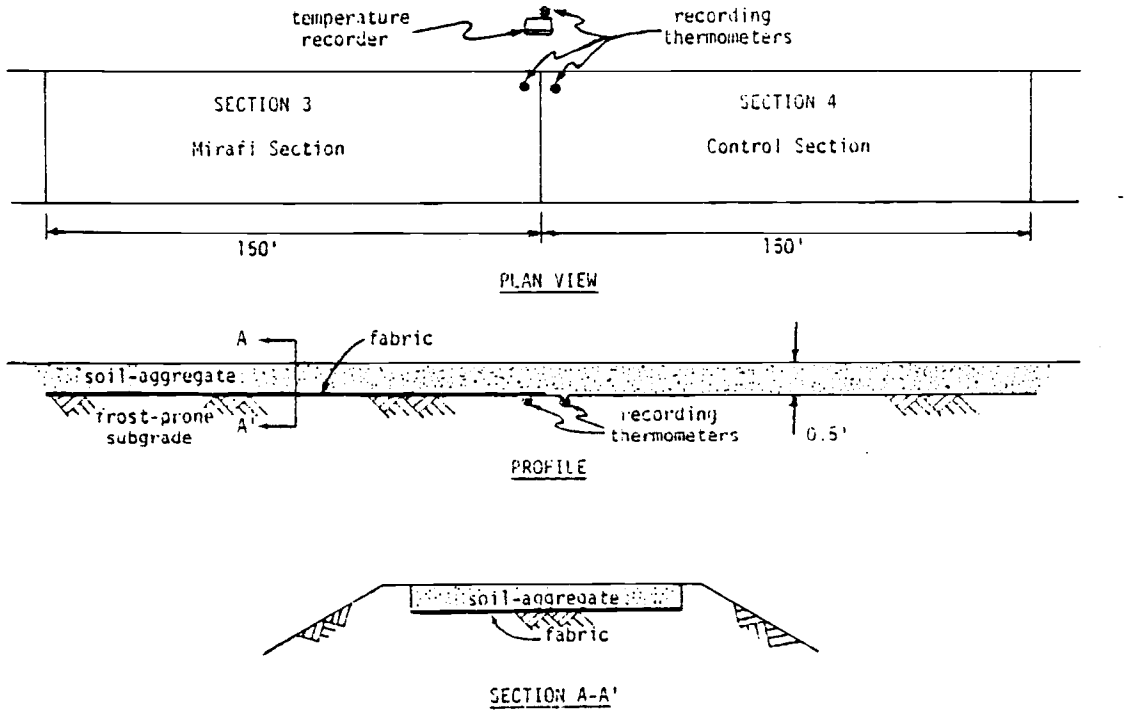

Figure 3.2: Mirafi fabric test sections 3 and 4 at Alburnett, Iowa (after Hoover, et al. (37)).

Geotextile layers have only recently been employed as capillary cut-off layers (3, 12, 37). A geotextile layer has as an advantage that the material of which it is made (e.g., polypropylene or polyester) is hydrophobic, making the capillary conductivity of the geotextile layer much lower than that of a soil layer (37).

3.3.1 Previous Field Studies of Geotextiles Used as a Capillary Barrier

Hoover, et al. (37) conducted field studies using only a geotextile layer (Mirafi 140) as a capillary barrier. These field studies were conducted on county roads in Linn County, Iowa. They found that 20 months after construction, limited moisture-density stability within the subgrade was obtained owing to the presence of a Mirafi 140 layer on top of the frost-susceptible road subgrade. A cross section of the successful test section is shown in Figure 3.2.

Andersson (3) reported the use of the geotextile Terram, (i.e., Mirafi 140) as a protective layer over a frost-susceptible subgrade in a test pit near the Stockholm Domestic Airport. He concluded that the geotextile layer had little effect on the road pavement system, at least in terms of deflection characteristics. However, laboratory tests performed on the test section subgrade soil using the geotextile layer as a capillary break indicated that water migration to the freezing front could be somewhat delayed by the geotextile layer (3).

Brantman, et al. (12) performed a study using Bidim as a capillary break to prevent frost heave in test sections constructed in roadways

near Soyuzdornii in the U.S.S.R. Information relating to the effectiveness of Bidim as a capillary break is not yet available.

3.3.2 Previous Laboratory Investigations

Roth (63) investigated the possibility of using geotextile layers in combination with a gravel layer as a capillary barrier. He found that a gravel layer 10 cm (3.9 in.) thick sandwiched between two geotextile layers worked very well as a capillary cut-off. However, he postulated that the thickness of the gravel layer was dependent on the maximum capillary head expected for the soil. He also concluded that the depth of the gravel layer relative to the depth of frost penetration was important, as the gravel layer should not be so low that the migration of pore water suspended in the soil could cause significant heaving. The gravel layer should not be so low that the water table could rise above the gravel layer (63). Of course, the gravel layer should not be so high that the freezing front could penetrate through this layer, or frost heaving could reoccur (63).

Hollingsworth (35) and Hoover, et al. (37) investigated the possibility of using only a geotextile layer in a frost-susceptible soil as a capillary break. Both Hollingsworth (35) and Hoover, et al. (37) used Mirafi 140 in their investigations. Both investigators found that a layer of Mirafi 140 reduces water migration to the freezing front (35, 37). Hoover, et al. (37) also found that two layers of Mirafi 140, each layer being placed at the third points of the sample, were more effective in reducing water migration to the freezing front than one layer. Since two geotextile layers work better than one

layer, obviously some water must be flowing through each of the layers. The reason for this water flowing through the geotextile layers was not clear.

Hoover, et al. (37) discussed the theory supporting the use of geotextiles as capillary barriers. He theorized that since the average pore size of the Mirafi 140 was equivalent to that of a medium fine sand, and since the soil used was a silty clay, the large pore size of the geotextile would cause the capillary conductivity of the geotextile to be lower than that of the soil. In addition, he reasoned that since the surface attraction between the geotextile and the water is considerably less than that between the soil and the water, the lower surface attraction of the geotextile should also inhibit capillary rise (37).

3.3.3 Discussion of Field and Laboratory Investigations of Geotextiles Used as Capillary Barriers

Since so little work has been performed relative to the use of a geotextile as a capillary barrier, general conclusions about the effectiveness of a geotextile layer in this application cannot be made. However, it is possible to point out several of the possible problems which may occur in the field. In particular, moisture may move across the geotextile layer in the vapor phase and condense on the colder, upper side of the geotextile layer (46, 68). This moisture movement in the vapor phase may be explained in terms of temperature and vapor pressure. Since vapor pressure increases with temperature, water vapor will flow from regions of high temperature (high vapor pressure) to regions of low temperature (low vapor pressure) and will condense in

the low temperature region (68). Vapor movements occur most readily in soils having low moisture contents (68). Increasing the number and/or size of the channels through which the water vapor can pass increases the rate of this moisture movement (68). After a long period of time, the amount of moisture which moves across the geotextile layer in the vapor phase may become significant. Therefore, in future long term investigations, water movement through the geotextile layer in the vapor phase should be observed.

The determination of the level within the road subgrade at which the geotextile layer should be placed can also be a problem. Hoover, et al. (37) suggested that the geotextile layer be placed on top of the subgrade. However, it is not obvious how a capillary cut-off layer placed on top of the subgrade would prevent water migration into the frost-susceptible subgrade. If the base layer was thick and composed of frost-susceptible material, a capillary cut-off layer placed on top of the subgrade would prevent water migration into the base, but not the subgrade. If the freezing line is expected to penetrate into the subgrade, the geotextile layer must be placed within the subgrade to prevent frost heave. This layer cannot be placed below the bottom of the side ditches (60),however, especially if the in-plane permeability of the geotextile layer is high. In areas where frost penetration is deep and the water table is high, the use of a capillary cut-off may not be possible.

3.4 Geotextile Properties Pertinent to the Frost Heave Problem

In light of the results obtained from previous investigations concerning the use of geotextiles as a capillary break, most of the properties which are important for geotextiles used in this application are probably related to geotextile permeability and/or pore size. The polymer of which the geotextile is constructed is also important as the different geotextile filaments have slightly different wetting angles (5).

Typically, geotextile permeabilities are comparable to a clean, medium to fine sand (5). Some monofilament woven geotextiles have permeabilities as great as fine gravels (5). Of the nonwoven geotextiles, the needled geotextiles tend to have the highest permeabilities, while the resin bonded geotextiles have the lowest and the heat bonded geotextiles intermediate (5). Typical geotextile permeabilities are presented in Table 3.1. However, the water-passing capabilities of a geotextile are also a function of the geotextile thickness (5). Geotextiles of greater thickness tend to pass less water for the same head loss than a geotextile of the same permeability but lesser thickness (5).

Geotextile permeabilities in the dry state are much less than in a saturated state (5). The pressure required to initiate flow in an initially dry geotextile is a function of the pore size and the wettability of the fibers (5). Some typical values for pertinent geotextile types of this critical pressure head are presented in Table 3.1.

Table 3.1: Geotextile permeabilities and critical pressure heads (after Mallard and Bell (48)).

Geotextile Filaments	Type Construction	Nominal Weight (oz/yd^2)	Coefficient of Permeability (cm/sec)	Critical Pressure Head cm)
Polyester (continuous)	Nonwoven Needlepunched	8.0	5.03×10^{-1}	3.5
Polyester (staple)	Nonwoven Resin Bonded	4.0	1.85×10^{-1}	0.4
Polypropylene & Polypropylene with nylon sheath	Nonwoven Melt Bonded	3.4	1.25×10^{-1}	5.5
Polypropylene (continuous)	Nonwoven Melt Bonded	4.0	2.0×10^{-2} *	7.5
Polypropylene (continuous)	Nonwoven Needlepunched	8.8	2.9×10^{1} +	

* obtained from manufacture (72)

\+ obtained from manufacture (24)

Also related to the permeability is the clogging and blinding behavior of the geotextile (5). Clogging or blinding may occur due to the pumping action caused by wheel loads passing over the road surface. clogging or blinding may reduce the permeability of the geotextile to that of the soil itself or less (5). This reduction in permeability may affect the ability of the geotextile to perform as a capillary break. However, more study in this area is needed to determine how clogging and blinding affect the performance of a geotextile in this application.

Finally, since geotextiles used as a capillary break must also function as a separation and/or reinforcement layer, properties relating to the separation and reinforcement functions must also be considered. These properties include high tensile strength, high modulus, high elongation at failure, high friction, high puncture and tear resistance, small pore size, high permeability, good durability, and good resistance to static and dynamic creep.

3.5 Summary

In view of the research conducted thus far, the use of a geotextile as a capillary break appears to be feasible. More work must be done in this area before geotextiles can be routinely incorporated into a frost action preventative design. In particular, more geotextile types should be tested in the field as well as in the laboratory as a capillary break, since only one geotextile type, namely Mirafi 140 (or Terram), has been tested thus far. Geotextile properties such as permeability, thickness, pore size, fiber polymer, clogging and

blinding should be observed and related to the capillary breaking potential. The long term performance of a geotextile layer should also be studied to determine if moisture transfer across the geotextile layer in the vapor phase occurs. Finally, the geotextiles selected for a capillary breaking potential test program should also possess the properties required for a geotextile used in the road subgrade stabilization application.

4.0 LABORATORY TEST PROGRAM AND PROCEDURES

The goals of the laboratory test program are as follows: (1) determine the effects of temperature (in the range likely to be experienced in cold regions) on geotextile load-strain and creep behavior, (2) determine the effects of moisture (fresh and saline) and freeze-thaw cycles on geotextile durability, and (3) establish the feasibility of using a geotextile layer as a capillary break to prevent frost heave.

To relate the geotextile properties obtained in the laboratory to the expected performance of the geotextile in situ, the laboratory test conditions should simulate the expected field conditions to as great a degree as possible. In particular, since geotextiles in situ are usually stressed in plane-strain conditions, the load-strain and creep tests conducted in the laboratory should simulate plane-strain conditions. As discussed in Section 2.3.1, plane-strain conditions can be adequately approximated with a 200 mm (8.0 in.) wide specimen tested in uniaxial tension. Therefore, the wide strip load-strain test described by Shrestha and Bell (66) was employed in the present test program. To reduce the amount of weight required, a 150 mm (6.0 in.) specimen width was used for the creep tests.

The field conditions which typically occur when frost heave is a problem may be simulated in a frost heave cell. A very simple frost heave cell was used in the test program. The simplicity of the frost heave cell allowed only qualitative information to be obtained.

4.1 Tensile Tests

Purpose and Scope: The purpose of the tensile tests was to determine the effect of temperature, moisture, and cycles of freezing and thawing on the load-strain behavior of geotextiles. The load-strain characteristics of geotextiles were studied at two temperatures.

4.1.1 Tensile Test Equipment

The test equipment used was as follows (66):

(1) Two MTS machines and an Instron machine were used to apply tensile loads to the specimens. The MTS machine used to determine the load-strain behavior of geotextiles at room temperature had a capacity of 101 kN (22,600 lbs) and a piston stroke of ±100 mm (±4.0 in.). The other MTS machine, which was installed in a walk-in cold room, was used to test the geotextiles at below freezing temperatures. This MTS machine had a capacity of 22.3 kN (5000 lbs) and a piston stroke of ±76 mm (±3.0 in.). The Instron has a very long stroke, making the Instron advantageous for testing specimens with a very high elongation at failure.

(2) An X-Y recorder was used to automatically record load and displacement.

(3) 230 mm (9.0 in.) wide grips were used to hold the specimens in the tensile testing machine. The grips are described in Section 4.1.1 of reference (66).

(4) The equipment used to cut, measure, and weigh the geotextile specimens was as follows: scissors and a paper cutter for cutting and trimming the specimens; a template and a 12.5 mm (0.50 in.) diameter leather punch for punching bolt holes in the specimens; a scale for measuring the dimensions of the geotextile specimens; and a micro-balance for weighing the geotextile specimens.

(5) A thermometer was used to measure the ambient temperature during the test.

4.1.2 Tensile Test Procedures

The following procedures are a modification of the wide strip tensile test procedures described by Shrestha and Bell (66).

Specimen preparation: The specimens were cut from different parts of the geotextile roll with a pair of scissors to the approximate dimensions required and, subsequently, trimmed with a paper cutter to the final dimensions. The specimens were trimmed to 200 mm (8.0 in.) width by 220 mm (8.5 in.) length to an accuracy of ±3.8 mm(±0.15 in.). All of the geotextile specimens were cut such that the length of the specimen was in the machine direction. The dimensions of each specimen were measured to an accuracy of 1.3 mm (0.05 in.). Each specimen was also weighed in the micro-balance, allowing the non-uniformity of the geotextile specimens to be determined. After being weighed, each specimen was laid flat on a

wooden board, and holes were punched on the clamping ends of the specimen for the bolts in the grips to pass through. The holes were punched using the 12.5 mm (0.50 in.) diameter punch and a template. Typically, five specimens were prepared for each test case.

For the determination of the geotextile wet strength, the specimens were soaked in water for at least 24 hours before testing. Prior to testing, the specimens were blotted to obtain a saturated-surface-dry condition. For the determination of the load-strain characteristics of geotextiles at -12°C (10°F), the specimens were placed in the walk-in freezer overnight (in a dry state).

Placement of specimen in testing machine: The grips in the tensile testing machine were spaced 100 mm (4.0 in.) apart so that a 100 mm (4.0 in.) specimen gauge length would be obtained. The specimen was placed in the grips as squarely as possible. All three bolts were tightened to give a uniform gripping pressure over the full width of the specimen. Any wrinkles on the specimen surface were removed by appropriate manipulation or by applying a small pre-tension corresponding to a strain of ½% to 1%.

Loading the specimen: The tensile load was applied at a preset constant rate of strain until the geotextile filaments failed by rupture, or until the load started to decline. The rate of strain was assumed to be the same as the rate of displacement of the piston for the MTS, or the rate of displacement of the cross-head for the Instron machine. Typically a rate of strain of 10%/min. was used, as recommended by Shrestha and Bell (66), which corresponds to a rate of displacement of 10 mm/min. (0.4 in./min.). Because of the small stroke range of the MTS machine, geotextile specimens which exhibited

high elongation were tested in the Instron machine. A rate of strain of 13%/min. (i.e., 13 mm/min. or 0.5 in./min.) was used for specimens tested on the Instron due to machine limitations. For both machines load and displacement were recorded automatically on X-Y recorders.

4.1.3 Test Variables

Geotextile selection: Five geotextile types, each with a different construction and/or material type, were selected for testing. The geotextiles which were selected are shown in Table 4.1.

All of the geotextiles selected have either been used frequently in separation and/or reinforcement applications or have construction and fiber characteristics similar to geotextiles used in those applications. The geotextiles were also selected such that the load-strain characteristics of several geotextile construction and material types may be compared in a meaningful way. For example, since the Bidim and the Fibretex have approximately the same weight and construction but have different material types (i.e., polyester and polypropylene), the behavior of the two material types may be compared. The two material types may also be compared using the Stabilenka and Typar. By comparing the Fibretex, Typar, and Propex geotextiles, the load-strain behavior of several different construction methods may also be compared.

Test Temperature: Each geotextile type was tested at room temperature (22°C (71°F)), and at the ambient temperature in the walk-in freezer (-12°C (10°F)). Testing each geotextile type at these

two temperatures allowed the effect of temperature on geotextile load-strain behavior to be determined.

Specimen Moisture: Each geotextile type was tested at room temperature in a dry state and also in a saturated-surface-dry state.

Specimen variability: Five specimens were tested for each test case. The strength of each specimen was normalized to a nominal weight per unit area to account for specimen weight variability. The normalized specimen strength is:

$$S_N = (M_n/M)S_u \qquad (4.1.1)$$

in which,

M_n = nominal mass per unit area of all specimens of a specific geotextile type,

M = mass per unit area of the specimen

S_u = ultimate geotextile strength,

S_N = normalized geotextile strength.

The normalized strengths of the five specimens for a test case were averaged. The significance of that average compared with the average normalized strength of other test cases was determined using a Student's t-distribution and assuming a 90% confidence level. The range in which 90% of the possible values for the mean should fall is (9):

$$\mu = \bar{S}_N \quad \frac{(t_{n-1,\alpha})(S)}{n} \qquad (4.1.2)$$

in which,

$\bar{S}_N$ = mean normalized strength of the five specimens

$T_{n-1,\alpha}$ = standard normal deviate in which

n is the number of samples and

α is the probability of exceeding a confidence level of $1-\alpha$

Table 4.1: Geotextiles selected for laboratory investigations.

Geotextile Name	Fiber Polymer	Geotextile Construction	Nominal Weight gm/m² (oz/yd²)
NONWOVEN			
Bidim C-34	Polyester	Needlepunched Continuous Filaments	272 (8.00)
Stabilenka T-100	Polyester	Resin Bonded Continuous Filaments	100 (2.94)
Typar 3401	Polypropylene	Heat Bonded Continuous Filaments	136 (4.00)
Fibretex 300	Polypropylene	Needlepunched Continuous Filaments	300 (8.82)
WOVEN			
Propex 2002	Polypropylene	Woven Slit Film	150 (4.41)

S = standard deviation of the sample population

n = number of specimens

μ = maximum or minimum value of the mean of a normal distribution.

4.2 Freeze-Thaw Test

Purpose and scope: The purpose of the freeze-thaw test was to determine the effect of freezing and thawing of fresh water and saline water on the load-strain behavior of geotextiles. The load-strain behavior of the specimens was determined after the specimens were subjected to 50 and 300 cycles of freezing and thawing.

4.2.1 Freeze-thaw Test Equipment

The test equipment used was as follows:

(1) Freeze-thaw chambers were used to subject the geotextile samples to cycles of freezing and thawing. The freeze-thaw chambers were 0.74 cubic meter (26 cubic foot) chest freezers. Wooden racks were placed in the freezers to support the samples. Two freeze-thaw chambers were required to accomodate the necessary samples. Heating coils of nichrome wire were placed in the freezers to provide heat for the thawing phase.

The voltage applied to the heating coils was controlled by a variable transformer. The heating and cooling of the chambers was controlled with a system of thermostats and relays. Air was circulat-

ed within each freezer by two small fans. The freeze-thaw chamber, racks, and temperature control system are shown in Figures 4.1, 4.2, and 4.3, respectively. Schematic diagrams of the heating and cooling control system circuitry are shown in Figure 4.5 (a and b).

(2) The geotextile specimens were sealed in Ziplock bags. The bagged specimens (dry or with fresh or saline water) were placed on aluminum pans supported by the racks as shown in Figure 4.4. The aluminum pans were needed to contain the fluids if the bags leaked.

(3) Thermistors were placed inside control bags to measure the specimen temperature. The specimen temperature was monitored to determine if complete freezing and thawing of the specimens was occurring. The thermistors were placed only with certain "critical" specimens such that complete freezing and thawing of all specimens could be insured. The locations of these critical specimens are shown in Figure 4.6.

(4) Electro-mechanical counters recorded the number of freeze-thaw cycles.

(5) Two recording thermometers (one in each chamber) recorded the chamber air temperature.

4.2.2 Freeze-Thaw Test Procedures

Specimen preparation: Five specimens were cut, measured, and weighed for each test case using the procedure described in Section 4.1.

Figure 4.1: Freeze-thaw chamber with racks for freeze-thaw test.

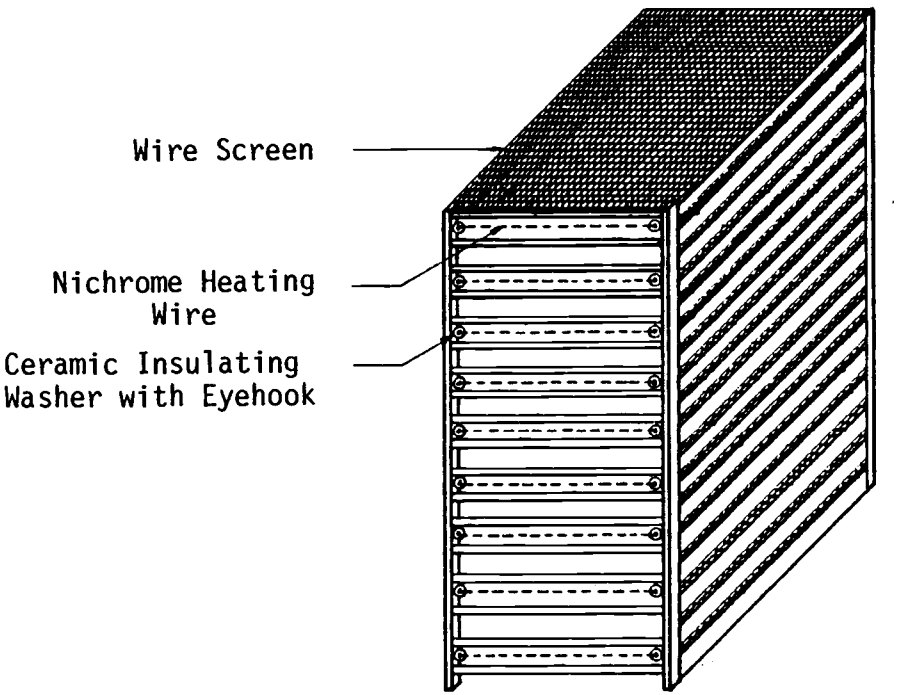

Figure 4.2: Wooden rack for supporting specimens in freeze-thaw chamber.

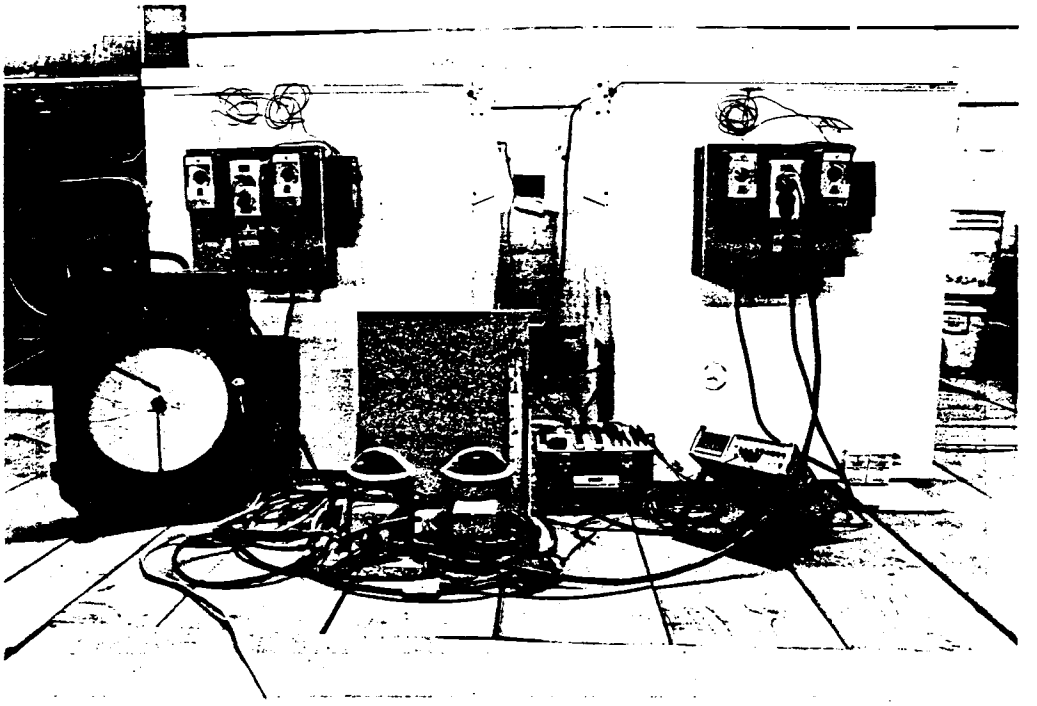

Figure 4.3: Temperature control system for freeze-thaw chambers.

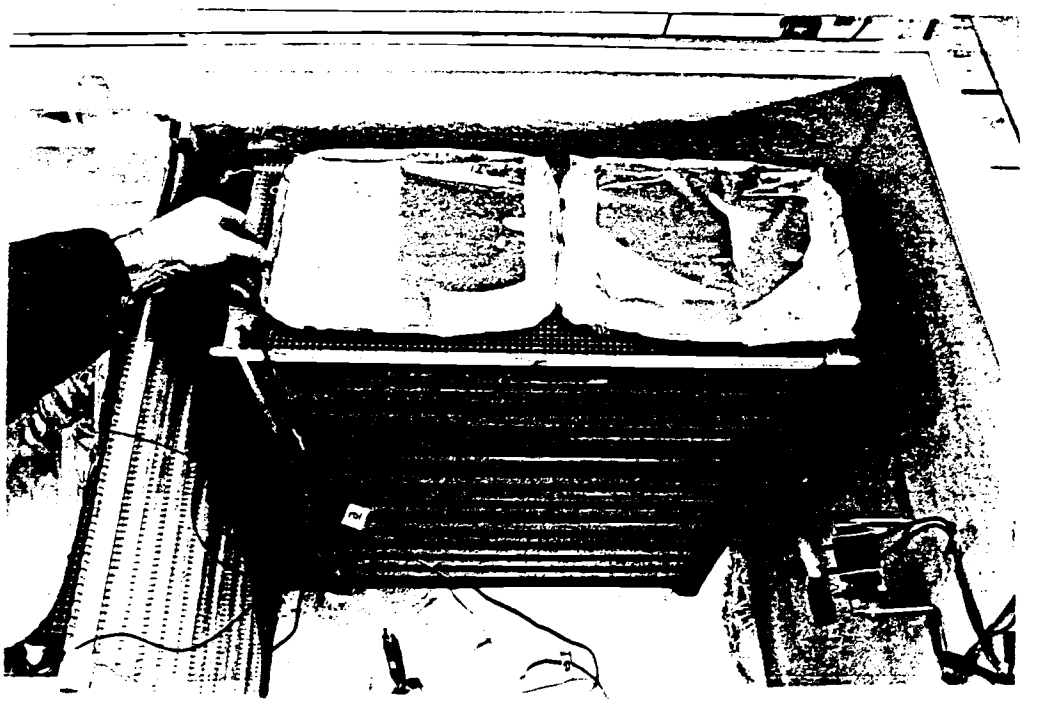

Figure 4.4: Aluminum pans with geotextile specimens in Ziplock bags in freeze-thaw chamber.

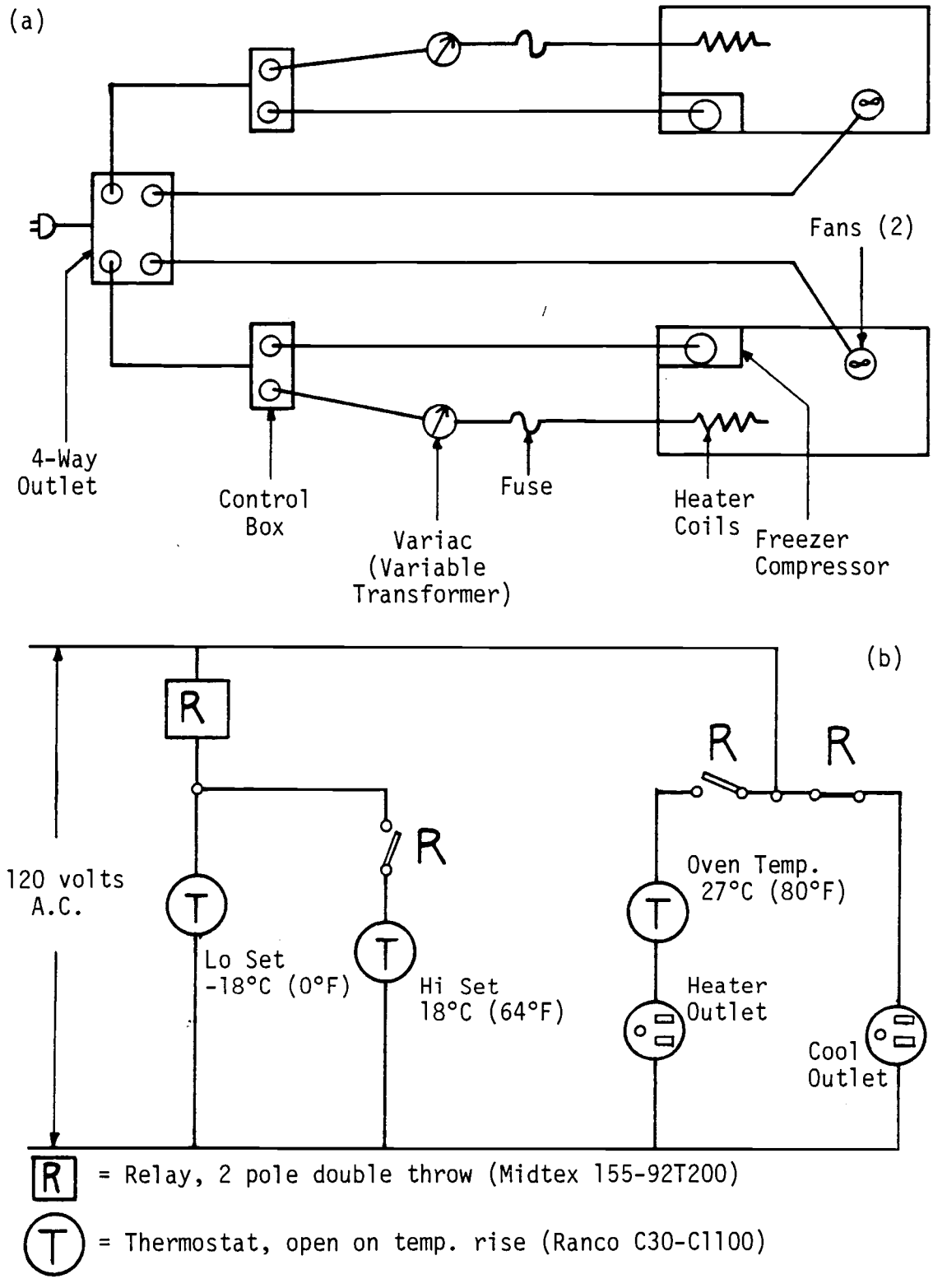

Figure 4.5: (a) One line wiring diagram of freeze-thaw chamber temperature control system. (b) Schematic diagram of the freeze-thaw chamber control box.

Placement of specimen in chamber: Each specimen was placed inside a Ziplock bag, and either the bag was filled with approximately 400 ml (.106 gal.) of distilled water or saline water, or the bag and the specimen were allowed to remain dry. After sealing, the bag was placed in an aluminum tray as shown in Figure 4.4. The tray (with specimen) was placed in the appropriate rack and chamber. A thermistor was placed inside the bag of each of the "critical" specimens.

Initialization of freeze-thaw cycling: The thermostats were adjusted such that the air temperature inside the chambers was cycling between -18°C (0°F) and 18°C (64°F). The chamber air temperature was adjusted by trial and error during the first few freeze-thaw cycles through the use of the recording thermometer. Initially, approximate settings were obtained from each thermostat dial. Cycling the freezer air temperature between these two values was found to insure complete freezing and thawing of all of the specimens, though thermistor readings were taken and the specimens visually inspected frequently through the end of the first few cycles as a check.

Once approximate thermostat settings were made, the voltage applied to the heating coils was set at 53 volts. This voltage corresponded to about 6.5 amperes for each freeze-thaw chamber. The heating coils in each of the racks were connected together in parallel. There were three racks and, therefore, three heating coils per freezer. Each freeze-thaw chamber was connected to an electrical outlet to begin the temperature cycling.

All of the geotextile specimens were allowed to go through the first 50 cycles of freezing and thawing. The chambers contained ten

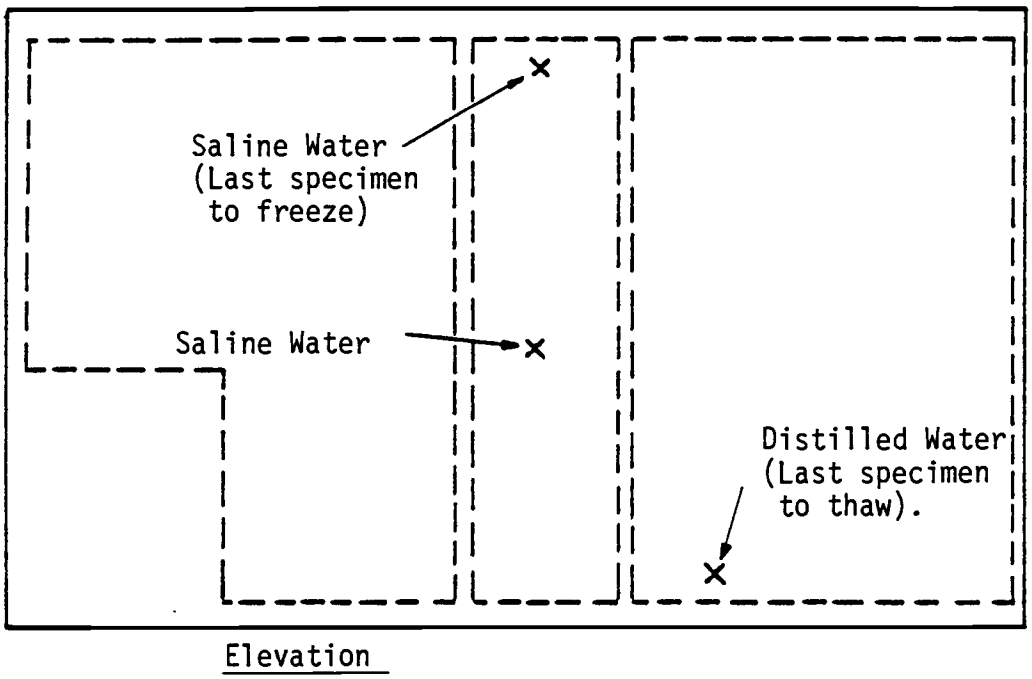

Figure 4.6: Locations of specimens with thermistors ("critical" specimens) in freeze-thaw chamber.

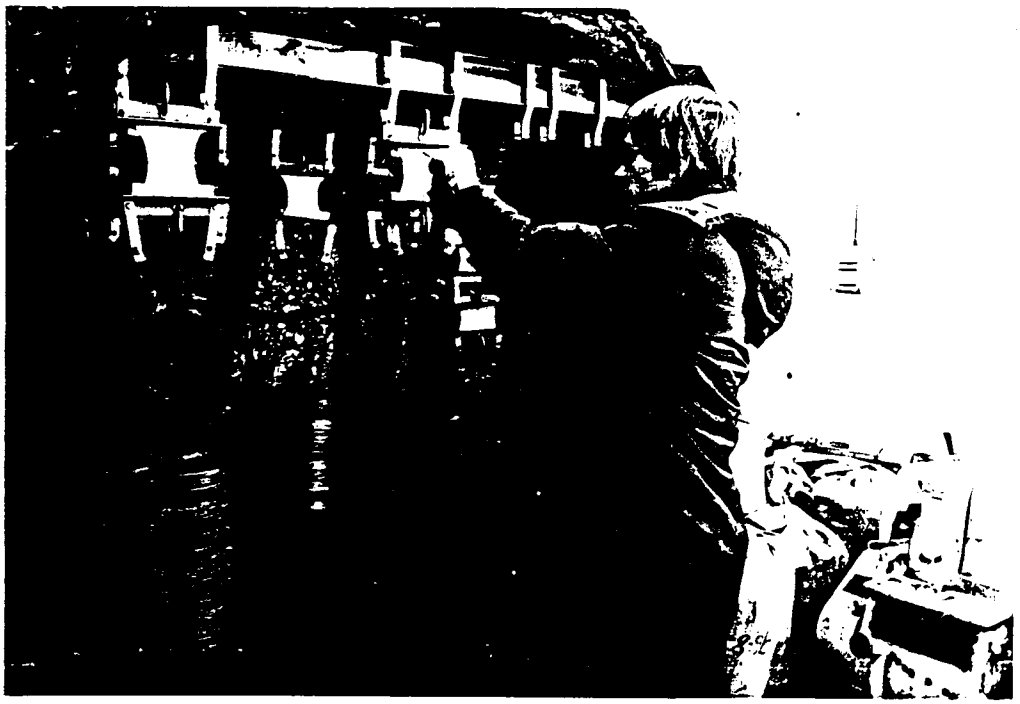

Figure 4.7: Creep test support system with weights, weight hangers, and specimens hung in series.

specimens of each test case. After 50 cycles were completed, five specimens of each test case were taken out of the chambers and tested for tensile strength. The other five specimens of each test case were distributed evenly between the two chambers and allowed to continue to cycle until 300 cycles were obtained.

When all of the specimens were in the two chambers (50 wet specimens and 25 dry specimens per chamber), the time required for each cycle was about 27 hours. With only one half of the specimens in the chambers (25 wet specimens and 12 dry specimens per chamber), the time required for each cycle was about 17 hours. The 50 cycle specimens (in particular, the specimens placed in saline water), were in the chambers for a total of 59 days, and the 300 cycle saline specimens were in the chambers for a total of 212 days.

Measurement of load-strain behavior of specimens: After the required number of freeze-thaw cycles were obtained, the specimens were taken from the chambers. Tensile tests were performed on those specimens using the procedures given in Section 4.1. The specimens which were originally dry were soaked in water for 24 hours before the tensile testing. All of the specimens were tested in a saturated-surface-dry condition.

4.2.3 Test Variables

Specimen selection: Five geotextile types were selected (see Table 4.1).

Specimen temperature: All specimens were tested at room temperature (approximately 22°C or 71°F).

Specimen moisture: Each geotextile type was subjected to freezing and thawing in distilled water, saline water, or in a dry state. The specimens subjected to cycles of freezing and thawing in a dry state were used as a control group to separate the effect of below freezing temperature on geotextile durability and strength from the effect of the freezing and thawing of water on geotextile strength.

Number of freeze-thaw cycles: The specimens were subjected to either 50 cycles or 300 cycles of freezing and thawing.

Specimen variability: Five specimens were tested for each test case. The same procedure as for the tensile tests was used to account for and evaluate specimen variability.

All of the test variables for the freeze-thaw test are summarized in Table 4.2.

4.3 Creep Test

Purpose and scope: The purpose of the creep tests was to determine the effect of temperature and load level on static geotextile creep. The creep characteristics of geotextiles were studied at two temperatures and four load levels (as a percent of ultimate strength). (See Table 4.3.).

4.3.1 Creep Test Equipment

The test equipment used was as follows:

(1) Two frames were used for hanging the geotextile specimens and weights. One frame was placed in the laboratory at room temperature, and the other frame was placed in the walk-in cold room at -12°C (10°F).

(2) Lead and/or steel weights were used to apply loads to the specimens. Weight hangers were used to support the weights. A 3.2 mm (0.13 in.) diameter steel cable was used to connect the weight hanger to the bottom grip. The frame, weights, and weight hangers (including specimens with grips) are shown in Figure 4.7.

(3) Non-slip grips were used to hold the specimens during the creep test. Due to the need to use many sets of these grips at one time (60 sets), the cost of the grips was of primary importance. Therefore, machining of the grips was kept to a minimum. Each set of grips consisted of four 200 mm (8.0 in.) long by 38 mm (1.5 in.) by 38 mm (1.5 in.) aluminum angles, using two of the aluminum angles for each end of the specimen. A piece of 200 mm (8.0 in.) by 38 mm (1.5 in.) by 3.2 mm (0.125 in.) aluminum bar stock was placed between each set of two aluminum angles. The geotextile specimen was wrapped around the aluminum bar stock. A bolt was placed at the ends of each grip to help clamp the specimen. A 76 mm (3.0 in.) C-clamp was placed in the center of each grip to keep the grip from bowing out when the bolts were tightened. Coarse sandpaper strips (D weight open coat aluminum oxide production paper, #36) were glued to the grip surfaces to limit specimen slippage within the grips. Aluminum strips were used to connect one set of grips (including specimen) to the next set of grips in series (three specimens were hung in series to conserve the number of weights required). The grips are shown in Figures 4.7 and 4.8.

Table 4.2: Test variables for freeze-thaw tests.

Geotextile Name	Specimen Temperature °C	°F	Specimen Size mm x mm	Specimen Moisture Condition	Number of Freeze-Thaw Cycles	Number of Specimens
Bidim C-34	22	(71)	200x100 MD	Dry	0*	5
				Saturated-Surface-Dry	0*	5
				Dry	50+	5
					300+	5
				Distilled Water	50	5
					300	5
				Saline Water	50	5
					300	5
Stabilenka T-100	22	(71)	200x100 MD	Dry	0	5
				Saturated-Surface-Dry	0	5
				Dry	50	5
					300	5
				Distilled Water	50	5
					300	5
				Saline Water	50	5
					300	5
Typar 3401	22	(71)	200x100 MD	Dry	0	5
				Saturated-Surface-Dry	0	5
				Dry	50	5
					300	5
				Distilled Water	50	5
					300	5
				Saline Water	50	5
					300	5

Table 4.2: Test variables for freeze-thaw tests. (cont.)

Geotextile Name	Specimen Temperature °C	°F	Specimen Size mm x mm	Specimen Moisture Condition	Number of Freeze-Thaw Cycles	Number of Specimens
Fibretex 300	22	(71)	200x100 MD	Dry	0	5
				Saturated-Surface-Dry	0	5
				Dry	50	5
					300	5
				Distilled Water	50	5
					300	5
				Saline Water	50	5
					300	5
Propex 2002	22	(71)	200x100 MD	Dry	0	5
				Saturated-Surface-Dry	0	5
				Dry	50	5
					300	5
				Distilled Water	50	5
					300	5
				Saline Water	50	5
					300	5

* Specimens which did not go through freeze-thaw cycles were part of the control group used to determine the effect of freezing and thawing on geotextile strength. The test procedures for these specimens are described in Section 4.1.

\+ These specimens were control specimens used to separate the effect of the temperature cycles from the effect of the freezing and thawing of water on geotextile strength.

Note: MD denotes machine direction.

(4) A small hydraulic jack was used to support the weights when loading the specimens. When the jack was released, the load was applied to the specimens smoothly and rapidly.

(5) Two MTS machines, one in the laboratory at room temperature (22°C or 71°F) and one in the walk-in cold room at -12°C (10°F), were used for applying constant tensile load to the specimens which required relatively high loads.

(6) An X-Y recorder was used for the automatic recording of displacement and time for specimens tested on the MTS.

(7) Miscellaneous equipment included the following: a micro-balance for weighing the geotextile specimens; scale for measuring the dimensions of the specimens; scissors and paper cutter for cutting and trimming the specimens; thermometer for measuring the temperature; dividers and calipers for measuring the deformation of the specimen; wrist watch for monitoring time; and small staples for marking the gauge length on the specimen for a reference for measuring deflections.

4.3.2 Creep Test Procedures

Specimen preparation: The specimens were cut, trimmed, measured, and weighed as described for the tensile tests, except that no holes were punched, and the specimen dimensions were 205 mm by 152 mm (12.0 in. by 6.0 in.). Staples were placed 64 mm (2.5 in.) apart in the center of the specimen for the measurement of deformation in the specimen.

Placement of specimen in grips: Each end of the specimen was wrapped around the aluminum bar as shown in Figure 4.9. The specimen was

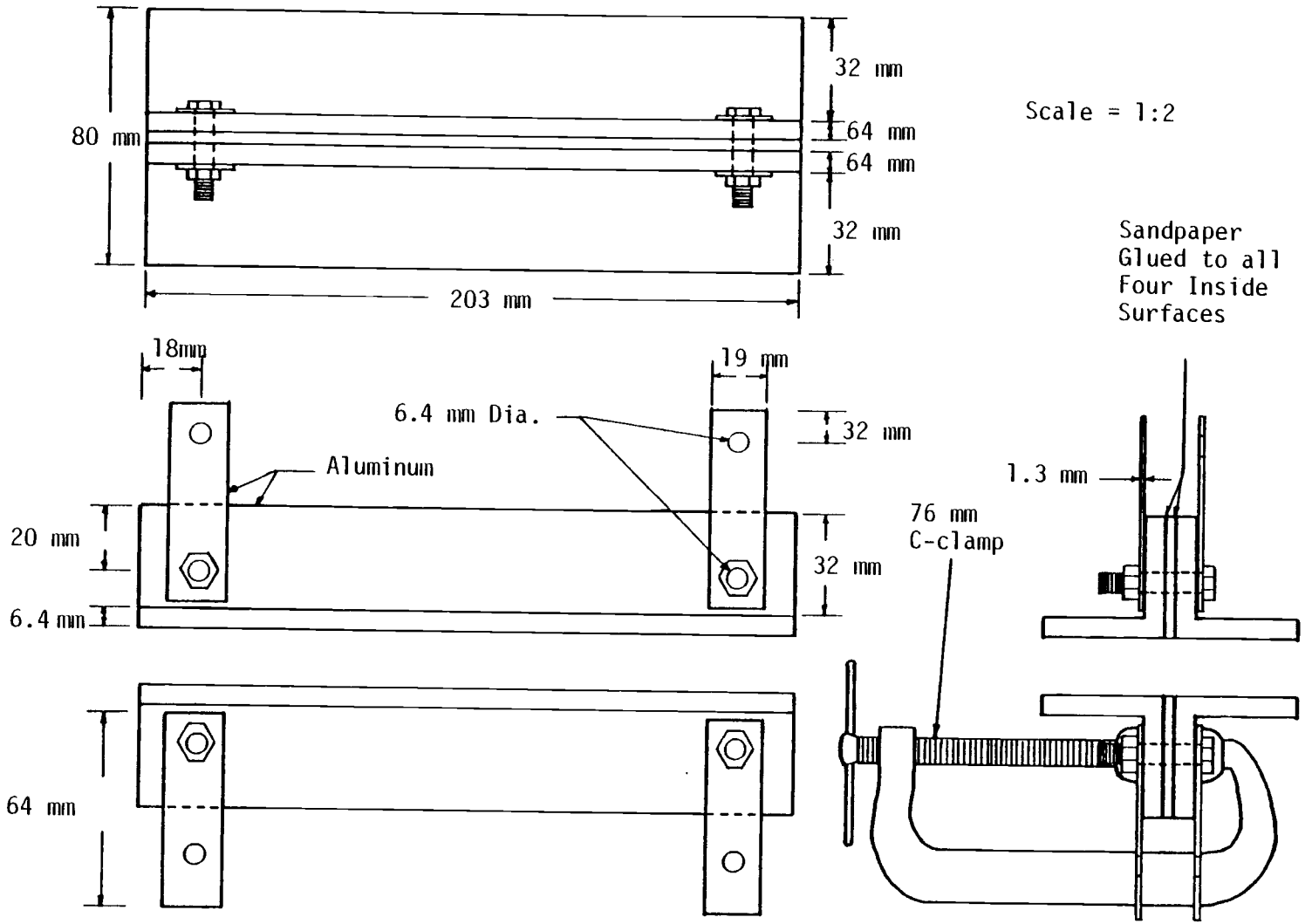

Figure 4.8: Grips used for creep test.

placed in the grips such that the distance from grip edge to grip edge was approximately 75 mm (3.0 in.). The aluminum angles were positioned as shown in Figure 4.9 and bolted together. A C-clamp was placed in the center of each grip and tightened. Subsequently the bolts were tightened, and the C-clamp was again checked for tightness to insure that a uniform pressure was obtained across the width of the grip. The specimen, with its grips, was connected in series with two other specimens through the use of aluminum strips, as shown in Figure 4.7. The three specimens connected in series represented one test case. If a specimen was likely to rupture under the applied load, the specimens were not hung in series but were tested individually.

Determination of load to be placed on specimen: Tensile tests were conducted on each geotextile type to determine an average ultimate strength for each geotextile. The procedures given in Section 4.1 were used, except the specimen size was 190 mm by 105 mm (7.5 in. by 6.0 in.), and a 76 mm (3.0 in.) gauge length was used. Five specimens of each geotextile type were tested (dry strength only). After the specimens were tested, the ultimate strength obtained for each specimen was normalized to a nominal mass per unit area. The normalized strengths of the samples for a geotextile type were averaged. The average normalized strength was used to determine the load required for each set of three creep specimens, as shown below:

$$\text{Load} = P_u \, (M_a/M_n) S_N \qquad (4.3.1)$$

in which,

P_u = percent of ultimate strength (typically 20%, 35%, 50%, or 65%)

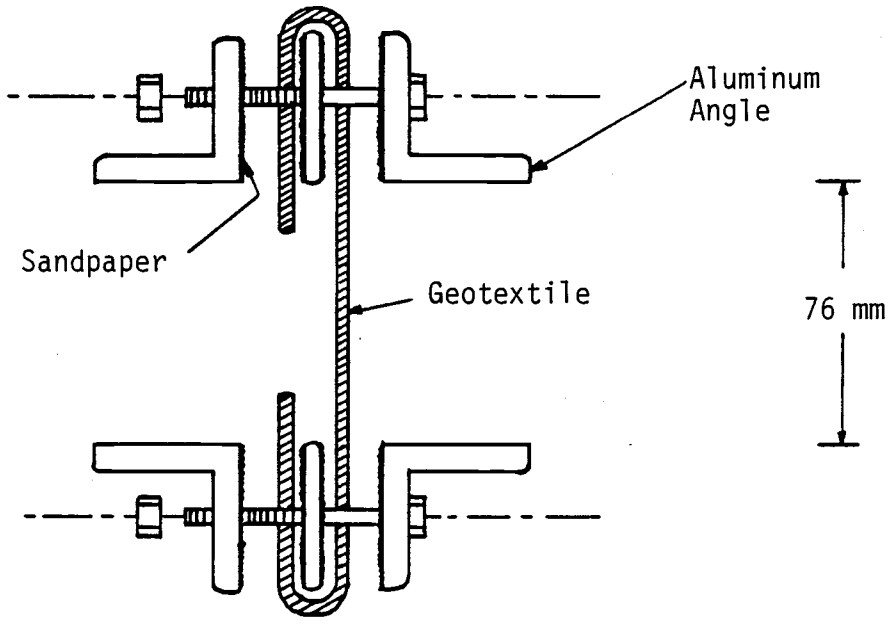

Figure 4.9: Placement of geotextile specimen in creep grips.

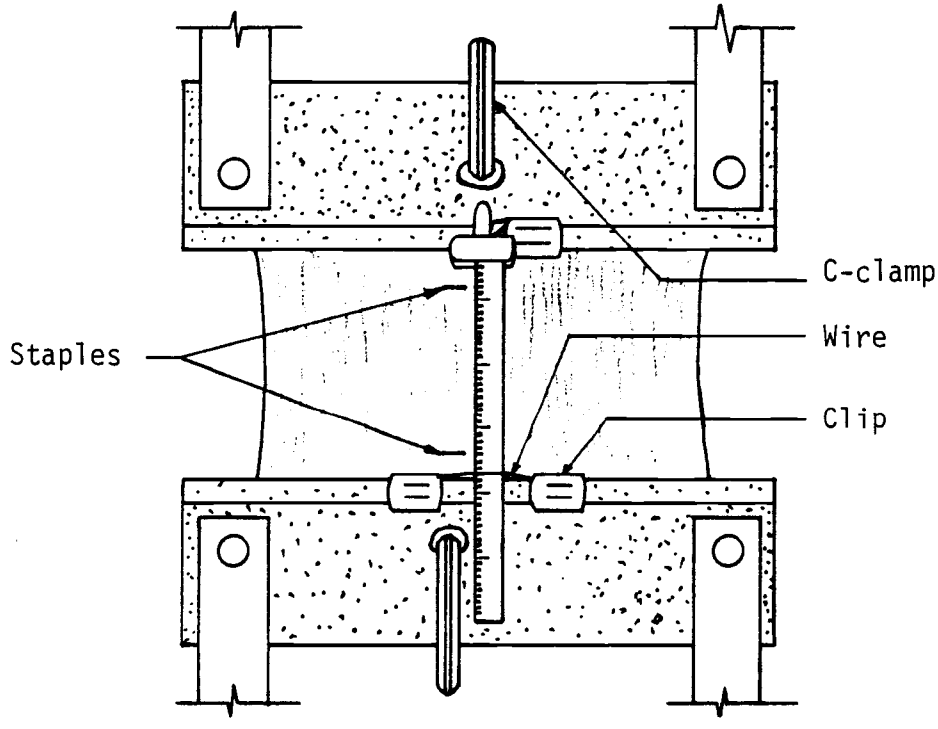

Figure 4.10: Creep specimen equipment configuration for the measurement of initial deflections.

M_a = average mass per unit area of the three specimens hung in series,

M_n = nominal mass per unit area of all specimens of a specific geotextile type,

S_N = average normalized ultimate strength for a geotextile type.

The weight of the weight hanger plus one half of the weight of the grips was considered to be part of the load determined from Equation 4.3.1. Lead and/or steel weights were used to make up the remainder of the load. All of the specimens for each geotextile type were arranged in groups of three (for a test case) such that the deviation of the weight per unit area of each specimen in the group was minimized.

Initialization of creep test: After hanging the three specimens connected in series from the support frame, the initial length of each specimen was measured using the calipers to measure from grip edge to grip edge and the dividers to measure from staple to staple. The measurement of the specimen length from staple to staple was made to determine if slippage was occurring between the specimen and the grips after the load was applied. Fortunately, slippage at the grips was never a problem during the testing program.

After the initial measurements were made, a small steel scale was clipped to the top grip edge (for each specimen), and a thin wire was clipped to the bottom grip edge such that the wire went around the steel scale, as shown in Figure 4.10. The steel scale was used to determine the initial, 1 minute, and 2 minute deformation of each specimen, as it was not possible to make the necessary measurements for

all three specimens at one time using the calipers and dividers.

After the steel scales were clipped to the grips, the jack was placed underneath the specimen to be loaded, and the jack was fully extended. The weight hanger was placed on the jack, and the required weights were stacked on the weight hanger. With three observers present, the jack was released, allowing the load to be placed on the specimens. After the load was placed on the specimens, each observer recorded the initial, 1 minute, and 2 minute deformation for a specific specimen. The time and the date were also noted.

After the 2 minute reading was taken, the scales and wires were unclipped from the grips. The calipers and dividers were used for future readings for these specimens. Typically, readings were taken at the following times: gauge length (before load was applied), 0 (immediately after load was applied), 1, 2, 5, 10, 30, 60, 120, 240, 1440, and 2880 minutes. After 2880 minutes had passed, readings were taken once every one or two weeks as time allowed, or until rupture occurred.

The grips shown in Figure 4.8 were used for creep tests performed using the MTS; however, only one specimen at a time could be tested on the MTS. Typically, only the specimens which were tested at 65 percent of the ultimate load were tested on the MTS. Specimen deformation was measured through the use of the calipers and the dividers. Scales were not used to get the initial deformation. The deformation versus time for each specimen was also recorded on the X-Y plotter as a check, with the plotter in the time sweep mode. The load was applied to the specimen using a ramp function in load control. The ramp was set such

that a preset load was reached in 2.0 seconds and held constant at the preset load thereafter. Typically, the specimens tested on the MTS were only allowed to creep for two days due to limited time and the limitations of the machine.

4.3.3 Test Variables

Specimen selection: Five geotextile types were selected (see Table 4.1).

Specimen temperature: Each geotextile type was tested at 22°C (71°F) and -12°C (10°F) to determine the effect of temperature on the creep behavior.

Load on specimen: To determine the effect of load on geotextile creep, each geotextile type was tested at four different loads expressed as a percent of the normalized ultimate strength: 20%, 25%, 50%, and 65%. However, for those geotextile types which stabilized at 50% or 65% ultimate load, the 35% load case was not considered; an 80% ultimate load case was substituted. For those geotextile types which failed rapidly at 50% ultimate load, the 65% load case was not considered (see Table 4.3).

Specimen variability: Three specimens were employed for each test case. To account for specimen variability, the load applied to each specimen was determined from the normalized strength of the geotextile as described in the creep test procedures.

Table 4.3: Test variables for creep tests.

Geotextile Name	Specimen Size mm x mm	Specimen Temperature °C	(°F)	Load Level (%)	Number of Specimens
Bidim C-34	150x76 MD	22	(71)	20	3
				50	3
				65	3
				80	3
		-12	(10)	20	3
				50	3
				65	3
				80	0
Stabilenka T-100	150x76 MD	22	(71)	20	3
				50	3
				65	3
				80	3
		-12	(10)	20	3
				50	3
				65	3
				80	0
Typar 3401	150x76 MD	22	(71)	20	3
				35	3
				50	3
				65	0
		-12	(10)	20	3
				35	0
				50	3
				65	3
Fibretex 300	150x76 MD	22	(71)	20	3
				35	3
				50	3
				65	0
		-12	(10)	20	3
				35	0
				50	3
				65	3

Table 4.3: Test variables for creep tests. (continued)

Geotextile Name	Specimen Size mm x mm	Specimen Temperature °C	(°F)	Load Level (%)	Number of Specimens
Propex 2002	150x76 MD	22	(71)	20	3
				35	3
				50	3
				65	3
		-12	(10)	20	3
				35	3
				50	3
				65	3

Length of test: Each specimen was allowed to creep for as long as time permitted up to over 150,000 minutes, or until rupture occurred. Most of the creep tests were terminated when creep had virtually stopped (i.e., an equilibrium point was reached). All of the test variables for the creep tests are summarized in Table 4.3.

4.4 Frost Heave Test

Purpose and scope: The purpose of the frost heave tests was to investigate the ability of a geotextile to act as a capillary break and thereby prevent frost heave. A simple frost heave cell was used in the study. The simplicity of the cell allowed only qualitative information to be obtained.

4.4.1 Frost Heave Test Equipment

The test equipment used was as follows: (1) A frost heave chamber placed inside a walk-in cold room was used to subject specimens of a frost-susceptible soil to the field conditions which typically occur during frost heaving (i.e., high water table, below freezing temperatures, and unidirectional freezing). This frost heave chamber is illustrated in Figures 4.11 and 4.12.

This chamber actually consisted of three separate cells (for three specimens), in which each cell consisted of a 171 mm (6.75 in.) high polystyrene cup which was 116 mm (4.56 in.) in diameter at the top and 105 mm (4.13 in.) in diameter at the bottom. Two cells had 22

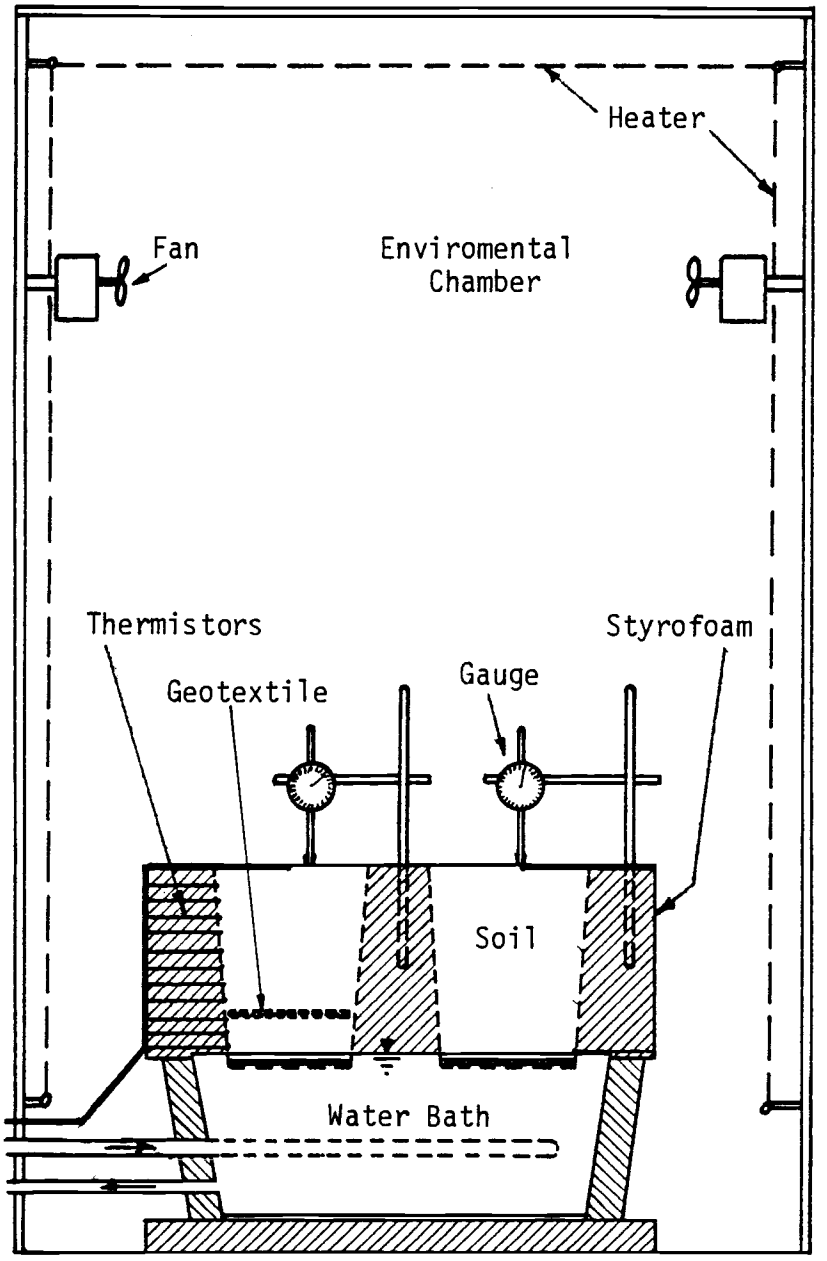

Figure 4.11: Frost heave test cell.

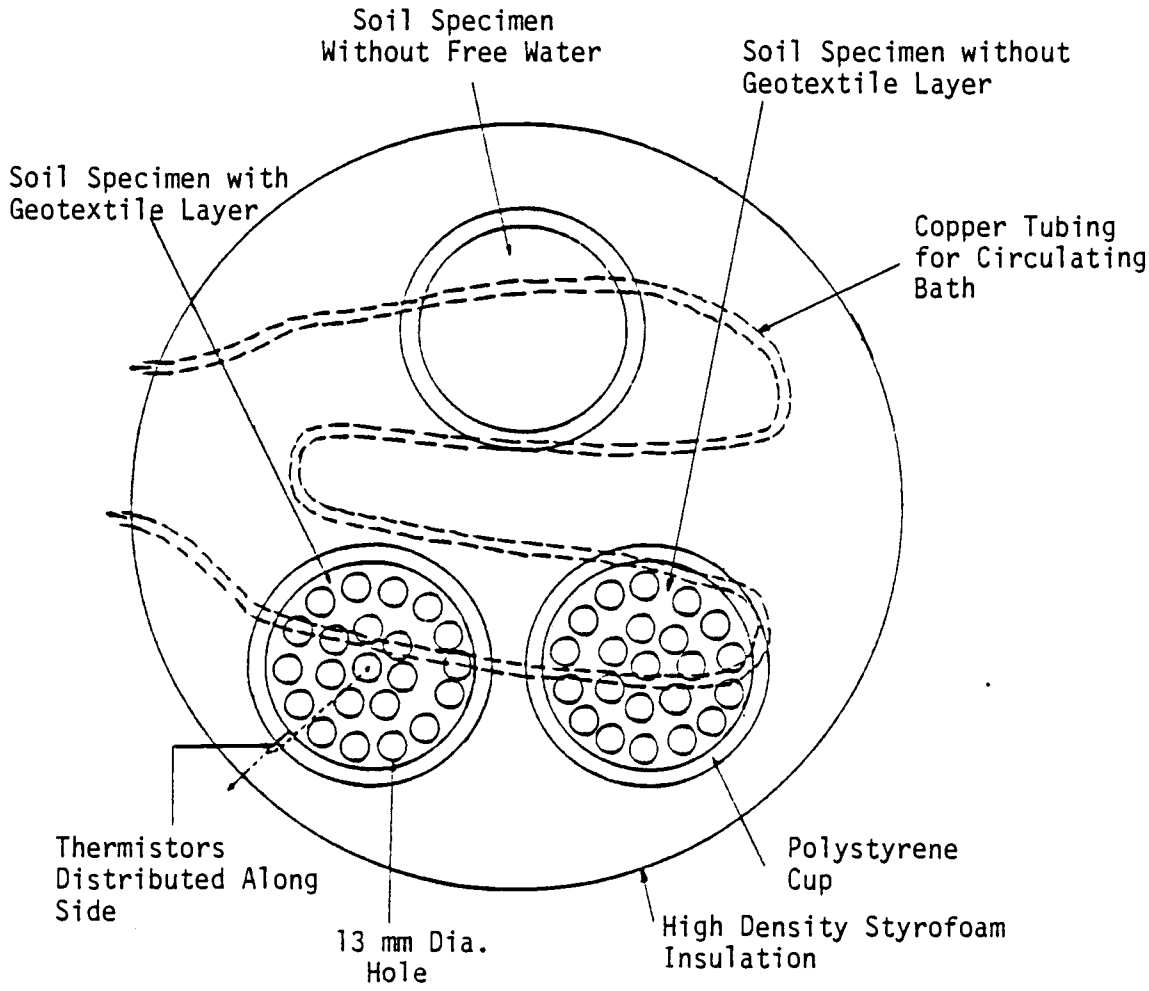

Figure 4.12: Locations of the three frost heave cells within the frost heave chamber.

13 mm (0.50 in.) diameter holes drilled through the bottom with a 100 mm (4.0 in.) diameter by 6.4 mm (0.25 in.) thick porous stone laying on the bottom. The third cell had no holes drilled through the bottom, thereby preventing water in the water supply from being drawn up into the specimen contained in the cell (closed system testing). All three cells were placed in a disk of high-density styrofoam insulation so that uniaxial freezing (from top to bottom) could be simulated. The disk was 0.394 m (15.5 in.) in diameter and 150 mm (6.0 in.) deep. The base of the cells extended 19 mm (0.75 in.) below the bottom of the styrofoam disk so that the water level in the water bath could be raised above the level of the porous stone. Thermistors were installed through the side of one of the polystyrene cells (with the holes in the bottom) and were spaced vertically at 14 mm (.56 in.) intervals. Thermistors were placed at only the top and bottom of the other cells.

The styrofoam disk (with the cells) was placed on the top of a 0.36 m (14 in.) diameter steel tub which was filled with water. The steel tub had two small viewing windows such that the level of the water in the tub could be checked. A plastic tube connected this tub with a tub outside of the walk-in cold room so that water could be added to the water bath without disturbing the frost heave test. The water bath (inside the freezer) was insulated with 25 mm (1.0 in.) of fiberglass insulation on the sides and a 25 mm (1.0 in.) styrofoam board on the bottom.

(2) A "Hotpack" constant temperature circulating bath was used to control the water bath temperature. Copper tubing was coiled

inside the center of the water bath as shown in Figure 4.12. The ends of the copper tubing were placed through the wall of the water bath, and plastic tubing connected the ends of the copper tubing to the circulating bath. Commercial grade antifreeze was used in the circulating bath. With the copper tubing acting as a heat exchanger to the water bath, the temperature of the circulating fluid, which was controlled by the "Hotpack" circulating bath, controlled the temperature of the water bath.

(3) An environmental chamber was used to control the temperature of the air surrounding the frost heave chamber and the top of the soil specimens. The environmental chamber consisted of 6.4 mm (0.25 in.) thick "plexiglass" sheets glued together to form a box which was open at the bottom. One side of the chamber was fastened to the chamber with bolts, and could be removed when necessary. Coiled nichrome heating wire was strung along the sides of the chamber to add heat to the system when required. The voltage applied to the heating wire was controlled with a Versatherm proportional temperature controller. Two fans were used to circulate the air within the chamber.

(4) A multimeter was used to measure the resistance, and thereby the temperature, read by each thermistor. A switch box was used for switching from one thermistor to another when reading each thermistor.

(5) Three dial gauges were used to measure the amount of heave in each specimen. Metal rods and clamps were used to support each dial gauge. The dial gauge probes were in contact with small aluminum plates placed on the top of each specimen.

(6) 100 mm (4.0 in.) diameter by 305 mm (12.0 in.) long thin (.30 mm or .012 in. thickness) rubber membranes were placed around each specimen. The sides of each cell were greased with a silicone grease (Molykote 44, medium consistency) to reduce side friction.

(7) Cellophane wrap was placed on the top of each specimen to reduce sublimation during freezing.

(8) A refrigerator was used to pre-cool the frost heave chamber and soil specimens prior to the beginning of the test.

(9) A small compaction hammer was used to compact each specimen in frost heave cells. The compaction hammer is shown in Figure 4.13.

(10) Scissors and a template were used to cut the geotextile specimens for the frost heave test.

4.4.2 Frost Heave Test Procedures

Specimen preparation: The soil specimen was thoroughly broken up, moistened, and mixed until a water content which was 2% above the optimum water content was obtained (i.e., 19.5%) the water content determined according to ASTM D2216, and the moisture-density relationship for the soil determined according to AASHTO T99. After the proper water content was obtained, the soil was allowed to cure for 12 hours in a moisture tight container. During the curing period, the porous stones to be used in the frost heave test were allowed to soak in water.

The geotextile specimen to be tested was cut from a randomly selected location in the geotextile roll. The specimen was subse-

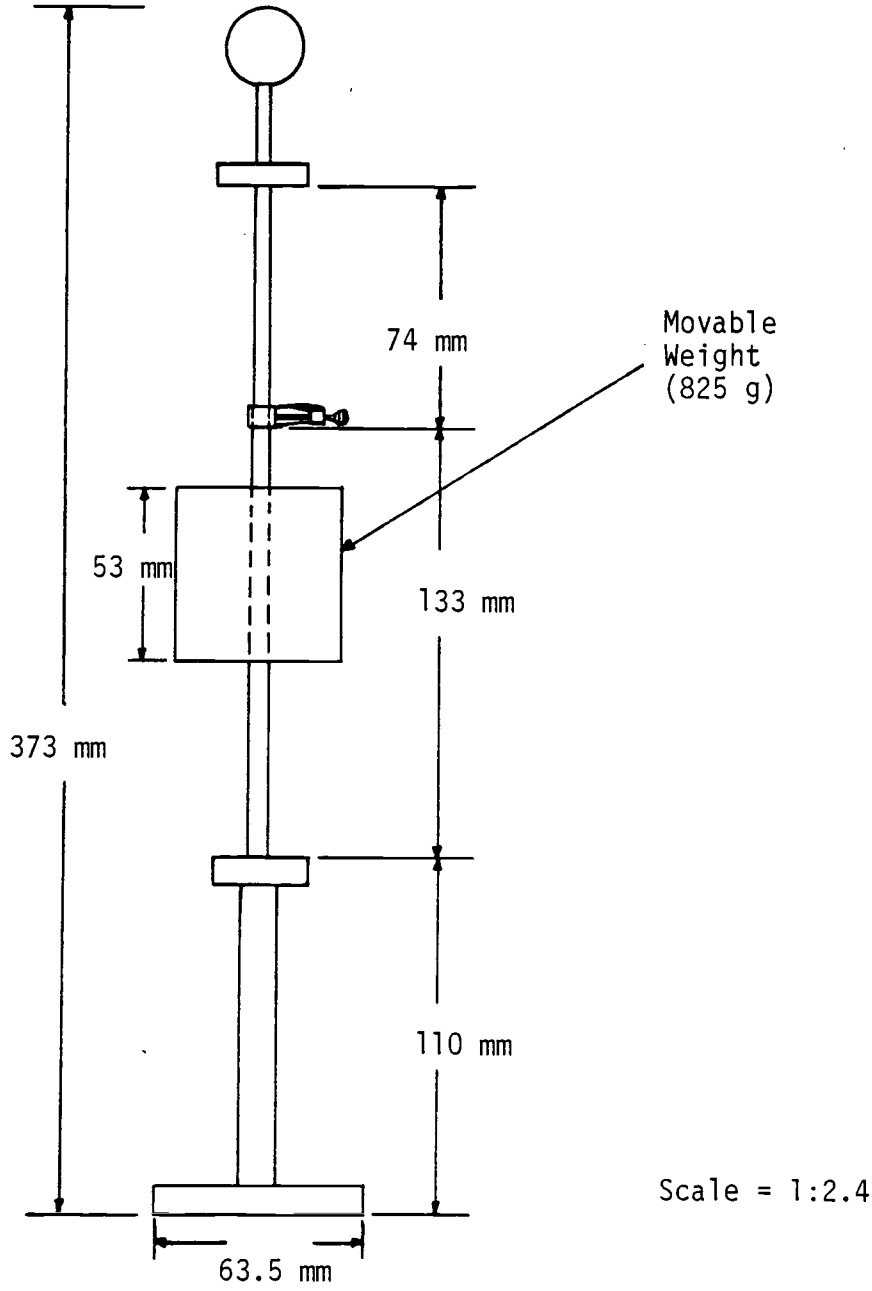

Figure 4.13: Compaction hammer used for compacting specimens for frost heave test.

quently trimmed using a circular template and a pair of scissors. The specimen was trimmed such that the edge of the geotextile specimen was in contact with the sides of the cell.

Placement of specimen in frost heave cell: A uniform coating of silicone grease was spread on the sides of each cell. Subsequently, a rubber membrane was placed inside each cell. After the soil had cured for 12 hours, the soil was placed inside the rubber membrane in each cell. To obtain a predetermined, standard density for every specimen, the weight of the soil placed in each cell had to be the same. The weight of the soil to be placed in each cell was determined by measuring the volume of each cell and by establishing a standard density to be used for every test. The standard density to be used was determined from the moisture-density relationship established during the specimen preparation (AASHTO T99). Ninety percent of the standard proctor density for the soil in this testing program was selected as the standard density. The soil was compacted in four lifts of equal thickness with the compaction hammer shown in Figure 4.13. The number of blows per layer varied from 20 blows for the bottom soil layer to 26 blows for the top soil layer. A geotextile specimen was positioned between the first (bottom) and second layer of the soil specimen placed in the cell with thermistors distributed throughout the full length of the cell.

After the soil specimens were compacted in the cells, the frost heave chamber was placed in a refrigerator for 12 hours. The refrigerator temperature was set at about 1°C (34°F). The portion of the rubber membrane extending above each specimen was twisted and tied such

that no moisture could escape from the specimens during this 12 hour cooling period. The bottoms of the cells were also set on a polyethylene sheet to prevent moisture loss from the bottom of the cells. Also during this 12 hour cooling period, the water bath (and the external water supply) was filled with distilled water such that when the frost heave cells were placed over the water bath, the water level would be about 6.4 mm (0.25 in.) above the level of the porous stones. The filling of the water bath during the 12 hour cooling period for the specimens allowed the water in the bath to cool to the approximate temperature required for the frost heave test (1°C (34°F)). The temperature of the circulating bath was also set such that the temperature of the water bath would stabilize at 1°C (34°F). A water bath temperature of 1°C (34°F) was found to correspond to a setting of 2.90 on the circulating bath. However, this setting was dependent on the ambient air temperature. A setting of 2.90 was satisfactory when the ambient air temperature was -5°C (23°F).

Frost heave test initialization: After the soil and cells were precooled in a refrigerator for 12 hours, the frost heave chamber was placed on the water bath, making sure that the cells were level. The excess rubber membrane for each specimen was untied, folded over to expose the surface of the specimen. A thin layer of ice shavings was placed on the surface of each specimen to reduce the time required to initiate freezing of the specimen. After placing the ice shavings on the surface, a piece of cellophane wrap was placed over the surface of each specimen to reduce moisture loss during the test. A thin aluminum plate was placed on the top of each specimen (on top of the

cellophane wrap) and the dial gauge probe was placed in contact with the plate. Three dial gauges, one for each specimen, were attached to the metal rods protruding from the styrofoam insulation such that the full throw of each dial gauge could be accomodated. After the dial gauges were attached to the metal rods and positioned over the center of the specimens, each dial gauge was zeroed. The environmental chamber was placed over the frost heave cell, and the Versatherm temperature controller was connected to the environmental chamber heating coils and set such that the air temperature inside the chamber was -5°C (23°F). An air temperature of -5°C (23°F) inside the chamber was found to correspond to a setting on the Versatherm of 42 for the coarse adjustment, 50 for the fine adjustment, and 5.0 for the voltage limit. After the Versatherm was set, the environmental chamber fans were started, and the heating coils were connected to the Verstherm. The air and the water bath temperature were allowed to stabilize until the 0°C (32°F) isotherm had propagated a maximum of 6.4 mm (0.25 in.) below the surface of the soil, which normally took about 12 hours.

Frost heave test measurements: After the air and water bath temperature stabilization was complete, initial readings of all thermistors and dial gauges were made. Additional readings were taken at the following times during the test: 0.5, 1, 2, 3, 5, 8, 12, 18, and 24 hours. After 24 hours, readings were taken at eight hour intervals over a one day period.

At the completion of the test, the frost heave chamber was taken out of the cold room. The specimens were carefully extruded from the cells and the rubber membranes. Each specimen was split horizontally

into sections approximately 19 mm (.75 in.) thick. The thickness and the position of each section within the specimen was noted. The location of the frozen part of the soil (the freezing front) was also noted. The section which contained the freezing front was split into two sections so that the water content immediately above and below the freezing front could be determined.

4.4.3 Test Variables

Specimen selection: Five geotextile types were selected (see Table 4.1). One soil type was used for the frost heave tests to allow the results of all of the frost heave tests to be compared. The soil used for the frost heave tests was a light brown non-plastic silt which was known to be frost-susceptible.

Specimen case: Two control specimens, along with a specimen which contained a geotextile layer, were tested simultaneously for frost heave. One of the control specimens was not allowed to draw water from the water supply, allowing the expansion upon freezing of in-situ moisture to be separated from the total heave obtained in the other two specimens. The other control specimen was allowed to draw water from the water supply, allowing the total amount of heave possible for the specimens with the existing thermal and moisture conditions to be determined. The third specimen was allowed to draw water from the water supply, but this specimen contained a geotextile layer which was located 38 mm (1.5 in.) above its base. The effectiveness of the geotextile layer as a capillary break was

determined through a comparison of the third specimen with the control specimens.

Specimen variability: One frost heave test was made for each geotextile type.

5.0 TEST PROGRAM RESULTS

5.1 Tensile Test Results

The results of the test program described in Sections 4.1 and 4.2 are presented in this section.

5.1.1 General Load-Strain Behavior

The tensile axial load versus strain relationships for all of the geotextiles tested, including the control test and the freeze-thaw test specimens, are given in Appendix A (Figures A.1 through A.10). Table 5.1 summarizes the breaking strength, strain at failure, and the secant modulus at 10% strain obtained in these load-strain tests. The results of the statistical analysis (using a Student's t-distribution) of the geotextile properties summarized in Table 5.1 are presented in Appendix A (Tables A.1 through A.3). For the geotextiles tested, the needlepunched geotextiles exhibited high strain at failure and intermediate strengths. The woven geotextile had the highest strength but the lowest failure strain. The bonded geotextiles had the lowest strengths and intermediate failure strains.

5.1.2 Effect of Temperature on Load-Strain Behavior

The five geotextiles described in Table 4.1 were tested at two temperatures, 22°C (71°F) and -12°C (10°F). All specimens were 200 mm (8.0 in.) wide with a 100 mm (4.0 in.) gauge length and were tested

Table 5.1: Geotextile load-strain characteristics.

Geotextile	Property	I	II	III	IV	V	VI	VII	VIII	IX
Bidim	Normalized strength (kN/m)*	18.5	17.5	16.0	16.1	15.3	16.7	16.7	16.0	15.6
C-34	% Strain at Peak Strength	53.2	60.0	59.9	54.8	59.0	54.5	64.6	58.2	59.0
	Normalized Secant Modulus at 10% strain (kN/m)	33.5	20.3	25.2	28.4	21.9	33.6	28.5	31.7	30.7
Stabilenka	Normalized Strength (kN/m)	5.9	5.6	5.3	5.7	5.8	5.4	5.4	5.4	5.3
T-100	% Strain at Peak Strength	32.6	27.9	44.0	43.8	44.0	43.9	44.1	41.6	43.9
	Normalized Secant Modulus at 10% strain (kN/m)	37.7	41.0	30.8	33.8	33.1	31.2	33.5	33.6	32.6
Typar	Normalized Strength (kN/m)	8.9	10.3	8.8	9.1	8.9	8.5	9.0	9.0	8.8
3401	% Strain at Peak Strength	53.3	31.3	43.8	48.2	17.3	16.7	40.4	43.4	42.3
	Normalized Secant Modulus at 10% strain (kN/m)	56.9	75.2	61.9	62.2	60.4	59.2	63.8	61.5	63.6
Fibretex	Normalized Strength (kN/m)	10.3	-	9.9	9.9	9.7	9.6	10.3	10.6	10.9
300	% Strain at Peak Strength	186	-	166	187	187	181	188	192	213
	Normalized Secant Modulus at 10% strain (kN/m)	6.1	7.5	7.5	5.8	4.9	6.1	4.7	5.5	5.4
Propex	Normalized Strength (kN/m)	24.2	23.7	24.4	25.4	24.7	24.2	23.3	21.3	22.9
2002	% Strain at Peak Strength	21.2	18.0	19.8	20.4	21.1	21.1	22.7	20.7	22.0
	Normalized Secant Modulus at 10% strain (kN/m)	151	163	162	162	151	148	146	144	151

I = Control, Dry Condition, 22° C (71°F)
II = Control, Dry Condition, -12°C (10°F)
III = Control, Wet Condition, 22°C (71°F)
IV = 50 Cycles Freeze/Thaw, Dry Environment, Wet Condition
V = 50 Cycles, Freeze/Thaw, Distilled Water Environment, Wet Condition
VI = 50 Cycles, Freeze/Thaw, Saline water Environment, Wet Condition
VII = 300 Cycles F/T, Dry Environment, Wet Conditions
VIII = 300 Cycles F/T, Distilled Water, Wet Conditions
IX = 300 Cycles, F/T, Saline Water Environment Wet Condition.

Note: Specimens which were subjected to freezing and thawing were cycled between -15 and +15°C (5° and 58°F).

*1 lbs/in. = 0.175 kN/m

in the machine direction. The tensile axial load versus strain relationships for the geotextiles tested at these two temperatures are shown in Figure 5.1. The error bars represent the maximum and minimum normalized loads obtained for the specimens tested. The symbol (i.e., circle, square, etc.) represents the mean normalized load obtained for the specimens tested. The breaking strength, strain at failure, and the secant modulus at 10% strain of these geotextiles are also tabulated in Table 5.1.

Decreasing the specimen temperature appeared to increase the modulus and decrease the strain at failure of the bonded and the slit film woven geotextiles. The secant modulus of Typar 3401, Stabilenka T-100, and Propex 2002 increased 32%, 8.8% and 8.4%, respectively, upon cooling to -12°C (10°F). Typar, Stabilenka, and Propex experienced a reduction of 22%, 5%, and 3% strain at failure, respectively, upon cooling. Geotextile strength increased with decreasing temperature only for the Typar 3401, in which a 16% increase in strength was observed. No other statistically significant (90% probability) variations in load-strain-strength characteristics with temperature were observed.

5.1.3 Effect of Moisture on Load-Strain Behavior

All five geotextile types (described in Table 4.1) were tensile tested in a saturated-surface-dry condition in the machine direction. The breaking strength, strain at failure, and secant modulus at 10% strain for the geotextiles tested in a saturated-surface-dry condition are presented in Table 5.1 under Condition III.

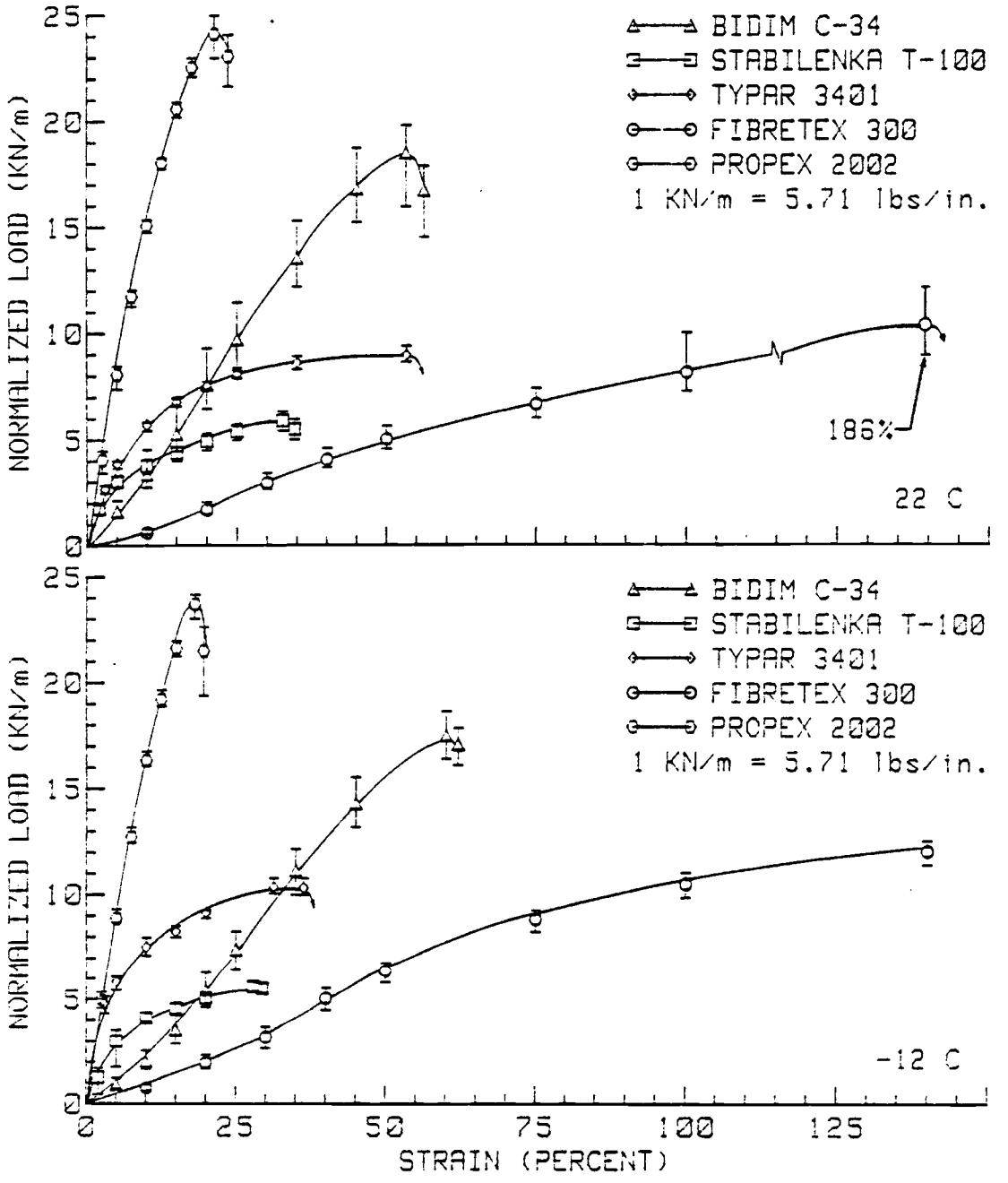

FIGURE 5.1: NORMALIZED AXIAL LOAD VS. STRAIN (DRY CONDITION).

Of the five geotextile types considered, only the polyester geotextiles exhibited changes in load-strain behavior due to moisture. The strain at failure for the Stabilenka T-100 increased from 27.9% to 44.0% upon wetting while the secant modulus decreased from 41.0 kN/m to 30.8 kN/m. The strength of the Stabilenka was not significantly affected by moisture. Though the strength, strain at failure, and secant modulus of the Bidim C-34 did not change upon wetting, the shape of the load-strain curve changed, as shown in Figure 5.2. As the Bidim C-34 was stretched in a wet condition, bundles of fibers apparently snapped loose from other bundles of fibers, resulting in an abrupt, temporary loss of load in the load-strain curve.

5.1.4 Effect of Freezing and Thawing on Load-Strain Behavior

Geotextile specimens were subjected to either 50 or 300 freeze-thaw cycles in a dry, distilled water, or saline water environment. After completion of the freeze-thaw cycles, all of the specimens were tensile tested in a saturated-surface-dry condition in the machine direction. The results of the freeze-thaw test are tabulated in Table 5.1.

The results indicate that normalized strength, percent strain at peak strength, and normalized secant modulus at 10% strain do not change appreciably when the geotextiles considered were tensile tested following 50 freeze-thaw cycles in a dry, distilled water or saline water environment. However, after 300 freeze-thaw cycles in a distilled water and a saline water environment, the strength of the

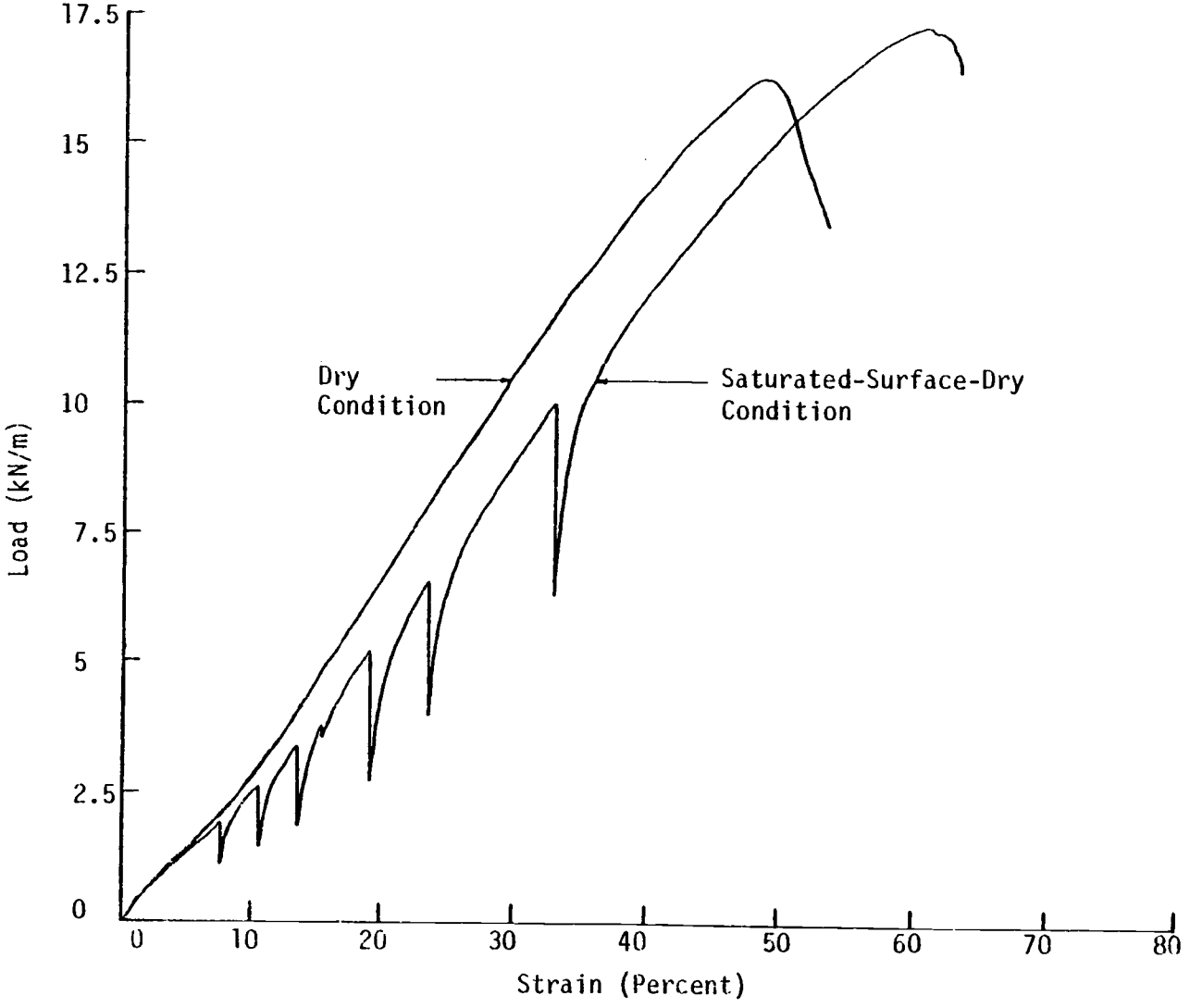

Figure 5.2: Effect of moisture on the load-strain behavior of Bidim C-34.

Propex 2002 was 12% and 6.5% less, respectively, than the strength of the geotextile (in a soaked condition) prior to freezing and thawing. An 11% decrease in the secant modulus of the Propex 2002 was also noted after 300 freeze-thaw cycles in distilled water. No other statistically significant (90% probability) deviations in the load-strain behavior of the specimens subjected to 300 freeze-thaw cycles were observed.

5.2 Creep Test Results

5.2.1 General Creep Behavior

Static creep tests were performed on the five geotextile types described in Table 4.1. All of the specimens were 150 mm (6.0 in.) wide with a grip to grip spacing of 76 mm (3.0 in.), and were oriented in the machine direction. Creep curves for all of the specimens tested are shown in Appendix B (Figures B.1 through B.7). In general, the needlepunched geotextiles exhibited the greatest short term creep strains, while the bonded and woven geotextiles exhibited the lowest short term creep strains. The polypropylene geotextiles exhibited greater short term creep strain than the polyester geotextiles, given geotextiles of the same construction. The difference in the creep characteristics of polypropylene and polyester geotextiles can be seen by either comparing the creep characteristics of Bidim C-34 and Fibretex 300 or Stabilenka T-100 and Typar 3401.

Interestingly, all of the geotextiles tested exhibited linear behavior for at least the first few minutes of creep when the creep strain was plotted as a function of the logarithm of time (see Figure 5.5). This linear behavior allowed primary creep to be characterized by a constant, logarithmic primary creep rate.

The polypropylene geotextiles exhibited the highest primary creep rates while the polyester geotextiles exhibited the lowest rates. The needlepunched geotextiles exhibited higher primary creep rates than did the bonded nonwoven or the slit film woven geotextiles. The primary creep rates are presented in Table 5.5.

Only seven failures by breaking of the specimen due to creep were noted, six of which occurred at room temperature. Both polyester geotextiles failed rapidly at room temperature at a load level of 80% of the ultimate tensile strength of the geotextiles. Failures were also noted for all three polypropylene geotextiles at room temperature at load levels of either 35% of 50% of the ultimate strength. Typar 3401 was the only geotextile which failed during the time of the test at -12°C (10°F). This failure occurred at a load level of 65% of ultimate load.

5.2.2 Effect of Load Level on Geotextile Creep

Five geotextile types (see Table 4.1) were tested at five load levels: 20%, 35%, 50%, 65%, and 80%. The load levels are expressed as a percent of the ultimate strength of each geotextile. Not all of the geotextiles were tested at all of the load levels.

At a load level of 20%, all of the geotextiles exhibited only primary creep and eventually stabilized (i.e., creep deformation stopped). The polyester geotextiles also stabilized at load levels of up to 50% at 22°C (71°F) and 65% at -12°C (10°F). The time required for a geotextile to stabilize, given in Table 5.2, appeared to be dependent on the filament polymer type and not on the geotextile construction. The load level had a variable effect on the stabilization time. In some cases the stabilization time increased with increasing load, while in other cases the stabilization time decreased.

The effect of load level on the geotextile creep strain at sixty minutes may readily be seen in Figure 5.3 and Tables 5.3 and 5.4. The increase in the sixty minute creep strain for an increase in load level from the 20% level to the 50% level, presented in Table 5.4, demonstrates the sensitivity of the various geotextiles to load level. The polypropylene geotextiles seemed to be more sensitive to increasing load at 22°C (71°F) than the polyester geotextiles. Needlepunched geotextiles showed greater sensitivity to increasing load than the bonded geotextiles, with the slit film woven geotextile exhibiting the lowest sensitivity to load. In general, the primary creep rate also demonstrated sensitivity to increasing load, though some decreases were noted, as shown in Figure 5.4 (a, b, and c) and Table 5.5.

The secondary creep rate, defined as the slope of the linear portion of a creep curve plotted using an arithmetic time scale, was very sensitive to changes in load level. The secondary creep rates for the geotextiles tested are presented in Table 5.6. The secondary creep rate of Typar 3401 increased by 300-fold when the load level was

Table 5.2: Time required for creep stabilization to occur.

Load (% of Ultimate)	Temperature (°C)	Time to Stabilization (Minutes) Bidim C-34	Stabilenka T-100	Typar 3401	Fibretex 300	Propex 2002
20	22	48,000	28,000	80,000	87,000	90,000
	-12	40,000	20,000	45,000	50,000	75,000
35	22			N.S.		N.S.
	-12					
50	22	30,000	30,000	N.S.	N.S.	N.S.
	-12	10,000	10,000	N.S.	N.S.	N.S.
65	22	N.S.*	N.S.		N.S.	
	-12	10,000	25,000	N.S.	N.S.	N.S.

*Specimens did not stabilize.

Table 5.3: Sixty minute creep strain.

Load (% of Ultimate)	Temperature (°C)	Creep Strain at Sixty Minutes (%) Bidim C-34	Stabilenka T-100	Typar 3401	Fibretex 300	Propex 2002
20	22	8.97	.80	2.08	20.7	2.87
	-12	12.7	1.09	1.99	13.1	2.50
35	22			7.14		7.97
	-12					
50	22	26.6	8.74	17.7	91.0	15.7
	-12	27.8	6.79	4.94	38.3	6.04
65	22	37.0	21.0		138	
	-12	34.5	10.9	10.8	54.1	9.70

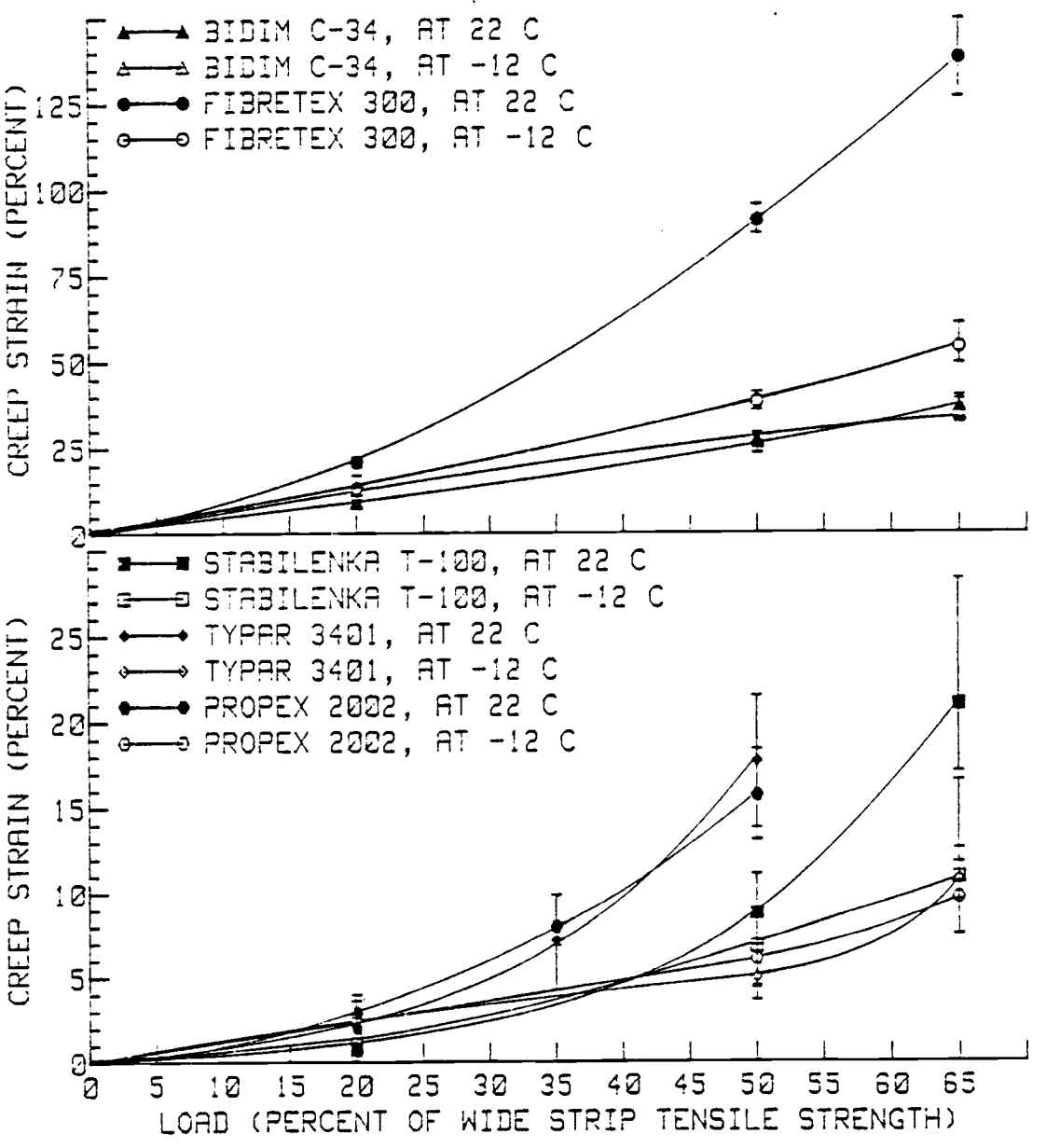

FIGURE 5.3: SIXTY MINUTE CREEP STRAIN VS. LOAD LEVEL.

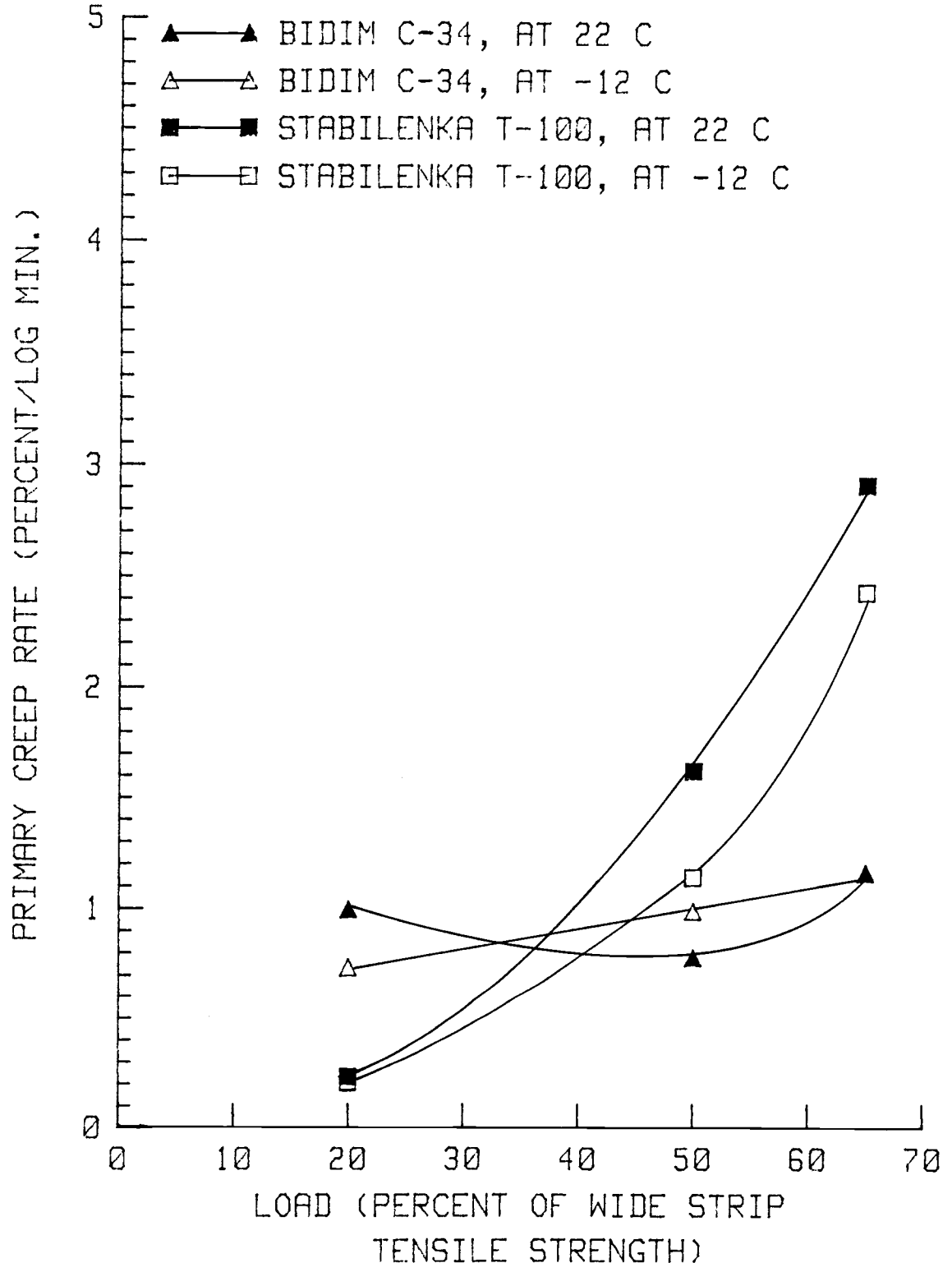

FIGURE 5.4(a): PRIMARY CREEP RATE VS. LOAD LEVEL.

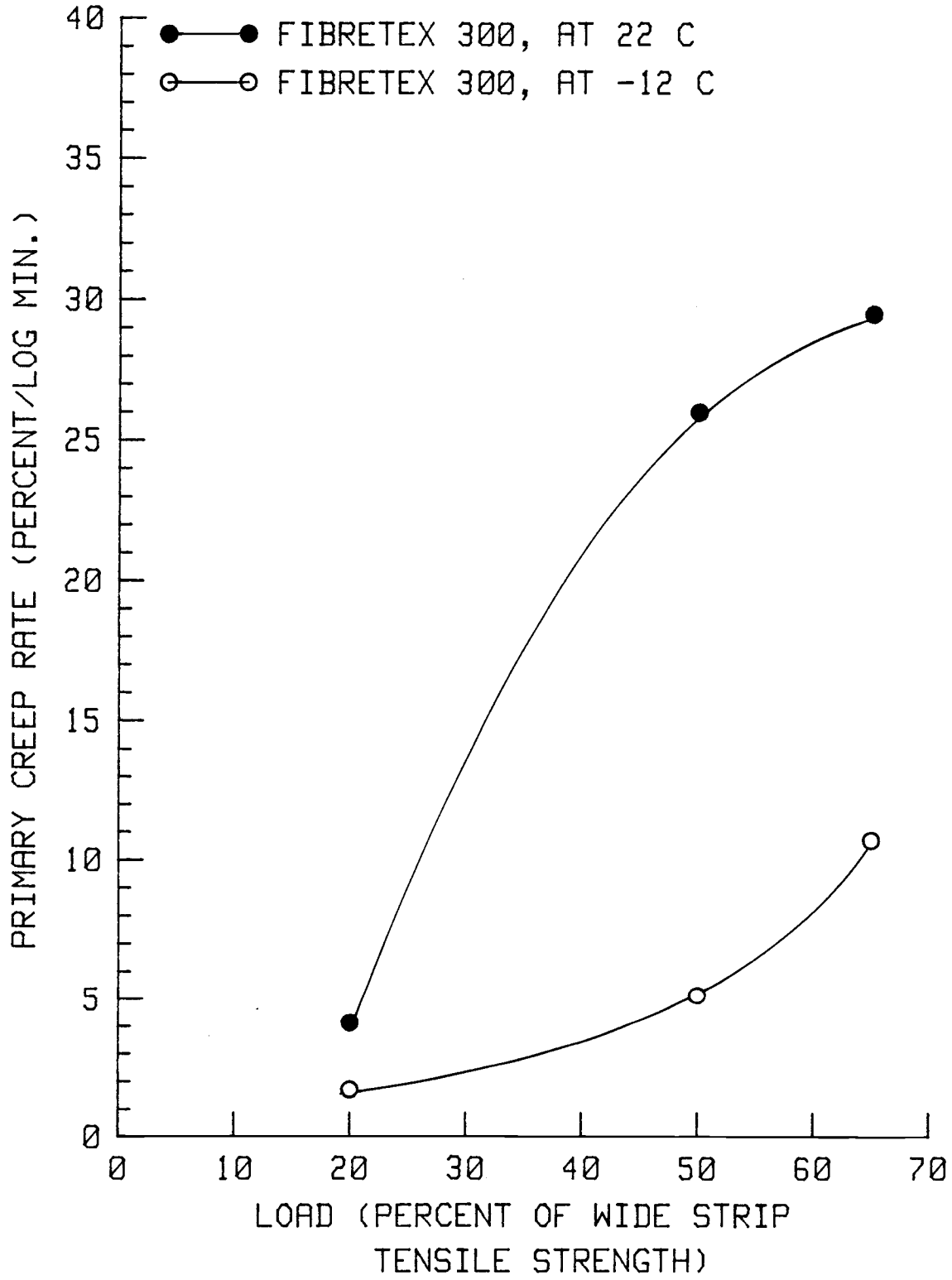

FIGURE 5.4(b): PRIMARY CREEP RATE VS. LOAD LEVEL.

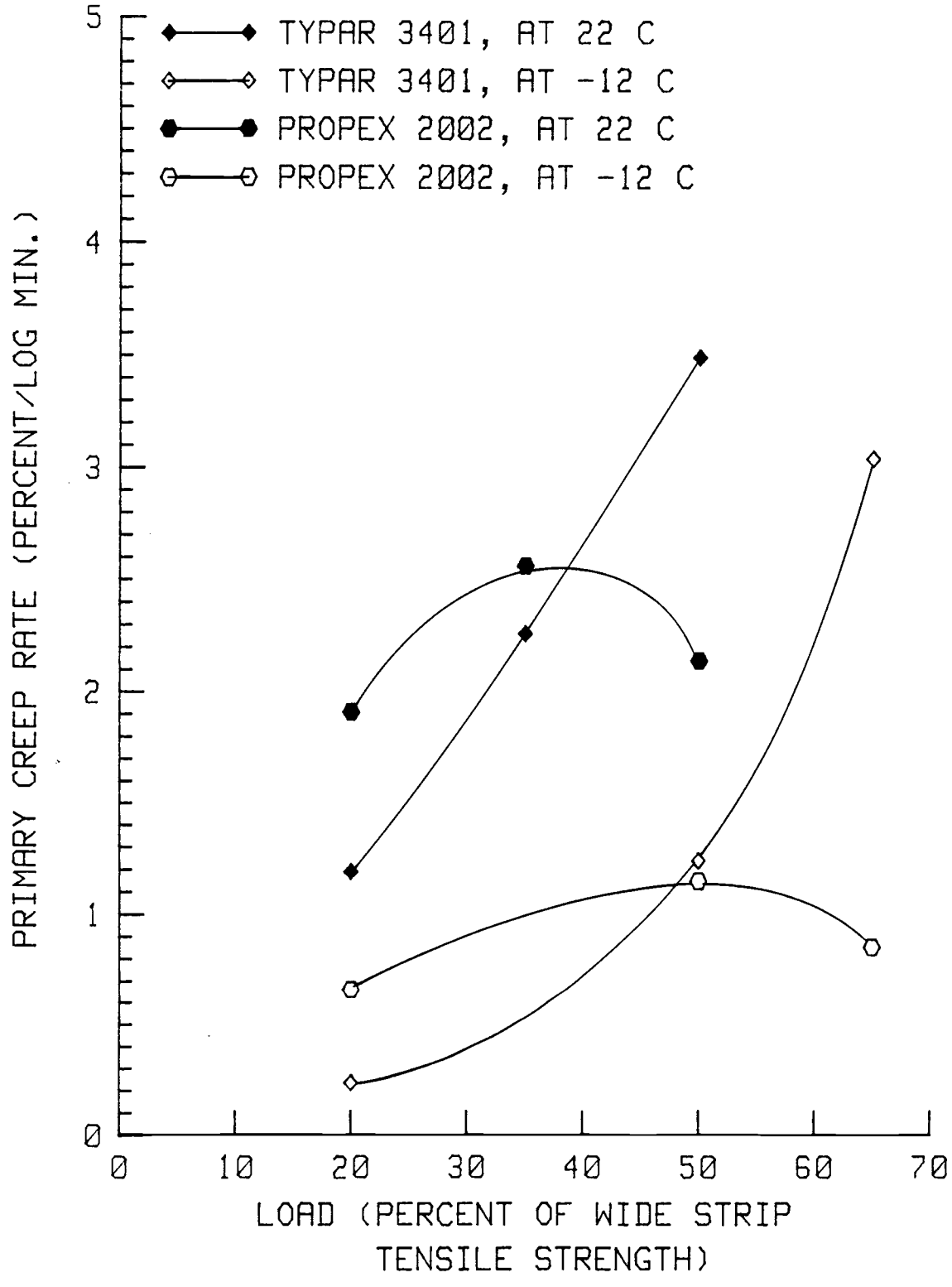

FIGURE 5.4(c): PRIMARY CREEP RATE VS. LOAD LEVEL.

Table 5.4: Increase in percent creep strain at sixty minutes for a load level increase of 30% (from a load level of 20% to a load level of 50%).

Temperature (°C)	Increase in % Creep Strain (20% to 50% Load Level)				
	Bidim C-34	Stabilenka T-100	Typar 3401	Fibretex 300	Propex 2002
22	17.6	7.9	15.6	70.2	12.8
-12	15.1	5.7	2.9	25.2	3.5

Table 5.5: Primary logarithmic creep rate at four load levels.

Load (% of Ultimate)	Temperature (°C)	Primary Logarithmic Creep Rate (%/log minutes)				
		Bidim C-34	Stabilenka T-100	Typar 3401	Fibretex 300	Propex 2002
20	22	.995	.231	1.19	4.12	1.91
	-12	.734	.307	.236	1.70	.662
35	22			2.26		2.56
	-12					
50	22	.780	1.62	3.49	26.0	2.14
	-12	.989	1.14	1.24	5.14	1.15
65	22	1.16	2.91		29.5	
	-12	1.16	2.43	3.04	10.7	.855

Table 5.6: Secondary creep rate.

Load (% of Ultimate)	Temperature (°C)	Secondary Creep Rate (%/minute) Bidim C-34	Stabilenka T-100	Typar 3401	Fibretex 300	Propex 2002
20	22	0	0	0	0	0
	-12	0	0	0	0	0
35	22			.0000670		.000158
	-12					
50	22	0	0	.0208	.000267	.0422
	-12	0	0	.0000247	.000150	.0000309
65	22	*	*[1]		.00593	
	-12	0	0	.000329	.000455	.000715

[1] Secondary creep was not observed within the time allowed for the test.

Table 5.7: Creep failure times for five geotextile types.

Load (% of Ultimate)	Temperature (°C)	Time to Failure (minutes) Bidim C-34	Stabilenka T-100	Typar 3401	Fibretex 300	Propex 200
35	22					186,000
	-12					
50	22			600		180
	-12					
65	22				7,560	
	-12			62,000		
80	22	1	1			

increased from 35% to 50% of the ultimate load, whereas only a 20-fold increase was observed for Fibretex 300. Similarly, a decrease in load level from 50% to 35% caused the time required for secondary creep to begin to increase by as much as 270-fold, as was noted for Propex 2002, or by as little as 30-fold, as for Fibretex 300 (see Table 5.8). The effect of load on the secondary creep rate of the polyester geotextiles could not be determined, as the polyester geotextiles did not exhibit secondary creep within the time allowed for the test.

The time required for the occurrence of creep failure by rupture, presented in Table 5.7, tended to increase dramatically with decreasing load. For example, the failure time for Propex 2002 increased 1000-fold when the load level was decreased by 15% of the ultimate load, from 50% to 35%. However, since so few failures were actually recorded, trends could not be well established.

5.2.3 Effect of Temperature on Geotextile Creep

All five geotextile types were tested at two temperatures: 22°C (71°F) and -12°C (10°F). The effect of temperature on geotextile creep may be observed by comparing geotextiles of the same construction but of different polymer type. For example, in Figure 5.5 the creep curves of the two needlepunched geotextiles, Bidim C-34 and Fibretex 300, are plotted together. At 22°C (71°F), the polypropylene geotextile exhibited much greater creep than the polyester geotextile. At -12°C (10°F), however, the creep of the polypropylene geotextile was reduced to that of the polyester geotextile, while the creep of the polyester geotextile changed little with decreasing temperature.

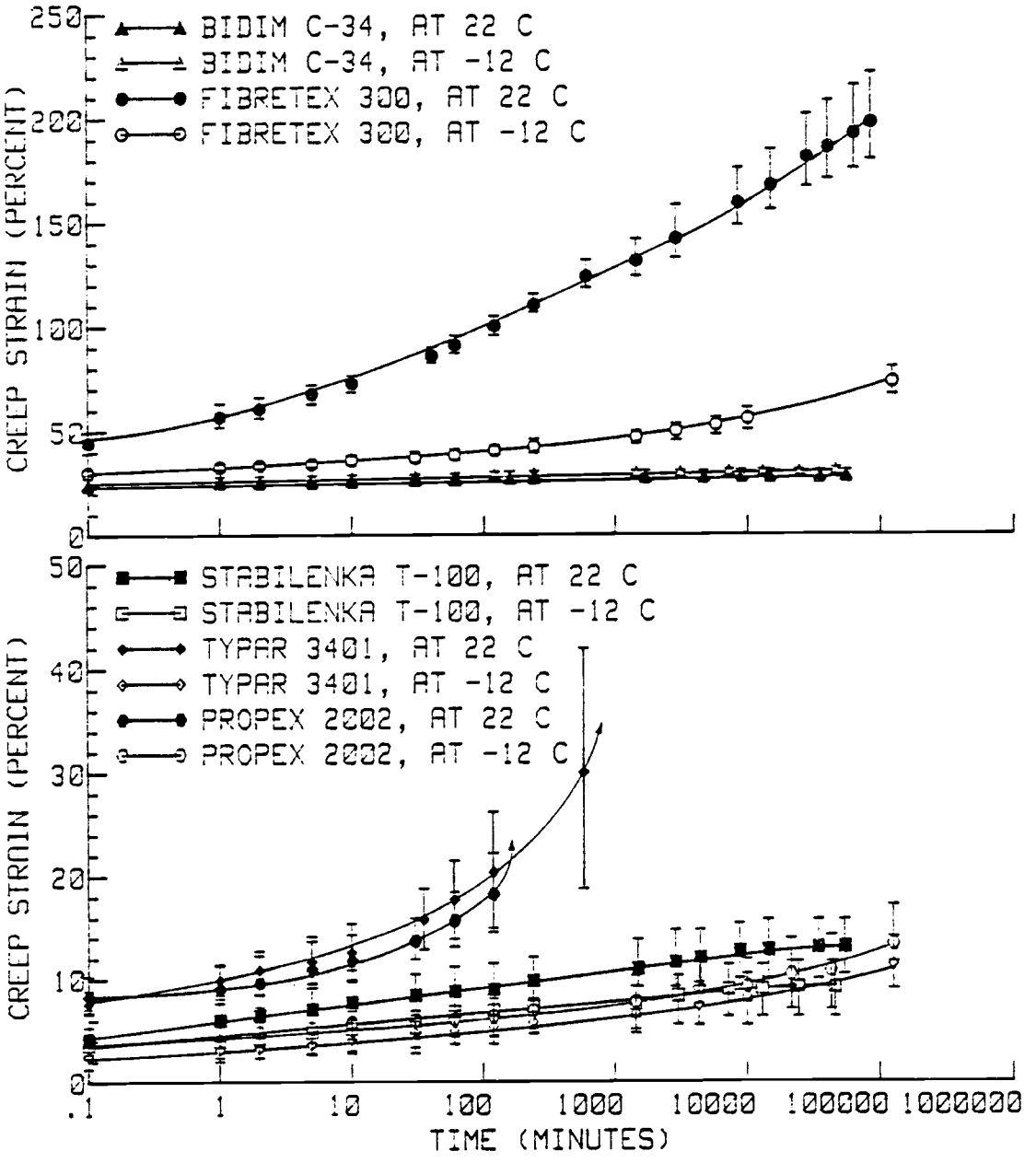

FIGURE 5.5: CREEP STRAIN VS. TIME AT 50% WIDE STRIP TENSILE STRENGTH.

Figure 5.3 shows that the dramatic reduction in the creep of the polypropylene geotextiles at sixty minutes with decreasing temperature occurred only at load levels of 35% of ultimate or above. At a load level of 20% of the ultimate strength, the decrease in creep strain with temperature was not statistically significant (90% probability) for any geotextile.

The time required for stabilization to occur was somewhat reduced due to decreasing temperature at a load level of 20% of the ultimate strength. Creep stabilization times are presented in Table 5.2. The percent reduction in stabilization time which occurred when the temperature was lowered from 22°C (71°F) to -12°C (10°F) varied from 17% for Bidim C-34 to 43% for Fibretex 300. This reduction in stabilization time indicates that the creep strain at a load level of 20% of ultimate strength may be influenced by temperature, but that a period of time greater than sixty minutes is required for the effect to become noticeable.

The primary creep rate generally decreased with decreasing temperature, though the primary creep rate of Bidim C-34 actually increased or remained the same when the temperature decreased. As may be seen in Figure 5.4 (a, b and c) and Table 5.5, the primary creep rate of the polypropylene geotextiles was most affected by temperature, with percent decreases as great as 80% being observed. The primary creep rate of Stabilenka T-100 exhibited a modest decrease of approximately 20% when the temperature was lowered.

The secondary creep rate of the polypropylene geotextiles decreased dramatically with decreasing temperature, as may be observed in Table 5.6. The ratio of the secondary creep rate at 22°C (71°F) to

the rate at -12°C (10°F) was as great as 1400:1 for Propex 2002 and as small as 13:1 for the Fibretex 300. Below freezing temperature also reduced the effect of the load level on the secondary creep rate. For example, at 22°C (71°F) an increase in load level of 15% of the ultimate strength increased the secondary creep rate of Typar 3401 by 300-fold. At -12°C (10°F), however, this increase in load produced only a 2-fold increase in the secondary creep rate of Typar 3401, indicating that decreasing the temperature greatly reduces the effect of load on the secondary creep rate.

The time required for secondary creep to begin increased 300-fold for Typar 3401 and Propex 2002 when the temperature was dropped to -12°C (10°F). However, the time required for secondary creep to begin was actually lower at -12°C (10°F) than it was at 22°C (71°F) for the Fibretex 300 (see Table 5.8).

The time required for rupture to occur seemed to increase with decreasing temperature, as shown in Table 5.7. The effect of temperature on the strain at failure could not be established, however, as only one creep failure was observed at -12°C (10°F).

5.2.4 Creep Failure Trends

The ability to predict the occurrence of creep failure based on parameters which may be obtained from a short term creep test is certainly desirable. However, a relationship between the primary or secondary creep rate and the occurrence of failure was not clear since so few specimens actually failed. No failures were observed for specimens which had a secondary creep rate below .0001% strain/minute.

Table 5.8: Time required for secondary creep to begin.

Load (% of Ultimate)	Temperature (°C)	Time to Beginning of Secondary Creep (minutes) Bidim C-34	Stabilenka T-100	Typar 3401	Fibretex 300	Propex 2002
20	22	S	S	S	S	S
	-12	S	S	S	S	S
35	22			27,000		17,000
	-12					
50	22	S	S	124	40,700	62
	-12	S	S	33,000	18,000	24,000
65	22	*	*		1,480	
	-12	S	S	10,200	10,000	400

S-Specimens stabilized.
*-Secondary creep was not observed within the time allowed for the test.

Table 5.9: Failure strains for creep and load-strain tests.

Load (% of Ultimate)	Temperature (°C)	Strain At The Beginning of Tertiary Creep (%)[1] Bidim C-34	Stabilenka T-100	Typar 3401	Fibretex 300	Propex 2002
Creep Tests						
35	22					43.3
	-12					
50	22			41.9		20.0
	-12					
65	22				227.3	
	-12			52.5		
Width of Specimen		Strain at Maximum Load for Load-Strain Tests (%)[2]				
200 mm	22	53.2	32.6	53.3	186	21.2
150 mm	22	54.9	32.9	49.0	226	21.6
200 mm	-12	60.0	27.9	31.3		18.0

[1] The failure strain for creep was defined to be the strain at the beginning of tertiary creep.
[2] The failure strain for load-strain tests was defined to be the strain at the maximum load.

If the specimens which did not fail were allowed to creep for longer periods of time, failures preceded by lower secondary creep rates may have been observed.

The failure strain of several specimens was nearly equal to the failure strain obtained in a load-strain test, as shown in Table 5.9. However, for the Propex at a load level of 35% of the ultimate strength (at room temperature), the failure strain was twice as large as the failure strain obtained for the load-strain test (see notes accompanying Table 5.9 for definition of "failure"). For extremely short failure times, such as that which occurred for Typar 3401 and Propex 2002 at a load level of 50% and room temperature, the failure strains appeared to be slightly lower than the strains obtained in the load-strain tests. In general, as the time to failure increased, the strain at failure appeared to increase.

5.3 Frost Heave Test Results

As described in Section 4.4, a geotextile layer was placed inside a soil specimen which was known to be frost-susceptible. A frost heave test was performed on the soil specimen, and the heaving which resulted was compared with the frost heave which was exhibited by a soil specimen which did not have a geotextile layer. All five of the geotextile types described in Table 4.1 were considered in the program. The same soil was used for all of the frost heave tests.

The frost penetration rates as well as the heave rates of soil specimens with and without a geotextile layer are presented in Table 5.10. All of the geotextile types tested except the Stabilenka T-100

reduced the heave rate of the soil. The heave rate of the soil was actually greater with the layer of Stabilenka T-100 than without the layer.

The percent reduction due to the geotextile layer of the heave rate and the volume of water drawn into the soil specimen (due to heaving) is presented in Table 5.11. The Fibretex 300 reduced the heave rate the greatest amount while the Typar 3401 had the greatest reduction in water content. Bidim C-34 also showed substantial reductions. Propex 2002 reduced the heave rate and the water content increase due to heaving only moderately. Though the average water content of the soil above the freezing line was slightly reduced with the layer of Stabilenka T-100 in place, the heave rate was actually 22.4% greater with the geotextile layer.

The dramatic difference in the effectiveness of each of the geotextiles as capillary barriers may be observed in Figures 5.6, 5.7, 5.8, 5.9, and 5.10. The water content data for these geotextiles are also presented in Appendix D. The profile of the water content versus depth in the soil specimen with and without the geotextile layer are nearly identical for the Stabilenka, while the Bidim, Typar and Fibretex prevented the water content profile from changing appreciably from its initial state.

Table 5.10: Frost penetration and heave rates for soil specimens with and without a geotextile layer.

Geotextile Type	Frost Penetration Steady State Rate (mm/hr)	Heave Rate (mm/hr)		
		No Water Supply	With Geotextile Layer	Without Geotextile Layer
Bidim C-34	0.914	0.076	0.18	0.46
Stabilenka T-100	0.584	0.013	0.56	0.46
Typar 3401	2.49	0.033	0.12	0.54
Fibretex 300	2.11	0.079	0.13	0.43
Propex 2002	1.75	0.081	0.32	0.58

Table 5.11: Reduction in heave rate and volume of water drawn into soil specimen (above the plane of the geotextile layer) due to geotextile layer.

Geotextile Type	Reduction in Heave Rate Due to Geotextile Layer (%)	Reduction in Volume of Water Drawn into Soil Specimen Due to Geotextile Layer (%)
Bidim C-34	72.9	25
Stabilenka T-100	-22.4*	3
Typar 3401	82.8	33
Fibretex 300	85.5	23
Propex 2002	52.1	18

*Heave rate increased with the geotextile layer.

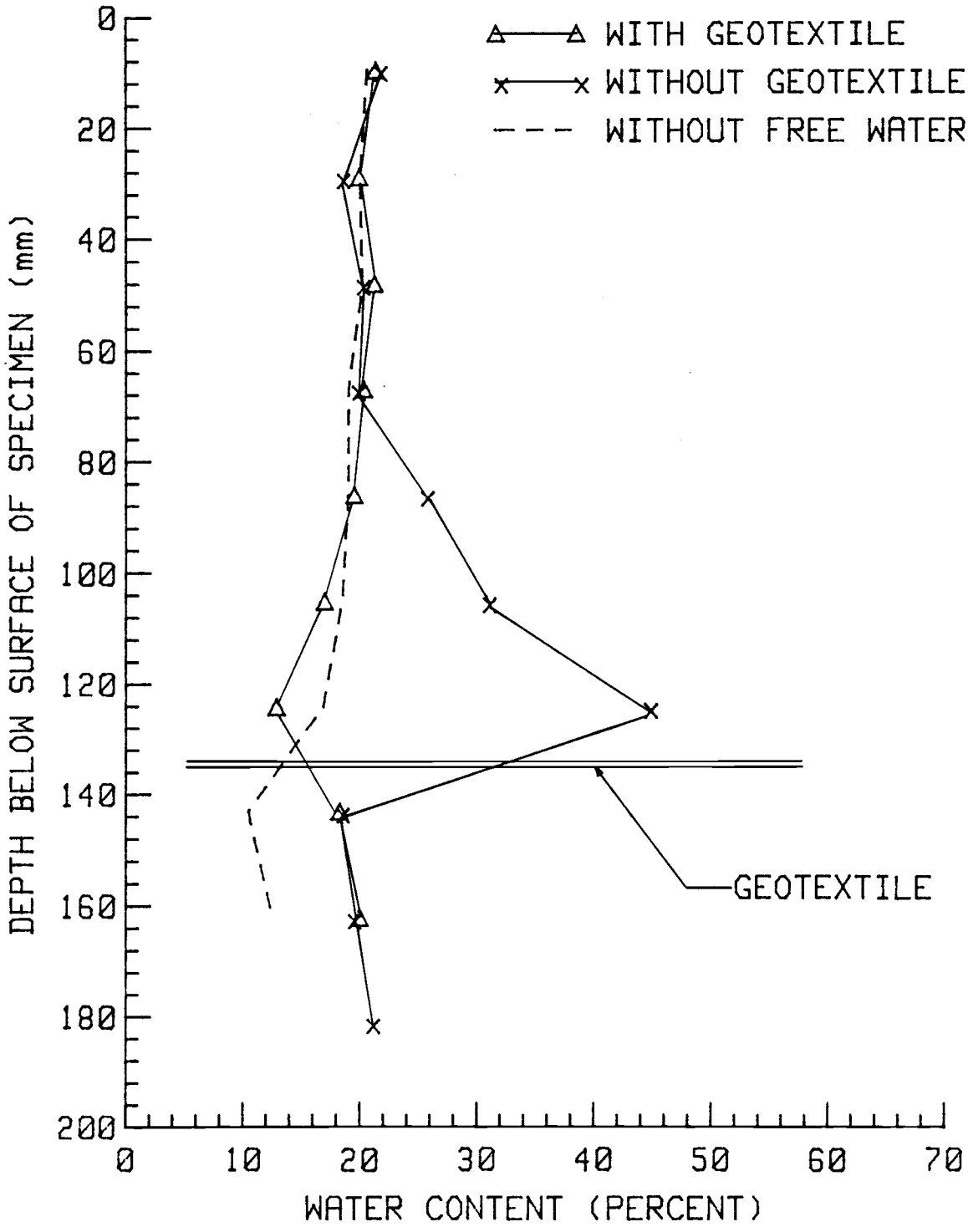

FIGURE 5.6: SOIL WATER CONTENT PROFILES AFTER FREEZING FOR SPECIMENS WITH AND WITHOUT LAYER OF BIDIM C-34.

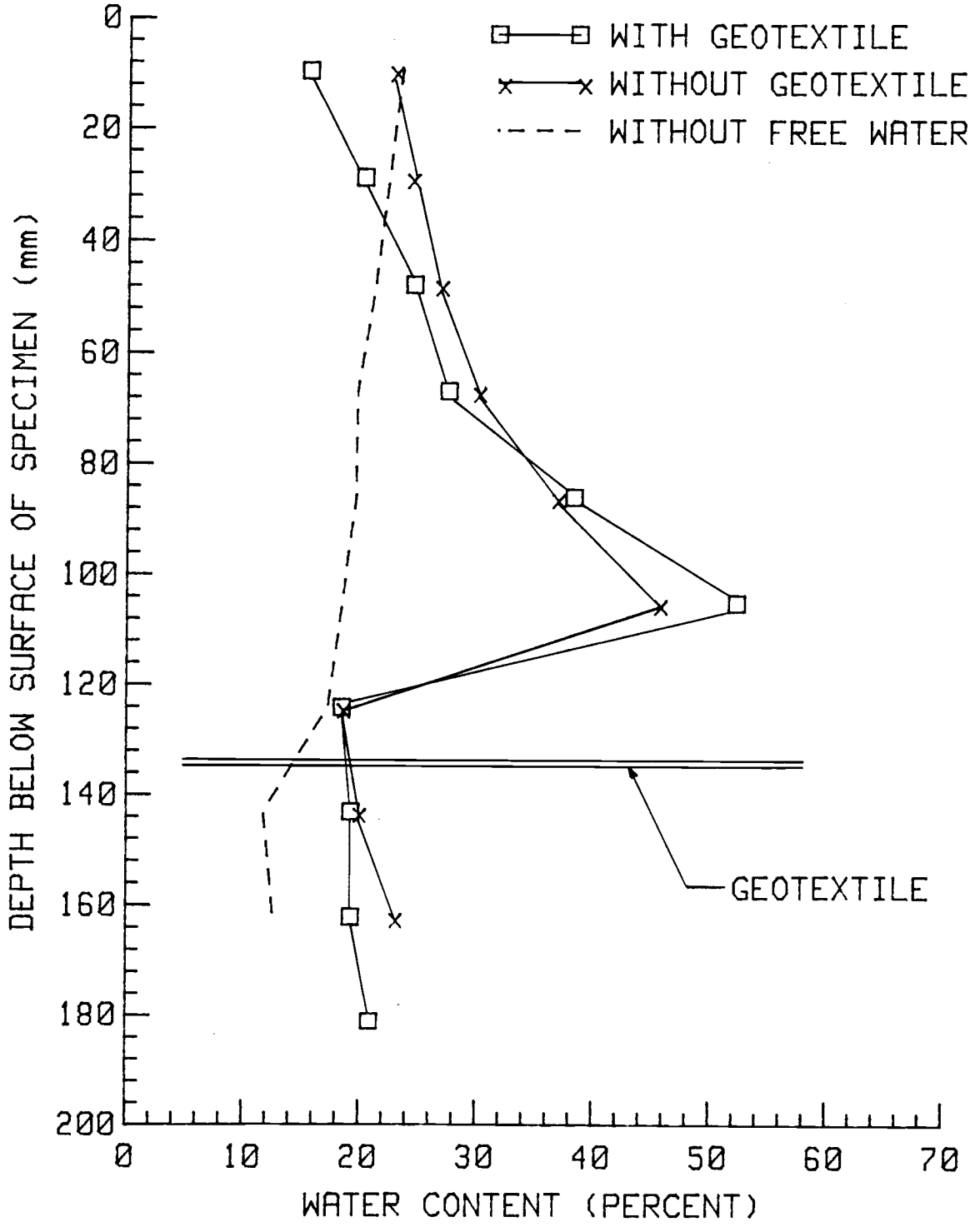

FIGURE 5.7: SOIL WATER CONTENT PROFILES AFTER FREEZING FOR SPECIMENS WITH AND WITHOUT LAYER OF STABILENKA T-100.

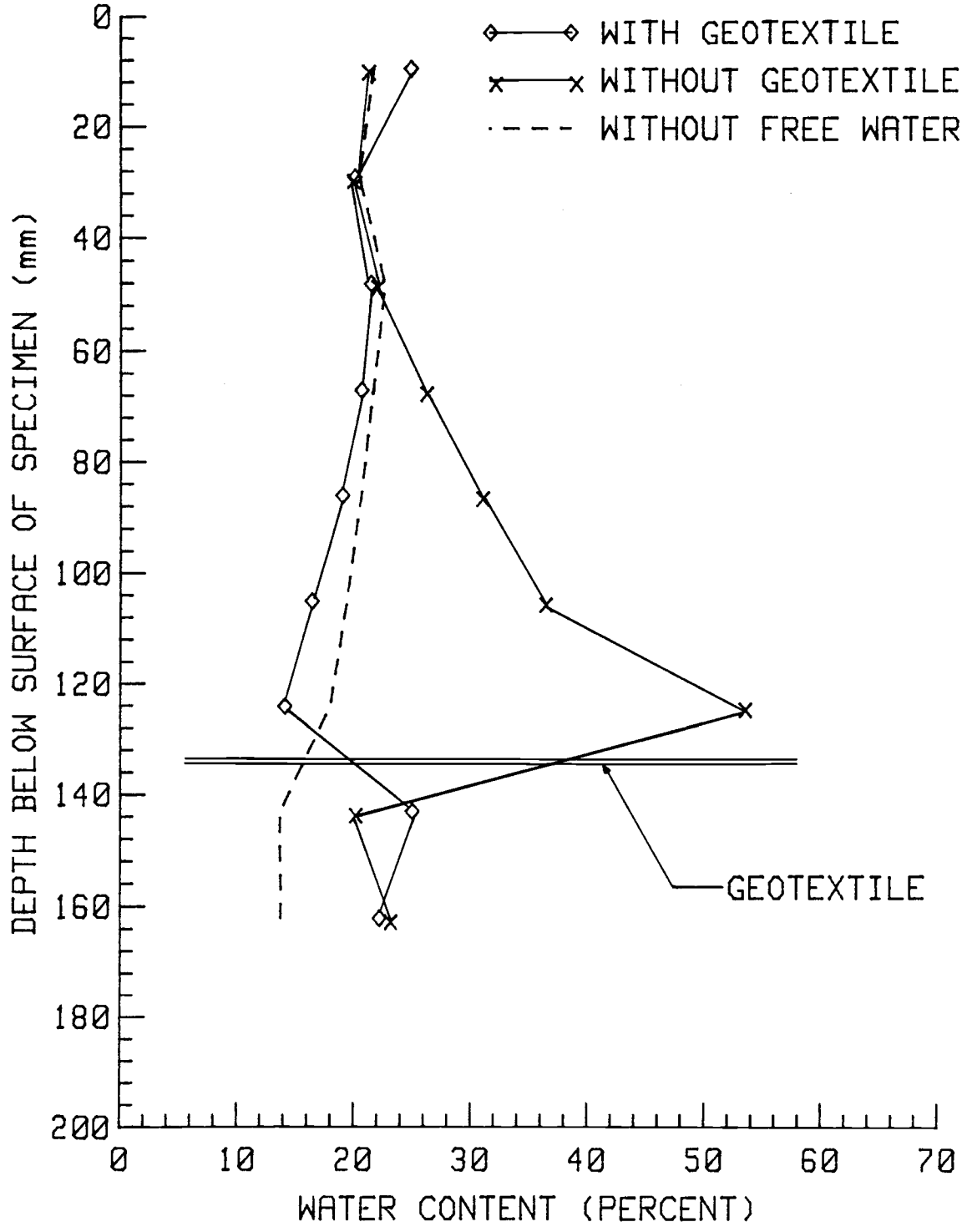

FIGURE 5.8: SOIL WATER CONTENT PROFILES AFTER FREEZING FOR SPECIMENS WITH AND WITHOUT LAYER OF TYPAR 3401.

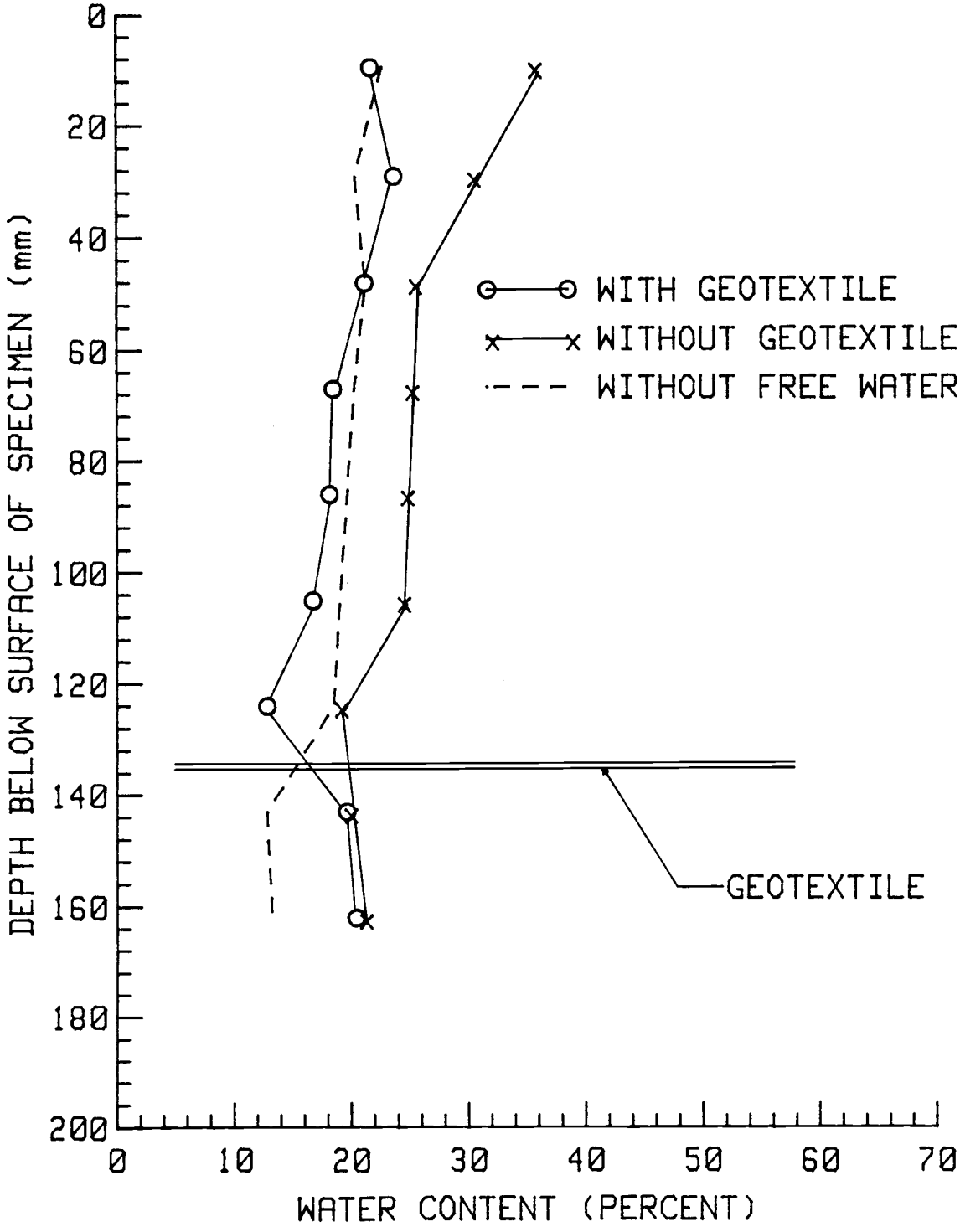

FIGURE 5.9: SOIL WATER CONTENT PROFILES AFTER FREEZING FOR SPECIMENS WITH AND WITHOUT LAYER OF FIBRETEX 300.

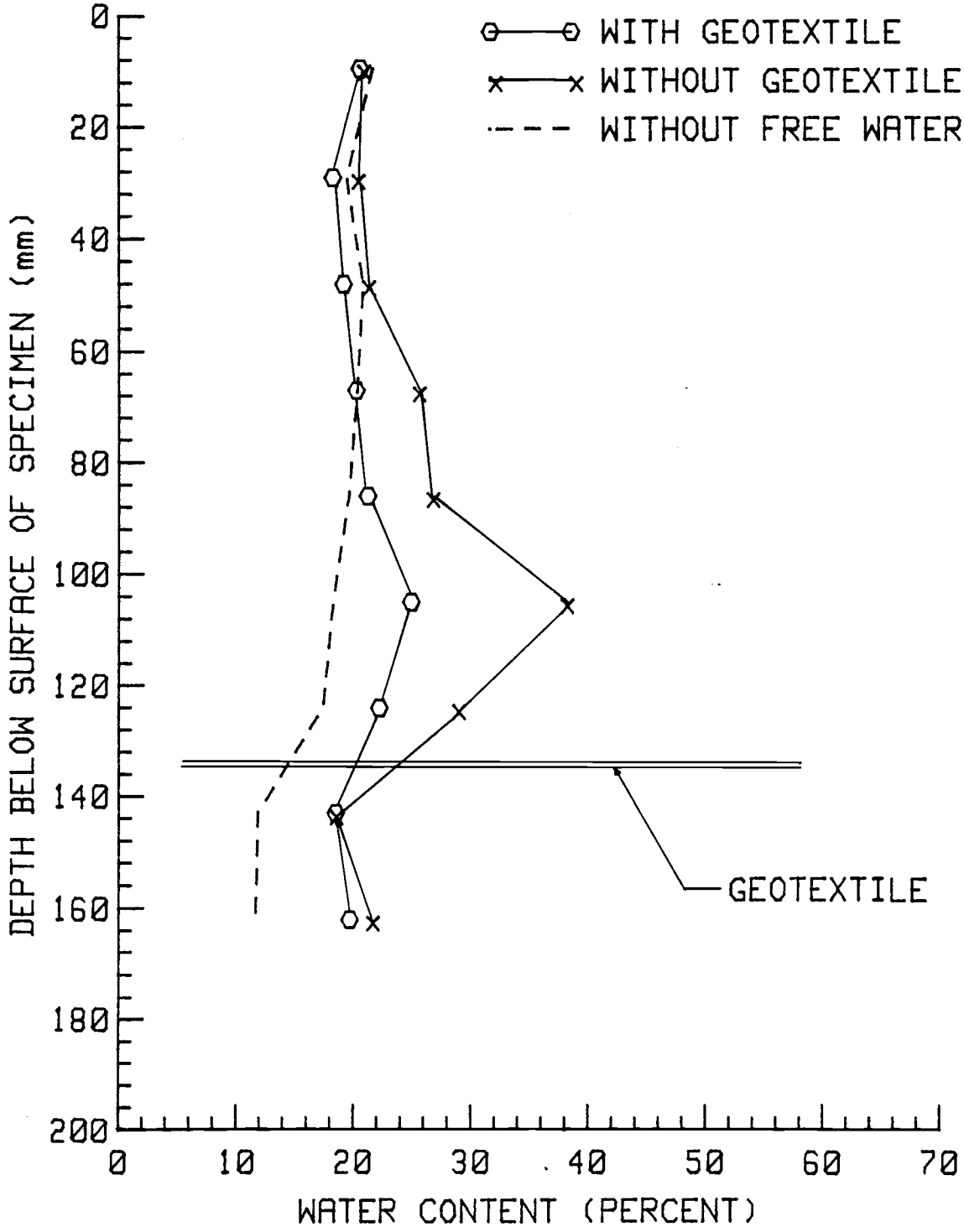

FIGURE 5.10: SOIL WATER CONTENT PROFILES AFTER FREEZING FOR SPECIMENS WITH AND WITHOUT LAYER OF PROPEX 2002.

6.0 DISCUSSION OF TEST RESULTS

6.1 Tensile Test Results

The effect of temperature on the load-strain-strength behavior of geotextiles may be discussed in terms of the filament material and the structure of the geotextile.

The modulus and strain at failure of the polypropylene geotextiles were more affected by temperature changes than that of the polyester geotextiles. Calhoun (15) also noted that decreasing the temperature increased the modulus and decreased the strain at failure of the polypropylene geotextiles. Information concerning the effect of temperature on the load-strain behavior of polyester geotextiles was not available. The decrease upon cooling in the ability of the geotextile to elongate under a tensile load is to be expected, considering that the glass transition temperature for polypropylene is about 0°C (32°F), which is between the two temperatures at which the geotextiles were tested. The molecular mobility of the polymer changes at the glass transition temperature.

With the exception of the Typar, in which a modest 16% strength increase was observed, the strength of the polypropylene geotextiles did not increase with decreasing temperature. Calhoun (15) and the supplier of Mirafi 140 (51) also noted that geotextile strength did not increase significantly with decreasing temperature. The reason for the slight increase in strength of the Typar 3401 upon cooling was not clear.

The presence of moisture affected only the polyester geotextiles, increasing the elongation of the Stabilenka under a tensile load and changing the shape of the load-strain curve for the Bidim (see Figure 5.2). Absorption of water into the filaments themselves probably accounts for this effect. Polyester will absorb about 0.5% water, while the absorption of water by polypropylene is nil (44). Koerner, et al. (44) concluded that any observed effect of moisture on geotextile load-strain behavior is most likely due to the effect of moisture on the bonding mechanisms between geotextile filaments. The load-strain behavior of the Bidim and the Stabilenka appears to support this conclusion. The amount of water held within the polyester filaments is most likely not enough to affect the load-strain behavior of the filaments. However, there may be enough water held within the filaments to act as a lubricant, allowing the filaments to slide past one another more easily.

Freeze-thaw cycles in a fresh or saline water environment did not adversely affect the load-strain characteristics of the five geotextiles tested. The results obtained by Calhoun (15) support the results obtained in the present study (see Table 2.4). Though the Propex did seem to lose some of its strength after being subjected to 300 freeze-thaw cycles, this strength loss was only 12%. Since many years would be required to obtain 300 freeze-thaw cycles in the Arctic environment, the 12% strength loss is of little concern from a practical standpoint.

6.2 Creep Test Results

The creep behavior of the geotextiles tested was a function of both the geotextile filament material and the geotextile construction.

The geotextile construction dominated the primary stage of creep. The needlepunched geotextiles exhibited the greatest creep strains during this primary stage of creep, while the bonded nonwoven and slit film woven geotextiles exhibited the lowest creep strains. The effect of geotextile structure on primary creep may be explained in terms of the ability of the individual filaments within the geotextile to reoriente in the direction of the applied load. The filaments within the needlepunched geotextiles are held together by only fiber to fiber friction and entanglement. Therefore, the filaments are relatively free to move and can straighten and become reoriented in the direction of the applied load. However, the filaments within the bonded geotextiles are held together at many locations along the length of the filament. Therefore, only a relatively short section of the filament can reorient and straighten out in the direction of the applied load. Since the filaments within the slit film woven geotextile are already oriented in the direction of the applied load, only a small amount of the deformation which occurs for the slit film woven geotextile may be attributed to reorientation of the filaments.

Finnigan (25) also observed that increasing the amount that the filaments are plied (twisted together) increased the amount of creep observed initially. Observations from the present study obviously support the results obtained by Finnigan.

The primary creep rate was also affected by geotextile structure, with the needlepunched geotextiles exhibiting the highest primary creep rates. Fiber reorientation seems to be a time-dependent process which occurs throughout the primary stage of creep, with the rate of fiber reorientation decreasing with time.

Though the rate of primary creep was dominated by the geotextile structure, the filament material and the specimen temperature also influenced the primary creep rate. Given two geotextiles with the same structure, the polypropylene geotextile exhibited a higher primary creep rate than the polyester geotextile at the 22°C (71°F) test temperature.

In general, the polypropylene geotextiles exhibited greater creep strains and creep rates than the polyester geotextiles at 22°C. The results obtained by other researchers (5, 73) agree with this observation.

The greatest influence of the filament material was in the later stages of creep. The secondary creep rate appeared to be a function of the filament polymer only. This observation is reasonable considering that most of the filament reorientation which will occur has already taken place by the time the secondary stage of creep is reached, and the only additional deformation that can occur must result from deformation or rupture of the filaments themselves.

Significant differences in the secondary creep rates of the three polypropylene geotextiles were observed. The Fibretex exhibited a significantly lower secondary creep rate than the other two polypropylene geotextiles. Since the Fibretex had the highest primary creep rate of the geotextiles tested, one would suspect that the secondary

creep rate of the Fibretex would also be the highest of the geotextiles tested, if the structure of the geotextile was influencing secondary creep. Since the Fibretex exhibited the lowest secondary creep rate, one must conclude that the structure of the geotextiles is not the cause of the observed differences in the secondary creep rates of the geotextiles.

Differences in the molecular structure of the filaments themselves may be causing the observed differences in the secondary creep rates of the three polypropylene geotextiles. The molecular structure of a polymeric filament, and its creep behavior, are strongly influenced by the drawing ratio of the filament (discussed in Section 2.4.2; see also Figure 2.16). Therefore, variations in the drawing ratios of the filaments of the various geotextiles may account for the differences in the secondary creep rates observed. Since the actual drawing ratios of these geotextiles were not available, this conclusion must be considered tentative until more is known about the variation from geotextile to geotextile of the filament drawing ratio.

Secondary creep was only observed at load levels above 20% of the ultimate strength for the polypropylene geotextiles. At a load level of 20%, the polypropylene geotextiles stabilized. Secondary creep was not observed for either of the polyester geotextiles. If the creep tests were allowed to continue for a longer period of time, secondary creep may have been observed at load levels above 50%. At a load level of less than or equal to 50%, the polyester geotextiles stabilized. Finnigan (25) also noted that polyester filaments would creep very little at load levels of 50% or below. Therefore, one may conclude that creep rupture is not likely if polypropylene geotextiles

are loaded to less than 20% and polyester geotextiles to less than 50% of their ultimate load.

Finnigan (25) noted that the primary creep rate of individual polyester filaments, as well as that of a polyester fabric, did not increase beyond a load level of 25% of the breaking load. This trend was not observed for the polyester geotextiles considered in the present study. Finnigan further noted that the transition from a primary creep rate which increased with load to a primary creep rate which is independent of the load level was somewhat less distinct for filaments which were plied than for filaments tested individually. These observations suggest that the large amount of plying and entanglement existing within the geotextile types tested almost completely masked the behavior of the primary creep rate of the individual filaments observed by Finnigan. Therefore, geotextile structure obviously plays an important role in determining the magnitude of the primary creep rate.

The time required for secondary creep to begin, and the secondary creep rate, were observed to be extremely sensitive to changes in load level. The time required for creep rupture to occur also reflects this sensitivity of secondary creep to changes in load level, as small changes in load caused changes of several orders of magnitude in the failure time. Tests performed by the plastics industry and summarized by Ogorkiewicz (55) also exhibited this "logarithmic" dependence of failure time on the stress level (see Figure 2.14).

As would be expected, the effect of temperature on creep was observed to be primarily a function of the filament polymer and not the geotextile construction. The effect of temperature on polypro-

pylene geotextiles versus that of polyester geotextiles may be explained in terms of the glass transition temperature and the "Principle of Corresponding States."

As explained in Section 2.4.3, changes in the polymer viscoelastic response to load with temperature below the glass transition are more gradual than the changes in this response with temperature above the glass transition, since so few molecular modes of motion are available below the glass transition. The "Principle of Corresponding States" relates these different viscoelastic responses to the glass transition temperature. Given that the glass transition temperature of polypropylene is approximately 0°C (32°F) and that of polyester is approximately 110°C (230°F), this principle may be applied as follows: the viscoelastic response of polypropylene at -12°C (10°F) is similar to that of polyester at 98°C (208°F), and at 22°C (71°F) the viscoelastic response of polypropylene is similar to that of polyester at 132°C (270°F). This principle appears to explain the dramatic reduction in creep of the polypropylene geotextiles upon cooling to -12°C (10°F) and the lack of change of the viscoelastic response of the polyester geotextiles upon cooling.

Below freezing temperature not only reduced the magnitude of the creep obtained for polypropylene geotextiles, but the rate at which these deformational processes occurred was also reduced dramatically (see Tables 5.5, 5.6 and 5.7). These decreased creep rates may explain why only one geotextile, Typar, failed at -12°C (10°F) at a load level of 65%. Perhaps, if the creep tests were conducted for longer periods of time, a greater number of creep failures would have been observed at -12°C (10°F).

In general, below freezing temperatures do not adversely affect the creep characteristics of geotextiles. For polypropylene geotextiles, the magnitude of the creep is reduced and the failure time is increased due to below freezing temperatures.

6.3 Creep Failure Trends

The objective of predicting rupture failure due to creep is to determine the critical (maximum) load level to which a geotextile may be subjected in the field without the occurrence of creep rupture within the design life of the soil/geotextile structure. Direct determination of the critical load level is difficult. With extensive creep testing of a given geotextile type a critical load level may be determined in the laboratory. However, the relationship between the laboratory results and field performance would be unknown.

Theoretical solutions to the problem of creep failure prediction for even an isolated geotextile filament have not been obtained due to the complexity of the molecular structure of a polymer which has been "drawn" (see Section 2.4). Theories which can model primary and secondary creep behavior, such as the Rate Process Theory, have been used to model geotextile creep with some success (66). However, Rate Process Theory requires that at least two creep tests for each geotextile type in question be carried out long enough to establish the secondary creep rate. As may be seen in Table 5.8, to establish the secondary creep rate, at least one month or more is required for a geotextile specimen which has a time to creep rupture of four to five months.

To establish a predictive method for geotextile creep failure based on a short term test, at least some creep tests must be carried out for long periods of time, as little creep test data for long creep rupture times is presently available.

Figures 6.1 and 6.2 show that it may be possible to predict geotextile creep based on a limited number of short term creep tests. Figure 6.1 is a log-log plot of the primary versus the secondary creep rate of several polypropylene geotextiles at various load levels and temperatures. Data from the present study and a previous study by Shrestha and Bell (66) are presented.

The data for the Typar and most of the data for the Propex falls on a single curve. The data for the Fibretex obviously lies well off the relationship for the Typar and Propex. This deviation may be at least partially accounted for by the differences in the amount of necking which occurs for each of these geotextiles. Fibretex exhibits a great deal of necking compared to Typar and Propex. Considering the effects of necking, the primary creep rate of the Fibretex would be reduced relative to Typar and Propex. Unfortunately, the actual amount of necking exhibited by these geotextiles was not measured, so a correction for necking cannot be made.

Geotextile necking is not likely to account for all of the scatter in the data, as the primary creep rate is strongly dependent upon geotextile structure (see Section 6.2). Unless some adjustment factor can be determined which would relate geotextile structure to primary creep rate, the relationship between the primary and secondary creep rates may only be applicable to geotextiles of similar construction. Since the secondary creep rate is dependent on the polymer

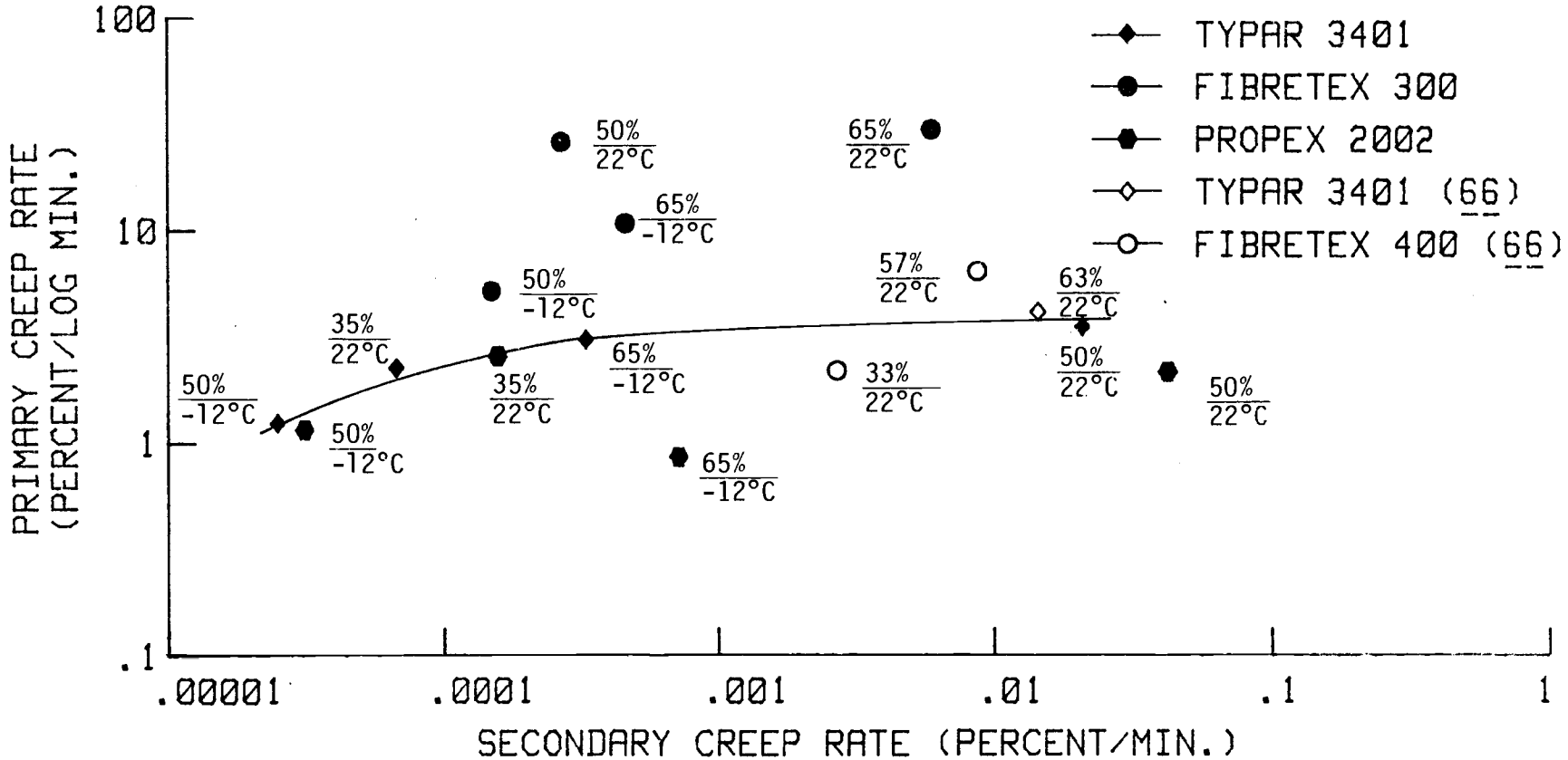

FIGURE 6.1: PRIMARY CREEP RATE VS. SECONDARY CREEP RATE FOR POLYPOPYLENE GEOTEXTILES AT VARIOUS LOAD LEVELS AND TEMPERATURES.

Note: $\frac{50\%}{22°C} = \frac{\text{Load Level (Percent of Wide Strip Tensile Strength)}}{\text{Specimen Temperature}}$

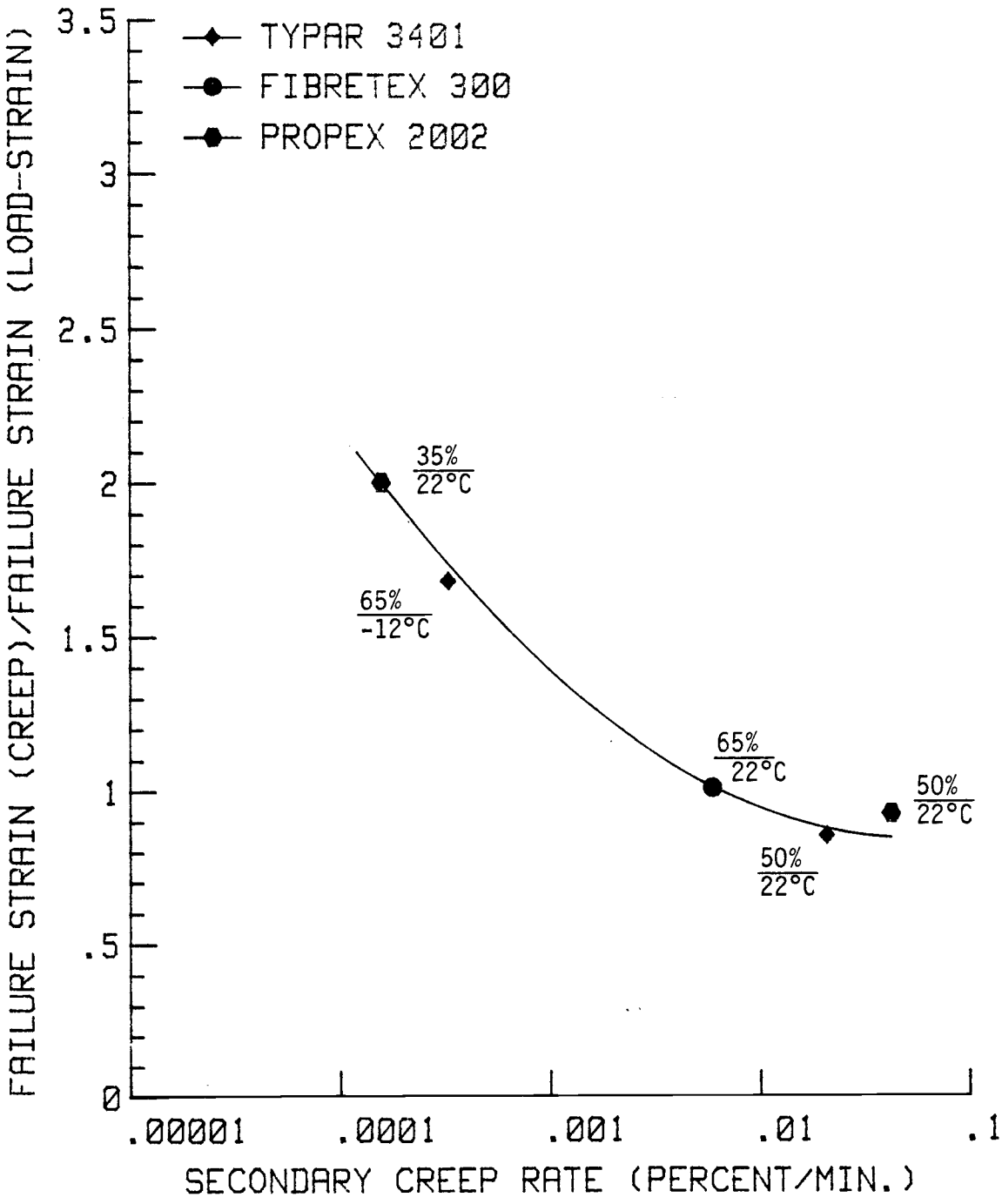

FIGURE 6.2: RATIO OF CREEP TO LOAD-STRAIN FAILURE STRAINS VS. SECONDARY CREEP RATE.

Note: $\frac{50\%}{22°C} = \frac{\text{Load Level (Percent of Wide Strip Tensile Strength)}}{\text{Specimen Temperature}}$

type, the data used to establish this relationship should be for geotextiles of the same polymer type as well.

Notwithstanding the limitations associated with the development of the relationship presented in Figure 6.1, this relationship could still be of value, as the relationship appears to be independent of load level and specimen temperature, at least for the Typar. When or if such a relationship can be established, a limited number of short term creep tests (e.g., less than a few hours each) could be performed on the geotextile in question and be used to determine the primary creep rates at the loads in question. From these primary creep rates and the relationship presented in Figure 6.1, the secondary creep rates could be obtained. From the primary and secondary creep rates, the time at which the geotextile will reach a specific strain may be determined. This strain could be a preselected allowable value, or the expected strain at the beginning of tertiary creep could be determined from a relationship similar to that presented in Figure 6.2.

As discussed in Section 5.2.4, the failure strain increased as time required for failure to occur increased. Since the secondary creep rate appears to control the time required for failure, a relationship between the creep rupture strain relative to the strain at failure for a load-strain test and the secondary creep rate is likely to exist. This relationship is also likely to be a function of the geotextile polymer, as the filament polymer tends to control geotextile creep behavior during secondary and tertiary creep.

For the relationships presented in Figures 6.1 and 6.2 to be truly useful, these relationships should be established for secondary creep rates less than .0001%/minute. At higher secondary creep rates, failure occurs rapidly, and these relationships are unnecessary.

If the relationship between primary and secondary creep rates can be established, an allowable load may be determined from a few very short creep tests. If this relationship cannot be established, the Rate Process Theory could still be used to predict the creep rates at new load levels, though additional research is still needed to establish the effectiveness of this theory in predicting geotextile creep.

6.4 Selection of Design Strength Parameters for Geotextiles Used in Cold Regions Applications

Once the required geotextile properties for design have been established (see Section 2.2.3), a geotextile may be selected using the following procedure:

(1) Determine the load-strain properties of the geotextiles in question using the test procedures outlined by Shrestha and Bell (66). Since below freezing temperature did not appreciably increase the strength and modulus of the geotextiles considered, the strength and modulus obtained at room temperature should not be increased owing to the expected below freezing temperatures in the field. However, the strain at failure obtained at room temperature should be reduced by 40% for polypropylene geotextiles if the field temperature is expected to be below freezing. 40% was the maximum reduction in failure

strain due to below freezing temperature obtained in the present study.

The allowable load for the geotextile need not be reduced owing to the freezing/thawing environment found in cold regions or due to continued exposure to saline water, as strength losses due to exposure to these conditions has so far proved to be minimal.

(2) Determine the creep properties of the geotextiles in question. The wide strip creep test used in the present study is recommended, except that a 200 mm (8.0 in.) wide specimen should be used to minimize the effects of necking. Until more is known about the relationship between primary and secondary creep rates, and the secondary creep rate and the failure strain, creep tests should be performed at two or more load levels for each geotextile type and should be carried out until the secondary creep rate is well established. Rate Process Theory may be used to extrapolate this data to other load levels if further refinement is needed.

From the test data and the analysis of the data using Rate Process Theory, the allowable load may be determined given the expected design life and the allowable strain. This allowable strain, however, should not exceed the failure strain obtained in the load-strain test.

Creep tests for polypropylene geotextiles should be performed at the temperature expected in the field since below freezing temperature reduces the rate of creep dramatically. For geotextiles made of polyester, or some polymers which have glass transition temperatures

above room temperature (i.e., 20°C or 70°F), the creep test may be performed at room temperature.

The geotextiles in question should be load-strain and creep tested confined in-soil, if possible.

(3) The load-strain properties of the geotextiles in question under repeated loading conditions should be determined when the selected geotextile is to be used in an application where fatigue is an important consideration (i.e., low embankments for highways).

6.5 Frost Heave Test Results

In general, geotextiles which were either thick and permeable or which were strongly hydrophobic and relatively impermeable performed well as a capillary cut-off layer.

The behavior of the two needlepunched geotextiles, which were thick and permeable, appears to be similar to that of the sand or gravel layers previously used in field and laboratory tests (4, 60, 61, 68). Since the size of the pores within these sand or gravel layers was much larger than that of the frost-susceptible soil below, the capillary conductivity of the sand or gravel layer was much lower than that of the soil. The lower capillary conductivity effectively reduced the height to which the capillary water could rise. If the air filled voids within the sand or gravel layer are so large that it is impossible for the voids to be bridged by capillarity, the capillaries can be effectively interrupted (63).

The high permeability (see Table 3.1) and, hence, the large pores within the needlepunched geotextiles caused the capillary conductivity

of the geotextile layers to be lower than that of the surrounding soil. However, the sand or gravel layer thickness required to effectively interrupt capillary rise in frost-susceptible soil was on the order of 10 cm to 20 cm (3.9 in. to 7.8 in.) (60, 63). Since the thickness of a geotextile layer is much less than 10 cm (3.9 in.), the lower capillary conductivity of the large air-filled pores within the geotextile could not account for the resistance to capillary flow needed to effectively interrupt the capillary tubes.

If a relatively thin geotextile layer is to prevent capillary rise in a soil, the geotextile layer must be hydrophobic as postulated by Hoover, et al. (37). In general, materials used for geotextile filaments are hydrophobic. The surface finish of the filaments may also change the wetting angle of the filaments, such that they are either more or less hydrophobic than the polymer of which they are made. In any case, the general hydrophobic nature of the geotextiles allows a much lower layer thickness than required of the sand or gravel. Increasing the thickness of the geotextile may improve the performance of the layer, however, as thick geotextiles can pass less water than can thin geotextiles, given the same head loss and coefficient of permeability (5).

The success of the relatively thin geotextile, Typar 3401, can be attributed to its relatively low permeability and highly hydrophobic nature. This highly hydrophobic nature requires that a relatively high head of water be present to allow flow to be initiated across the geotextile layer (see Table 3.1).

Though the Propex did exhibit some degree of success, some water did get through the layer. The Propex was quite thin relative to the

three geotextiles which were most successful. The Propex was also not as hydrophobic as the Typar. These two factors may have contributed to the mediocre performance of the Propex.

The Stabilenka, in contrast to the Bidim, Fibretex, and Typar geotextiles, had virtually no influence on water migration to the freezing front (see Tables 5.10, 5.11, and Figures 5.6 and 5.7). Of the geotextiles tested, only the Stabilenka was truly hydrophillic and readily absorbed water. The Stabilenka was also relatively thin. As was the case for the Propex, geotextile thickness and fiber wettability contributed to the lack of success of the Stabilenka geotextile.

Though thick geotextiles with high permeability and low wettability, or thin geotextiles with relatively low permeability and low wettability were most effective in stopping water migration and frost heave in the laboratory, these geotextiles may not be without problems in the field. For example, as discussed in Section 3.3.3, permeable geotextiles may be subject to problems with moisture flow across the geotextile layer in the vapor phase. Clogging may be a problem for the thick geotextiles as well.

In areas where frost penetration is deep and the water table is high, the use of a geotextile as a capillary cut-off layer may be difficult, if not impossible to apply (discussed in Section 3.3.3). If the water table is allowed to rise above the level of the geotextile layer, or if the freezing front propagates below the geotextile layer, the geotextile layer would be rendered useless (63).

Even with the possible existence of these problems, the use of a geotextile layer as a capillary break is still very promising. Further laboratory work is needed to better define the factors

affecting the effectiveness of geotextiles as capillary breaks. Further field work is needed to determine if these possible long term problems will be realized in practical applications.

7.0 CONCLUSIONS AND RECOMMENDATIONS

7.1 Conclusions

Based upon the laboratory test program results presented for the five geotextiles considered in this research program, the following conclusions have been reached:

(1) The mechanical properties of geotextiles, in terms of load-strain-strength and creep characteristics, are not adversely affected by subfreezing temperatures in a temperature range associated with many cold regions engineering applications.

(2) The presence of moisture does not adversely affect geotextile load-strain-strength characteristics.

(3) Freeze-thaw cycling in a dry, distilled water, or saline water environment has little influence on the load-strain-strength characteristics of geotextiles.

(4) Geotextile structure tends to control primary creep strains.

(5) The fiber polymer controls the secondary creep rate and the effect temperature has on geotextile creep.

(6) Above temperatures of about 0°C (32°F), polyester geotextiles have much lower creep rates and higher thresholds of tertiary creep than polypropylene; however, below this

temperature there is much less difference between the two polymers.

(7) The fiber drawing ratio influences the creep characteristics of geotextiles. However, since the actual drawing ratios of the filaments of the five geotextiles considered in this research program were not known, the magnitude of this effect could not be ascertained.

(8) Geotextile primary and secondary creep rates are very sensitive to changes in load level.

(9) A relationship between the primary creep rate and the secondary creep rate for the same polymer and geotextile structure may exist; however, additional geotextile creep tests are required to establish this relationship. To date, this relationship seems to be independent of temperature and load level, at least for Typar.

(10) A relationship may exist between the ratio of the strain at the beginning of tertiary creep (creep failure) to the strain at peak load for a load-strain test and the secondary creep rate for geotextiles with the same polymer type. If this relationship could be established, Rate Process Theory or the relationship between the primary and secondary creep rates could be used to predict the time and load level associated with geotextile rupture due to creep.

(11) Geotextiles have considerable potential as capillary breaks to limit frost heave.

(12) Geotextiles which are hydrophobic are more effective capillary cut-offs than those which absorb water readily.

7.2 Recommendations for Future Research

(1) The effect of fiber drawing ratio on geotextile creep should be thoroughly investigated.

(2) The relationship between the primary and secondary creep rate for secondary creep rates less than .0001 percent strain/minute should be investigated. A method for taking into account the dependence of the primary creep rate on geotextile structure should be determined.

(3) The relationship between the secondary creep rate and failure strain should be investigated, especially at low secondary creep rates.

(4) The effect of geotextile confinement within a soil on creep behavior should be investigated.

(5) The geotextile properties which affect the ability of a geotextile to perform as a capillary break must be better defined through continued laboratory research.

(6) Composite geotextile materials to reduce frost heave deserve study to combine the desirable properties of more than one material.

(7) Long term problems such as moisture migration in the vapor phase and geotextile clogging should be investigated through closely monitored field installations of geotextiles as capillary breaks.

BIBLIOGRAPHY

1. Alfrey, T. and Gurnee, E.F., Organic Polymers, Prentice-Hall, Inc., Englewood Cliffs, New Jersey, 1967.

2. Andersland, O.B. and Anderson, D.M., ed., Geotechnical Engineering for Cold Regions, McGraw-Hill Book company, New York, 1978.

3. Andersson, O., "The Use of Plastic Fabric for Pavement Protection During Frost Break," Proceedings, International Conference on the Use of Fabrics in Geotechnics, Ecole Nationale Des Ponts et Chaussees, Paris, April 1977, Vol. 1, pp. 143-149.

4. Armstrong, M.D., and Csathy, T.I., "Frost Design Practice in Canada," Pavement Design in Frost Areas, II: Design Considerations, Highway Research Record, No. 33, 1963, pp. 170-201.

5. Bell, J R., Hicks, R.G., Copeland, J., Evans, G.L., Cogne, J.J., Mallard, P., Jahn, S., and Lewis, M., "Evaluation of Test Methods and Use Criteria for Geotechnical Fabrics in Highway Applications," FHWA Report 80-021, Federal Highway Administration, Washington, D.C., June 1980.

6. Bell, J.R., Greenway, D.R., and Vischer, W., "Construction and Analysis of a Fabric Reinforced Low Embankment on Muskeg," Proceedings, International Conference on the Use of Fabrics in Geotechnics, Ecole Nationale Des Ponts et Chaussees, Paris, April 1977, Vol. 1, pp. 71-76.

7. Bell, J.R. and Lavansiri, D., Evaluation of Fabric Reinforcement of the Roadway Structure, Department of Civil Engineering, Oregon State University, June 1977.

8. Bell, J.R. and Steward, J.E., "Construction and Observation of Fabric Retained Soil Walls," Proceedings, International Conference on the use of Fabrics in Geotechnics, Ecole National Des Ponts et Chaussees, Paris, April 1977, Vol. 1, pp. 123-128.

9. Bennet, C.A. and Franklin, N.L., Statistical Analysis in Chemistry and the Chemical Industry, John Wiley and Sons, New York, 1954.

10. Berry, J.P., "Fracture of Polymeric Glasses," Fracture, an Advanced Treatise, Vol. 7, H. Liebowitz, ed., Academic Press, New York, 1972, pp. 38-93.

11. Brandt, G.H., "Chemical Additives to Reduce Frost Heave and Water Accumulation in Soils," Highway Research Board Bulletin, Washington, D.C., No. 393, 1972, pp. 45-55.

12. Brantman, B.P., Kazarnovsky, V.D., Polunovsky, A.G., and Ruvinsky, V.I., "Experiments on the Use of Synthetic Non-woven Materials for Road Structures," Proceedings, International Conference on the Use of Fabrics in Geotechnics, Ecole Nationale Des Ponts et Chaussees, Paris, April 1977, Vol. 1, pp. 35-40.

13. Broms, B.B., "Polyester Fabric as Reinforcement in Soil," Proceedings, International Conference on the Use of Fabrics in Geotechnics, Ecole Nationale Des Ponts et Chaussees, Paris, April 1977, Vol. 1, pp. 129-125.

14. Burwash, W.J., "A Case History Involving the Use of a Geotextile for a Highway Embankment on Muskeg," Proceedings, First Canadian Symposium on Geotextiles, Calgary, Alberta, Canada, September 23, 1980, pp. 225-235.

15. Calhoun, C.C., "Development of Design Criteria and Acceptance Specifications for Plastic Filter Cloths," Technical Report S-72-7, Army Engineer Waterways Experiment Station, Vicksburg, Mississippi, June 1972.

16. Clark, E.S., Polymeric Materials, American Society for Metals, Metals Park, Ohio, 1975.

17. Coleman, B.D. and Knox, A.G., "The Interpretation of Creep Failure in Textile Fibers as a Rate Process," Textile Research Journal, May 1957, pp. 393-399.

18. Cragg, C.B.H., "Geotextile Applications within the Ontario Hydro," Proceedings, First Canadian Symposium on Geotextiles, Calgary, Alberta, Canada, September 23, 1980, pp. 125-136.

19. Dickerson, R.E., Gray, H.B., and Haight, G.P., Chemical Principles, Second Edition, W.A. Benjamin, Inc., Menlo Park, California, 1974.

20. Dunham, J.W. and Barrett, R.J., "Woven Plastic Cloth Filters for Stone Seawalls," Journal of the Waterways Harbors and Coastal Engineering Division, ASCE, February 1976.

21. Eirich, F.R. and Smith, T.L., "Molecular Mechanical Aspects of the Isothermal Rupture of Elastomers," Fracture, and Advanced Treatise, Vol. 7, H. Liebowitz, ed., Academic Press, New York, 1972, pp. 352-611.

22. El-Fermaoui, A. and Nowatzki, E., "Effect of Confining Pressure on Performance of Geotextiles in soils," Proceedings, Second International Conference on Geotextiles, Industrial Fabrics Association International, St. Paul, Vol. 3, August 1982, pp. 799-804.

23. Ferry, J.D., Viscoelastic Properties of Polymers, Third Edition, John Wiley and Sons, Inc., New York, 1980.

24. _____, "Fibretex," Crown Zellerbach, Nonwoven Fabrics Division, Camas, Washington.

25. Finnigan, J.A., "The Creep Behavior of High Tenacity Yarns and Fabrics Used in Civil Engineering Applications," Proceedings, International Conference on the Use of Fabrics in Geotechnics, Ecole Nationale Des Ponts et Chaussees, Paris, April 1977, Vol. 2, pp. 305-310.

26. Geil, P.H., "Polymer Morphology," Chemical and Engineering News, Vol. 43, No. 33, August 16, 1965, pp. 72-84.

27. Goodman, I. and Rhys, J.A., Polyesters, Vol. 1, American Elsevier Publishing Company Inc., New York, 1965.

28. Greenway, D.R. and Bell, J.R., "The Role of Fabric in Low Embankments on Muskeg," Proceedings, Seventeenth Muskeg Research Conference, Saskatoon, Saskatchewan, Canada, October 4, 1977.

29. Haliburton, T.A., Anglin, C.C., and Lawmaster, J.D., "Selection of Geotechnical Fabrics for Embankment Reinforcement," Report of Contract No. DACW01-78-C-0055 for U.S. Army Engineer District, Mobile, Alabama. Oklahoma State University, May 1978.

30. Hall, C., Polymer Materials, John Wiley and Sons, Inc., New York, 1981.

31. Hearle, J.W.S., Groseberg, P., and Backer, S., Structural Mechanics of Fibers, Yarns, and Fabrics, John Wiley and Sons, Inc., New York, 1969.

32. Herrin, M. and Jones, G.E., "The Behavior of Bituminous Materials from the Viewpoint of the Absolute Rate Theory," Proceedings, The Association of Asphalt Paving Technologists, Vol. 32, February 1963, pp. 82-105.

33. Hertzberg, R.W., Deformation and Fracture Mechanics of Engineering Materials, John Wiley and Sons, Inc., New York, 1976.

34. Hogan, H.B., "The Engineering Application of the Absolute Rate Theory to Plastics: I-Laminates," Bulletin, Vol. 42, No. 6, University of Utah, Logan, Utah, August 1951, pp. 1-147.

35. Hollingsworth, H., Evaluation of Mirafi 140 Fabric as a Capillary Water Barrier, Unpublished Report, Chen and Associates, Inc., Casper, Wyoming, June 17, 1976.

36. Holtz, R.D., Tobin, W.R., and Burke, W.W., "Creep Characteristics and Stress-Strain Behavior of a Geotextile-Reinforced Sand," Proceedings, Second International Conference on Geotextiles, Industrial Fabrics Association International, St. Paul, Vol. III, August 1982, pp 805-810.

37. Hoover, J.M., Pitt, J.M., Handfelt, L.D., and Stanley, R.L., "Performance of Soil-Aggregate-Fabric Systems in Frost-Susceptible Roads, Linn County, Iowa," Transportation Research Record, No. 827, 1981, pp. 6-14.

38. Hull, D., "The Microstructure and Porperties of Crazes," Proceedings, Battelle Institute Materials Science Colloquia, Deformation and Fracture of High Polymers, H.H. Kausch, ed., Kronberg, Germany, September 11-16, 1972, Plenum Press, New York, pp. 301-316.

39. Jenkins, A.D., ed., Polymer Science, Vol. 1, American Elsevier Publishing Co., Inc., New York, 1972.

40. Kerr, J.R. and Townsend, D.L., "Experiences with Geotextiles on Soft Subgrade Clays," Proceedings, First Canadian Symposium on Geotextiles, Calgary, Alberta, Canada, Spetember 23, 1980, pp. 215-224.

41. Kinney, T.C., Expanded Report on the Use of Geotextiles to Bridge Thermokarsts, Report to the Alaska Department of Transportation (Unpublished), Fairbanks, Alaska, August 27, 1981.

42. Kinney, T.C., Fabric Induced Changes in High Deformation Soil-Fabric-Aggregate Systems, Thesis for Ph.D., University of Illinois, Urbana, 1978.

43. Kinney, T.C., Personal Communication, Shannon and Wilson, Inc., Fairbanks, Alaska, 1981.

44. Koerner, R.M., Rosenfarb, J.L., Dougherty, W.W., and McElroy, J.J., "Stress-Strain-Time Behavior of Geotextiles," The Use of Geotextiles for Soil Improvements, Preprint 80-177, ASCE Convention, Portland, OR, April 17, 1980, pp. 31-52.

45. Leidersdorf, C.B., Potter, R.E., and Goff, R.D., Slope Protection for Artificial Exploration Islands Off Prudoe Bay, Proceedings, 13th Annual Conference, Vol. VIII, Houston, Texas, Offshore Technology Conference, 1981, pp. 437-447.

46. Low, P.F. and Lovell, C.W., "The Factor of Moisture in Frost Action," Highway Research Board Bulletin, Washington, D.C., No. 225, 1959, pp. 23-44.

47. Maagdenberg, A.C., "Fabrics Below Sand Embankments Over Weak Soils, Their Technical Specifications and Their Application in a Test Area," Proceedings, International Conference on the Use of Fabrics in Geotechnics, Ecole Nationale Des Ponts et Chaussees, Paris, April 1977, Vol. 1, pp. 77-82.

48. Mallard, Pierre and Bell, J R., "Use of Fabrics In Erosion Control," Transportation Research Report 81-4, Department of Civil Engineering, Oregon State University, Corvallis, Oregon, January 1981.

49. McGaw, R., "Frost Heaving Versus Depth to Water Table," Highway Research Board Bulletin, Washington, D.C., No. 393,1972, pp.45-55.

50. McGown, A., Andrawes, K.Z., and Kabir, M.H., "Load-Extension Testing of Geotextiles Confined In-Soil," Proceedings, Second International Conference on Geotextiles, Industrial Fabrics Association International, St. Paul, Vol. III, August 1982, pp. 793-798.

51. McGown, A., The Properties of Non Woven Fabrics Presently Identified as Being Important in Public Works Applications, University of Strathclyde, Glasgow, Scotland, U.K., 1978.

52. Menges, G., "Attempt to Explain Crazing in Amorphous Thermoplastics and Adhesion Fractures in Semicrystalline Thermoplastics and Filled Polymers," Proceedings, Battelle Institute Materials Science Colloquia on Deformation and Fracture of High Polymers, H.H. Kausch, ed., Kronberg, Germany, September 11-16, 1972, Plenum Press, New York, pp. 301-316.

53. _____, "Mirafi 140 Construction Fabric," Publication PM-5, Celanese Fibers Marketing Co., Charlotte, N.C., 1975.

54. Mitchell, J.K., Campanella, R.G., and Sinjh, A., "Soil Creep as a Rate Process," ASCE, Journal of the Soil Mechanics and Foundation Division, January 1968, pp. 231-253.

55. Ogorkiewicz, R.M., ed., Engineering Properties of Thermoplastics, John Wiley and Sons, Inc., New York, 1970.

56. Pare, J.-J., "Use of Geotextiles in James Bay Hydroelectric Projects," Proceedings, First Canadian Symposium on Geotextiles, Calgary, Alberta, Canada, September 23, 1980. pp. 188-200.

57. Penner, E., "The Mechanisms of Frost Heaving in Soils," Highway Research Board Bulletin, Washington, D.C., No. 225, 1959, pp. 1-22.

58. Peterlin, A., "Mechanisms of Deformation in Polymeric Solids," Polymeric Materials, American Society for Metals, 1975, p. 208.

59. Raumann, G., "A Hydraulic Tensile Test with Zero Transverse Strain for Geotechnical Fabrics," Geotechnical Testing Journal, Vol. 2, No. 2, June 1979, pp. 69-76.

60. Rengmark, F., "Highway Pavement Design in Frost Areas in Sweden," Highway Research Record, No. 33, 1963, pp. 137-157.

61. _____, "Roadway Design in Seasonal Frost Areas," NHCRP Synthesis of Highway Practice, No. 26, Transportation Research Board, Washington, D.C., 1974.

62. Rodriguez, F., Principles of Polymer Systems, McGraw-Hill, New York, 1970.

63. Roth, W.H., "Fabric Filter for Improving Frost Susceptible Soils," Proceedings, International Conference on the Use of Fabrics in Geotechnics, Ecole Nationale Des Ponts et Chaussees, Paris, April 1977, Vol. 1, pp. 23-28.

64. Sale, J.P., Parker, F., and Barker, W.R., "Membrane Ecapsulated Soil Layers," Journal of the Soil Mechanics and Foundations Division, ASCE, New York, Vol. 99, SM 12, 1973, pp 1077-1089.

65. Sauer, J.A., Marin, J., and Hsiao, C.C., "Creep and Damping Properties of Polystyrene," Journal of Applied Physics, Vol. 20, No. 6, June 1949, pp. 507-517.

66. Shrestha, S.C. and Bell, J R., "Tensile and Creep Behavior of Geotextiles," Transportation Research Report 81-3, Department of Civil Engineering, Oregon State University, Corvallis, Oregon, January 1981.

67. Shrestha, S.C. and Bell, J R., "A Wide Strip Tensile Test of Geotextiles," Proceedings, Second International Conference on Geotextiles, Industrial Fabrics Association International, St. Paul, Vol. III, August 1982, pp. 739-744

68. _____, Soil Mechanics for Road Engineers, Her Majesty's Stationery Office, London, 1955.

69. Steward, J.E., Williamson, R., and Mohney, J., Guidelines for the Use of Fabrics in Construction and Maintenance of Low Volume Roads, U.S. Department of Agriculture, U.S. Forest Service, Portland, Oregon, 1977.

70. Taivainen, O.A., "Preventive Measures to Reduce Frost Action on Highways in Finland," Highway Research Record, No. 33, 1963, pp. 202-216.

71. Tart, R.G. and Luscher, U., "Construction and Performance of Frozen Gravel Fills," Proceedings, Specialty Conference on the Northern Community: A Search for a Quality Environment, ASCE, Seattle, Washington, April 1981, pp. 693-704.

72. _____, Typar, Du Pont Company, Typar Sales, Wilmington, Delaware, January 1978.

73. _____, The Use of Non-Woven Fabrics in Civil Engineering Structures, Rhone-Poulenc-Textile Co., Non-woven Development Division, Lyons, France, 1975.

74. _____, Unpublished Results of Geotextile Creep Test Program, New York State Department of Transportation, Soil Mechanics Bureau, Albany, New York, 1981.

75. Van Vlack, L.H., Elements of Materials Science and Engineering, Third Edition, Addison-Wesley Publishing Company, Reading, Massachusetts, 1977.

76. Webster, S.L. and Watkins, J.E., "Investigation of Construction Techniques for Tactical Bridge Approach Roads Across Soft Ground," Technical Report S-77-1, U.S. Army Engineer Waterways Experiment Station, Vicksburg, Mississippi, February 1977.

77. Wilson, C.D., Personal Communication, Synflex Industries, Inc., Vancouver, British Columbia, 1981.

78. Yoder, E.J. and Witczak, M.W., Principles of Pavement Design, Second Edition, John Wiley and Sons, Inc., New York, 1975.

GLOSSARY

Chain Packing Efficiency: The closeness with which polymer molecular chains may be packed together.

Conformation: The symmetrical arrangement of molecules within a crystal.

Covalent Bond: An atomic bond formed by the sharing of two electrons between two atoms.

Copolymer: A polymer whose molecular chain is a combination of two kinds of mers.

Crimp: The waviness of a fiber woven in a fabric.

Cross-link: An atom (e.g., sulfur) which rigidly joins two adjacent polymer molecular chains with primary covalent bonds.

Drawing Ratio: The ratio of the length of a fiber after drawing to its length before drawing.

Dtex: A linear weight in units of grams/1000 meters.

Fiber Drawing: The process of stretching polymer fibers while being heated to above the glass transition temperature to induce molecular orientation and crystallinity within the fiber.

Glossary (continued)

Five Fold Yarn: Five filaments twisted together to form a yarn.

Homopolymer: A polymer whose molecular chain is composed of only one kind of mer.

Mer: The basic structural unit of a polymer molecular chain.

Microfibril: A polymer cyrstal in which the molecules have become aligned due to fiber drawing.

Nonlinear Viscoelasticity: Time-dependent deformational behavior in which the relationship between stress and strain is not linear.

Ply: To twist together two or more filaments.

Tenacity: The breaking tensile stress for a fiber in terms of the size of the unstrained fiber expressed as grams-force per denier.

Tensile Creep Modulus: The ratio of the applied stress to the creep strain at a given time.

Van der Waals Bond: An intramolecular bond resulting from a dipole-induced dipole attraction of electrons in orbitals of atoms belonging to the interacting molecules.

Glossary (continued)

Warps: Yarns or fibers aligned in the warp direction.

APPENDICES

APPENDIX A

Load-Strain and Freeze-Thaw Test Data

Figures A.1 through A.10 represent load-strain data in which the load has been normalized using the ratio of the actual mass per unit area to the nominal per unit area of the geotextile (see Equation 4.1.1). The symbol (i.e., circle, square, triangle, etc.) represents the mean normalized load for all of the specimens (typically, five specimens were tested for each case) of a particular geotextile and case. The error bars represent the maximum and minimum normalized loads obtained for the group of specimens. Tables A.1 through A.3 summarize the results of the statistical analysis of the normalized strength, strain at failure, and normalized secant modulus at 10% strain of the load-strain tests. The statistical analysis was performed using a student's t-distribution assuming a 90% confidence level (see Equation 4.1.2).

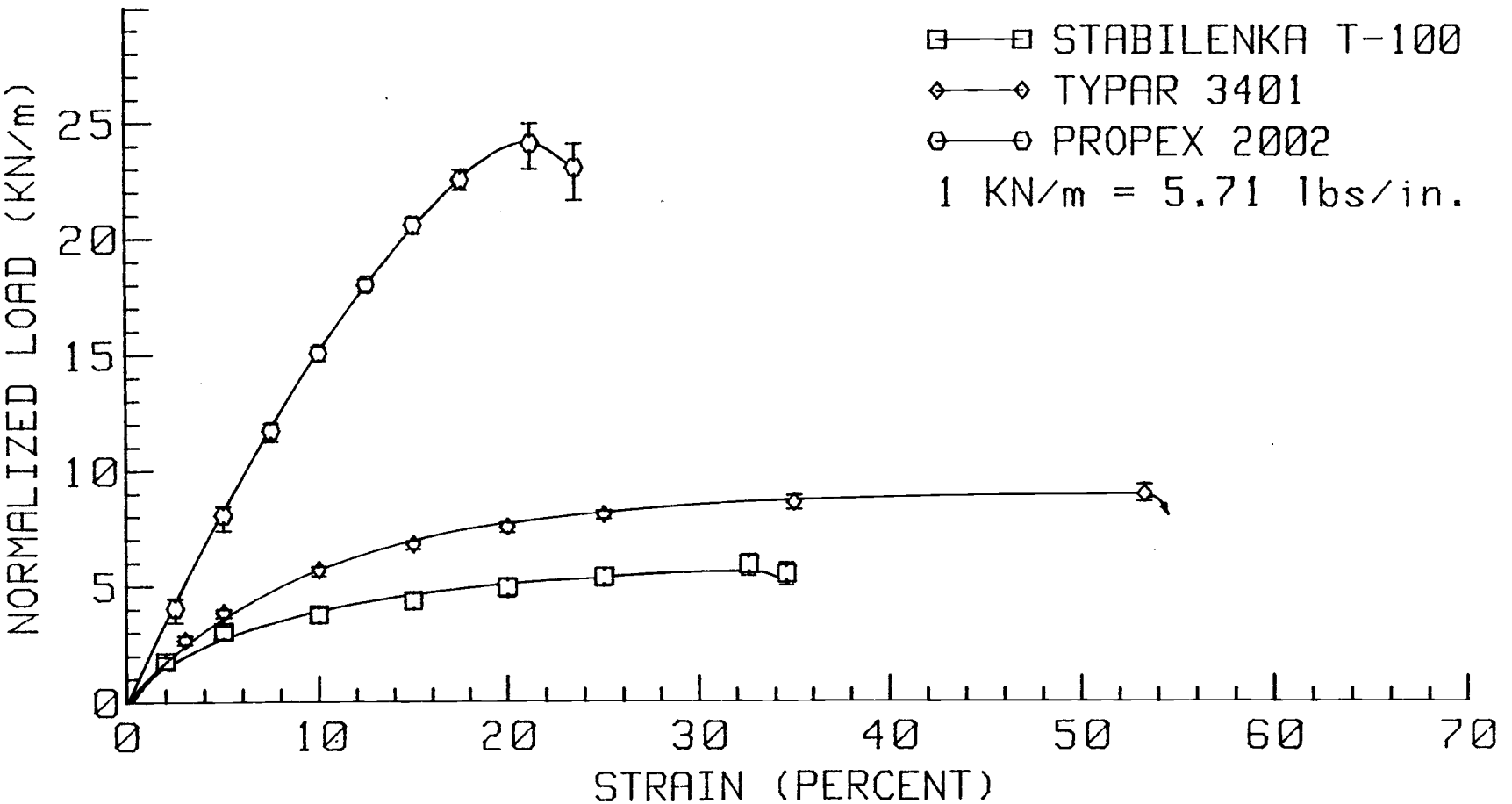

FIGURE A.1(a): NORMALIZED AXIAL LOAD VS. STRAIN AT 22 C (DRY CONDITION).

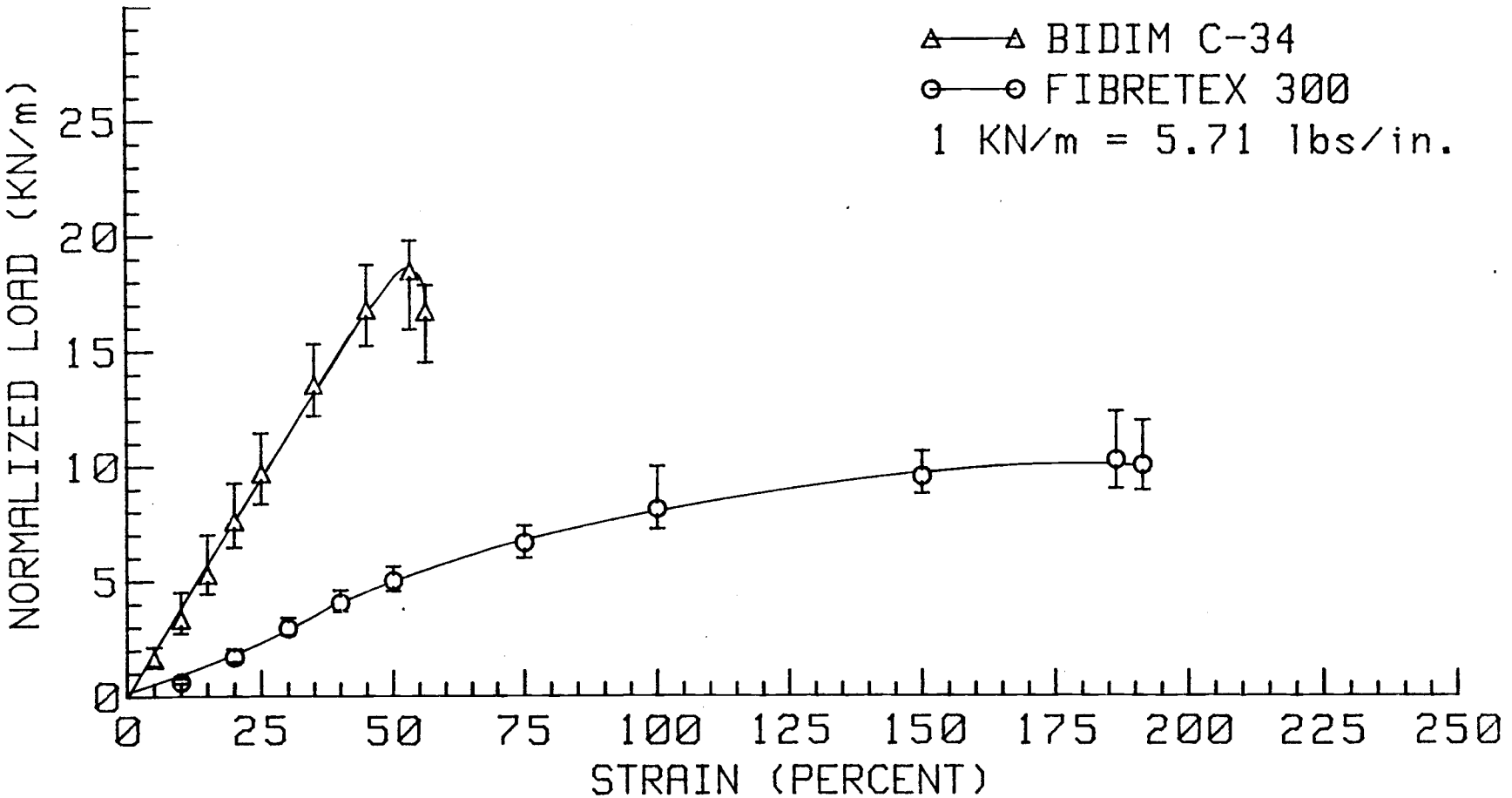

FIGURE A.1(b): NORMALIZED AXIAL LOAD VS. STRAIN AT 22 C (DRY CONDITION).

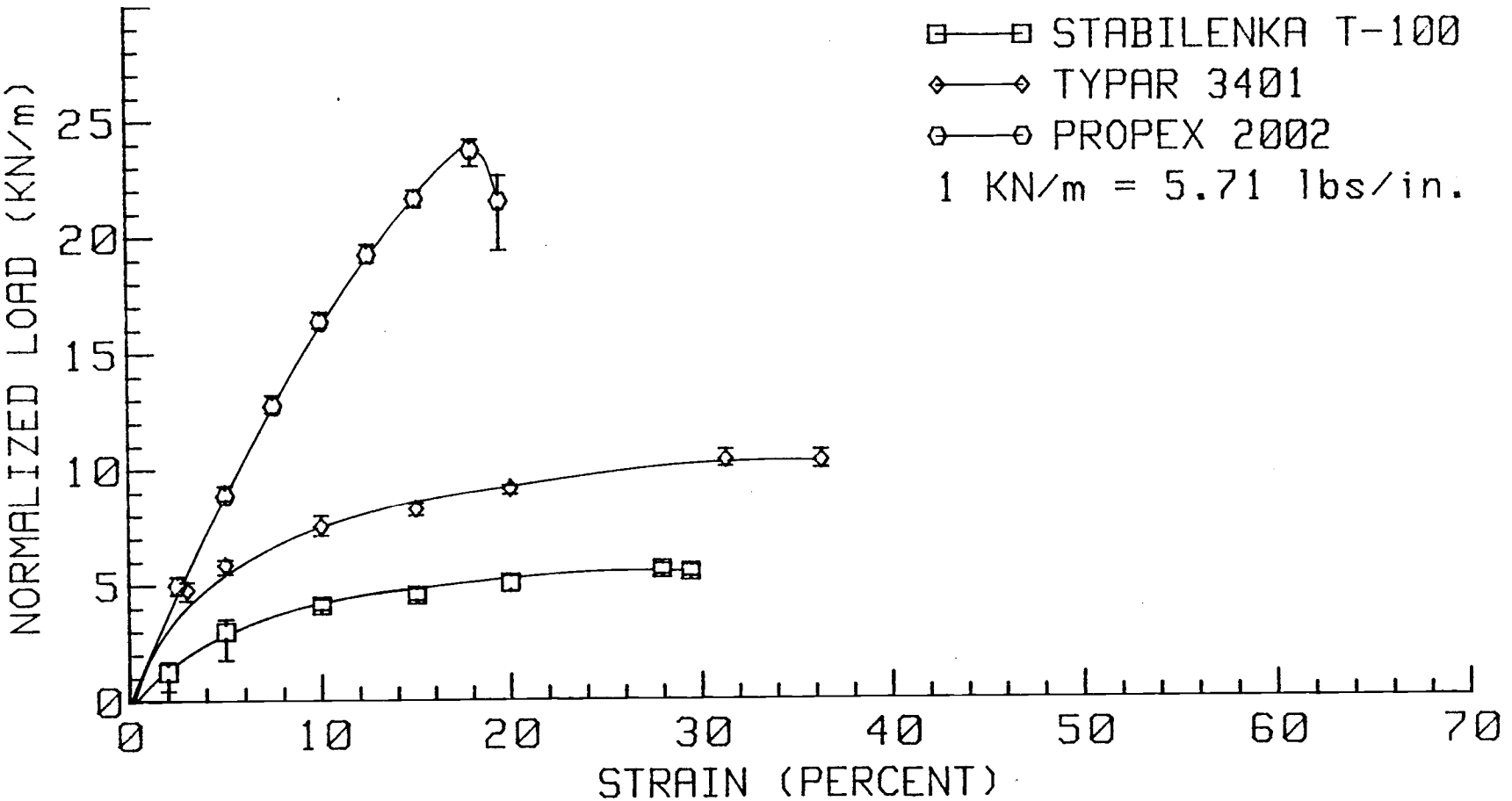

FIGURE A.2(a): NORMALIZED AXIAL LOAD VS. STRAIN AT -12 C (DRY CONDITION).

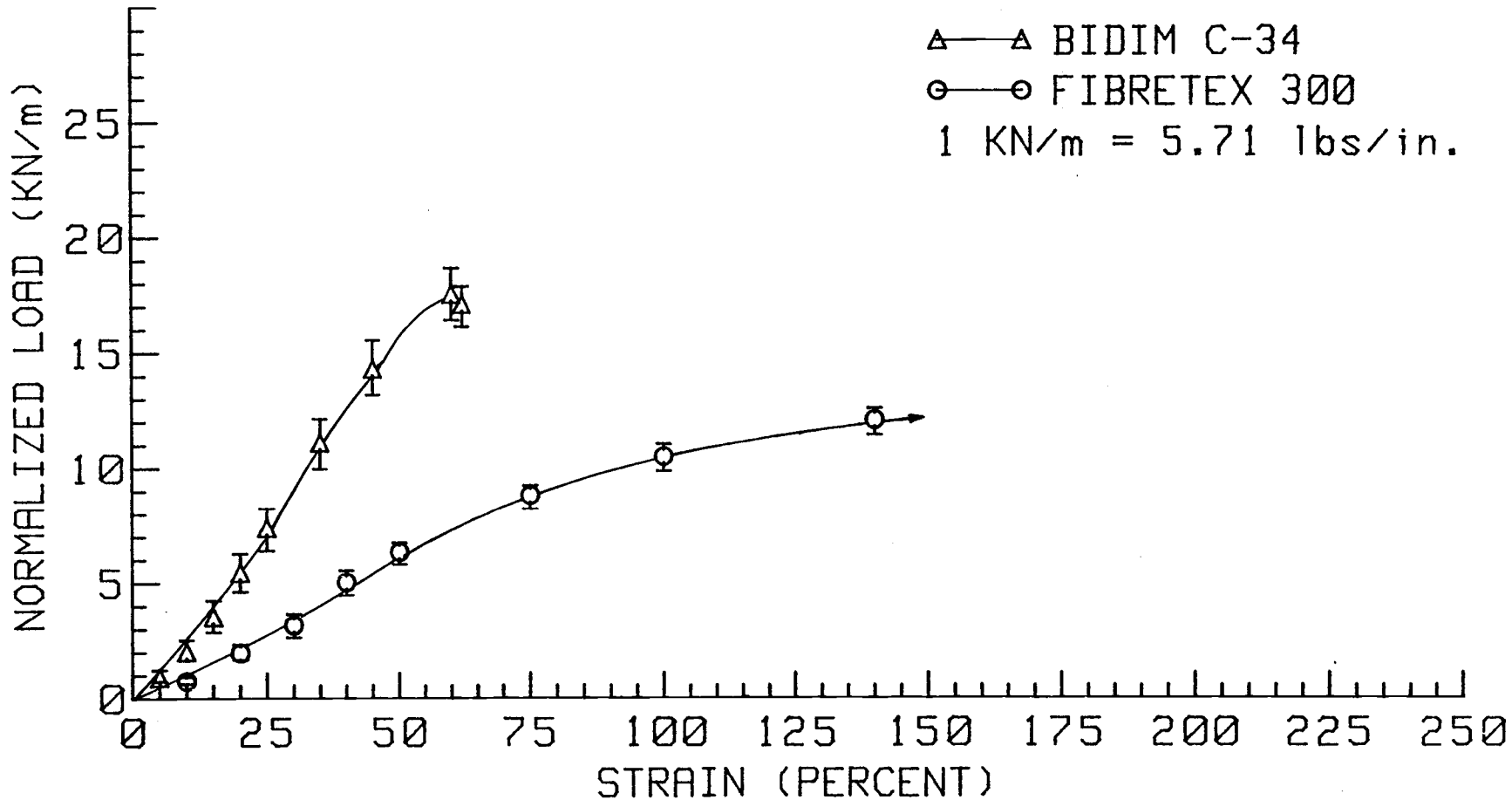

FIGURE A.2(b): NORMALIZED AXIAL LOAD VS. STRAIN AT -12 C (DRY CONDITION).

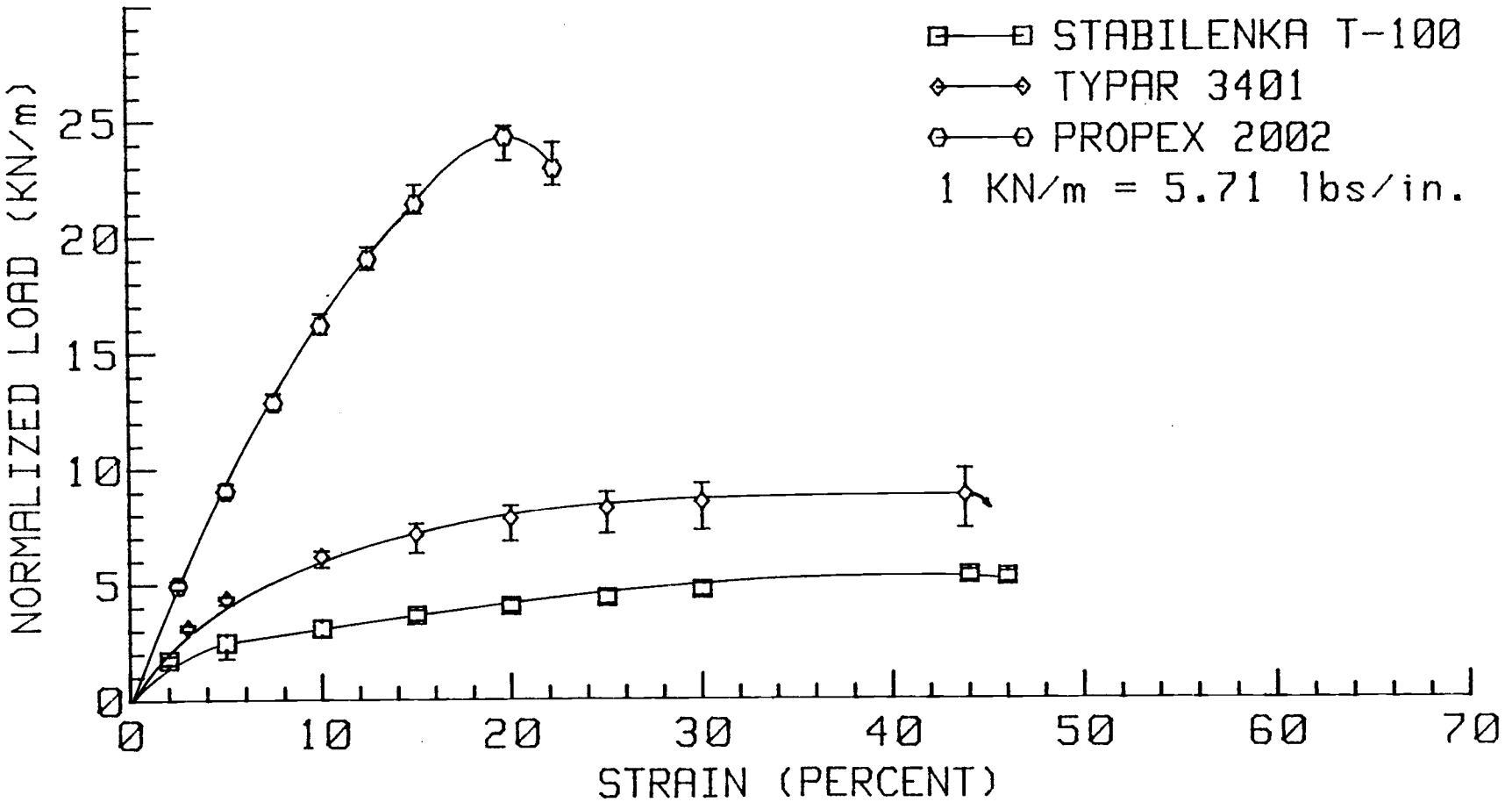

FIGURE A.3(a): NORMALIZED AXIAL LOAD VS. STRAIN AT 22 C (WET CONDITION).

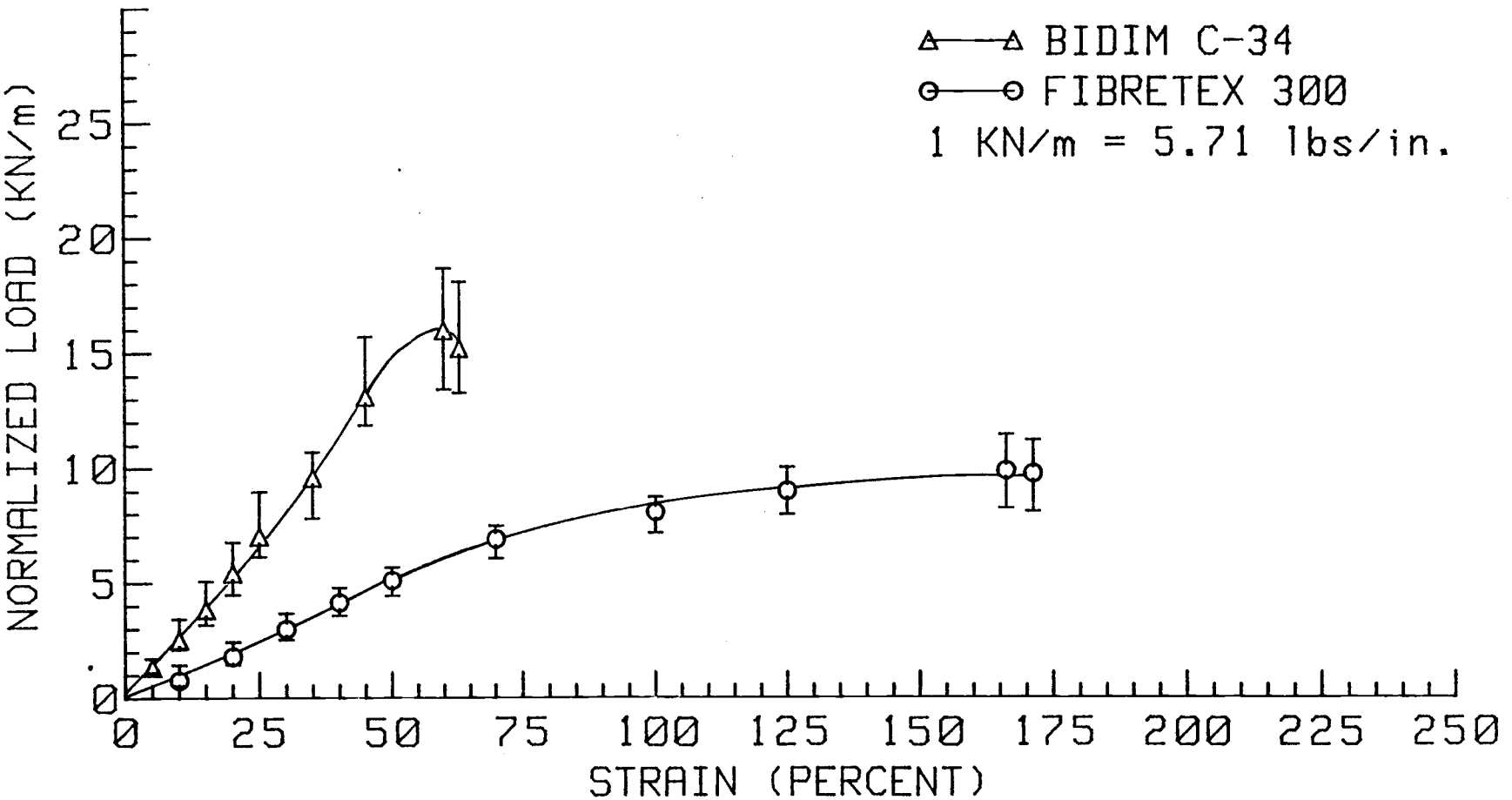

FIGURE A.3(b): NORMALIZED AXIAL LOAD VS. STRAIN AT 22 C (WET CONDITION).

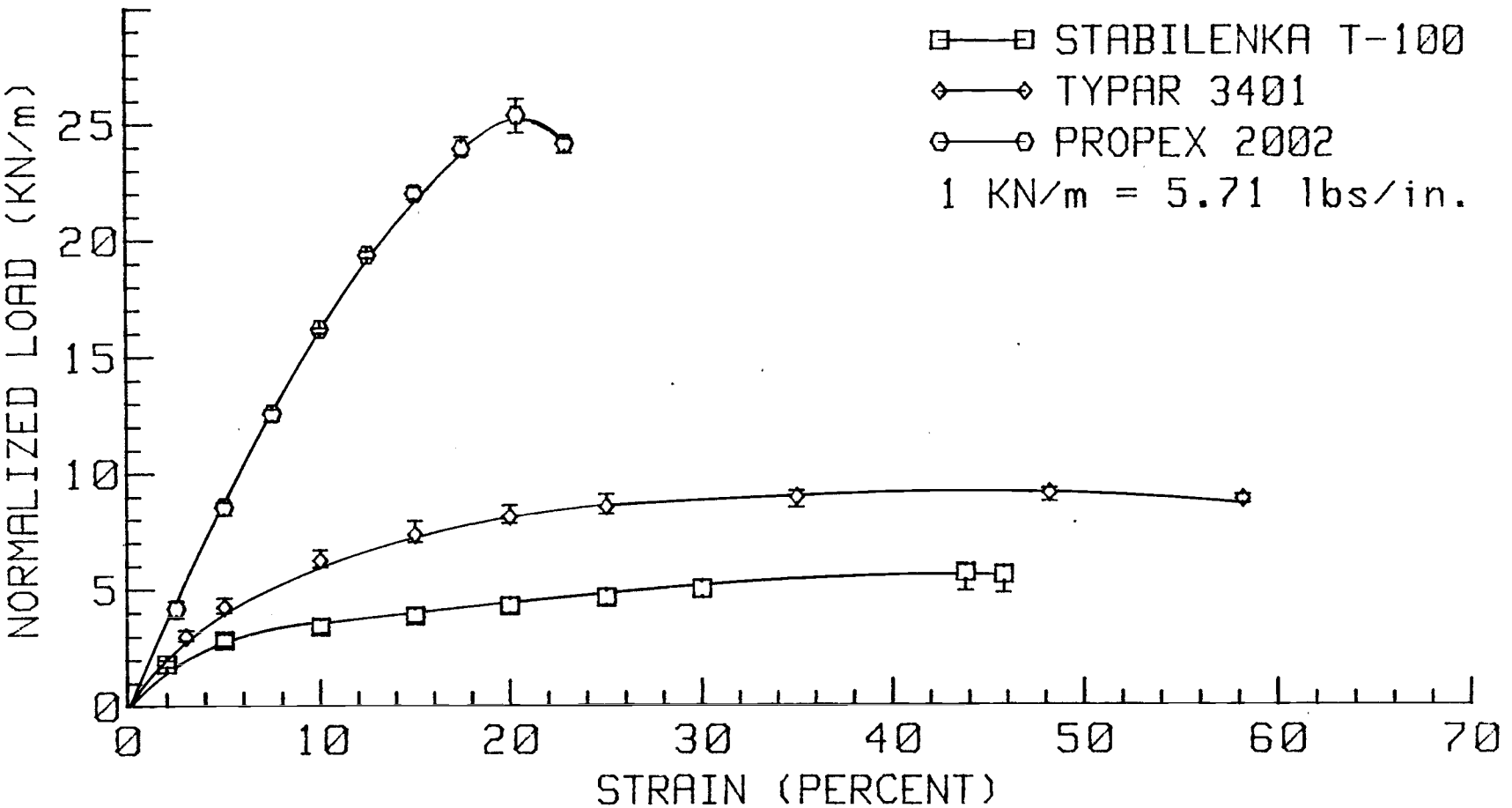

FIGURE A.4(a): NORMALIZED AXIAL LOAD VS. STRAIN AFTER 50 FREEZE-THAW CYCLES IN A DRY ENVIRONMENT (22 C, WET CONDITION).

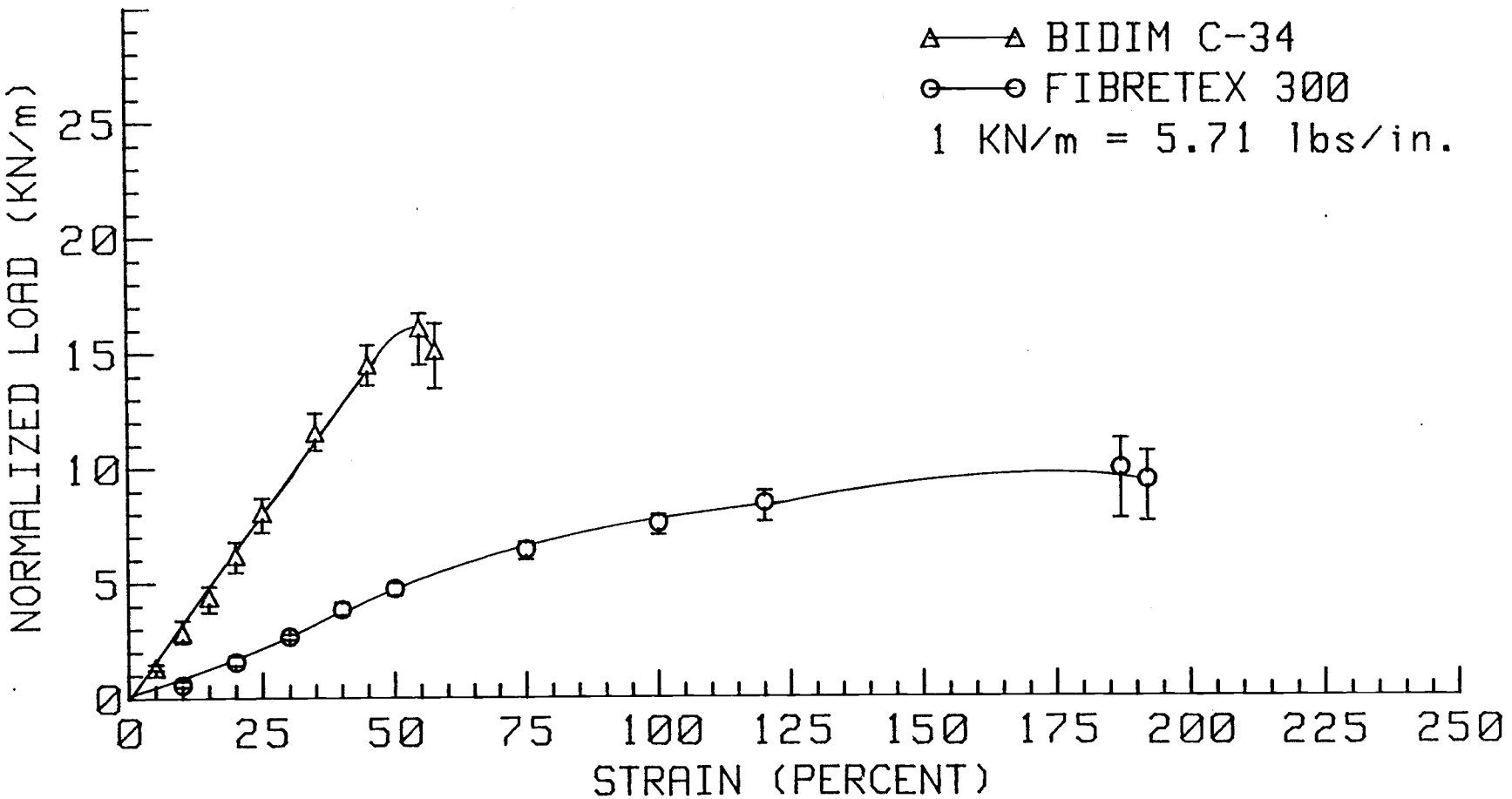

FIGURE A.4(b): NORMALIZED AXIAL LOAD VS. STRAIN AFTER 50 FREEZE-THAW CYCLES IN A DRY ENVIRONMENT (22 C, WET CONDITION).

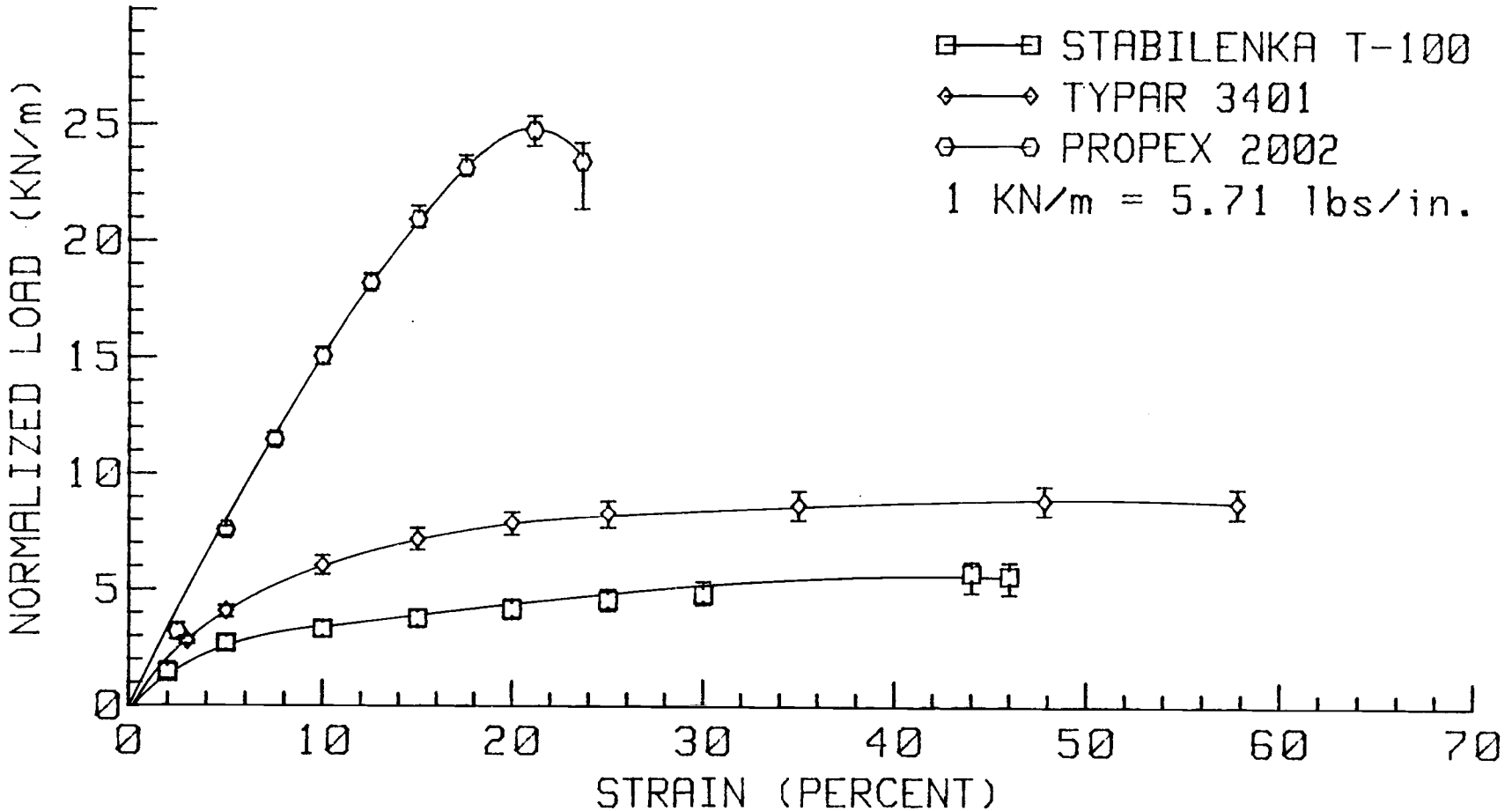

FIGURE A.5(a): NORMALIZED AXIAL LOAD VS. STRAIN AFTER 50 FREEZE-THAW CYCLES IN A DISTILLED WATER ENVIRONMENT (22 C, WET CONDITION).

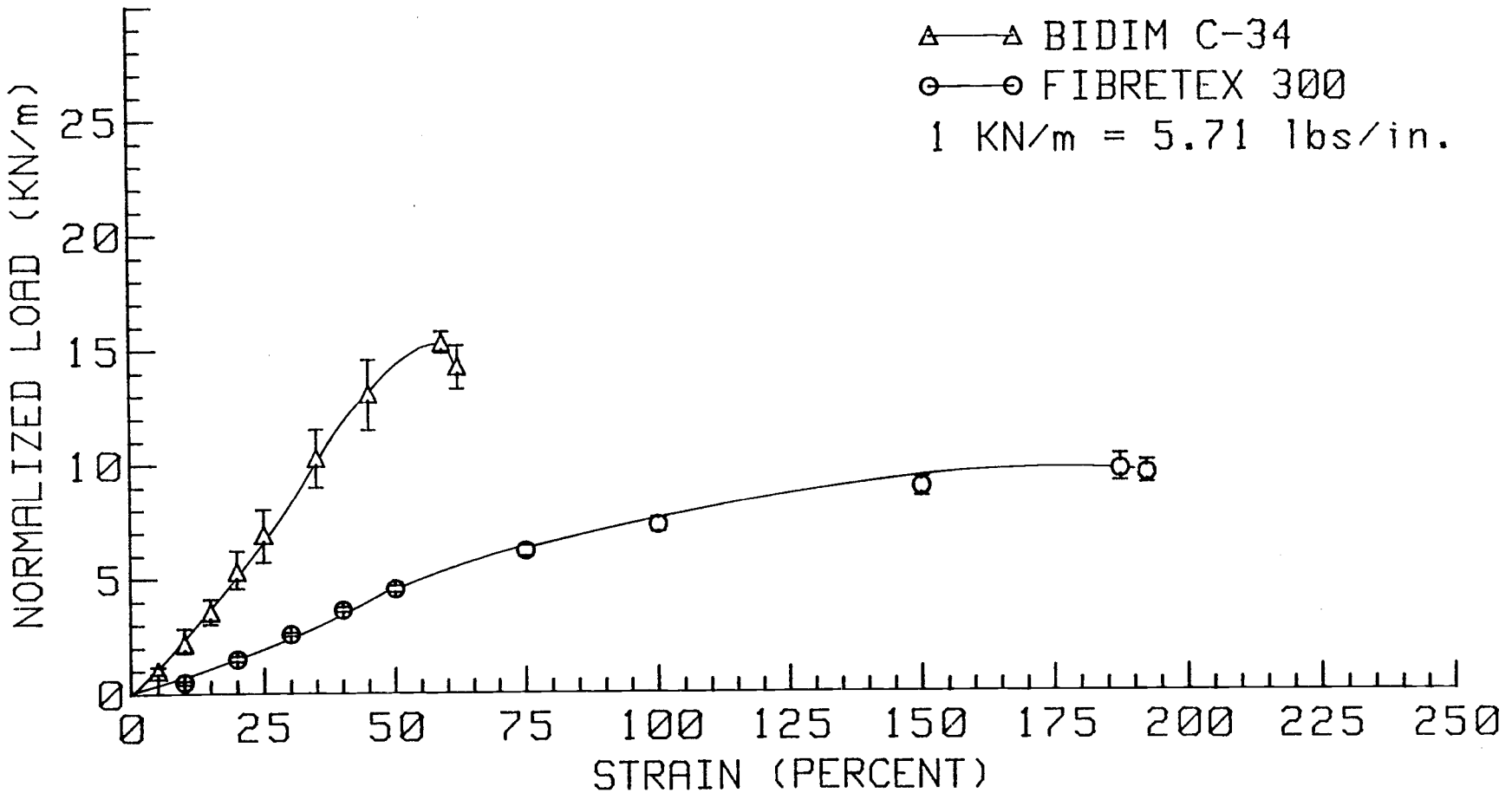

FIGURE A.5(b): NORMALIZED AXIAL LOAD VS. STRAIN AFTER 50 FREEZE-THAW CYCLES IN A DISTILLED WATER ENVIRONMENT (22 C, WET CONDITION).

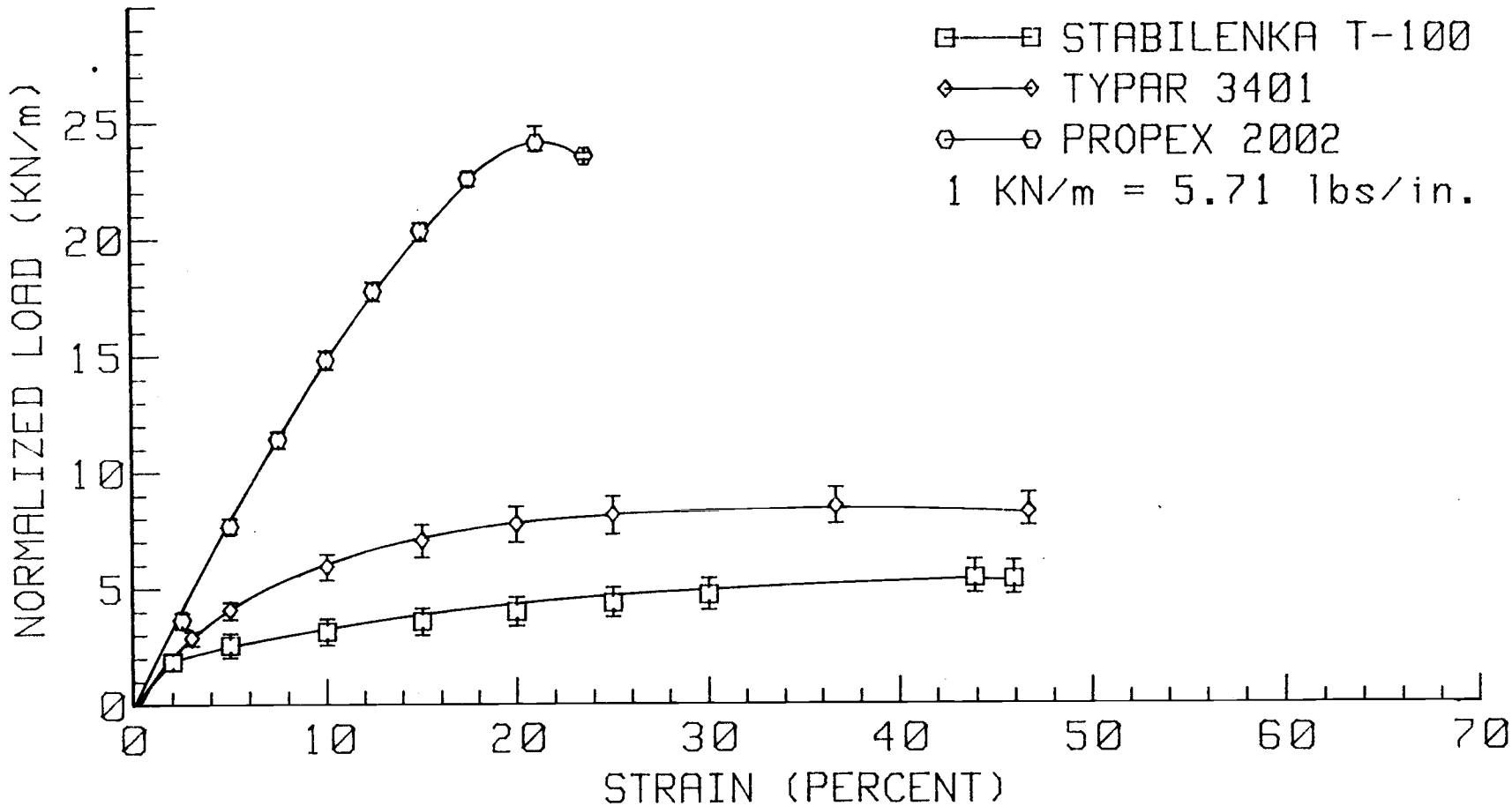

FIGURE A.6(a): NORMALIZED AXIAL LOAD VS. STRAIN AFTER 50 FREEZE-THAW CYCLES IN A SALINE WATER ENVIRONMENT (22 C, WET CONDITION).

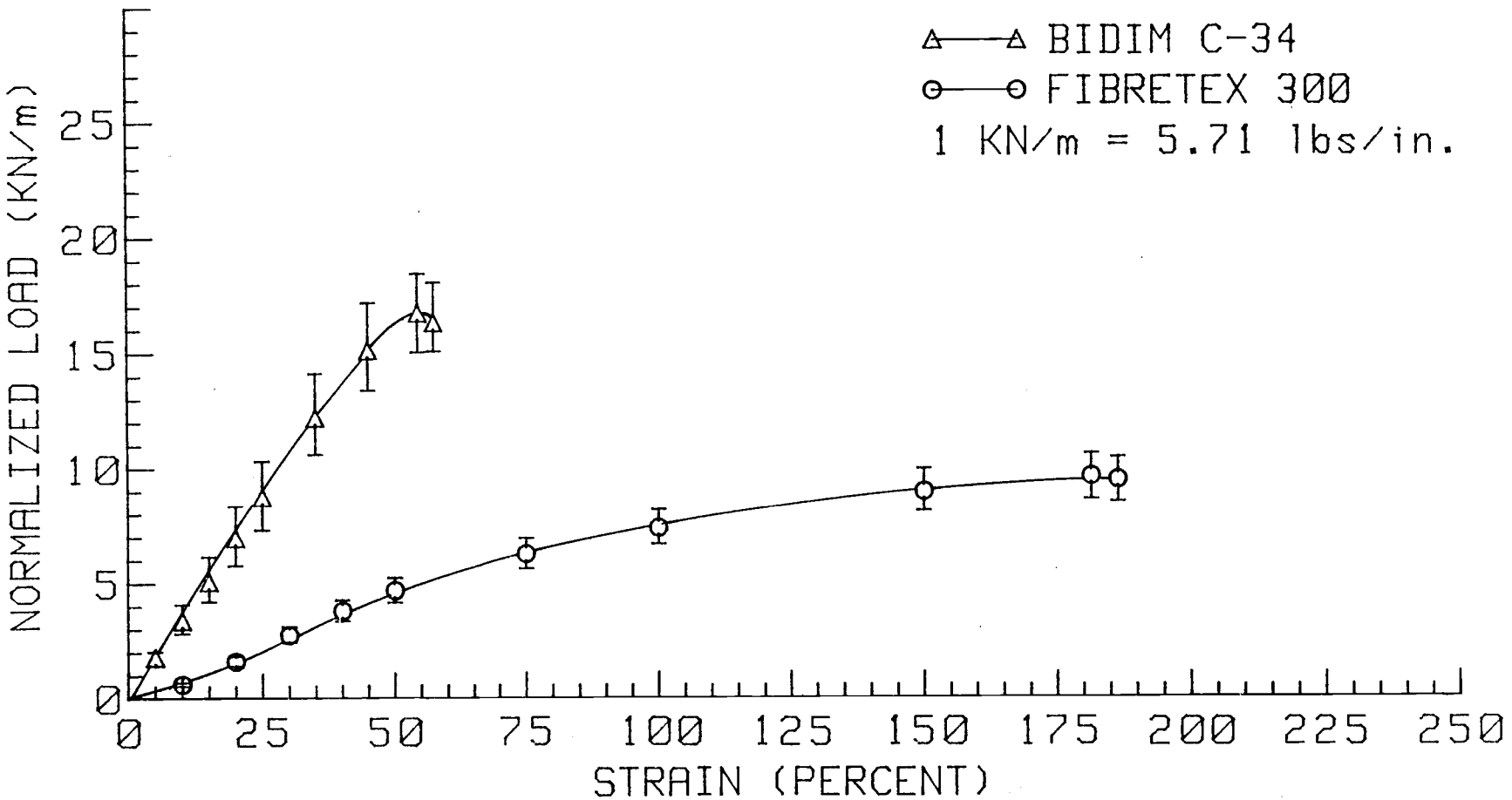

FIGURE A.6(b): NORMALIZED AXIAL LOAD VS. STRAIN AFTER 50 FREEZE-THAW CYCLES IN A SALINE WATER ENVIRONMENT (22 C, WET CONDITION).

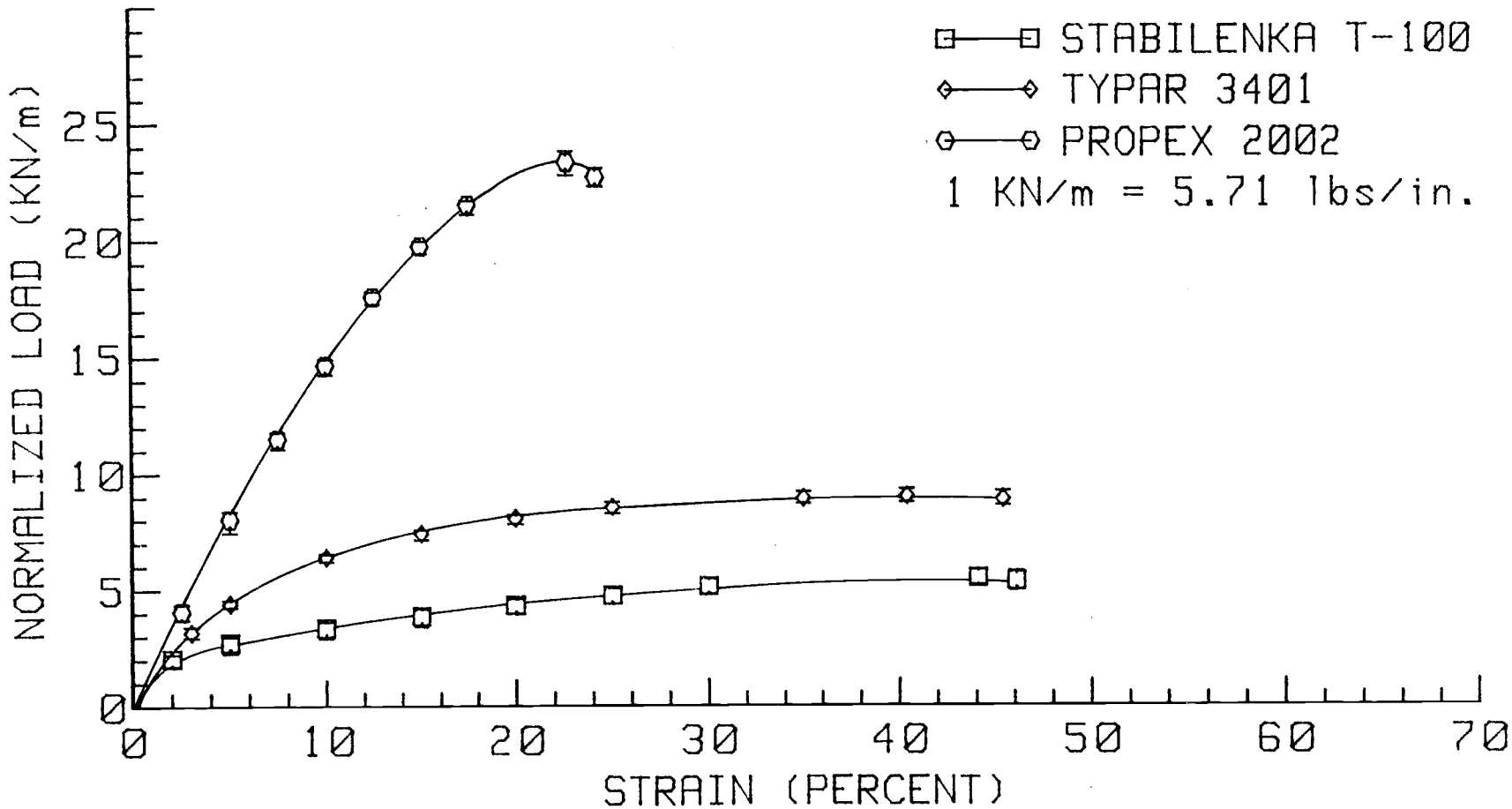

FIGURE A.7(a): NORMALIZED AXIAL LOAD VS. STRAIN AFTER 300 FREEZE-THAW CYCLES IN A DRY ENVIRONMENT (22 C, WET CONDITION).

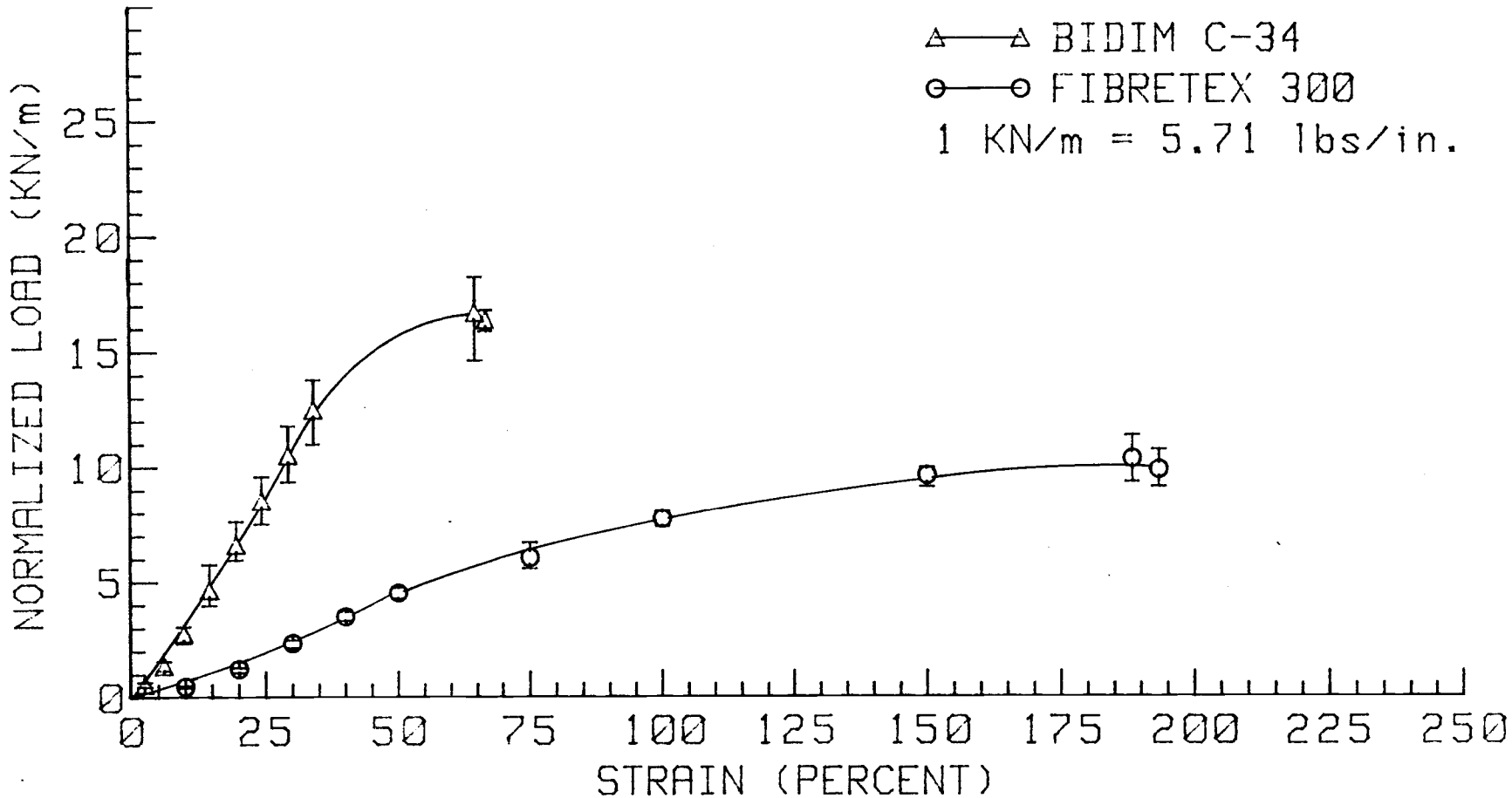

FIGURE A.7(b): NORMALIZED AXIAL LOAD VS. STRAIN AFTER 300 FREEZE-THAW CYCLES IN A DRY ENVIRONMENT (22 C, WET CONDITION).

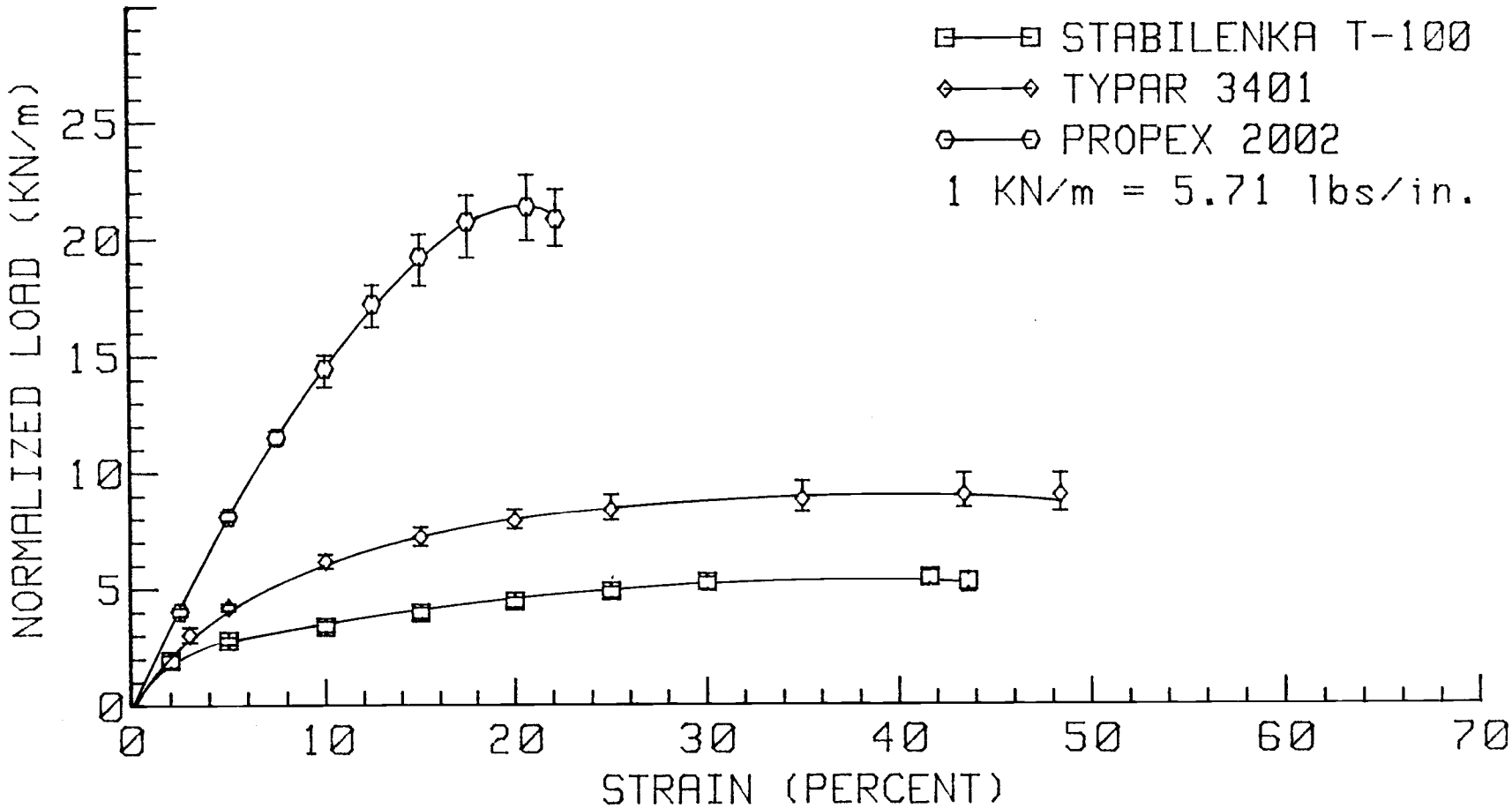

FIGURE A.8(a): NORMALIZED AXIAL LOAD VS. STRAIN AFTER 300 FREEZE-THAW CYCLES IN A DISTILLED WATER ENVIRONMENT (22 C, WET CONDITION).

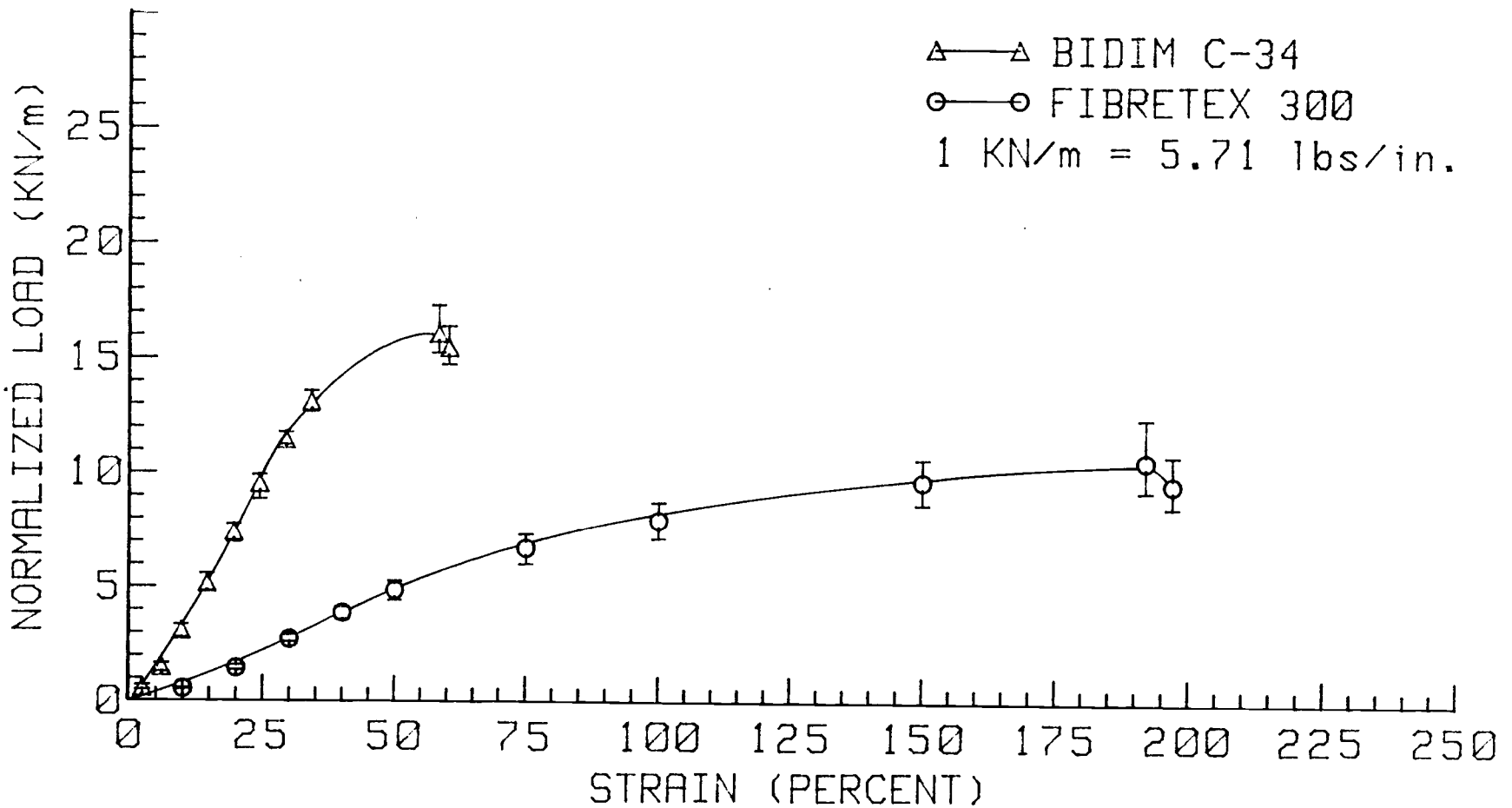

FIGURE A.8(b): NORMALIZED AXIAL LOAD VS. STRAIN AFTER 300 FREEZE-THAW CYCLES IN A DISTILLED WATER ENVIRONMENT (22 C, WET CONDITION).

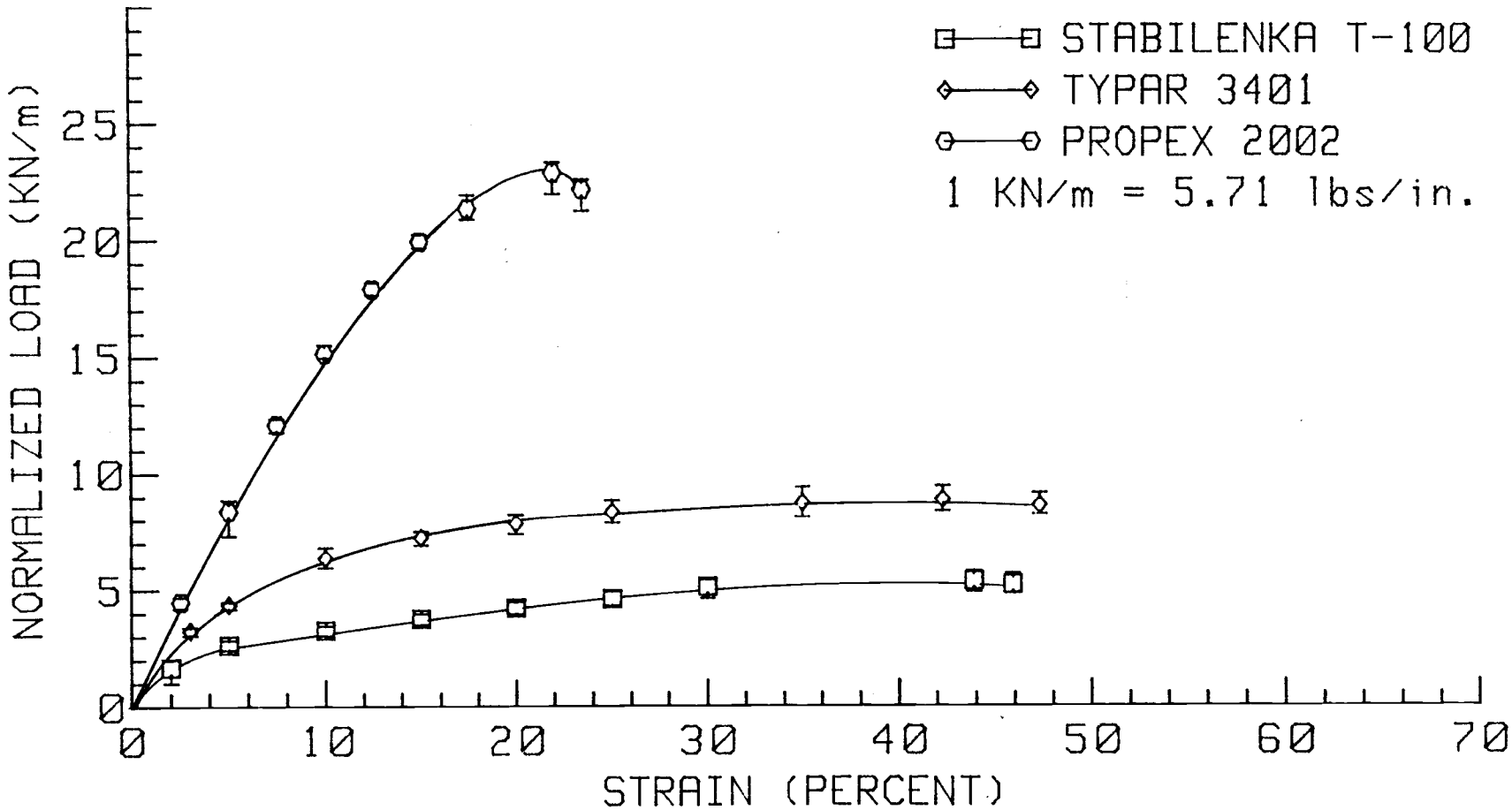

FIGURE A.9(a): NORMALIZED AXIAL LOAD VS. STRAIN AFTER 300 FREEZE-THAW CYCLES IN A SALINE WATER ENVIRONMENT (22 C, WET CONDITION).

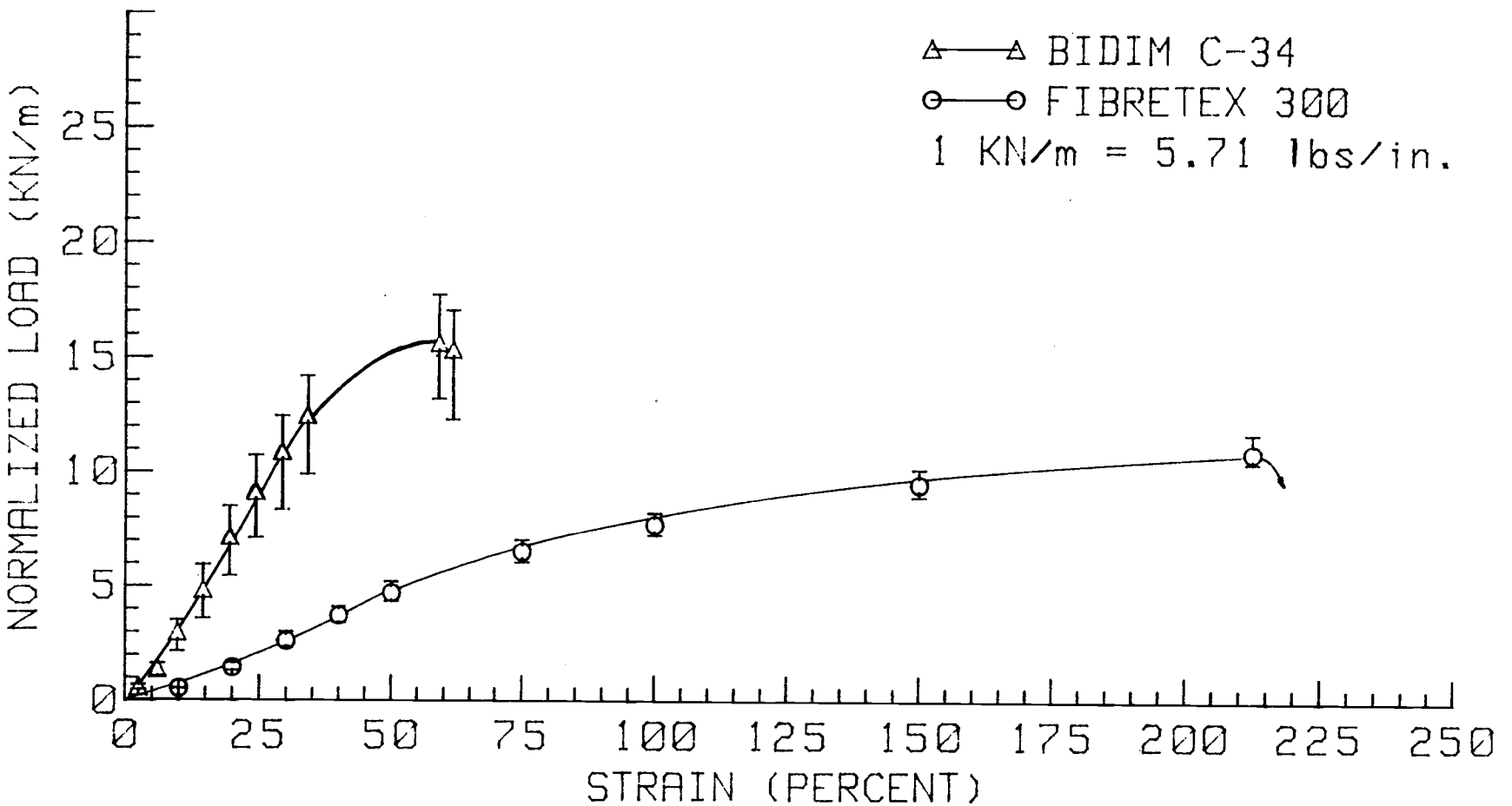

FIGURE A.9(b): NORMALIZED AXIAL LOAD VS. STRAIN AFTER 300 FREEZE-THAW CYCLES IN A SALINE WATER ENVIRONMENT (22 C, WET CONDITION).

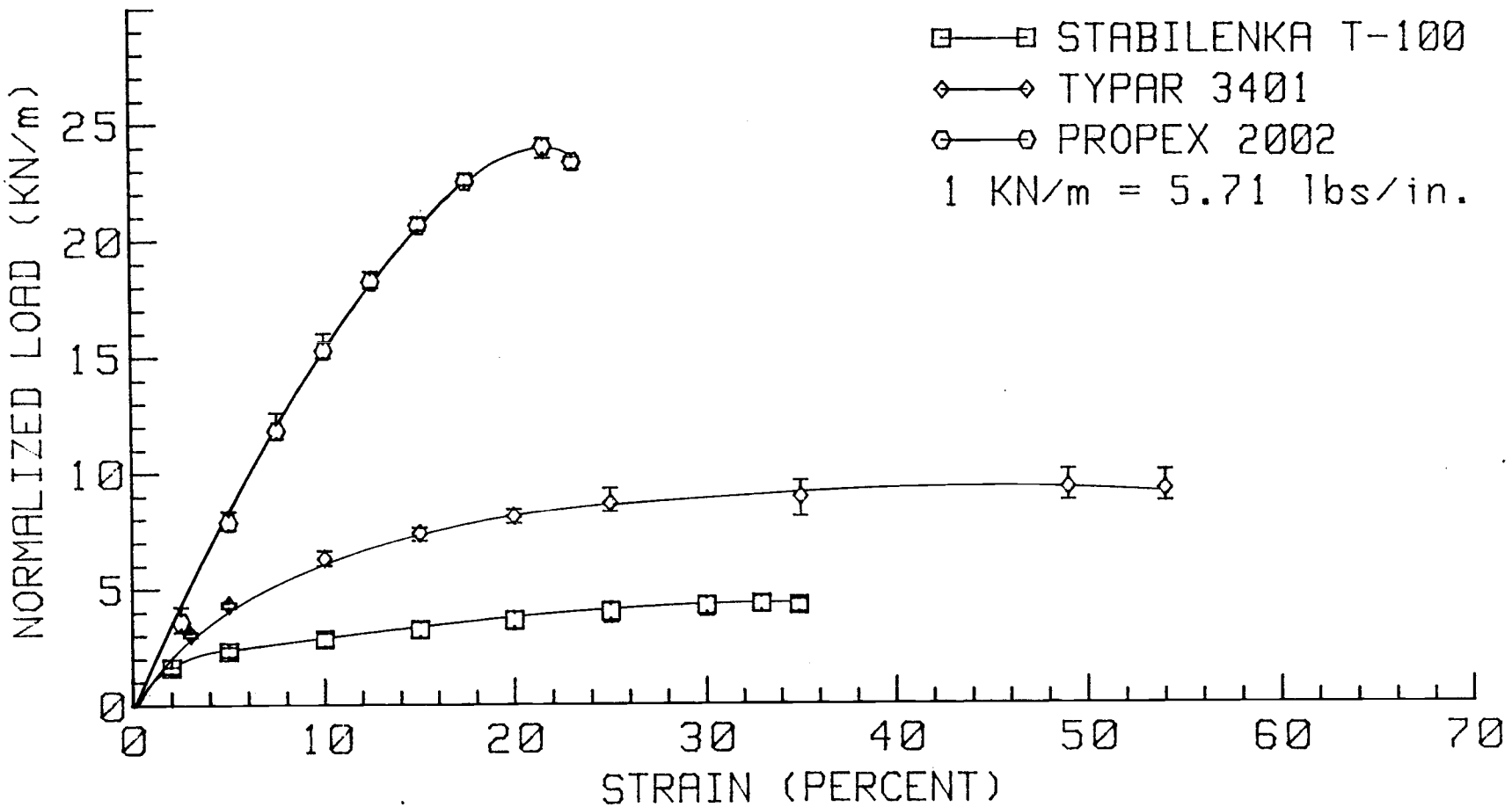

FIGURE A.10(a): NORMALIZED AXIAL LOAD VS. STRAIN AT 22 C (DRY CONDITION, 150 mm SAMPLE WIDTH).

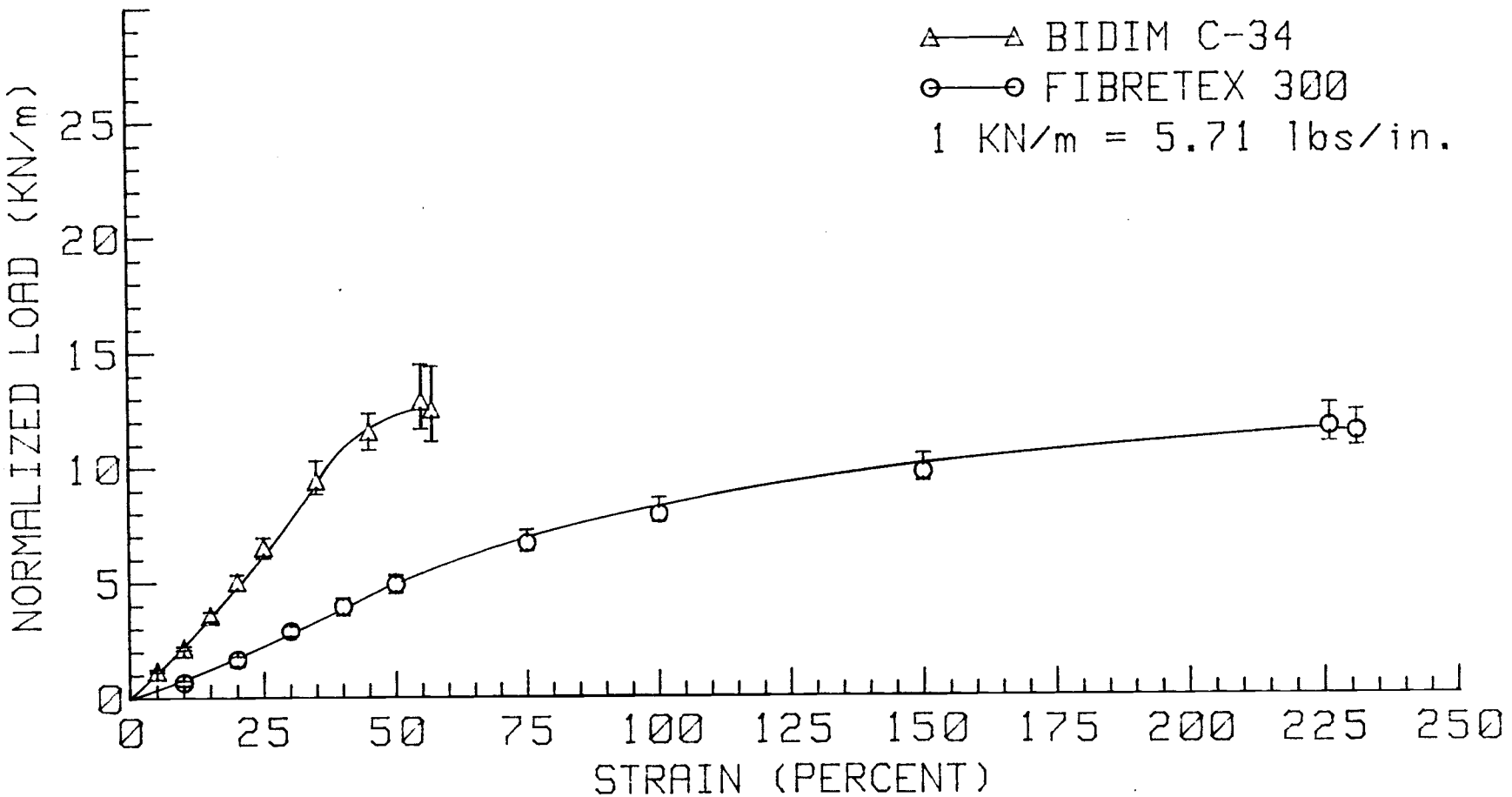

FIGURE A.10(b): NORMALIZED AXIAL LOAD VS. STRAIN AT 22 C (DRY CONDITION, 150 mm SAMPLE WIDTH).

Table A.1: Statistical analysis of normalized geotextile strengths obtained in load-strain tests.

Geotextile	Case	Number of Specimens	Standard Deviation (kN/m)	Mean Normalized Strength (kN/m)	90% Confidence Limits of Strength (kN/m)
Bidim C-34	I	5	1.5	18.6	17.1 to 20.0
	II	5	1.0	17.5	16.6 to 18.6
	III	5	1.9	16.0	14.2 to 17.7
	IV	5	0.89	16.1	15.2 to 16.9
	V	5	0.45	15.3	14.9 to 15.7
	VI	5	1.3	16.7	15.5 to 17.9
	VII	5	1.3	16.7	15.4 to 17.9
	VIII	5	1.0	16.0	15.0 to 17.0
	IX	5	1.9	15.6	13.8 to 17.4
Stabilenka T-100	I	5	0.41	4.90	5.52 to 6.29
	II	5	0.20	5.60	5.41 to 5.80
	III	5	0.20	5.34	5.15 to 5.53
	IV	5	0.44	5.69	5.27 to 6.11
	V	5	0.56	6.74	5.22 to 6.27
	VI	5	0.51	5.38	4.89 to 5.87
	VII	5	0.29	5.45	5.17 to 5.73
	VIII	5	0.23	5.43	5.20 to 5.66
	IX	5	0.35	5.34	5.01 to 5.67
Typar 3401	I	5	0.31	8.95	8.65 to 9.25
	II	5	0.31	10.3	10.0 to 10.6
	III	5	0.93	8.81	7.92 to 9.70
	IV	5	0.23	9.11	8.88 to 9.33
	V	5	0.54	8.86	8.23 to 9.51
	VI	5	0.57	8.48	7.93 to 9.02
	VII	5	0.28	8.97	8.70 to 9.23
	VIII	5	0.56	8.98	8.46 to 9.51
	IX	5	0.48	8.84	8.39 to 9.30
Fibretex 300	I	5	1.5	10.3	8.83 to 11.7
	II	0			
	III	5	1.5	9.86	8.42 to 11.3
	IV	5	1.4	9.91	8.60 to 11.2
	V	4	0.50	9.68	9.09 to 10.3
	VI	5	0.91	9.60	8.74 to 10.5
	VII	4	0.90	10.3	9.25 to 11.4
	VIII	5	1.3	10.6	9.35 to 11.8
	IX	3	0.72	10.9	9.68 to 12.1

Table A.1 (continued)

Geotextile	Case	Number of Specimens	Standard Deviation (kN/m)	Mean Normalized Strength (kN/m)	90% Confidence Limits of Strength (kN/m)
Propex 2002	I	5	0.81	24.1	23.5 to 24.9
	II	5	0.44	23.6	23.3 to 24.0
	III	5	0.64	24.3	23.8 to 24.9
	IV	4	0.62	25.4	24.7 to 26.1
	V	5	0.52	24.7	24.2 to 25.2
	VI	4	0.14	23.5	23.3 to 23.6
	VII	5	0.40	23.3	22.9 to 23.6
	VIII	5	1.0	21.4	20.3 to 22.4
	IX	5	0.54	22.8	22.2 to 23.3

I = Control, Dry Condition, 22°C (71°F)
II = Control, Dry Condition, -12°C (10°F)
III = Control, Wet Condition, 22°C (71°F)
IV = 50 Cycles Freeze/Thaw, Dry Environment, Wet Condition
V = 50 Cycles Freeze/Thaw, Distilled Water Environment, Wet Condition
VI = 50 Cycles Freeze/Thaw, Saline Water Environment, Wet Condition
VII = 300 Cycles Freeze/Thaw, Dry Environment, Wet Condition
VIII = 300 Cycles Freeze/Thaw, Distilled Water Environment, Wet Condition
IX = 300 Cycles Freeze/Thaw, Saline Water Environment, Wet Condition

Table A.2: Statistical analysis of percent strain at peak strength obtained in load-strain tests.

Geotextile	Case	Number of Specimens	Standard Deviation (%)	Mean Strain At Peak Strength(%)	90% Confidence Limits of Strain (%)
Bidim C-34	I	5	4.6	53.2	48.8 to 57.6
	II	5	1.3	60.0	58.8 to 61.2
	III	5	4.0	59.9	56.1 to 63.7
	IV	5	3.2	54.8	51.7 to 57.9
	V	5	4.5	58.9	54.7 to 63.2
	VI	5	2.5	54.5	52.2 to 56.8
	VII	5	2.5	64.7	62.3 to 67.1
	VIII	5	5.4	58.0	52.8 to 63.2
	IX	5	4.1	59.8	55.9 to 63.7
Stabilenka	I	5	1.7	32.9	31.3 to 34.5
	II	5	3.9	27.9	24.2 to 31.6
	III	5	2.6	44.0	41.5 to 46.5
	IV	5	4.2	43.8	39.8 to 47.8
	V	5	1.8	44.0	42.3 to 45.7
	VI	5	1.5	43.9	42.5 to 45.4
	VII	5	1.5	44.1	42.7 to 45.5
	VIII	5	3.5	41.6	38.3 to 44.9
	IV	5	2.2	43.9	41.8 to 46.0
Typar 3401	I	5	7.0	53.3	46.7 to 60.0
	II	5	5.2	31.3	27.3 to 35.3
	III	5	6.4	43.8	37.7 to 49.9
	IV	5	11.4	48.2	37.3 to 59.1
	V	4	7.5	47.8	39.0 to 56.6
	VI	5	2.9	36.9	34.2 to 39.7
	VII	5	5.9	40.4	34.8 to 46.0
	VIII	5	5.0	43.4	38.6 to 48.2
	IX	5	6.8	42.3	35.8 to 48.8
Fibretex	I	5	20.8	186	166 to 206
	II	0			
	III	5	27.5	166	140 to 192
	IV	5	39.7	187	149 to 225
	V	4	23.1	187	160 to 214
	VI	5	12.2	181	169 to 193
	VII	4	22.3	188	162 to 214
	VIII	5	22.0	192	171 to 213
	IX	3	13.2	213	191 to 235

Table A.2 (continued)

Geotextile	Case	Number of Specimens	Standard Deviation (%)	Mean Strain At Peak Strength(%)	90% Confidence Limits of Strain (%)
Propex 2002	I	5	0.99	21.2	20.3 to 22.1
	II	5	1.2	18.0	16.9 to 19.1
	III	5	1.4	19.8	18.4 to 21.2
	IV	4	0.66	20.4	19.6 to 21.2
	V	5	1.4	21.1	19.7 to 22.5
	VI	4	0.95	21.1	20.0 to 22.2
	VII	5	0.83	22.7	21.9 to 23.5
	IX	5	1.3	21.9	20.7 to 23.2

I = Control, Dry Condition, 22°C (71°F)
II = Control, Dry Condition, -12°C (10°F)
III = Control, Wet Condition, 22°C (71°F)
IV = 50 Cycles Freeze/Thaw, Dry Environment, Wet Condition
V = 50 Cycles Freeze/Thaw, Distilled Water Environment, Wet Condition
VI = 50 Cycles Freeze/Thaw, Saline Water Environment, Wet Condition
VII = 300 Cycles Freeze/Thaw, Dry Environment, Wet Condition
VIII = 300 Cycles Freeze/Thaw, Distilled Water Environment, Wet Condition
IX = 300 Cycles Freeze/Thaw, Saline Water Environment, Wet Condition

Table A.3: Statistical analysis of normalized secant moduli at 10% strain for load-strain tests.

Geotextile	Case	Number of Specimens	Standard Deviation (kN/m)	Mean Secant Modulus at 10% Strain (kN/m)	90% Confidence Limits of Secant Modulus (kN/m)
Bidim C-34	I	5	7.5	33.5	26.3 to 40.6
	II	5	3.7	20.3	16.8 to 23.8
	III	5	5.6	25.2	19.8 to 30.7
	IV	5	3.7	28.3	24.9 to 31.9
	V	5	4.2	21.9	17.9 to 25.9
	VI	5	5.5	33.6	28.4 to 38.9
	VII	5	2.8	28.6	25.9 to 31.2
	VIII	5	2.4	31.7	29.4 to 34.0
	IX	5	5.7	30.7	25.2 to 36.1
Stabilenka T-100	I	5	2.6	37.7	35.2 to 40.1
	II	5	1.7	41.0	39.4 to 42.6
	III	5	2.6	30.8	28.4 to 33.3
	IV	5	2.7	33.8	31.2 to 36.4
	V	5	2.8	33.1	30.5 to 35.7
	VI	5	4.1	31.2	27.3 to 35.0
	VII	5	2.9	33.4	30.7 to 36.3
	VIII	5	2.0	33.4	31.5 to 35.4
	IX	5	1.8	32.6	30.8 to 34.3
Typar 3401	I	5	1.7	56.9	55.3 to 58.5
	II	5	3.1	75.1	72.2 to 78.1
	III	5	2.7	61.8	59.2 to 64.3
	IV	5	2.8	62.2	59.5 to 64.8
	V	5	2.8	62.2	59.5 to 64.8
	VI	5	4.0	59.2	55.3 to 63.1
	VII	5	1.2	63.8	62.7 to 64.8
	VIII	5	2.2	61.5	57.2 to 65.9
	IX	5	3.2	63.6	60.4 to 66.7
Fibretex 300	I	5	0.96	6.20	5.29 to 7.11
	II	5	1.3	7.46	6.27 to 8.65
	III	5	3.9	7.50	3.80 to 11.2
	IV	5	1.1	5.74	4.75 to 6.74
	V	4	0.66	4.96	4.19 to 5.73
	VI	5	0.57	6.09	5.55 to 6.65
	VII	4	0.46	4.71	4.17 to 5.25
	VIII	5	0.22	5.46	5.25 to 5.67
	IX	3	0.11	5.36	5.17 to 5.55

Table A.3 (continued)

Geotextile	Case	Number of Specimens	Standard Deviation (kN/m)	Mean Secant Modulus at 10% Strain (kN/m)	90% Confidence Limits of Secant Modulus (kN/m)
Propex 2002	I	5	2.9	151	148 to 153
	II	5	2.7	163	161 to 166
	III	5	3.1	162	159 to 165
	IV	4	1.2	162	160 to 163
	V	5	2.6	150	148 to 153
	VI	4	3.7	148	144 to 152
	VII	5	2.6	146	144 to 149
	VIII	5	5.4	144	139 to 149
	IX	5	2.2	151	149 to 153

I = Control, Dry Condition, 22°C (71°F)
II = Control, Dry Condition, -12°C (10°F)
III = Control, Wet Condition, 22°C (71°F)
IV = 50 Cycles Freeze/Thaw, Dry Environment, Wet Condition
V = 50 Cycles Freeze/Thaw, Distilled Water Environment, Wet Condition
VI = 50 Cycles Freeze/Thaw, Saline Water Environment, Wet Condition
VII = 300 Cycles Freeze/Thaw, Dry Environment, Wet Condition
VIII = 300 Cycles Freeze/Thaw, Distilled Water Environment, Wet Condition
IX = 300 Cycles Freeze/Thaw, Saline Water Environment, Wet Condition

APPENDIX B

Creep Test Data

The load levels (as a percent of the wide strip tensile strength) of the creep curves presented in Figures B.1 through B.7 have been normalized to the nominal geotextile weight per unit area using Equation 4.3.1. The symbol (i.e., circle, square, etc.) represents the mean strain of all of the specimens (three specimens were tested for each case) of a particular geotextile and case. The error bars represent the maximum and minimum strains obtained for the group of specimens. The actual values of the strains obtained for each specimen tested are presented in Tables B.1 through B.30. Columns with the heading "Staples" contain strains measured using the staples placed on the geotextile. Columns with the heading "Grips" contain strains measured using the edges of the grips. The column with the heading "Average" represents the average strain for all six strains (three specimens, strain measured using both staples and grips).

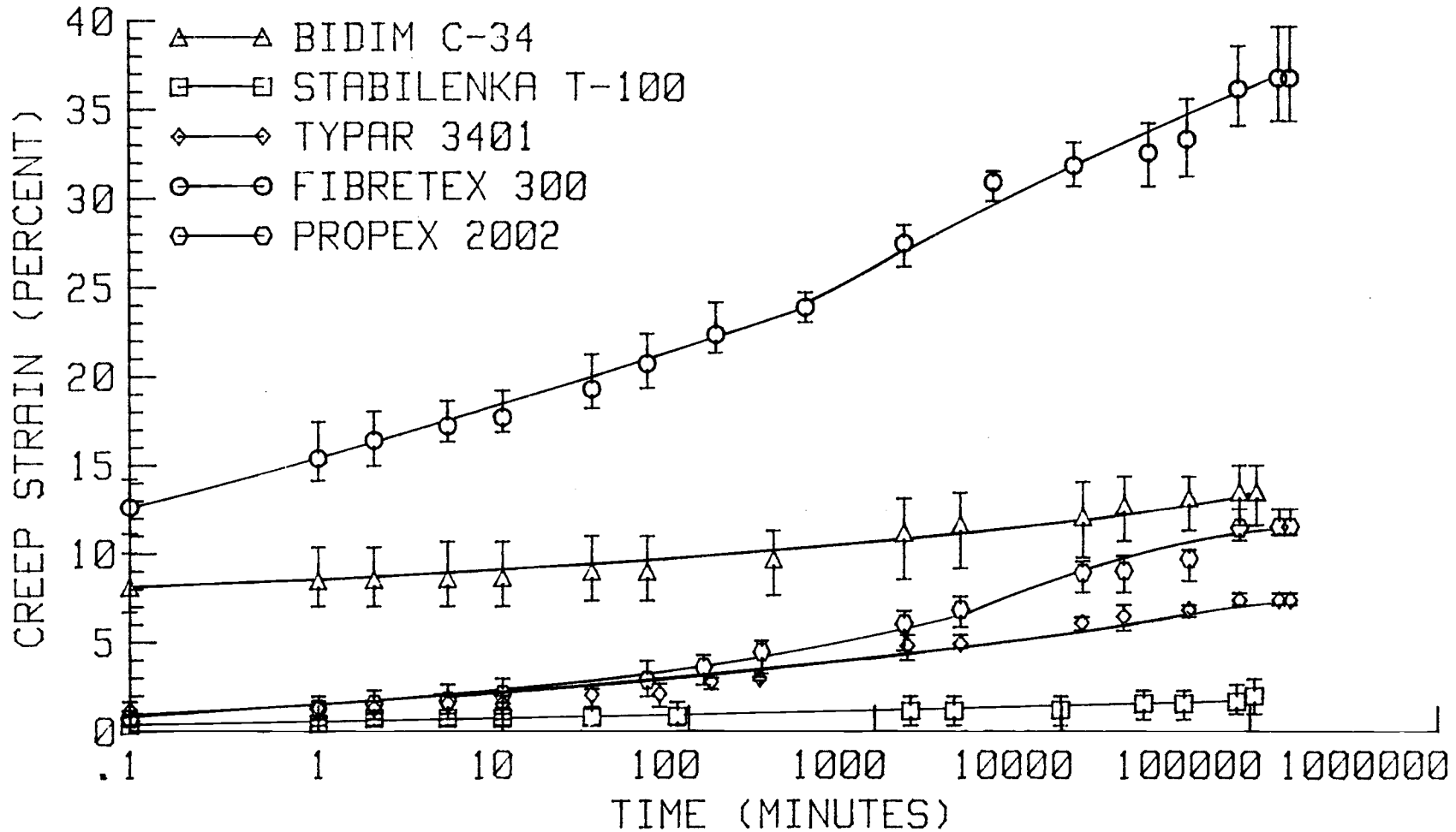

FIGURE B.1: CREEP STRAIN VS. TIME AT 20% WIDE STRIP TENSILE STRENGTH AND 22 C.

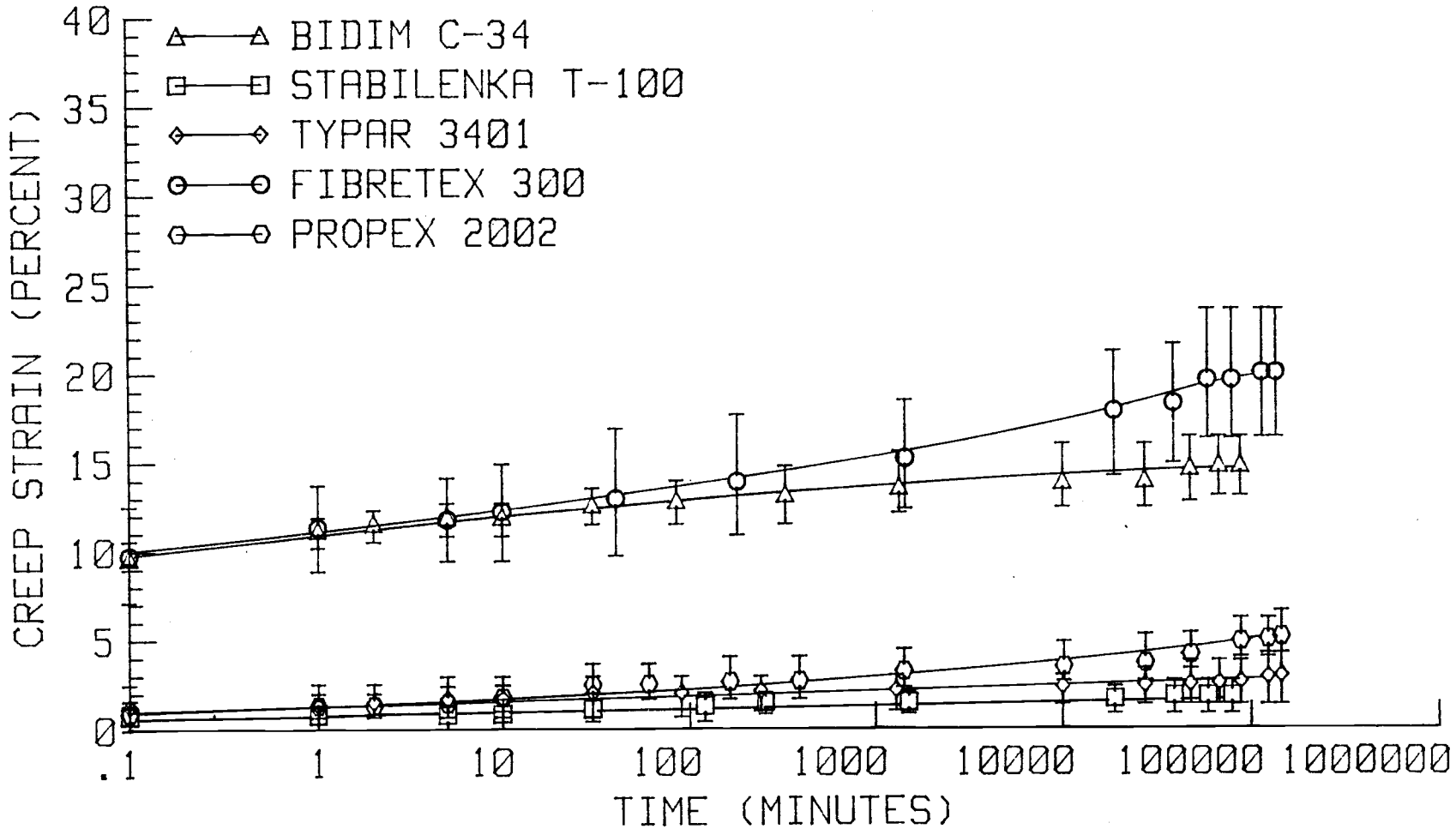

FIGURE B.2: CREEP STRAIN VS. TIME AT 20% WIDE STRIP TENSILE STRENGTH AND -12 C.

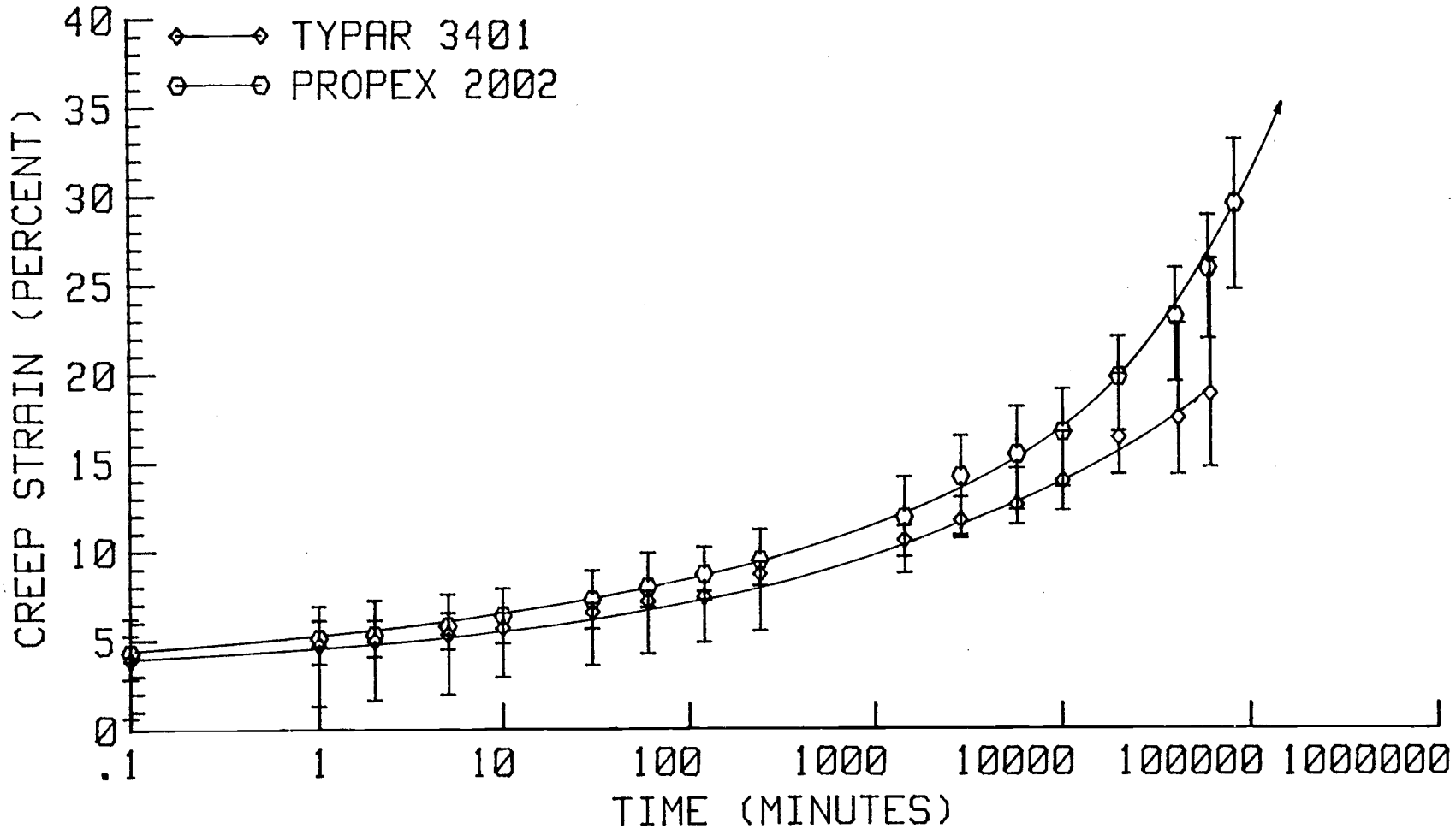

FIGURE B.3: CREEP STRAIN VS. TIME AT 35% WIDE STRIP TENSILE STRENGTH AND 22 C.

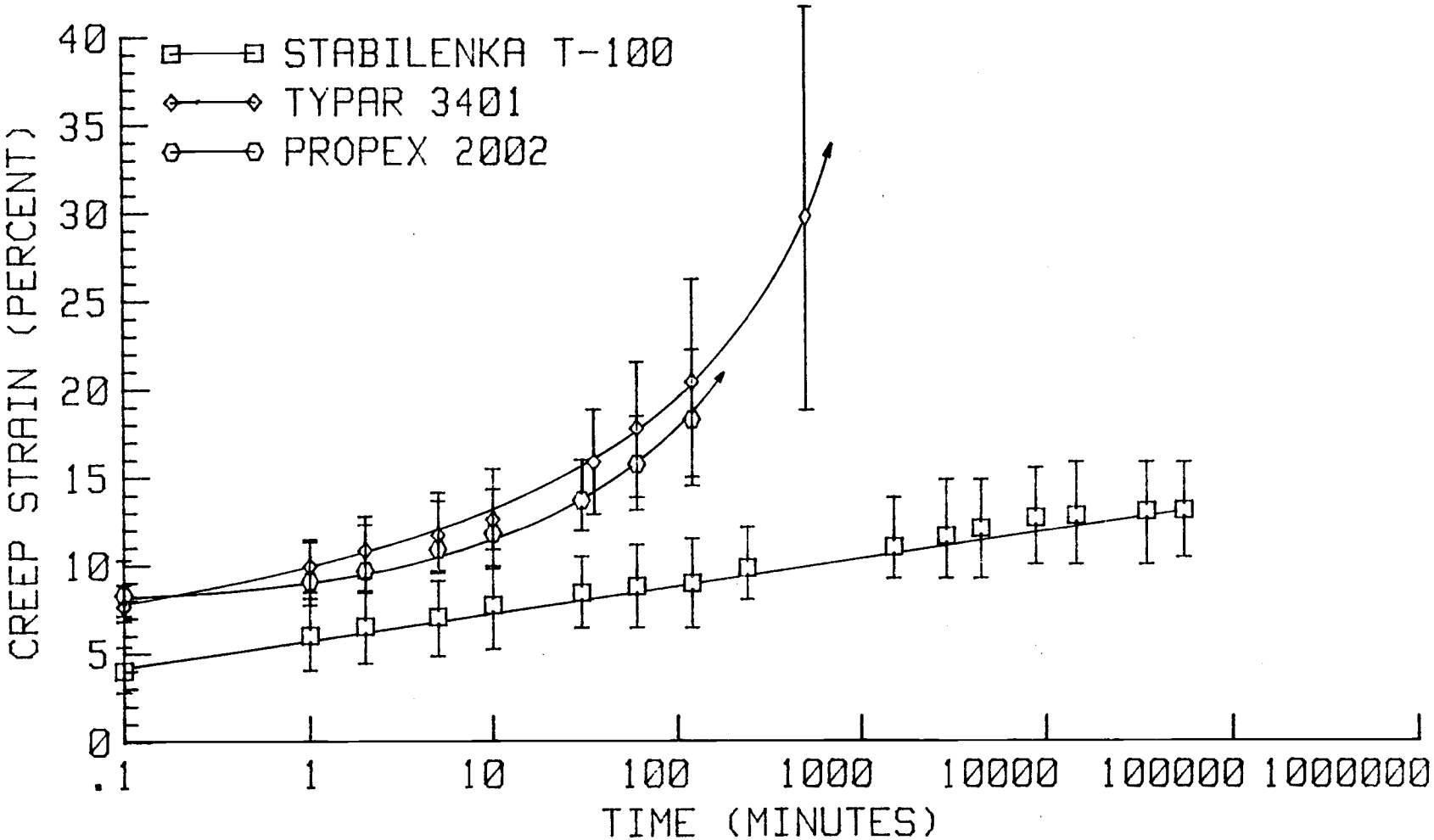

FIGURE B.4(a): CREEP STRAIN VS. TIME AT 50% WIDE STRIP TENSILE STRENGTH AND 22 C.

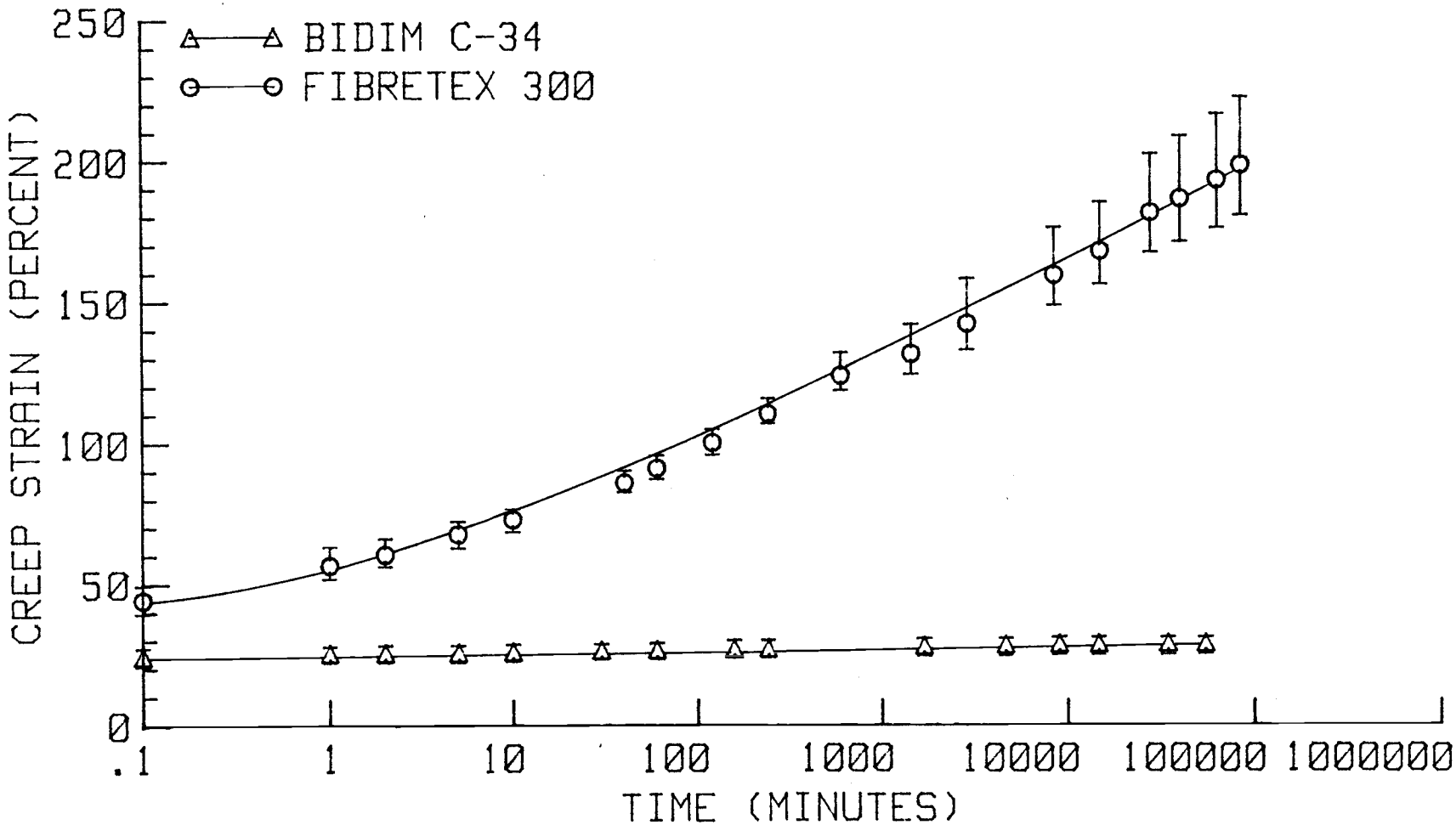

FIGURE B.4(b): CREEP STRAIN VS. TIME AT 50% WIDE STRIP TENSILE STRENGTH AND 22 C.

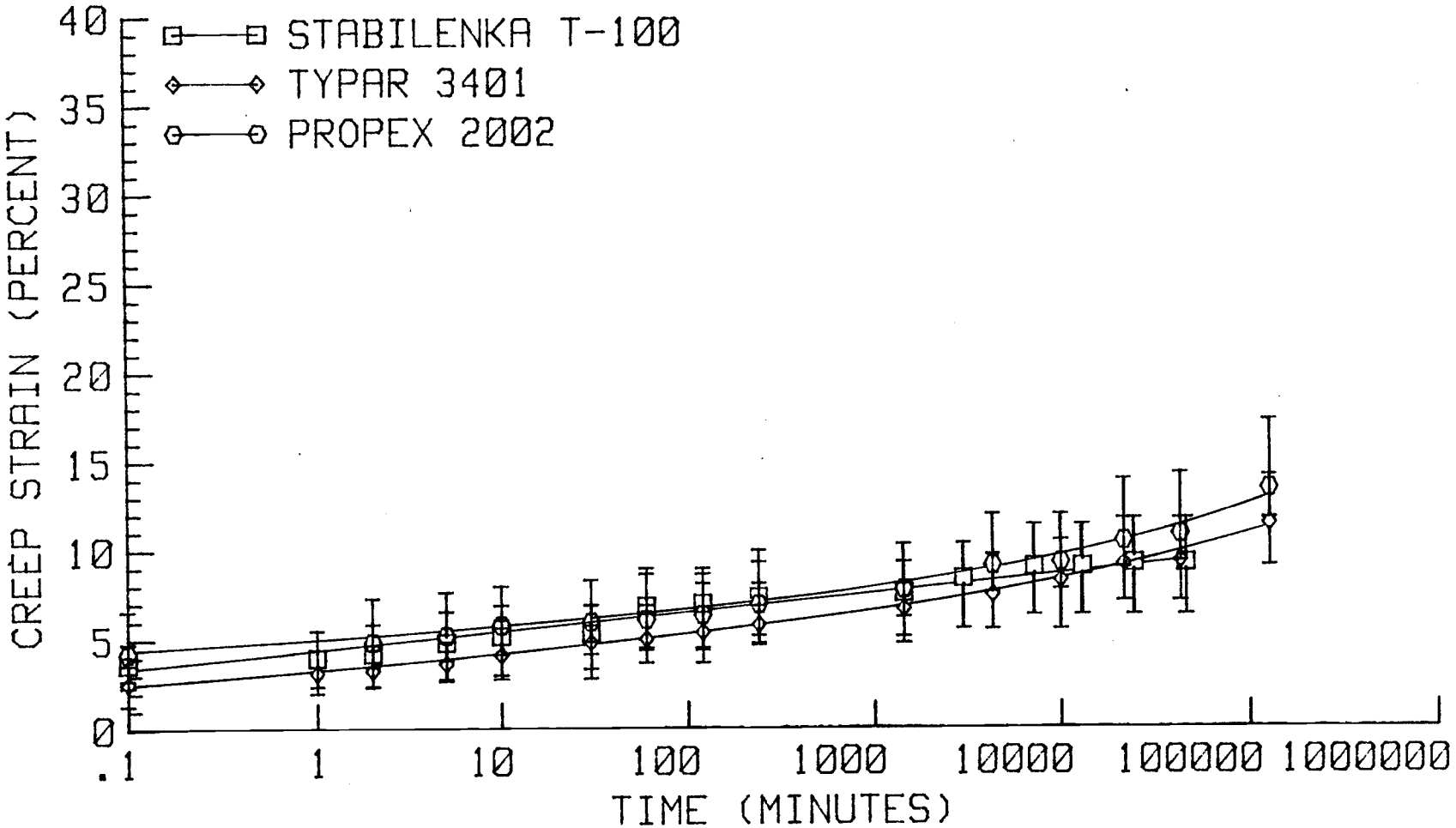

FIGURE B.5(a): CREEP STRAIN VS. TIME AT 50% WIDE STRIP TENSILE STRENGTH AND -12 C.

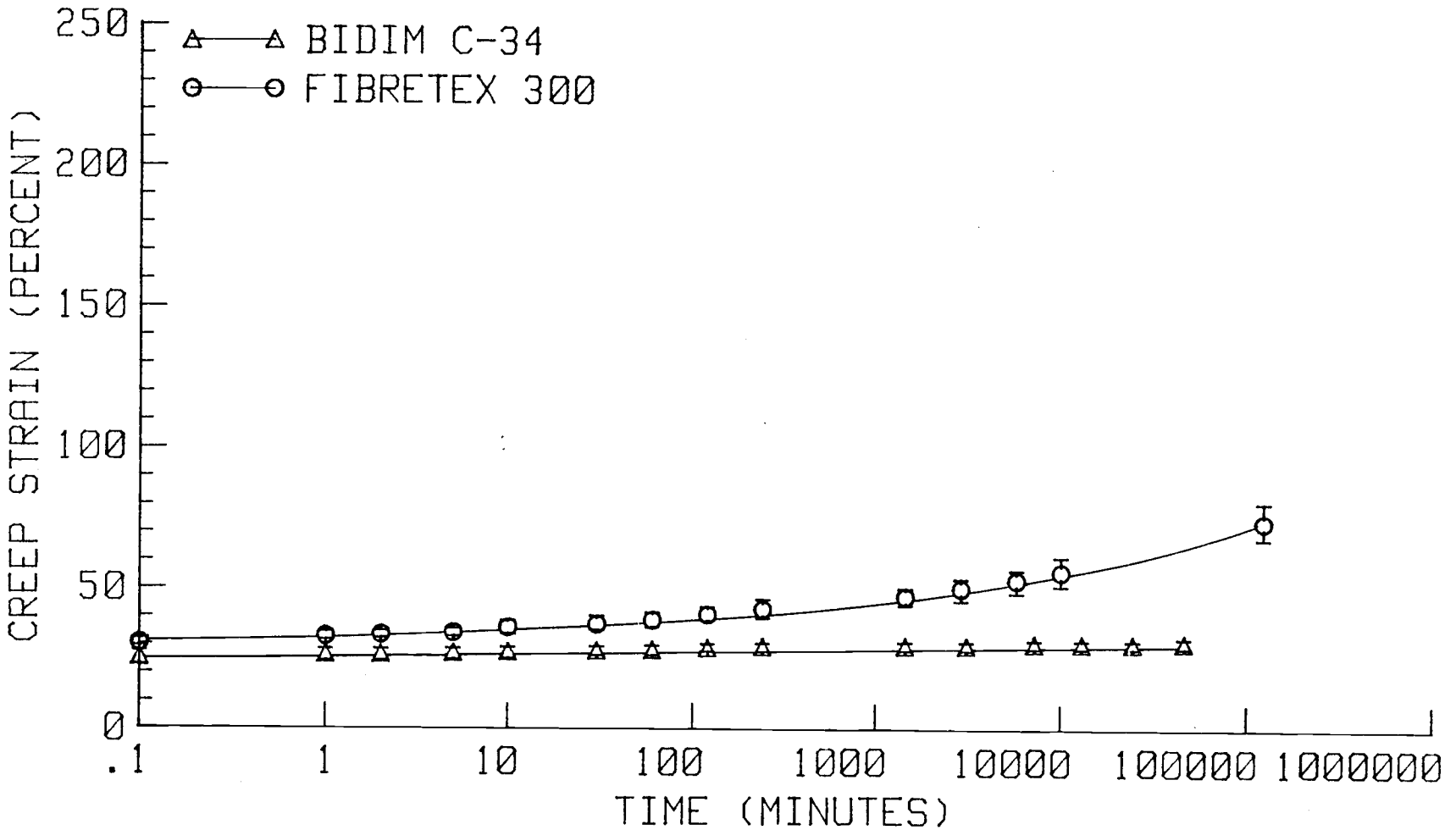

FIGURE B.5(b): CREEP STRAIN VS. TIME AT 50% WIDE STRIP TENSILE STRENGTH AND -12 C.

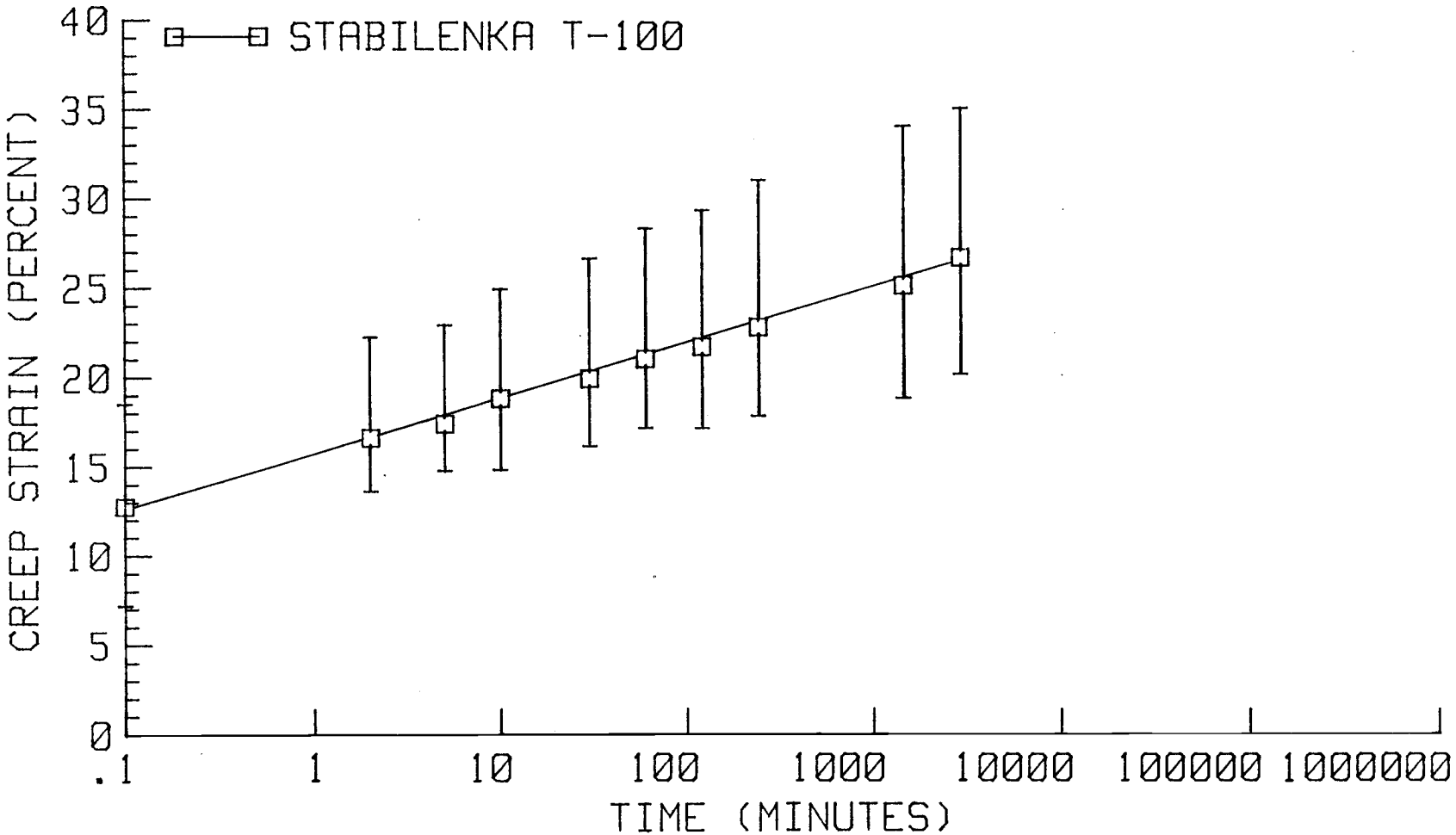

FIGURE B.6(a): CREEP STRAIN VS. TIME AT 65% WIDE STRIP TENSILE STRENGTH AND 22 C.

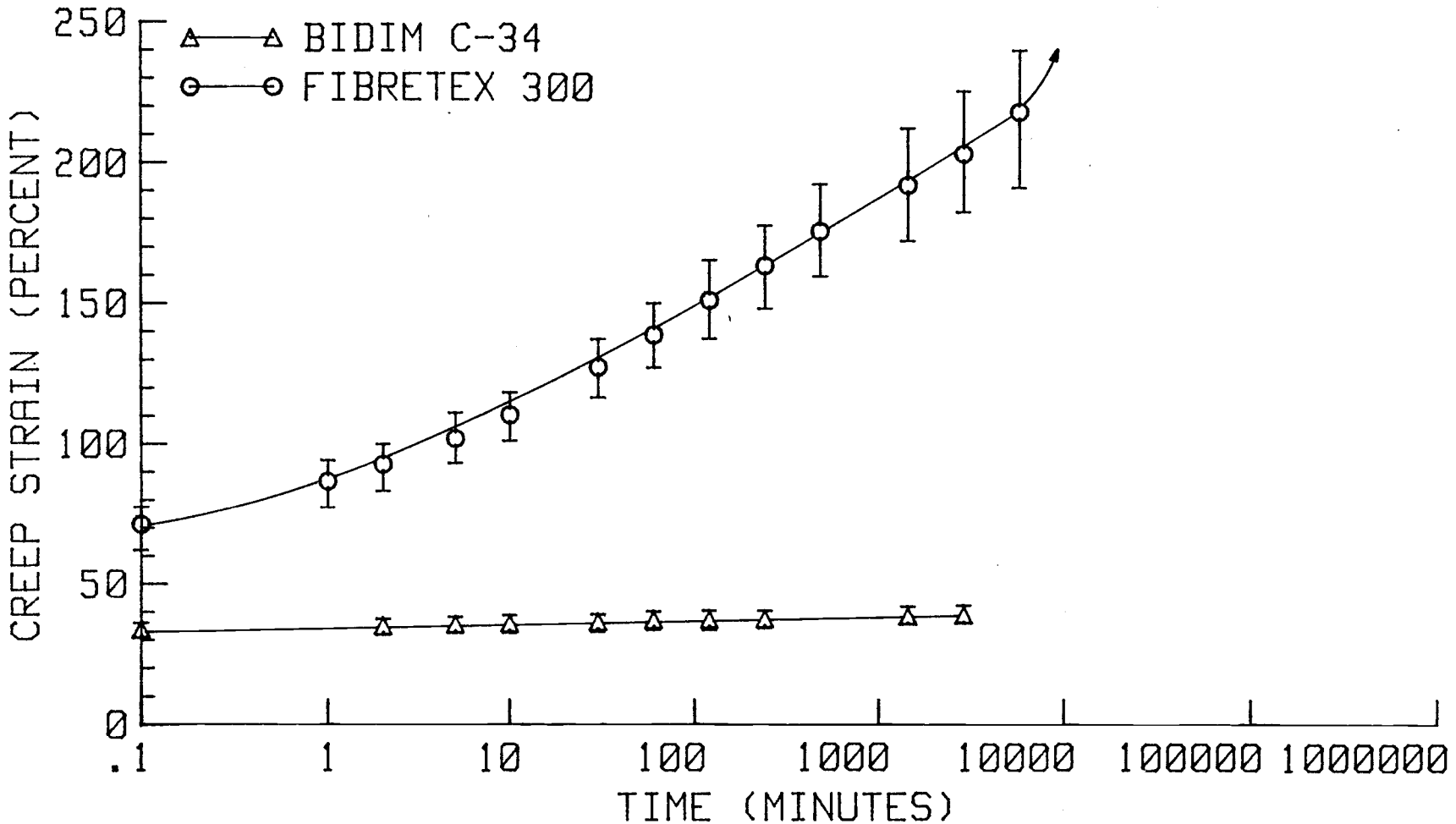

FIGURE B.6(b): CREEP STRAIN VS. TIME AT 65% WIDE STRIP TENSILE STRENGTH AND 22 C.

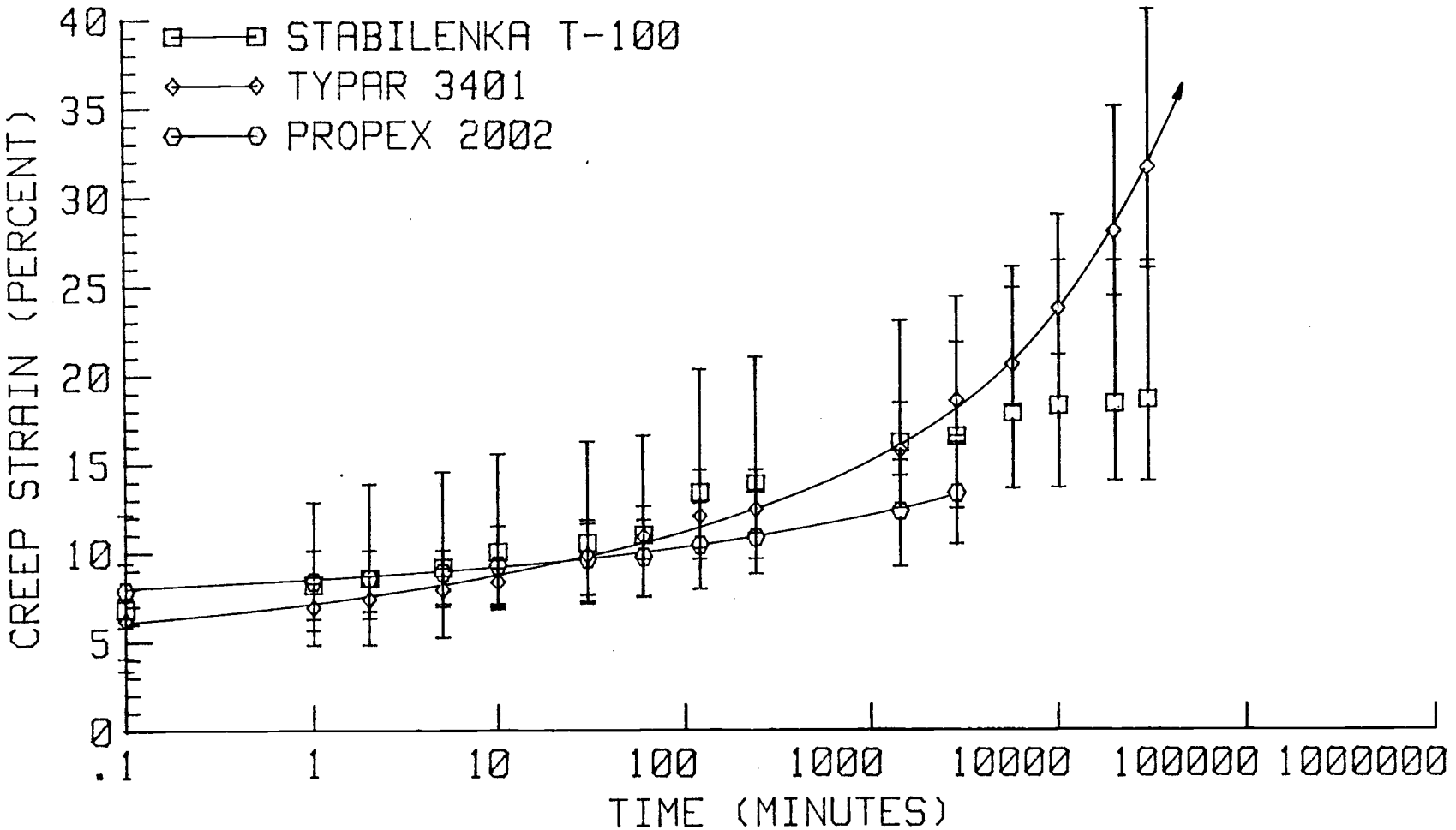

FIGURE B.7(a): CREEP STRAIN VS. TIME AT 65% WIDE STRIP TENSILE STRENGTH AND -12 C.

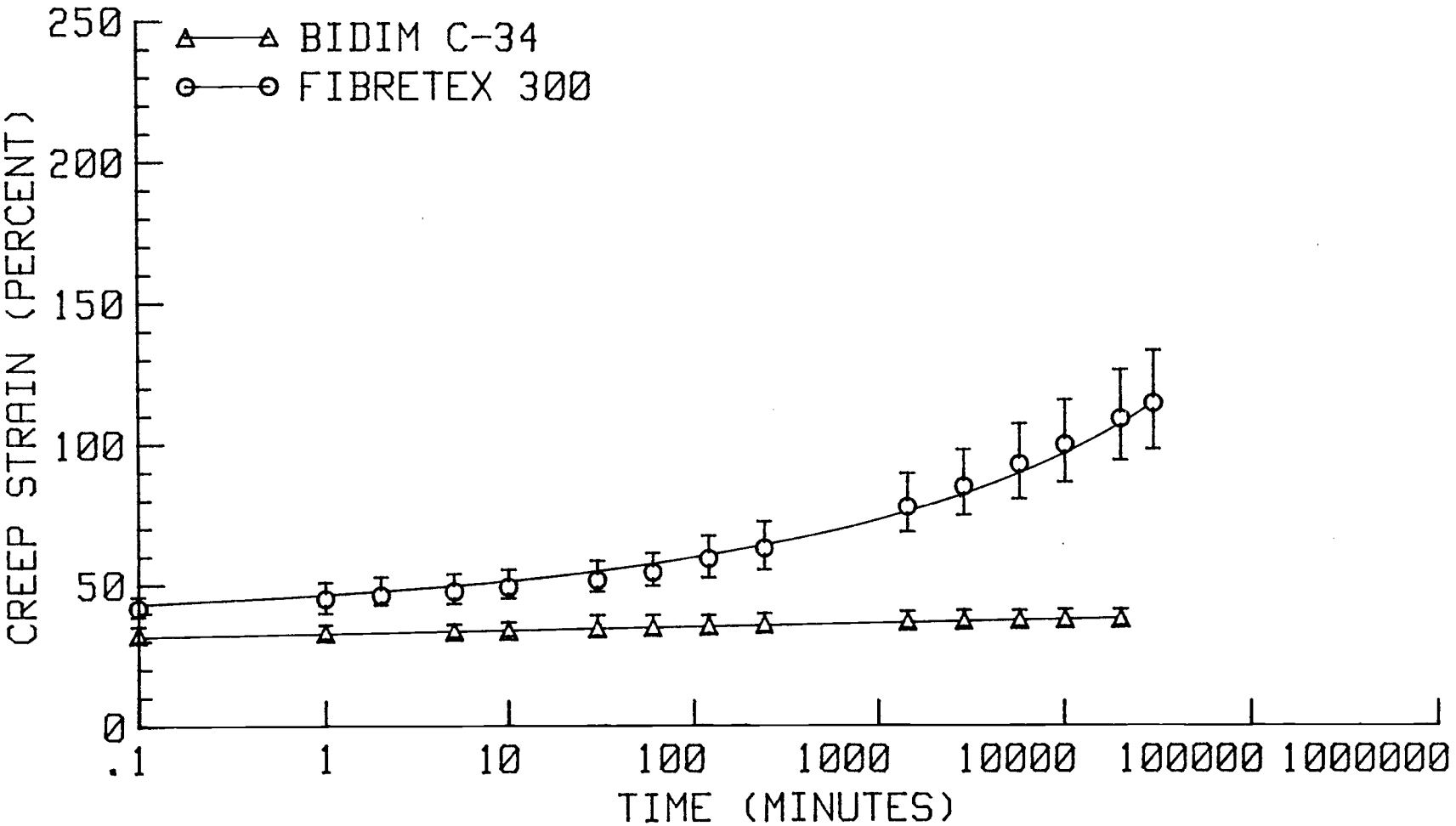

FIGURE B.7(b): CREEP STRAIN VS. TIME AT 65% WIDE STRIP TENSILE STRENGTH AND -12 C.

TABLE B.1 : CREEP STRAIN VS. TIME AT 20 % WIDE STRIP TENSILE STRENGTH AND -12 C FOR BIDIM C-34.

TIME (MIN.)	% STRAIN SAMPLE 1		% STRAIN SAMPLE 2		% STRAIN SAMPLE 3		% STRAIN AVERAGE
	STAPLES	GRIPS	STAPLES	GRIPS	STAPLES	GRIPS	
.10	9.63	10.28	10.61	9.24	9.43	9.00	9.70
1.00	10.74	11.84	11.43	10.19	11.89	11.25	11.22
2.00	11.11	12.15	11.84	10.51	12.30	11.58	11.58
5.00	11.48	12.46	12.24	10.83	12.70	11.90	11.94
10.00	11.48	12.46	12.24	10.83	12.70	11.90	11.94
30.00	13.33	12.77	12.24	11.46	13.52	12.22	12.59
85.00	13.33	13.08	12.65	11.46	13.93	12.54	12.84
330.00	13.33	13.08	13.88	11.46	14.75	12.54	13.18
1340.00	13.70	13.08	13.88	12.10	15.57	13.18	13.59
10030.00	14.07	13.71	13.88	12.42	15.98	13.18	13.87
27505.00	14.07	13.71	14.29	12.42	15.98	13.18	13.94
47760.00	15.19	14.33	14.69	12.74	16.39	14.47	14.64
67680.00	15.56	14.33	14.69	13.06	16.39	14.79	14.80
87840.00	15.56	14.33	14.69	13.06	16.39	14.79	14.80

TABLE B.2 : CREEP STRAIN VS. TIME AT 20 % WIDE STRIP TENSILE STRENGTH AND -12 C FOR STABILENKA T-100.

TIME (MIN.)	% STRAIN SAMPLE 1		% STRAIN SAMPLE 2		% STRAIN SAMPLE 3		% STRAIN AVERAGE
	STAPLES	GRIPS	STAPLES	GRIPS	STAPLES	GRIPS	
.10	0.00	.68	.82	1.34	.83	1.01	.78
1.00	0.00	.68	.82	1.34	.83	1.01	.78
5.00	0.00	.68	.82	1.34	.83	1.01	.78
10.00	0.00	.68	.82	1.68	.83	1.01	.84
30.00	.40	1.02	1.22	1.68	.83	1.35	1.08
120.00	.40	1.02	1.22	2.01	1.24	1.68	1.26
255.00	.81	1.02	1.63	2.01	1.24	2.02	1.46
1500.00	.81	1.02	1.63	2.01	1.24	2.02	1.46
18970.00	.81	1.02	1.63	2.35	1.66	2.36	1.64
39240.00	.81	1.69	1.63	2.68	1.66	2.36	1.81
59040.00	.81	1.69	1.63	2.68	1.66	2.36	1.81
79200.00	.81	1.69	1.63	2.68	1.66	2.36	1.81

TABLE B.3 : CREEP STRAIN VS. TIME AT 20 % WIDE STRIP TENSILE STRENGTH AND -12 C FOR TYPAR 3401.

TIME (MIN.)	% STRAIN SAMPLE 1		% STRAIN SAMPLE 2		% STRAIN SAMPLE 3		% STRAIN AVERAGE
	STAPLES	GRIPS	STAPLES	GRIPS	STAPLES	GRIPS	
.10	.84	.33	1.20	1.66	2.52	1.33	1.31
1.00	.84	.33	1.20	1.66	2.52	1.33	1.31
2.00	1.67	.66	1.20	1.66	2.52	1.33	1.51
5.00	1.67	.66	1.20	1.99	2.94	1.66	1.69
10.00	1.67	.66	1.20	1.99	2.94	1.66	1.69
30.00	1.67	.66	2.01	2.65	2.94	1.99	1.99
90.00	1.67	.66	2.01	2.65	2.94	1.99	1.99
240.00	1.67	.99	2.01	2.65	2.94	2.33	2.10
1285.00	1.67	.99	2.01	2.98	2.94	2.33	2.15
9970.00	1.67	1.32	2.01	2.98	2.94	2.99	2.32
27445.00	1.67	1.32	2.01	2.98	3.36	2.99	2.39
47700.00	1.67	1.32	2.01	2.98	3.78	2.99	2.46
67680.00	1.67	1.32	2.01	3.31	3.78	2.99	2.51
87840.00	2.09	1.32	2.01	3.31	3.78	2.99	2.58
122400.00	2.93	1.32	2.41	3.31	4.20	2.99	2.86
144000.00	3.35	1.32	2.41	3.31	4.20	2.99	2.93

TABLE B.4 : CREEP STRAIN VS. TIME AT 20 % WIDE STRIP TENSILE STRENGTH AND -12 C FOR FIBRETEX 300.

TIME (MIN.)	% STRAIN SAMPLE 1		% STRAIN SAMPLE 2		% STRAIN SAMPLE 3		% STRAIN AVERAGE
	STAPLES	GRIPS	STAPLES	GRIPS	STAPLES	GRIPS	
.10	7.64	7.14	9.81	9.57	12.55	12.01	9.79
1.00	9.45	8.86	11.70	11.30	13.73	12.91	11.33
5.00	10.18	9.43	11.70	11.59	14.12	13.51	11.76
10.00	10.18	9.43	12.45	12.17	14.90	14.11	12.21
40.00	10.55	9.71	13.58	12.46	16.86	14.41	12.93
180.00	11.64	10.86	14.72	13.04	17.65	15.32	13.87
1440.00	12.36	12.86	15.47	15.65	18.43	16.22	15.17
18914.00	14.18	15.43	18.87	17.39	21.18	19.82	17.81
39100.00	14.91	15.71	18.87	17.97	21.57	20.42	18.24
59040.00	16.36	16.29	20.38	19.13	23.53	21.62	19.55
79200.00	16.36	16.29	20.38	19.13	23.53	21.62	19.55
113800.00	16.36	17.43	20.75	19.42	23.53	22.22	19.95
135400.00	16.36	17.43	20.75	19.42	23.53	22.22	19.95

TABLE B.5 : CREEP STRAIN VS. TIME AT 20 % WIDE STRIP TENSILE STRENGTH AND -12 C FOR PROPEX 2002.

TIME (MIN.)	% STRAIN SAMPLE 1		% STRAIN SAMPLE 2		% STRAIN SAMPLE 3		% STRAIN AVERAGE
	STAPLES	GRIPS	STAPLES	GRIPS	STAPLES	GRIPS	
.10	1.20	.65	.81	.33	1.65	1.00	.94
1.00	2.00	.97	1.62	.66	1.65	1.00	1.32
2.00	2.00	.97	1.62	.66	1.65	1.00	1.32
5.00	2.40	1.29	1.62	.66	1.65	1.00	1.44
10.00	2.40	1.29	2.02	.99	2.47	1.33	1.75
30.00	3.20	1.62	3.64	1.66	2.88	1.66	2.44
60.00	3.20	1.94	3.64	1.66	2.88	1.66	2.50
164.00	3.20	1.94	4.05	1.66	2.88	1.99	2.62
390.00	3.20	2.27	4.05	1.66	2.88	1.99	2.67
1414.00	3.60	2.91	4.45	2.32	3.29	2.66	3.21
10129.00	3.60	3.24	4.86	2.65	3.70	2.66	3.45
27600.00	3.60	3.24	5.26	2.98	4.12	2.66	3.64
47850.00	3.60	3.56	5.26	3.64	5.35	3.32	4.12
87840.00	4.80	4.21	5.67	4.30	6.17	3.99	4.86
122400.00	5.60	4.21	5.67	4.30	6.17	3.99	4.99
144000.00	5.60	4.21	5.67	4.30	6.58	4.32	5.11

TABLE B.6 : CREEP STRAIN VS. TIME AT 20 % WIDE STRIP TENSILE STRENGTH AND 22 C FOR BIDIM C-34.

TIME (MIN.)	% STRAIN SAMPLE 1		% STRAIN SAMPLE 2		% STRAIN SAMPLE 3		% STRAIN AVERAGE
	STAPLES	GRIPS	STAPLES	GRIPS	STAPLES	GRIPS	
.10	8.14	6.73	8.14	10.06	8.14	7.50	8.12
1.00	8.53	7.03	8.53	10.37	8.53	7.81	8.47
2.00	8.53	7.03	8.53	10.37	8.53	8.13	8.52
5.00	8.53	7.03	8.53	10.67	8.53	8.13	8.57
10.00	8.53	7.03	8.53	10.67	8.53	8.44	8.62
30.00	8.91	7.34	8.91	10.98	8.91	8.75	8.97
60.00	8.91	7.34	8.91	10.98	8.91	8.75	8.97
287.00	9.69	7.65	9.69	11.28	9.69	10.00	9.67
1440.00	11.24	8.56	11.24	11.59	11.24	13.13	11.17
2880.00	11.63	9.17	11.63	12.20	11.63	13.44	11.62
12927.00	12.02	9.79	12.02	12.50	12.02	14.06	12.07
21567.00	12.79	10.70	12.79	12.80	12.79	14.38	12.71
47682.00	13.18	11.31	13.18	13.72	13.18	14.38	13.16
87840.00	13.57	11.62	13.57	13.72	13.57	15.00	13.51
108000.00	13.57	11.62	13.57	13.72	13.57	15.00	13.51

TABLE B.7 : CREEP STRAIN VS. TIME AT 20 % WIDE STRIP TENSILE STRENGTH AND 22 C FOR STABILENKA T-100.

TIME (MIN.)	% STRAIN SAMPLE 1		% STRAIN SAMPLE 2		% STRAIN SAMPLE 3		% STRAIN AVERAGE
	STAPLES	GRIPS	STAPLES	GRIPS	STAPLES	GRIPS	
.10	.40	.33	.40	.33	.40	.33	.36
1.00	.40	.33	.40	.33	.40	.66	.42
2.00	.80	.33	.80	.65	.80	.99	.73
5.00	.80	.33	.80	.65	.80	.99	.73
10.00	.80	.33	.80	.65	.80	.99	.73
30.00	.80	.33	.80	.65	.80	1.32	.78
87.00	.80	.33	.80	.65	.80	1.65	.84
1560.00	1.20	.33	1.20	.98	1.20	1.98	1.15
2665.00	1.20	.33	1.20	.98	1.20	1.98	1.15
9885.00	1.20	.33	1.20	1.31	1.20	1.98	1.20
27212.00	1.60	.66	1.60	1.63	1.60	2.31	1.57
44647.00	1.60	.66	1.60	1.63	1.60	2.31	1.57
84960.00	1.60	.99	1.60	1.63	1.60	2.64	1.68
105100.00	2.00	.99	2.00	1.96	2.00	2.97	1.99

TABLE B.8 : CREEP STRAIN VS. TIME AT 20 % WIDE STRIP TENSILE STRENGTH AND 22 C FOR TYPAR 3401.

TIME (MIN.)	% STRAIN SAMPLE 1		% STRAIN SAMPLE 2		% STRAIN SAMPLE 3		% STRAIN AVERAGE
	STAPLES	GRIPS	STAPLES	GRIPS	STAPLES	GRIPS	
.10 •	1.22	1.69	1.22	1.33	1.22	.34	1.17
1.00	1.22	1.69	1.22	1.67	1.22	.68	1.29
2.00	1.22	1.69	1.22	1.67	1.22	.68	1.29
5.00	1.63	1.69	1.63	2.00	1.63	.68	1.55
10.00	1.63	1.69	1.63	2.00	1.63	.68	1.55
30.00	2.04	2.37	2.04	2.33	2.04	1.36	2.03
70.00	2.04	2.37	2.04	2.67	2.04	1.36	2.09
132.00	2.86	2.71	2.86	3.00	2.86	2.37	2.78
240.00	2.86	3.05	2.86	3.00	2.86	3.05	2.95
1500.00	4.90	4.75	4.90	4.00	4.90	5.42	4.81
2880.00	4.90	4.75	4.90	4.67	4.90	5.42	4.92
12790.00	6.12	6.10	6.12	5.67	6.12	6.44	6.10
21420.00	6.53	6.44	6.53	5.67	6.53	7.12	6.47
47540.00	6.94	6.44	6.94	6.67	6.94	7.12	6.84
87840.00	7.35	7.80	7.35	7.33	7.35	7.12	7.38
142600.00	7.35	7.80	7.35	7.33	7.35	7.12	7.38
164200.00	7.35	7.80	7.35	7.33	7.35	7.12	7.38

TABLE B.9 : CREEP STRAIN VS. TIME AT 20 % WIDE STRIP TENSILE STRENGTH AND 22 C FOR FIBRETEX 300.

TIME (MIN.)	% STRAIN SAMPLE 1		% STRAIN SAMPLE 2		% STRAIN SAMPLE 3		% STRAIN AVERAGE
	STAPLES	GRIPS	STAPLES	GRIPS	STAPLES	GRIPS	
.10	12.55	11.14	12.55	12.78	12.55	14.24	12.64
1.00	15.29	14.13	15.29	14.77	15.29	17.44	15.37
2.00	16.47	14.95	16.47	15.91	16.47	18.02	16.38
5.00	17.25	16.30	17.25	16.48	17.25	18.60	17.19
10.00	17.65	16.85	17.65	17.05	17.65	19.19	17.67
30.00	19.22	18.48	19.22	18.18	19.22	21.22	19.25
60.00	20.78	20.11	20.78	19.32	20.78	22.38	20.69
140.00	22.35	21.47	22.35	21.31	22.35	24.13	22.33
424.00	23.92	23.64	23.92	23.01	23.92	24.71	23.85
1440.00	27.45	27.72	27.45	26.14	27.45	28.49	27.45
4320.00	30.98	31.52	30.98	29.83	30.98	31.10	30.90
11560.00	31.76	33.15	31.76	30.68	31.76	31.98	31.85
28862.00	32.55	34.24	32.55	30.68	32.55	32.85	32.57
46307.00	33.33	35.60	33.33	31.25	33.33	33.14	33.33
86400.00	36.08	38.59	36.08	34.09	36.08	36.05	36.16
141100.00	36.86	39.67	36.86	34.38	36.86	36.05	36.78
162700.00	36.86	39.67	36.86	34.38	36.86	36.05	36.78

TABLE B.10 : CREEP STRAIN VS. TIME AT 20 % WIDE STRIP TENSILE STRENGTH AND 22 C FOR PROPEX 2002.

TIME (MIN.)	% STRAIN SAMPLE 1		% STRAIN SAMPLE 2		% STRAIN SAMPLE 3		% STRAIN AVERAGE
	STAPLES	GRIPS	STAPLES	GRIPS	STAPLES	GRIPS	
.10	.82	.33	.82	.99	.82	.68	.74
1.00	1.22	.65	1.22	1.98	1.22	1.36	1.28
2.00	1.63	.65	1.63	2.31	1.63	1.36	1.54
5.00	1.63	.98	1.63	2.64	1.63	1.69	1.70
10.00	2.04	1.30	2.04	2.97	2.04	2.03	2.07
60.00	2.86	1.95	2.86	3.96	2.86	2.71	2.87
120.00	3.67	2.61	3.67	4.29	3.67	3.73	3.61
246.00	4.49	3.26	4.49	4.95	4.49	5.08	4.46
1440.00	6.12	4.56	6.12	6.60	6.12	6.78	6.05
2880.00	6.94	5.86	6.94	7.59	6.94	6.78	6.84
12870.00	8.98	7.82	8.98	9.57	8.98	9.15	8.91
21476.00	8.98	7.82	8.98	9.90	8.98	9.49	9.02
47596.00	9.80	8.47	9.80	10.23	9.80	10.17	9.71
87840.00	11.43	10.75	11.43	12.54	11.43	11.19	11.46
142600.00	11.43	11.07	11.43	12.54	11.43	11.19	11.51
164200.00	11.43	11.07	11.43	12.54	11.43	11.19	11.51

TABLE B.11 : CREEP STRAIN VS. TIME AT 35 % WIDE STRIP TENSILE STRENGTH AND 22 C FOR TYPAR 3401.

TIME (MIN.)	% STRAIN SAMPLE 1		% STRAIN SAMPLE 2		% STRAIN SAMPLE 3		% STRAIN AVERAGE
	STAPLES	GRIPS	STAPLES	GRIPS	STAPLES	GRIPS	
.10	2.85	3.69	3.21	3.97	5.31	4.35	3.90
1.00	3.66	4.70	4.02	4.64	6.12	5.02	4.69
2.00	4.07	5.03	4.42	4.97	6.12	5.02	4.94
5.00	4.47	5.37	4.82	5.30	6.53	5.35	5.31
10.00	5.28	6.04	4.82	5.63	6.53	5.69	5.66
30.00	6.91	7.05	5.62	6.62	6.94	6.02	6.53
60.00	7.72	7.05	6.83	7.28	6.94	7.02	7.14
120.00	7.72	7.38	7.23	7.28	7.35	7.36	7.39
240.00	9.35	8.72	8.03	8.61	8.57	8.70	8.66
1440.00	11.38	10.40	9.64	10.60	10.61	10.70	10.56
2880.00	13.01	11.74	10.84	11.59	11.02	11.71	11.65
5760.00	14.63	12.42	11.65	12.58	11.43	12.71	12.57
10080.00	16.67	13.76	12.85	13.91	12.24	14.05	13.91
20200.00	19.92	16.44	14.86	16.23	14.29	16.39	16.35
41760.00	22.76	17.45	15.26	17.55	14.29	17.39	17.45
61920.00	26.42	18.79	15.26	18.87	14.69	18.73	18.80

TABLE B.12 : CREEP STRAIN VS. TIME AT 35 % WIDE STRIP TENSILE STRENGTH AND 22 C FOR PROPEX 2002.

TIME	% STRAIN SAMPLE 1		% STRAIN SAMPLE 2		% STRAIN SAMPLE 3		% STRAIN AVERAGE
(MIN.)	STAPLES	GRIPS	STAPLES	GRIPS	STAPLES	GRIPS	
.10	5.65	4.26	3.98	6.25	5.02	.65	4.30
1.00	6.45	5.25	4.78	6.91	5.86	1.29	5.09
2.00	6.45	5.25	4.78	7.24	6.28	1.62	5.27
5.00	7.26	5.90	5.18	7.57	6.69	1.94	5.76
10.00	7.66	6.56	5.58	7.89	7.53	2.91	6.36
30.00	8.47	7.21	6.77	8.88	8.37	3.56	7.21
60.00	8.87	8.20	7.57	9.87	8.79	4.21	7.92
120.00	9.68	8.85	8.37	10.20	10.04	4.85	8.67
240.00	10.48	9.84	9.16	11.18	10.46	5.50	9.44
1440.00	12.10	13.11	10.36	14.14	12.55	8.74	11.83
2880.00	14.52	15.08	13.15	16.45	15.06	10.68	14.16
5760.00	15.32	16.39	13.55	18.09	16.74	12.30	15.40
10080.00	16.94	18.36	14.34	19.08	17.57	13.59	16.65
20160.00	19.76	21.64	16.73	22.04	20.92	17.48	19.76
40320.00	22.98	25.90	19.52	25.66	23.85	21.04	23.16
60480.00	25.00	28.85	21.91	28.62	26.78	23.95	25.85
83520.00	29.84	33.11	24.70	31.58	30.54	27.18	29.49
148000.00	42.74	43.93	31.47	37.83	43.51	40.78	40.05

TABLE B.13 : CREEP STRAIN VS. TIME AT 50 % WIDE STRIP TENSILE STRENGTH AND -12 C FOR BIDIM C-34.

TIME (MIN.)	% STRAIN SAMPLE 1		% STRAIN SAMPLE 2		% STRAIN SAMPLE 3		% STRAIN AVERAGE
	STAPLES	GRIPS	STAPLES	GRIPS	STAPLES	GRIPS	
.10	22.59	24.28	24.81	27.48	26.38	26.26	25.30
1.00	24.07	25.88	25.19	28.12	27.17	27.27	26.28
2.00	24.07	25.88	25.19	28.12	27.17	27.27	26.28
5.00	24.44	26.20	25.57	28.43	27.95	27.95	26.76
10.00	24.81	26.52	25.95	28.75	28.35	28.28	27.11
30.00	25.93	27.16	26.34	29.07	28.74	28.28	27.59
60.00	25.93	27.80	26.34	29.39	29.13	28.28	27.81
120.00	27.41	27.80	27.48	30.03	29.13	29.63	28.58
240.00	27.41	28.75	28.63	30.03	30.31	29.63	29.13
1440.00	27.78	29.07	28.63	30.67	30.71	29.63	29.41
3100.00	27.78	29.39	28.63	30.67	30.71	29.97	29.52
7200.00	28.52	30.35	29.39	31.31	31.10	30.98	30.27
13000.00	28.52	30.35	29.39	31.31	31.10	30.98	30.27
24500.00	28.52	30.35	29.39	31.31	31.10	30.98	30.27
46100.00	28.89	30.67	30.53	32.27	31.10	30.98	30.74

TABLE B.14 : CREEP STRAIN VS. TIME AT 50 % WIDE STRIP TENSILE STRENGTH AND -12 C FOR STABILENKA T-100.

TIME (MIN.)	% STRAIN SAMPLE 1		% STRAIN SAMPLE 2		% STRAIN SAMPLE 3		% STRAIN AVERAGE
	STAPLES	GRIPS	STAPLES	GRIPS	STAPLES	GRIPS	
.10	2.73	4.01	2.36	3.73	4.28	4.81	3.65
1.00	3.13	4.35	2.36	3.73	4.67	5.50	3.96
2.00	3.13	4.68	2.36	4.07	5.06	5.84	4.19
5.00	3.91	5.69	2.76	4.41	5.45	6.53	4.79
10.00	4.30	6.35	2.76	4.75	5.84	6.87	5.14
30.00	4.69	6.69	2.76	4.75	5.84	6.87	5.26
60.00	6.64	7.36	4.33	6.10	7.39	8.93	6.79
120.00	6.64	7.36	4.33	6.10	8.17	8.93	6.92
240.00	7.42	7.36	4.72	6.44	8.56	9.28	7.30
1440.00	7.42	8.03	4.72	6.78	8.95	9.28	7.53
3000.00	8.59	8.36	5.51	7.46	9.73	10.31	8.33
7200.00	8.59	9.36	6.30	7.80	10.51	11.34	8.98
13000.00	8.59	9.36	6.30	7.80	10.51	11.34	8.98
24500.00	8.98	9.36	6.30	7.80	10.89	11.68	9.17
46100.00	8.98	9.36	6.30	7.80	10.89	11.68	9.17

TABLE B.15 : CREEP STRAIN VS. TIME AT 50 % WIDE STRIP TENSILE STRENGTH AND -12 C FOR TYPAR 3401.

TIME (MIN.)	% STRAIN SAMPLE 1		% STRAIN SAMPLE 2		% STRAIN SAMPLE 3		% STRAIN AVERAGE
	STAPLES	GRIPS	STAPLES	GRIPS	STAPLES	GRIPS	
.10	2.75	3.03	3.63	2.67	1.99	1.32	2.56
1.00	2.75	3.37	4.44	3.33	2.79	1.98	3.11
2.00	2.75	3.37	4.44	3.33	3.19	2.31	3.23
5.00	3.14	3.70	4.84	3.67	3.59	2.64	3.60
10.00	3.14	4.04	6.05	4.33	3.98	2.97	4.09
30.00	3.53	4.04	6.85	5.67	5.18	3.30	4.76
60.00	3.92	4.38	6.85	5.67	5.18	3.63	4.94
120.00	4.71	4.71	8.06	5.67	5.18	3.63	5.33
240.00	4.71	4.71	8.06	6.33	5.98	4.62	5.74
1440.00	5.10	5.39	9.27	8.00	6.37	5.61	6.62
4320.00	5.49	6.40	9.68	8.67	7.57	6.60	7.40
10000.00	5.49	7.74	10.48	10.00	7.97	7.59	8.21
21600.00	7.06	7.74	11.69	10.33	10.36	7.59	9.13
43200.00	7.06	7.74	11.69	10.67	10.76	7.92	9.31
127000.00	9.02	9.43	14.11	12.67	13.15	9.90	11.38

TABLE B.16 : CREEP STRAIN VS. TIME AT 50 % WIDE STRIP TENSILE STRENGTH AND -12 C FOR FIBRETEX 300.

TIME	% STRAIN SAMPLE 1		% STRAIN SAMPLE 2		% STRAIN SAMPLE 3		% STRAIN AVERAGE
(MIN.)	STAPLES	GRIPS	STAPLES	GRIPS	STAPLES	GRIPS	
.10	30.12	29.57	30.74	30.06	31.85	29.32	30.28
1.00	33.20	32.62	32.30	31.60	34.27	31.48	32.58
2.00	33.98	33.54	32.68	32.21	34.68	32.10	33.20
5.00	34.75	34.15	33.46	32.82	35.48	32.72	33.90
10.00	37.45	35.06	35.02	34.66	38.31	33.64	35.69
30.00	38.22	36.28	36.19	35.28	39.92	34.88	36.79
60.00	40.15	37.80	38.52	35.89	41.13	36.42	38.32
120.00	42.08	40.55	39.69	38.34	43.15	38.27	40.35
240.00	45.95	42.38	42.02	39.88	44.35	39.20	42.30
1440.00	49.81	47.87	46.30	44.17	49.19	43.83	46.86
2880.00	53.28	51.52	49.81	46.32	52.42	45.37	49.79
5760.00	56.37	55.49	53.31	48.77	54.44	48.15	52.75
10000.00	61.00	58.54	54.86	52.15	57.26	50.62	55.74
122000.00	80.69	78.66	70.43	69.02	75.40	67.59	73.63

TABLE B.17 : CREEP STRAIN VS. TIME AT 50 % WIDE STRIP TENSILE STRENGTH AND -12 C FOR PROPEX 2002.

TIME (MIN.)	% STRAIN SAMPLE 1		% STRAIN SAMPLE 2		% STRAIN SAMPLE 3		% STRAIN AVERAGE
	STAPLES	GRIPS	STAPLES	GRIPS	STAPLES	GRIPS	
.10	3.16	2.75	5.43	6.62	3.95	3.70	4.27
2.00	3.95	3.44	5.81	7.28	4.35	4.04	4.81
5.00	4.35	3.78	6.20	7.62	4.74	4.38	5.18
10.00	5.53	4.12	6.59	7.95	5.93	4.38	5.75
30.00	5.53	4.12	6.98	8.28	5.93	4.71	5.93
60.00	5.53	4.47	6.98	8.61	5.93	4.71	6.04
120.00	5.53	4.47	7.36	8.61	6.72	5.05	6.29
240.00	6.32	5.15	7.36	9.93	7.11	5.39	6.88
1440.00	6.72	6.19	8.95	10.26	7.51	6.73	7.73
4320.00	8.70	7.56	9.69	11.92	8.70	7.74	9.05
10000.00	8.70	8.59	9.69	11.92	8.70	7.74	9.22
21600.00	9.09	8.93	11.63	13.91	9.49	9.43	10.41
43200.00	9.49	9.28	12.02	14.24	9.88	9.76	10.78
127000.00	12.25	11.68	14.34	17.22	12.25	12.46	13.37

TABLE B.18 : CREEP STRAIN VS. TIME AT 50 % WIDE STRIP TENSILE STRENGTH AND 22 C FOR BIDIM C-34.

TIME (MIN.)	% STRAIN SAMPLE 1		% STRAIN SAMPLE 2		% STRAIN SAMPLE 3		% STRAIN AVERAGE
	STAPLES	GRIPS	STAPLES	GRIPS	STAPLES	GRIPS	
.10	21.05	23.32	25.00	24.92	27.42	26.14	24.64
1.00	22.18	24.60	25.78	25.87	27.82	26.47	25.45
2.00	22.18	24.60	25.78	25.87	28.23	26.80	25.58
5.00	22.18	24.60	26.17	26.18	28.23	26.80	25.69
10.00	22.56	24.92	26.56	26.50	28.63	27.12	26.05
30.00	23.31	25.56	26.56	27.44	28.63	27.12	26.44
60.00	23.31	25.88	26.56	27.44	29.03	27.12	26.56
157.00	24.06	25.88	27.34	27.76	30.24	27.78	27.18
240.00	24.06	26.20	27.34	27.76	30.24	28.10	27.28
1682.00	24.44	27.16	28.13	28.39	30.65	28.76	27.92
4620.00	24.44	27.80	28.13	29.02	30.65	29.74	28.29
8982.00	24.81	28.12	28.52	29.02	31.05	30.07	28.60
14680.00	24.81	28.12	28.52	29.02	31.05	30.07	28.60
34560.00	24.81	28.43	28.91	29.34	31.05	30.39	28.82
54700.00	25.19	28.43	28.91	29.34	31.05	30.39	28.88

TABLE B.19 : CREEP STRAIN VS. TIME AT 50 % WIDE STRIP TENSILE STRENGTH AND 22 C FOR STABILENKA T-100.

TIME (MIN.)	% STRAIN SAMPLE 1		% STRAIN SAMPLE 2		% STRAIN SAMPLE 3		% STRAIN AVERAGE
	STAPLES	GRIPS	STAPLES	GRIPS	STAPLES	GRIPS	
.10	3.73	3.40	4.84	5.39	2.80	3.99	4.02
1.00	5.81	5.44	7.26	8.08	4.00	5.32	5.98
2.00	6.64	6.12	7.66	8.42	4.40	5.65	6.48
5.00	7.05	6.80	8.06	9.09	4.80	6.31	7.02
10.00	7.88	7.48	8.87	9.76	5.20	6.98	7.70
30.00	8.71	8.16	8.87	10.44	6.40	7.64	8.37
60.00	8.71	8.50	10.08	11.11	6.40	7.64	8.74
120.00	9.13	8.84	10.08	11.45	6.40	7.64	8.92
240.00	10.37	9.18	10.08	12.12	8.00	8.97	9.79
1500.00	11.20	10.20	12.10	13.80	9.20	9.30	10.97
2873.00	12.03	10.54	13.31	14.81	9.20	9.63	11.59
4440.00	12.03	12.24	13.31	14.81	9.20	10.63	12.04
8798.00	12.45	12.24	14.11	15.49	10.00	11.63	12.65
14500.00	12.45	12.24	14.52	15.82	10.00	11.63	12.78
34560.00	13.28	12.93	14.52	15.82	10.00	11.63	13.03
54700.00	13.28	12.93	14.52	15.82	10.40	11.63	13.10

TABLE B.20 : CREEP STRAIN VS. TIME AT 50 % WIDE STRIP TENSILE STRENGTH AND 22 C FOR TYPAR 3401.

TIME (MIN.)	% STRAIN SAMPLE 1		% STRAIN SAMPLE 2		% STRAIN SAMPLE 3		% STRAIN AVERAGE
	STAPLES	GRIPS	STAPLES	GRIPS	STAPLES	GRIPS	
.10	7.38	8.39	7.57	8.91	6.83	6.91	7.66
1.00	9.84	11.41	9.56	11.22	8.43	8.88	9.89
2.00	11.07	12.75	9.96	11.88	9.24	9.87	10.79
5.00	12.30	14.09	10.76	12.54	9.64	10.53	11.64
10.00	13.52	15.44	11.16	13.20	10.84	11.18	12.56
35.00	18.03	18.79	15.14	16.50	12.85	13.49	15.80
60.00	20.90	21.48	17.13	18.48	14.46	13.82	17.71
120.00	25.00	26.17	19.52	20.79	16.06	14.47	20.34
584.00	41.80	41.95	29.48	29.04	18.88	18.75	29.98

TABLE B.21 : CREEP STRAIN VS. TIME AT 50 % WIDE STRIP TENSILE STRENGTH AND 22 C FOR FIBRETEX 300.

TIME	% STRAIN SAMPLE 1		% STRAIN SAMPLE 2		% STRAIN SAMPLE 3		% STRAIN AVERAGE
(MIN.)	STAPLES	GRIPS	STAPLES	GRIPS	STAPLES	GRIPS	
.10	39.60	39.51	44.36	44.78	48.63	49.55	44.40
1.00	52.15	51.77	54.89	55.22	61.96	63.06	56.51
2.00	56.44	56.13	59.02	59.70	64.71	66.07	60.34
5.00	63.04	62.67	68.05	68.66	70.59	72.07	67.51
10.00	68.32	68.66	73.31	74.33	74.90	76.58	72.68
40.00	82.51	83.38	84.59	87.16	86.67	90.09	85.73
60.00	87.13	89.65	88.72	92.54	92.16	95.50	90.95
120.00	95.71	100.00	97.74	101.79	100.00	104.80	100.01
240.00	107.59	110.08	106.77	111.94	109.02	115.62	110.17
600.00	118.81	124.52	118.42	125.07	123.14	131.83	123.63
1440.00	125.41	131.88	124.06	132.24	132.16	141.74	131.25
2880.00	133.66	141.14	132.71	141.19	144.71	157.96	141.90
8480.00	151.82	159.67	148.50	158.51	160.39	175.98	159.14
15000.00	159.41	170.03	156.02	168.36	167.06	184.98	167.64
28000.00	171.62	183.65	167.29	182.69	180.00	202.10	181.23
40320.00	176.24	188.01	171.05	186.27	187.45	208.41	186.24
63400.00	182.18	195.64	175.94	192.84	194.12	216.22	192.82
84900.00	187.79	201.09	180.45	197.61	199.61	222.22	198.13

TABLE B.22 : CREEP STRAIN VS. TIME AT 50 % WIDE STRIP TENSILE STRENGTH AND 22 C FOR PROPEX 2002.

TIME	% STRAIN SAMPLE 1		% STRAIN SAMPLE 2		% STRAIN SAMPLE 3		% STRAIN AVERAGE
(MIN.)	STAPLES	GRIPS	STAPLES	GRIPS	STAPLES	GRIPS	
.10	8.13	8.87	7.14	10.30	7.29	8.08	8.30
1.00	8.54	9.56	8.33	11.30	7.69	8.75	9.03
2.00	8.94	9.90	8.73	12.29	8.50	9.43	9.63
5.00	10.16	11.26	9.52	13.62	9.72	10.77	10.84
10.00	11.38	12.63	9.92	14.29	10.53	11.78	11.75
30.00	13.01	15.36	11.90	15.95	12.15	13.47	13.64
60.00	15.04	18.43	13.10	18.27	13.77	15.49	15.68
120.00	17.89	22.18	15.08	20.60	14.98	18.52	18.21

TABLE B.23 : CREEP STRAIN VS. TIME AT 65 % WIDE STRIP TENSILE STRENGTH AND -12 C FOR BIDIM C-34.

TIME (MIN.)	% STRAIN SAMPLE 1		% STRAIN SAMPLE 2		% STRAIN SAMPLE 3		% STRAIN AVERAGE
	STAPLES	GRIPS	STAPLES	GRIPS	STAPLES	GRIPS	
.10	31.03	34.38	31.25	35.27	29.84	30.97	32.13
1.00	31.80	35.02	31.25	35.62	30.62	31.61	32.65
5.00	31.80	35.33	31.25	35.96	31.78	32.58	33.12
10.00	31.80	35.65	31.67	36.64	31.78	32.58	33.35
30.00	31.80	36.59	31.67	39.04	32.56	33.23	34.15
60.00	32.57	36.91	32.08	39.04	32.95	33.55	34.52
120.00	34.10	37.54	32.50	39.04	33.33	33.87	35.06
240.00	34.48	38.80	33.33	39.73	33.33	34.19	35.65
1440.00	35.25	39.12	34.58	40.41	34.50	35.48	36.56
2880.00	35.25	39.43	35.00	40.75	34.88	35.81	36.85
5760.00	36.02	39.75	35.00	40.75	35.27	36.13	37.15
10100.00	36.40	40.06	35.00	41.10	35.66	36.45	37.44
20200.00	36.40	40.06	35.42	41.10	35.66	36.45	37.51

TABLE B.24 : CREEP STRAIN VS. TIME AT 65 % WIDE STRIP TENSILE STRENGTH AND -12 C FOR STABILENKA T-100.

TIME (MIN.)	% STRAIN SAMPLE 1		% STRAIN SAMPLE 2		% STRAIN SAMPLE 3		% STRAIN AVERAGE
	STAPLES	GRIPS	STAPLES	GRIPS	STAPLES	GRIPS	
.10	10.84	12.16	3.89	3.39	4.00	6.73	6.84
1.00	11.24	12.84	6.23	5.42	4.80	8.42	8.16
2.00	12.45	13.85	6.23	5.42	4.80	8.42	8.53
5.00	12.85	14.53	7.00	6.10	5.20	9.09	9.13
10.00	14.46	15.54	7.39	6.78	6.80	9.09	10.01
30.00	14.46	16.22	7.78	7.46	7.20	9.76	10.48
60.00	14.86	16.55	8.17	7.46	8.80	9.76	10.93
120.00	18.47	20.27	9.73	9.83	9.60	12.12	13.34
240.00	18.47	20.95	10.89	10.51	9.60	12.46	13.81
1440.00	20.88	22.97	12.45	12.54	12.80	15.15	16.13
2880.00	20.88	24.32	12.45	13.22	12.80	15.15	16.47
5760.00	23.69	26.01	14.01	13.56	13.60	15.82	17.78
10100.00	24.50	26.35	14.01	14.24	13.60	16.50	18.20
20200.00	24.50	26.35	14.01	14.24	14.00	16.84	18.32
30200.00	24.50	26.35	14.40	14.92	14.00	17.17	18.56

TABLE B.25 : CREEP STRAIN VS. TIME AT 65 % WIDE STRIP TENSILE STRENGTH AND -12 C FOR TYPAR 3401.

TIME	% STRAIN SAMPLE 1		% STRAIN SAMPLE 2		% STRAIN SAMPLE 3		% STRAIN AVERAGE
(MIN.)	STAPLES	GRIPS	STAPLES	GRIPS	STAPLES	GRIPS	
.10	7.44	4.95	6.64	7.48	4.08	6.56	6.19
1.00	8.26	5.61	6.64	7.82	5.71	7.21	6.88
2.00	8.68	6.27	7.05	7.82	6.94	7.21	7.33
5.00	9.09	6.93	7.47	8.50	7.35	7.87	7.87
10.00	9.09	6.93	8.71	8.50	7.76	8.85	8.31
30.00	11.16	7.59	9.54	11.56	9.39	9.51	9.79
60.00	11.57	9.57	11.20	12.59	10.20	9.84	10.83
120.00	12.81	10.56	12.86	14.63	10.20	10.82	11.98
240.00	13.22	11.22	12.86	14.63	11.02	11.15	12.35
1440.00	15.70	15.18	16.18	18.37	14.29	14.43	15.69
2880.00	18.60	16.50	19.09	21.77	17.14	17.70	18.47
5760.00	19.42	18.15	21.16	24.83	19.18	20.33	20.51
10100.00	21.07	21.12	24.48	28.91	23.27	22.95	23.63
20200.00	24.38	24.42	29.05	35.03	26.53	28.52	27.99
30200.00	26.03	26.73	34.44	40.48	30.61	32.13	31.74
62000.00	31.82	31.68	48.96	56.12	39.18	38.69	41.08

TABLE B.26 : CREEP STRAIN VS. TIME AT 65 % WIDE STRIP TENSILE STRENGTH AND -12 C FOR FIBRETEX 300.

TIME (MIN.)	% STRAIN SAMPLE 1		% STRAIN SAMPLE 2		% STRAIN SAMPLE 3		% STRAIN AVERAGE
	STAPLES	GRIPS	STAPLES	GRIPS	STAPLES	GRIPS	
.10	40.08	38.89	45.83	44.83	38.58	41.75	41.66
1.00	43.51	42.48	50.76	49.53	39.76	43.04	44.85
2.00	43.89	42.81	52.65	50.47	42.91	43.69	46.07
5.00	44.27	43.14	53.79	52.66	44.88	45.95	47.45
10.00	45.42	45.10	55.30	53.92	46.46	47.90	49.02
30.00	47.33	47.39	58.33	56.74	48.03	50.16	51.33
60.00	51.15	49.35	60.98	59.87	49.61	53.72	54.11
120.00	52.29	54.25	66.67	67.08	54.72	58.58	58.93
240.00	56.49	59.15	71.59	72.10	55.12	61.17	62.60
1440.00	70.23	73.53	87.88	89.34	68.50	74.76	77.37
2880.00	76.34	81.37	95.83	97.81	74.41	81.88	84.61
5760.00	84.35	89.54	104.92	106.90	80.31	89.32	92.56
10100.00	89.69	97.39	112.50	115.36	86.22	95.79	99.49
20200.00	97.33	106.86	122.35	126.02	94.09	105.50	108.69
30200.00	103.82	111.76	127.65	132.92	98.03	111.00	114.20

TABLE B.27 : CREEP STRAIN VS. TIME AT 65 % WIDE STRIP TENSILE STRENGTH AND -12 C FOR PROPEX 2002.

TIME (MIN.)	% STRAIN SAMPLE 1		% STRAIN SAMPLE 2		% STRAIN SAMPLE 3		% STRAIN AVERAGE
	STAPLES	GRIPS	STAPLES	GRIPS	STAPLES	GRIPS	
.10	6.83	8.25	7.87	9.43	5.83	9.00	7.87
1.00	7.23	8.91	8.27	10.10	6.25	9.33	8.35
2.00	7.23	9.24	8.27	10.10	6.67	9.67	8.53
5.00	8.03	9.57	8.27	10.10	7.08	10.00	8.84
10.00	8.03	10.23	8.27	11.45	7.08	10.33	9.23
30.00	8.03	10.89	8.66	11.78	7.08	11.00	9.58
60.00	8.03	11.22	8.66	11.78	7.50	11.00	9.70
120.00	8.84	11.55	9.06	12.79	7.92	12.00	10.36
240.00	8.84	11.88	9.06	13.47	8.75	12.67	10.78
1440.00	10.44	14.52	10.24	15.15	9.17	14.00	12.25
2880.00	11.24	15.18	11.02	16.16	10.42	15.67	13.28

TABLE B.28 : CREEP STRAIN VS. TIME AT 65 % WIDE STRIP TENSILE STRENGTH AND 22 C FOR BIDIM C-34.

TIME	% STRAIN SAMPLE 1		% STRAIN SAMPLE 2		% STRAIN SAMPLE 3		% STRAIN AVERAGE
(MIN.)	STAPLES	GRIPS	STAPLES	GRIPS	STAPLES	GRIPS	
.10	31.22	31.01	35.41	36.13	33.07	35.28	33.69
2.00	33.03	31.71	35.80	37.42	34.66	36.57	34.86
5.00	33.03	32.40	36.96	38.06	35.06	37.22	35.46
10.00	33.03	32.40	38.13	38.71	35.06	37.22	35.76
30.00	33.48	32.75	38.13	39.03	35.86	38.51	36.29
60.00	34.39	33.45	39.69	40.00	35.86	38.51	36.98
120.00	34.84	33.45	40.08	40.32	35.86	38.51	37.18
240.00	34.84	34.15	40.08	40.32	36.25	39.16	37.47
1440.00	35.75	36.24	41.25	41.94	36.25	39.16	38.43
2880.00	36.20	36.24	42.02	42.26	36.65	39.81	38.86

TABLE B.29 : CREEP STRAIN VS. TIME AT 65 % WIDE STRIP TENSILE STRENGTH AND 22 C FOR STABILENKA T-100.

TIME (MIN.)	% STRAIN SAMPLE 1		% STRAIN SAMPLE 2		% STRAIN SAMPLE 3		% STRAIN AVERAGE
	STAPLES	GRIPS	STAPLES	GRIPS	STAPLES	GRIPS	
.10	13.23	13.09	13.36	18.52	7.20	11.26	12.78
2.00	14.79	14.43	19.43	22.22	13.60	15.02	16.58
5.00	14.79	14.77	19.84	22.90	14.80	17.06	17.36
10.00	17.12	15.44	22.67	24.92	14.80	17.75	18.78
30.00	17.12	16.11	23.89	26.60	16.80	18.77	19.88
60.00	17.51	17.11	25.91	28.28	17.60	19.45	20.98
120.00	18.29	17.11	26.32	29.29	18.40	20.48	21.65
240.00	19.07	17.79	27.94	30.98	19.20	21.50	22.74
1440.00	20.23	18.79	30.77	34.01	22.40	24.23	25.07
2880.00	21.01	20.13	31.17	35.02	24.80	27.65	26.63

TABLE B.30 : CREEP STRAIN VS. TIME AT 65 % WIDE STRIP TENSILE STRENGTH AND 22 C FOR FIBRETEX 300.

TIME (MIN.)	% STRAIN SAMPLE 1		% STRAIN SAMPLE 2		% STRAIN SAMPLE 3		% STRAIN AVERAGE
	STAPLES	GRIPS	STAPLES	GRIPS	STAPLES	GRIPS	
.10	62.06	63.36	77.44	76.81	69.88	77.16	71.12
1.00	77.08	78.68	93.98	93.37	87.64	87.96	86.45
2.00	83.00	84.68	99.62	99.70	93.44	94.14	92.43
5.00	92.89	94.59	106.77	110.84	100.39	103.70	101.53
10.00	100.79	102.70	115.41	118.07	110.04	112.65	109.95
30.00	116.21	119.52	131.58	137.05	125.87	131.48	126.95
60.00	126.88	131.23	143.23	149.70	136.29	143.21	138.42
120.00	137.15	143.84	156.77	165.06	146.33	154.94	150.68
240.00	147.83	156.46	168.42	177.41	159.46	168.52	163.02
480.00	159.29	170.87	179.70	192.17	167.95	181.79	175.30
1440.00	171.94	185.89	195.49	212.05	183.78	200.93	191.68
2880.00	182.21	197.30	207.52	225.30	192.66	212.04	202.84
5760.00	190.91	206.91	218.80	239.76	211.58	238.89	217.81

APPENDIX C

Method of Evaluation of Parameters of the Four Element Mechanical Model Using the Rate Process Theory

APPENDIX C

As discussed in Section 2.4.4, Burger's rheological model in conjunction with the Rate Process Theory may be used to characterize the creep behavior of geotextiles. Since more work is needed to ascertain the effectiveness of this model for geotextiles, the method of applying the model to creep is presented below. For the derivation of the equations that follow, the reader is referred to Hogan (34).

The constants of the open elements E, K and α [1] are determined as follows: Initially, accurate scale drawings of the experimental creep curves in question must be made, as shown in Figure C.1(a). These experimental creep curves (only two or three are needed) should be for the same geotextile at constant temperature but for two or three different load levels. Using one of the experimental creep curves, measure the instantaneous creep strain ε_o and determine E, given the stress σ:

$$E = \frac{\sigma}{\varepsilon_o} \tag{C.1}$$

As discussed by Hogan (34),

$$\ln \dot{\varepsilon}_d = \ln \frac{K}{2} + \alpha\sigma \tag{C.2}$$

in which $\dot{\varepsilon}_d$ is the secondary creep rate, shown in Figure C.1(c). Hence, if the logarithm of the secondary creep rate at constant stress is plotted against the corresponding stress for each experimentally

---

[1] Note: See Figure 2.32, Burger's rheological model.

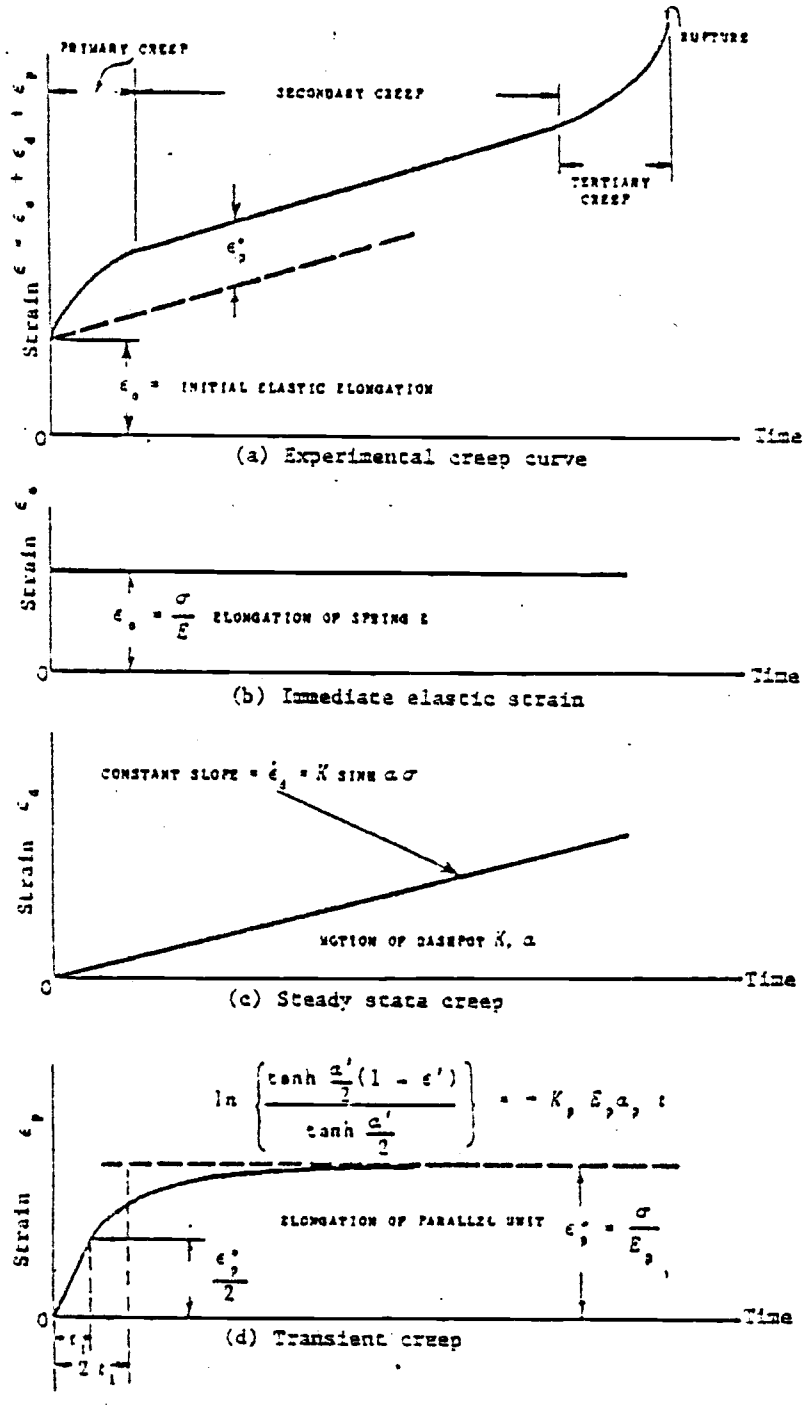

Figure C.1: Picturization of creep (after Hogan (34)).

determined creep curve, the resulting curve is a straight line with a slope α and whose intercept on the ordinate is K/2. In this manner, K and α, the constants for the open viscous element, may be determined.

The constants of the closed parallel elements, E_p, K_p, and α_p[1], are determined as follows:

From the same experimental creep curve in which ε_o was determined, measure the total creep strain due to primary (or transient) creep, ε_p^*, as shown in Figure C.1 (a and d). Then,

$$E_p = \frac{\sigma}{\varepsilon_p^*} \tag{C.3}$$

Again, from the same experimental creep curve, determine the point on the experimental creep curve at which the creep strain due only to primary creep is one half of ε_p^*. At this point time $t = t_1$, as shown in Figure C.1(d). From the scale drawing of the experimental creep curve, measure the creep strain due to primary creep, ε_p, at time $t = 2t_1$. ε'' is defined as follows:

$$\varepsilon'' = \frac{\varepsilon_p}{\varepsilon_p^*} \text{ at } t = 2t_1 \tag{C.4}$$

Following a determination of ε'' a constant, α', may be determined from the curve shown in Figure C.2, provided that the following condition exists (34):

$$0.55 < \varepsilon'' < 0.75.$$

Thus

$$\alpha_p = \frac{\alpha'}{\sigma} \tag{C.5}$$

---

[1]Note: See Figure 2.32, Burger's rheological model.

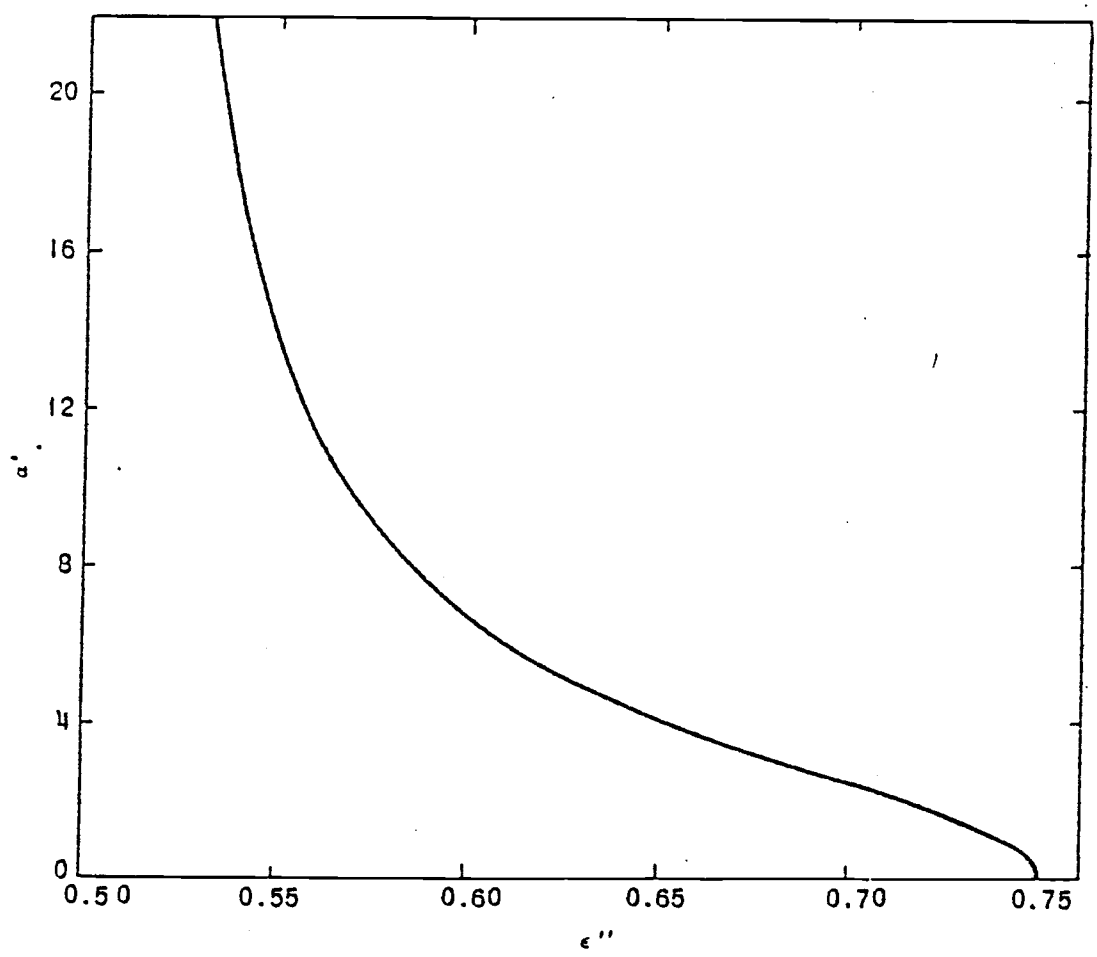

Figure C.2: α' versus ε'' (after Hogan (34)).

K_p may be determined from the following equation:

$$K_p = \frac{1}{E_p \alpha_p t_1} \left[\ln \frac{\tanh \frac{\alpha_p \sigma}{2}}{\tanh \frac{\alpha_p \sigma}{4}} \right] \qquad (C.6)$$

Once the constants E, K, α, E_p, K_p, and α_p have been determined, the creep strains ε_o and ε_p^*, as well as the creep rate $\dot{\varepsilon}_d$, may be determined for any new stress σ' using equations C.1, C.3, and C.2, respectively. The new time t_1 at stress σ', when $\varepsilon_p = \frac{\varepsilon_p^*}{2}$, may be determined from Equations C.6 and C.5, Figure C.2, and finally Equation C.4.

The variation in creep rate with temperature can be determined from the following equation (32):

$$\frac{\ln(\dot{\varepsilon}/T)}{(1/T)} = -\frac{\bar{E}}{R} \qquad (C.7)$$

in which, $\bar{E}$ = the experimental activation energy

R = universal gas constant = 1.98 cal°K^{-1} $mole^{-1}$

$\dot{\varepsilon}$ = rate of creep strain at temperature T

T = absolute specimen temperature.

From Equation C.7 it follows that if identical specimens are subjected to creep tests under the same stress intensity but at different temperatures, there should be a linear variation between $\ln(\dot{\varepsilon}/T)$ and $1/T$ having a slope of $-\bar{E}/R$ (32). Therefore, once this linear relationship has been established for a given material, the creep rate for the material at a new temperature may be determined. The validity of this relationship for geotextiles has not been demonstrated.

APPENDIX D

Water Content Distributions for Frost Heave Test Specimens

Tables D.1 through D.5 contain the water content values for all of the soil columns considered in the frost heave program. The specimen depth was measured from the top of the specimen after heaving.

Table D.1: Soil water content versus depth after freezing for specimens with and without layer of Bidim C-34.

Depth Below Top of Specimen (mm)	Water Content %		
	No Free Water	Free Water	
	Without Geotextile	With Geotextile	Without Geotextile
9.5	20.6	21.3	21.3
29	20.0	19.9	18.1
48	20.2	21.2	19.8
67	19.0	20.3	19.4
86	19.0	19.5	25.3
105	18.5	17.0	30.6
124	16.9	12.9 *	44.4
143	10.5	18.3	18.1
162	12.6	20.0	19.1
181			20.7

*Geotextile Layer.

Table D.2: Soil water content versus depth after freezing for specimens with and without layer of Stabilenka T-100.

Depth Below Top of Specimen (mm)	Water Content %		
	No Free Water	Free Water	
	Without Geotextile	With Geotextile	Without Geotextile
9.5	23.4	15.5	22.4
29	22.3	20.2	23.9
48	21.2	24.5	26.4
67	19.7	27.5	29.7
86	19.6	38.3	36.5
105	18.5	52.3	45.3
124	17.3	18.5 *	18.2
143	11.8	19.3	19.6
162	12.7	19.3	22.7
181		20.9	

*Geotextile Layer.

Table D.3: Soil water content versus depth after freezing for specimens with and without layer of Typar 3401.

Depth Below Top of Specimen (mm)	Water Content %		
	No Free Water	Free Water	
	Without Geotextile	With Geotextile	Without Geotextile
9.5	21.6	24.8	20.7
29	20.4	20.0	19.4
48	22.6	21.4	21.5
67	21.6	20.6	25.7
86	20.6	19.0	30.5
105	19.4	16.4	35.9
124	18.0	14.1 *	53.0
143	13.7	25.0	19.7
162	13.8	22.2	22.7

*Geotextile layer.

Table D.4: Soil water content versus depth after freezing for specimens with and without layer of Fibretex 300.

Depth Below Top of Specimen (mm)	Water Content %		
	No Free Water	Free Water	
	Without Geotextile	With Geotextile	Without Geotextile
9.5	22.6	21.6	35.2
29	20.3	23.6	30.0
48	21.2	21.1	25.0
67	20.2	18.4	24.7
86	19.6	18.1	24.3
105	19.0	16.7	24.0
124	18.5	12.8 *	18.7
143	12.8	19.6	19.5
162	13.3	20.4	20.8

*Geotextile layer.

Table D.5: Soil water content versus depth after freezing for specimens with and without layer of Propex 2002.

Depth Below Top of Specimen (mm)	Water Content %		
	No Free Water	Free Water	
	Without Geotextile	With Geotextile	Without Geotextile
9.5	21.6	20.5	20.4
29	19.4	18.2	19.9
48	20.8	19.1	20.8
67	20.3	20.2	25.1
86	19.6	21.2	26.3
105	18.3	24.9	37.7
124	17.4	22.2*	28.5
143	11.9	18.5	18.1
162	11.7	19.7	21.2

*Geotextile layer.